

Studies of Linear and Nonlinear Acoustic Waves in Space Plasmas

Thomas K. Baluku

Submitted in fulfilment of the academic requirements

for the degree of Doctor of Philosophy

in the School of Physics

University of KwaZulu-Natal,

Durban

January, 2011

Preface

The theoretical work described in this thesis was carried out in the School of Physics, University of KwaZulu-Natal, Durban, from August 2007 to June 2010, under the supervision of Professor Manfred A. Hellberg and Prof. Richard L. Mace.

These studies represent original work by the author and have not otherwise been submitted in any form for any degree or diploma to any tertiary institution. Where use has been made of the work of others it is duly acknowledged in the text.

Declaration 1 – Plagiarism

I,, declare that

1. The research reported in this thesis, except where otherwise indicated, is my original research.
2. This thesis has not been submitted for any degree or examination at any other university.
3. This thesis does not contain other persons' data, pictures, graphs or other information, unless specifically acknowledged as being sourced from other persons.
4. This thesis does not contain other persons' writing, unless specifically acknowledged as being sourced from other researchers. Where other written sources have been quoted, then:
 - (a) Their words have been re-written but the general information attributed to them has been referenced.
 - (b) Where their exact words have been used, then their writing has been placed in italics and inside quotation marks, and referenced.
5. This thesis does not contain text, graphics or tables copied and pasted from the Internet, unless specifically acknowledged, and the source being detailed in the thesis and in the References sections

Signed

Declaration 2 – Publications

The research work presented in this thesis includes results in three articles (as a leading author) that have been published in peer-review journals (with double asterisks) and three articles that are either in advanced stages to be submitted or have been submitted for publication in various journals (with an asterisk). Besides, I have also been involved in two other published articles (as a third author).

Publication 1: T. K. Baluku and M. A. Hellberg, Dust acoustic solitons in plasmas with kappa-distributed electrons and/or ions, *Physics of Plasmas*, **15, 123705 (2008)

Publication 2: M. A. Hellberg, R. L. Mace, T. K. Baluku, I. Kourakis and N. S. Saini, Comment on “Mathematical and physical aspects of Kappa velocity distribution” [*Phys. Plasmas* 14, 110702 (2007)], *Physics of Plasmas*, **16**, 094701 (2009)

Publication 3: T. K. Baluku, M. A. Hellberg, I. Kourakis and S. N. Saini, Dust ion acoustic solitons in a plasma with kappa distributed electrons, *Physics of Plasmas*, **17, 053702 (2010)

Publication 4: T. K. Baluku, M. A. Hellberg and F. Verheest, New light on ion acoustic solitons in a plasma with two temperature electrons, *Europhysics Letters* **91, 15001 (2010)

In preparation:

Publication 5: F. Verheest, M. A. Hellberg and T. K. Baluku, Finite amplitude electrostatic solitons at the acoustic speed, *Journal of Plasma Physics*, submitted (2010)

*Publication 6: T. K. Baluku, M. A. Hellberg and R. L. Mace, Electron-acoustic waves in double-kappa plasmas: Application to Saturn's magnetosphere, *Journal of Geophysical Research*, submitted (2010)

*Publication 7: T. K. Baluku and M. A. Hellberg, Ion acoustic solitary waves in an electron-positron-ion plasma with nonthermal electrons, *Plasma Physics and Controlled Fusion*, submitted (2010)

*Publication 8: T. K. Baluku and M. A. Hellberg, Ion acoustic solitons in a plasma with two-temperature kappa distributed electrons (to be submitted to *Planetary and Space Science*)

Signed

Dedication

In memory of our late daughter Masika Claret, and to my wife Biirah Judith for her enduring love.

Acknowledgements

I express my sincere gratitude to Professors Manfred A. Hellberg and Richard L. Mace, for their guidance during the course of this work. Their constant criticism was inspiring and gave me confidence. I am greatly indebted to Prof. Manfred Hellberg for being patient with and kind to me, and for his expertise and commitment in nurturing young researchers. This has been an exciting experience, your support has been invaluable.

I also would like to thank Professor Frank Verheest (Ghent Belgium), Doctors Ioannis Kourakis (Belfast, Ireland) and Naresh N. S. Saini (Amritsar, India) for your collaboration. I learnt a lot from you all.

Financial support of the National Astrophysics and Space Science Programme (NASSP), the National Research Foundation (NRF), and the University of KwaZulu-Natal (through Prof. Manfred Hellberg) is greatly acknowledged.

Finally, I thank my wife Biirah Judith for her love, encouragement and all the support. It is very unfortunate that I began this programme at a time when we still had fresh memories of the loss of our beloved daughter Claret. Thank you Judith, your efforts and support are an invaluable asset.

Abstract

This thesis is about a study of the behaviour of linear and nonlinear electrostatic waves in a variety of multi-component plasma configurations in space physics, including species whose velocity distributions are represented by kappa distributions. Kappa distributions commonly occur in space plasmas, and are characterized by a spectral index parameter κ , which ranges from low values (representing a more enhanced superthermal tail and “hard” particle spectra) to very high values (with $\kappa \rightarrow \infty$ representing a Maxwellian distribution).

The linear theory of the electron-acoustic waves (EAWs), which commonly occur in two-temperature plasmas, is investigated within a kinetic-theoretical paradigm using the kappa velocity distribution as metastable state. The results of this calculation are directly applicable to the Saturnian magnetosphere where the electrons are well represented by the superposition of two kappa distributions, with distinct temperatures and values of κ . According to our findings, weakly damped EAWs are likely to occur at around $13 - 18 R_S$, where the densities of the hot and cool electron populations are of similar magnitude, the kappa index values are more or less constant around $\kappa_c \simeq 2$ and $\kappa_h \simeq 4$, and the hot to cool temperature ratio is about 10^2 .

In the nonlinear wave studies described in this thesis, a variety of different three-species plasma models are investigated, including dusty (complex) plasmas which are observed in a number of different space environments. In addition to electrons and ions, dusty plasmas contain massive heavily charged dust grains typically of micron size. This additional component has a significant effect on the overall wave behaviour compared to an electron-ion

plasma, and introduces new eigenmodes such as dust acoustic waves and dust ion-acoustic waves, as examples, which are discussed in detail in this thesis.

Nonlinear electrostatic waves, such as solitons and double layers, are reported from satellite observations. Propagation of these solitary structures, including their existence domains, structure behaviour and characteristics, in a variety of different multi-component plasma configurations is investigated in this thesis. These nonlinear studies encompass both small amplitude (Korteweg-de Vries) and fully nonlinear (Sagdeev pseudopotential) investigations, and comparison of results from these methods is presented.

According to the conventional Sagdeev and small amplitude (KdV) approaches, the existence of solitons requires Mach numbers which exceed a critical value (M_s), the phase velocity of the acoustic waves in the plasma configuration. The KdV soliton solutions have amplitudes that go to zero as the Mach number approaches the critical value. Results in this thesis show that in plasmas where solitons of both polarities can be supported, under certain conditions, electrostatic solitons with finite amplitudes can be obtained at the critical Mach number, and therefore such structures can propagate at the acoustic phase velocity. This is an important finding that goes counter to conventional wisdom on this topic. In addition, the appearance of double layers has usually been considered to mark the end of soliton occurrence in plasma models. From the nonlinear studies of the different plasma configurations discussed in this thesis, it is shown that for some models, and for certain plasma parameters, solitons can also be obtained for Mach numbers that exceed those leading to the occurrence of double layers.

Contents

1	General Introduction	1
1.1	Aspects of Kappa Distributions	1
1.1.1	Introduction	1
1.1.2	Kappa Distributions: Velocity Moments and the Most Probable Speed	2
1.1.3	Kappa Distributions: Application to Plasma Experiments and Space Plasma Observations	5
1.1.4	Modified Forms of Kappa Distributions and other Non-Maxwellian Distributions	7
1.2	Dusty Plasmas	14
1.2.1	Dust and Dusty Plasmas	14
1.2.2	Fundamental Length Scales	16
1.2.3	Charging Process of Dust Grains	19
1.2.4	Waves in Dusty Plasmas	22
1.3	Solitons and Double Layers	24
1.3.1	Solitons	24
1.3.2	Double Layers	25
1.4	Methods Used in the Study of Solitary Structures	26
1.4.1	The Reductive Perturbation Theory	28
1.4.2	The Sagdeev Pseudopotential Theory	30

1.5	Outline of Thesis	34
2	Electron-Acoustic Waves in Bi-kappa Plasmas	37
2.1	Introduction	37
2.2	Description of Electron-Acoustic Waves	40
2.3	Theoretical Model and Basic Equations	43
2.4	Analytic Solutions	45
2.5	Numerical Solutions	50
2.6	Results: Effects of Density, Temperature and Spectral Index	52
2.6.1	Effect of Electron Spectral Indices	54
2.6.2	Effect of Temperature Ratio	58
2.6.3	Effect of the Hot Electron Density Fraction	58
2.7	Results: Application to Saturn's Magnetosphere	60
2.8	Conclusions and Chapter Summary	66
3	Dust Acoustic Solitons in Plasmas with Kappa-Distributed Electrons and/or Ions	69
3.1	Introduction	69
3.2	Model and Basic Equations	70
3.3	Small Amplitude Dust Acoustic Solitons (DAS) and Double Layers	75
3.3.1	Small Amplitude Solitons	76
3.3.2	Small Amplitude Double Layers	78
3.4	Arbitrary Amplitude DAS and Double Layers	81
3.4.1	Positive Potential Solitons	81
3.4.2	Negative Potential Solitons	83
3.4.3	Numerical Results and Discussion	84
3.5	Dust Acoustic Structures with Positive Dust	88
3.6	Chapter Summary	92
4	Dust Ion-Acoustic Solitons in a Plasma with Kappa-Distributed Elec- trons	94
4.1	Introduction	94

4.2	Basic Equations	96
4.3	Linear Dispersion Relation	98
4.4	Small Amplitude Solitons: Reductive Perturbation Technique	100
4.4.1	Korteweg-de Vries (KdV) Equation	102
4.4.2	Modified Korteweg-de Vries (mKdV) Equation	104
4.5	Arbitrary Amplitude Solitons: Pseudopotential Approach	106
4.5.1	Electrostatic potential limitations	110
4.6	Negative Dust	115
4.6.1	Effect of Dust Grain Mass–Charge Ratio (through z)	115
4.6.2	Effect of Ion Temperature (through σ)	116
4.7	Results and Discussion	117
4.8	Positive Dust	127
4.9	Comment	129
4.10	Discussion and Chapter Summary	130
5	Ion-Acoustic Solitons in a Plasma with Two-Temperature κ-distributed Electrons	133
5.1	Introduction	133
5.2	Model and Basic Equations	135
5.3	The Linear Dispersion Relation	136
5.4	Small Amplitude Solitons	138
5.4.1	The Korteweg-de Vries (KdV) Equation	138
5.4.2	The Modified Korteweg-de Vries (mKdV) Equation	143
5.5	Arbitrary Amplitude IA Solitons	148
5.5.1	Pseudopotential Approach	150
5.5.2	Potential Limitations	151
5.5.3	Existence Domain for Ion-Acoustic Solitons and Double Layers	153
5.5.4	Variation of Soliton Potential Amplitude (ϕ_m) with Mach Number	154
5.5.5	Sagdeev (Pseudopotential) Approach vs. Perturbation Technique	159
5.6	Positive Potential Double Layers	160
5.7	Conclusions and Chapter Summary	163

6	Ion-Acoustic Solitary Waves in an Electron-Positron-Ion (e-p-i) Plasma	165
6.1	Introduction	165
6.1.1	Nonthermal Distributions: The Cairns Distribution	167
6.2	Plasma Model and Basic Equations	168
6.3	Linear Dispersion Relation	169
6.4	Arbitrary Amplitude Solitary Waves	170
6.4.1	Numerical Results and Discussion	172
6.4.2	Critical Composition	174
6.5	Summary and Remarks	177
7	Ion-Acoustic Solitary Waves in a Plasma With Two-Temperature Elec-	
	trons	179
7.1	Introduction	179
7.2	Plasma Model and Basic Equations	181
7.3	Numerical Results and Discussion	185
7.3.1	$\tau > \tau_{c1} = 5 - 2\sqrt{6}$	185
7.3.2	$\tau_{c2} \simeq 0.075 < \tau < \tau_{c1}$	186
7.3.3	$\tau < \tau_{c2} \simeq 0.075$	190
7.4	Conclusions and Chapter Summary	200
8	General Summary and Conclusions	203
8.1	Linear Electron-Acoustic Waves	203
8.2	Nonlinear Acoustic Waves	204
A		212
A.1	Derivation of Density and Pressure for Kappa Distributions	212
A.1.1	Special Integrals for Kappa Distributions	212
A.1.2	Density and Pressure Expressions for Kappa Distributions	213
B		217
B.1	Dispersion Relation of Electron-Acoustic Waves from Linear Kinetic Theory.	217
C		223

C.1 Derivation of the Modified Korteweg de-Vries (mKdV) Equation 223

C.2 Solution of the mKdV Equation 227

List of Figures

1.1	Comparison of generalized Lorentzian distributions for different spectral indices	4
1.2	The normalized form of Eq. (1.26) for different values of β	13
1.3	A typical soliton structure in terms of the electrostatic potential and the electric field	24
1.4	A schematic picture of (a) potential profile, (b) phase space for the ions, and (c) phase space for the electrons, for a typical double layer structure . . .	27
2.1	Analytical results discussed in Eqs. (2.6)–(2.14), applied to a plasma system corresponding to a radial distance of about $13.1 R_S$ in Saturn’s magnetosphere	49
2.2	A graph showing $\xi_c = \text{Re}(\xi_c) + i \text{Im}(\xi_c)$ satisfying both $D_r(k, \omega) = 0$ and $D_i(k, \omega) = 0$ for $k\lambda_{De} = 1$ (<i>left panel</i>), and dispersion and damping rate curves corresponding to the initial estimates of ξ_c (<i>right panel</i>)	53
2.3	Dispersion and damping for different cool electron kappa indices, κ_c	55
2.4	Dispersion and damping for different hot electron kappa indices, κ_h	57
2.5	Dispersion and damping for different temperature ratios, $\beta = T_h/T_c$	59
2.6	Dispersion and damping for different density ratios, $f = n_{0h}/n_{0e}$	60
2.7	Same as in Fig. 2.6, here for $f = 0.1$ (blue) and $f = 0.2$ (red), respectively . . .	61

2.8	Dispersion (ω_r/ω_{pe}) and damping (γ/ω_{pe}) versus $k\lambda_{Dc}$ for parameters corresponding to the Saturnian magnetosphere at about $13.1 R_S$ (<i>left panel</i>) and $14 R_S$ (<i>right panel</i>)	63
2.9	Same as in Fig. 2.8, at about $15 R_S$ (<i>left panel</i>) and $17.8 R_S$ (<i>right panel</i>)	63
2.10	Same as in Fig. 2.8, at about $12 R_S$ (<i>left panel</i>) and $9.8 R_S$ (<i>right panel</i>)	65
2.11	Same as in Fig. 2.8, at about $15.2 R_S$ (<i>left panel</i>) and $16 R_S$ (<i>right panel</i>)	65
2.12	Same as in Fig. 2.8, at about $5.4 R_S$ (<i>left panel</i>) and $6.3 R_S$ (<i>right panel</i>)	67
3.1	Existence domain for weak negative potential dust acoustic solitary waves, from the small amplitude theory (M_s, M_β, M_α) for $\sigma = 0.5$	79
3.2	Same as Fig. 3.1, here for $\sigma = 1$	79
3.3	Existence domains for negative potential solitons for $\sigma = 1$ and varying κ values	85
3.4	Typical Sagdeev potentials for the case of Fig 3.3(b)	85
3.5	Same as Fig. 3.3, here for $\kappa_i = 25; \kappa_e = 4$ (<i>left panel</i>) and $\kappa_i = 4; \kappa_e = 25$ (<i>right panel</i>)	87
3.6	Existence domains for negative potential solitons for $\kappa_e = \kappa_i = 2$	88
3.7	Existence domains for positive potential solitons in the presence of positive dust for near-Maxwellian ions and varying κ_e (<i>upper panel</i>), and variation with temperature ratio, σ for $\kappa_e = \kappa_i = 2$ (<i>lower panel</i>)	90
3.8	Existence domains for positive potential solitons in a positive dusty plasma, plotted as a function of the alternative fractional density variable, $g = N_{i0}/N_{e0}$	91
4.1	Variation of critical density fraction, f_c , with κ in the small amplitude (KdV) theory	104
4.2	Variation of the thermal velocity-to-phase speed ratio, U_{ti}/M_s with fractional density, f	109
4.3	Schematic representation of Bernoulli integrals for cool, supersonic ($M_j > 1$) and hot, subsonic ($M_j < 1$) species	112
4.4	Existence domain for dust ion-acoustic solitons with varying z	115
4.5	Existence domain for dust ion-acoustic solitons with varying σ	117

4.6	Existence domain for DIA solitons with cold ions ($\sigma = 0$), <i>left panel</i> , and cool ions ($\sigma = 0.01$), <i>right panel</i>	119
4.7	Variation of potential amplitude, ϕ_m , with κ for different values of M	121
4.8	Variation of potential amplitude, ϕ_m with the ratio M/M_s for various values of κ	122
4.9	Plot of ϕ_m vs. M/M_s (<i>upper panel</i>), and pseudopotential plots (<i>middle and lower panels</i>)	124
4.10	Soliton amplitudes obtained at $M = M_s$ for f in the range (f_p, f_n)	126
4.11	Existence domains for positive potential DIA solitons, for both negatively charged dust ($f < 1$) and positive dust ($f > 1$)	128
4.12	Sagdeev potential for $f < f_c$ (<i>left panel</i>) and $f > f_c$ (<i>right panel</i>)	130
5.1	f -solutions of $\alpha_{s4}(f) = 0$ and $\alpha_{s5}(f) = 0$ as functions of τ	146
5.2	f -solutions of $\alpha_{s4} = 0$ and $\alpha_{s5} = 0$ as functions of β	147
5.3	Same as in Fig. 5.2, here for $\beta = 1/10$ (<i>left panel</i>) and $\beta = 3/100$ (<i>right panel</i>)	147
5.4	Restriction of solitons by double layers, obtained for the parameters typical for Saturn's outer magnetosphere at about $16 R_S$	152
5.5	Existence domain for ion-acoustic solitons	153
5.6	Soliton profiles for different spectral index values $\kappa = \kappa_c = \kappa_h$	155
5.7	Variation of soliton potential amplitude with $\delta M = M - M_s$ for a 'hard' electron spectrum (low κ values)	155
5.8	Same as in Fig. 5.7, now for the Maxwellian equivalent ($\kappa_c = \kappa_h = \infty$)	156
5.9	Finite solitons at $M = M_s$ in the "coexistence" region	157
5.10	Typical soliton profiles at the lowest Mach number M_s	158
5.11	Soliton amplitude (ϕ_0) as a function of Mach number, M	159
5.12	Variation of f_c with temperature ratio, β	160
5.13	Existence domain for positive double layers for a plasma with Maxwellian electron components and cold ions, with $\beta = 0.09$	161
5.14	Same as in Fig. 5.13, now with $\beta = 0.3$	162

6.1	Existence domain of solitons or double layers corresponding to a plasma with equal positron and electron temperatures ($\sigma = 1$) and $\beta = 0.5$ (<i>left panel</i>), and for different β values (<i>right panel</i>)	173
6.2	Existence domain of positive potential solitons, in the $(M - \beta)$ plane, for different values of p	174
6.3	Curves for $\Psi'''(\phi = 0, M = M_s) = 0$ giving $p = p_c$ for different values of $\sigma = T_p/T_e$	176
6.4	Typical Sagdeev potential curves for $\sigma = 1, \beta = 0.5$, and $p = 0.03 < p_c = 0.04904$ (<i>upper panel</i>) and $p = 0.0494 > p_c$ (<i>lower panel</i>)	177
7.1	Variation of the critical density fraction, f_c , with τ	185
7.2	Existence domain of ion-acoustic solitons for $\tau = 1/5 > \tau_{c1}$	186
7.3	Existence domain of ion-acoustic solitons for $\tau = 0.09$ (<i>left panel</i>), and typical soliton potential amplitude at $M = M_s = 1$ (<i>right panel</i>)	187
7.4	Soliton amplitude variation with M for $\tau = 0.09$ and different f values (<i>left panel</i>), and typical Sagdeev curves for $f = 0.01$ and different Mach numbers, both below and above M_{dl} (<i>right panel</i>)	189
7.5	Typical soliton pulse curves corresponding to $\tau = 0.09, f = 0.01$ in Fig. 7.4 for different Mach numbers, both below and above the positive double layer (<i>left panel</i>), and phase space curves (<i>right panel</i>)	190
7.6	Existence domain (<i>left panel</i>) of ion-acoustic solitons, and soliton amplitudes at $M = M_s$ for the values of f encompassing the coexistence region (<i>right panel</i>), for $\tau = 0.1$	190
7.7	Existence domain of ion-acoustic solitons for $\tau = 1/15$, and amplitude variation with f at $M = M_s$	191
7.8	Variation of solitary structure amplitude with f for $\tau = 1/15$ (<i>top panel</i>), and typical Sagdeev potentials around M_{dl} (<i>bottom panel</i>)	193
7.9	Sagdeev potential curves for $\tau = 1/15, f = f_*$ and M around $M = M_{li} = M_{dl}$	194
7.10	Sagdeev potential curves for $\tau = 1/15, f_* < f < f_{p1}$, for Mach numbers very close to M_{li} (<i>left panel</i>), and the behaviour of $\Psi(\phi, M)$ around $\phi = \phi_{li}$ (<i>right panel</i>)	196

7.11 Existence domain of ion-acoustic solitons for $\tau = 1/30$ (*left panel*), and
amplitude variation at $M = M_s$ with f in the coexistence region (*right panel*) 198

7.12 As in Fig. 7.11, for $\tau = 1/100$ 199

List of Tables

2.1	Parameter estimates from Fig. 3 of Schippers <i>et al.</i> [2008], corresponding to radial distances (R) in Saturn's magnetosphere	62
2.2	Range of wavelength, λ (m), and frequency, f (kHz), of the EPW and EAW modes	64
3.1	Double layer conditions arising from Eq. (3.15)	81
3.2	Behaviour of $\Psi'(\phi)$ for both $\phi < 0$ and $\phi > 0$	82
4.1	Coefficients, c_j/f in Eq. (4.21) for some values of κ	101
4.2	Upper limits of f for different values of z and spectral indices, κ	116
4.3	Soliton amplitude, ϕ_m for $f = 0.7$ and $M = 1.75$, with Maxwellian electrons	123
4.4	Maximum potential amplitudes, $\phi_{li1} = (M_s^2 - \sqrt{3\sigma})^2/2$ and $\phi_{ld} = M_s^2/2z$ at $f = f_p$ and f_n , respectively, for the parameters in Fig. 4.10	127
7.1	Roots of $\Psi(\phi, M)$ for values of M close to M_{li}	196

In this chapter we discuss the general aspects of kappa distributions, their characteristics and how they have been used in the analysis of observational data from space satellites and laboratory experimental data.

Since most of the work discussed in this thesis is linked to nonlinear solitary waves or structures (solitons and double layers) that exist in a number of plasma models, including dusty plasmas, in this chapter we also highlight properties of dust particles or dust grains and general characteristics of dusty plasmas. In addition, we briefly describe solitons and double layers, including the theoretical approaches to modelling these solitary structures.

1.1 Aspects of Kappa Distributions

1.1.1 Introduction

Kappa distributions were first introduced by Olbert [1968] and co-workers when they were analyzing the isotropic background currents measured in the Earth's magnetosheath by the M.I.T detector on IMP-1. Around the same time, based on observations of electrons of energy in the range (125 eV to ~ 2 keV), with OGO 1 satellite, and (40 eV to ~ 2 keV), with OGO 3, Vasyliunas [1968] used the same distribution to fit the low-energy electron population in the Earth's magnetosphere. In the analysis of Olbert [1968] and coworkers,

they assumed that the electron speed distribution in the satellite frame of reference is of the form [Olbert, 1968]:

$$f_e v^2 dv = \text{constant} \frac{v^2 dv}{\left(1 + \frac{v^2}{\kappa w_0^2}\right)^{(\kappa+1)}}, \quad (1.1)$$

where v is the actual speed, w_0 is the most probable speed of the electrons, and κ is a ‘free’ parameter whose value is a measure of the departure of the distribution from its Maxwellian character (with $\kappa \rightarrow \infty$ leading to the Maxwellian distribution). This distribution provides a good fit to those that are commonly observed, being Maxwellian-like at low speeds and obeying a power-law form at high speeds.

Following the empirical formula in Eq. (1.1), the isotropic (3-D) kappa velocity distribution of particles of mass m is written in the form [Vasyliunas, 1968; Marsch and Livi, 1985; Summers and Thorne, 1991; Kivelson and Russell, 1995]

$$F_\kappa(v) = A_\kappa \left[1 + \frac{v^2}{\kappa \theta^2}\right]^{-(\kappa+1)}, \quad (1.2)$$

where $v^2 = v_x^2 + v_y^2 + v_z^2$; A_κ is a normalization parameter, θ is an “effective or characteristic thermal speed” parameter, that is, the most probable speed [Vasyliunas, 1968], and κ is a spectral index, which is a free parameter. The parameters A_κ and θ are obtained self-consistently from the lowest even moments [Podesta, 2005; Hellberg *et al.*, 2009] of the distribution function in (1.2).

1.1.2 Kappa Distributions: Velocity Moments and the Most Probable Speed

The velocity moments of the kappa distribution are given by [Podesta, 2005]

$$\begin{aligned} \langle v^n \rangle &= 4\pi \int_0^\infty v^{(n+2)} F_\kappa(v) dv = 4\pi A_\kappa \int_0^\infty v^{(n+2)} \left(1 + \frac{v^2}{\kappa \theta^2}\right)^{-(\kappa+1)} dv \\ &= 2\pi A_\kappa (\kappa \theta^2)^{(n+3)/2} B[(n+3)/2, \kappa - (n+1)/2] \\ &= \frac{2(\kappa \theta^2)^{n/2} \Gamma\left(\frac{n+3}{2}\right) \Gamma\left(\kappa - \frac{n+1}{2}\right)}{\sqrt{\pi} \Gamma(\kappa - 1/2)} \end{aligned}$$

where $\Gamma(a)$ and $B(a, b)$ are the usual gamma and beta functions, respectively. For arbitrary real values of κ and $n \geq 0$, the integral is finite for $n < (2\kappa - 1)$, that is, $\kappa > (n+1)/2$.

The expression for A_κ is obtained from the zeroth moment of velocity, that is,

$$\begin{aligned} N_0 = \langle v^0 \rangle &= 4\pi \int_0^\infty v^2 F_\kappa(v) dv \\ &= \pi A_\kappa (\kappa \theta^2)^{3/2} \frac{\Gamma(\kappa - 1/2)}{\Gamma(\kappa + 1)}, \quad \text{giving} \\ A_\kappa &= \frac{N_0}{(\pi \kappa \theta^2)^{3/2}} \frac{\Gamma(\kappa + 1)}{\Gamma(\kappa - 1/2)}. \end{aligned} \quad (1.3)$$

In the normalization parameter expression (1.3), N_0 is the unperturbed equilibrium density, given by $N_0 = \langle v^0 \rangle$, the zeroth moment of the distribution, and Γ is the usual gamma function, $\Gamma(a) = \int_0^\infty t^{a-1} e^{-t} dt$;

Also, for $n = 2$, the second moment of velocity gives $\langle v^2 \rangle = 3\kappa\theta^2/(2\kappa - 3)$ or $\theta^2 = \langle v^2 \rangle (2\kappa - 3)/3\kappa$. Using the energy relation $m\langle v^2 \rangle/2 = 3K_B T/2$, where K_B is the Boltzmann constant, and T is the characteristic kinetic temperature, that is, the temperature of the equivalent Maxwellian distribution [Podesta, 2005; Hellberg *et al.*, 2009; Livadiotis and McComas, 2009] with the same average kinetic energy $m\langle v^2 \rangle/2$ per particle, we obtain $\langle v^2 \rangle = 3K_B T/m$. Therefore the most probable speed, θ , is related to the thermal speed of the particle species [Goldston and Rutherford, 1995; Shukla and Mamun, 2002], $v_{th} = (K_B T/m)^{1/2}$, by

$$\theta^2 = v_{th}^2 \frac{(2\kappa - 3)}{\kappa} = v_{mp}^2 \frac{(\kappa - 3/2)}{\kappa}, \quad (1.4)$$

where $v_{mp} = \sqrt{2} v_{th}$ is the most probable speed for a Maxwellian velocity distribution [Kivelson and Russell, 1995, p.38]. However, we point out that in some textbooks [Swanson, 2003, p.86], the most probable speed is sometimes referred to as the thermal speed. The expression in Eq. (1.4) shows clearly that the characteristic thermal speed θ is κ dependent, and reduces to the thermal speed v_{mp} when $\kappa \rightarrow \infty$.

The spectral index κ is a measure of the slope of the energy spectrum of the superthermal particles ($v^2 \gg \kappa\theta^2$) forming the tail of the velocity distribution function. The kappa distribution thus approximates a family of ‘‘power law distributions’’ $F_\kappa(v) \propto v^{-2(\kappa+1)}$ for $v \gg \theta$. The smaller the value of κ the more superthermal particles in the tail of the distribution function and the harder the energy spectrum. That is, low values of κ represent a more enhanced and ‘‘hard’’ spectrum (strong non-Maxwellian tail with more superthermal particles in the tail of the distribution function), resulting in an enhanced velocity distri-

bution at low speeds, a depressed distribution that is Maxwellian-like at medium speeds and an enhanced power law tail at high speeds (see Fig. 1.1). As already mentioned, when $\kappa \rightarrow \infty$ the Maxwellian distribution function,

$$F_\infty(v) = N_0 \left(\frac{m}{2\pi K_B T} \right)^{3/2} \exp \left(\frac{-mv^2}{K_B T} \right), \quad (1.5)$$

is recovered. The features described above are shown in Fig. 1.1, where we have plotted the normalized distribution (1.2) as a function of the normalized velocity. In particular, the figure shows that kappa distributions have higher and narrower peaks, and broader base tails, than the Maxwellian distributions [Hellberg *et al.*, 2009]. In addition, very large values of κ approximate the Maxwellian distribution. Note that the expression for the

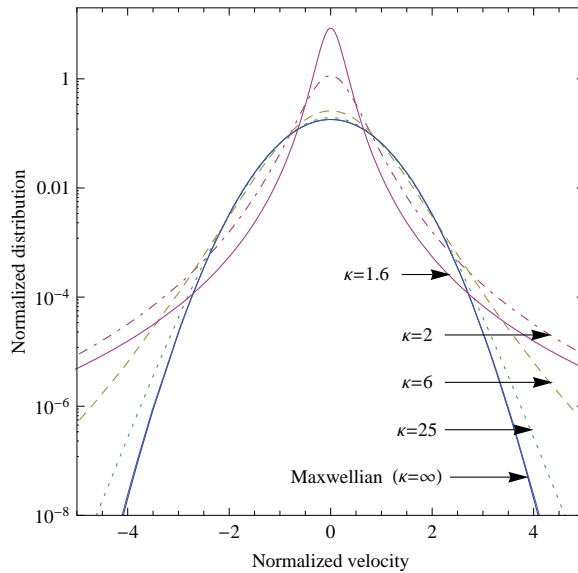


Figure 1.1: Comparison of generalized Lorentzian distributions for the spectral index $\kappa = 1.6$, and 2, 6, 25 and $\kappa = \infty$ (the corresponding Maxwellian distribution), based on Fig. 1 of Summers and Thorne [1991]

characteristic velocity θ , (1.4), is only valid for $\kappa > 3/2$, and thus in the application of the physical quantities derived from Eq. (1.2), like density, we shall use κ values that exceed 1.5. The origin of this constraint comes from the requirement that $\langle v^2 \rangle = 3\kappa\theta^2/(2\kappa - 3)$ does not diverge.

The 1-D kappa distribution is obtained from Eq. (1.2) by integrating over two velocity-

space coordinates, giving [Summers and Thorne, 1991]

$$F_{1\kappa}(v) = \frac{N_0}{(\pi\kappa\theta^2)^{1/2}} \frac{\Gamma(\kappa)}{\Gamma(\kappa - 1/2)} \left(1 + \frac{v^2}{\kappa\theta^2}\right)^{-\kappa}, \quad (1.6)$$

where, here, v is a signed velocity component.

1.1.3 Kappa Distributions: Application to Plasma Experiments and Space Plasma Observations

Kappa distributions have been used by a number of authors [Summers and Thorne, 1991; Mace and Hellberg, 1993; Mace and Hellberg, 1995; Hellberg and Mace, 2002; Podesta, 2005; Mace and Hellberg, 2009; Mace and Sydora, 2010] in studying the effect of Landau damping on various plasma modes. Summers and Thorne [1991] introduced the modified plasma dispersion function $Z_{\kappa}^*(\xi)$ analogous to the standard plasma dispersion function, $Z(\xi)$, based on the Maxwellian distribution [Fried and Conte, 1961]. Mace and Hellberg [1995] generalized $Z_{\kappa}^*(\xi)$, lifting the constraint that κ be an integer, and showed its close relationship to the Gauss hypergeometric function.

Kappa distributions are convenient in analyzing and interpreting observational data in space plasmas which show a Maxwellian “core” at low energies and a power-law tail distribution for higher energies. Some examples of its application include the Earth’s magnetospheric plasma sheet [Christon *et al.*, 1988], the solar wind [Pierrard and Lemaire, 1996] and solar corona [Scudder, 1992; Pierrard and Lemaire, 1996], the magnetospheres of Jupiter and Saturn [Krimigis *et al.*, 1983; Sittler *et al.*, 1983; Schippers *et al.*, 2008; Dialynas *et al.*, 2009], and the auroral region [Olsson and Janhunen, 1998].

Based on the observational data from the European satellite Heos 1, Formisano *et al.* [1973] studied plasma properties as a result of the solar wind interactions in the Earth’s magnetosheath. In their work, they described the proton velocity distribution function by a function similar to that used by Vasyliunas [1968], though they called it a “K distribution function”, with the spectral index K (in their case) chosen only from four values: 2, 3, 5, ∞ . In particular, when no upstream waves were detected in the interplanetary region, the Maxwellian distribution function for protons did not clearly fit the positive ion energy spectra observed inside the magnetosheath for higher energies (above 0.9 keV) while with a “K distribution function”, with $K = 2$, there was close agreement with the

experimental data, as illustrated in their Fig. 2.

In the early 1990s, Scudder [1992] proposed that the high coronal temperature is a consequence of the “velocity filtration effect” when he assumed a non-Maxwellian velocity distribution in the chromosphere (see also Pierrard and Lemaire [1996]; Maksimovic *et al.* [1997]; Shizgal [2007]). With typical κ values ranging from 2.5 to 7, Scudder [1992] found that the plasma temperature increased from 10^3 K at the altitude of the chromosphere up to $(1 - 2) \times 10^6$ K in the solar corona without additional heat deposition or dissipation of wave energy in the solar corona [Pierrard and Lemaire, 1996]. The “velocity filtration effect” was also found to apply to the topside ionopause [Pierrard and Lemaire, 1996] to explain the increase of the plasma temperature as a function of altitude in the outer plasmasphere. With $\kappa = 3 - 5$, temperatures in the outer plasmasphere increased up to values of $(10 - 20) \times 10^3$ K which are comparable to those measured with the satellites at high altitudes (see Pierrard and Lemaire [1996]).

Results from the Voyager 1 and 2 spacecraft [Krimigis *et al.*, 1983], during their encounters with the magnetosphere of Saturn, indicated that the typical energy spectrum of the ions (assumed protons) is like a Maxwellian at low energies (≤ 200 keV) and a power law at high energies (≥ 200 keV). Krimigis *et al.* [1983] used κ distributions to fit ion spectral observations in the magnetosphere of Saturn, with typical values of κ in the range 6 – 8 and thermal energy $K_B T$ in the range ~ 16 keV to ~ 28 keV matching the observations extremely well in general, though with a few exceptions.

In analyzing the field-aligned conductance values, Olsson and Janhunen [1998] used the Freja electron data to compare the Maxwellian and kappa distribution fits of low-orbiting satellite electron flux spectra in the auroral region. Kappa fits with $\kappa \simeq 6$ (κ in the range 4-7) gave better fits to the observed distribution, though the difference in conductance values was not large.

More recent measurements of Saturn’s magnetosphere from the Cassini-Huygens satellite [Schippers *et al.*, 2008] have shown that the electron distribution is very well fitted by the sum of two kappa distributions, the hot (superthermal) component having a much lower density than the bulk (‘thermal’ component). These bi-kappa¹ fits were observed over a wide range of the magnetosphere, the measurements encompassing the range from 5.4 to

¹Bi-kappa is used in this thesis to refer to the sum of two components, each being kappa-distributed

18 R_S (Saturn radii). The bulk component has a very hard spectrum, with typical kappa values ≤ 2 , while the minority hot component (which at 9 R_S makes up less than 10% of the electrons) has $\kappa \sim 4$. A typical value for the bulk component is $\kappa \simeq 2$ throughout most of the magnetosphere, apart from the region $R < 7 R_S$ (where $2 < \kappa_{\text{bulk}} < 8$, increasing rapidly for decreasing R), whereas the hot component has a highly variable value of κ , lying between 3 and 9.

1.1.4 Modified Forms of Kappa Distributions and other Non-Maxwellian Distributions

Since the empirical formula of Olbert [1968] and Vasyliunas [1968], modifications to Kappa distributions have been introduced and applied in the analysis of observation data from satellites.

One such form is the distribution function $f_0(v)$ of a test particle in the presence of radiation fields of nonequilibrium photons, introduced by Hasegawa *et al.* [1985]. This takes the form

$$f_0(v) = A \left(1 + \frac{v^2}{2\kappa v_{te}^2} \right)^{-\kappa}, \quad (1.7)$$

where, v_{te} is the thermal velocity, and with the normalization $\int_0^\infty f_0(v) 4\pi v^2 dv = 1$,

$$A = \frac{2\kappa - 3}{4\sqrt{2}(\pi\kappa)^{3/2}v_{Te}^3} \frac{\Gamma(\kappa)}{\Gamma(\kappa - 1/2)}.$$

Equation (1.7) has considerable resemblance to the one-dimensional standard kappa distribution function in Eq. (1.6) used to fit particle data in space plasmas [Hasegawa *et al.*, 1985], although it is expressed in terms of the thermal velocity, and not the generalized most probable speed $\theta = \theta(\kappa, v_{Te})$.

Apart from kappa distributions, the Tsallis distribution [Tsallis, 1988, 1995], that is characterized by a Tsallis parameter q (which is closely related to κ), has been urged to be an alternative model for non-Maxwellian distributions. The Tsallis distribution, denoted p is a probability distribution given by [Tsallis, 1995]

$$p_q(x) = \frac{1}{Z_q} [1 - (1 - q)\beta x^2]^{1/(q-1)}, \quad (1.8)$$

where $Z_q = \int [1 - (1 - q)\beta x^2]^{1/(q-1)} dx$, and β is defined as the Lagrange parameter associated with the q -expectation $\langle x^2 \rangle_q$ [in (1.11) below]. The distribution in (1.8) extremizes the Tsallis entropy $S_q(p)$ defined by [Tsallis, 1988, 1995]

$$S_q(p) = \frac{K_B}{q-1} \left(1 - \int [p(x)]^q dx \right), \quad (1.9)$$

with x a dimensionless parameter. Thus, the Tsallis entropy is a generalization of the Boltzmann-Gibbs entropy, since it recovers the Boltzmann-Gibbs Shannon form,

$S_1(p) = -K_B \sum_i p_i \ln(p_i)$ in the limit $q \rightarrow 1$. In addition, the Tsallis distribution (1.8) extremizes the generalized Tsallis entropy (1.9) subject to the constraints [Tsallis, 1995]

$$\int p(x) dx = 1, \quad (1.10)$$

and

$$\langle x^2 \rangle_q = \int x^2 [p(x)]^q dx = \sigma^2 < \infty, \quad (1.11)$$

with $q < 3$, in order to satisfy (1.10) [Tsallis, 1995].

Another approach, introduced by Leubner [2002], makes use of the Tsallis q -statistics [Tsallis, 1999]. Using the generalized entropy from the Tsallis q -statistics, Leubner [2002] showed that with the transformation $\kappa = 1/(1 - q)$, where q is a parameter quantifying the degree of non-extensivity, and κ is a spectral index of the kappa distribution, the one-dimensional and isotropic three-dimensional equilibrium velocity space distributions, in kappa notation, can be written as

$$F_{L_1}(v) = \frac{N}{v_{th}} \frac{1}{\sqrt{\kappa}} \frac{\Gamma(\kappa)}{\Gamma(\kappa - 1/2)} \left(1 + \frac{1}{\kappa} \frac{v^2}{v_{th}^2} \right)^{-\kappa} \quad \text{and} \quad (1.12)$$

$$F_{L_3}(v) = \frac{N}{\pi^{3/2} v_{th}^3} \frac{1}{\kappa^{3/2}} \frac{\Gamma(\kappa)}{\Gamma(\kappa - 3/2)} \left(1 + \frac{1}{\kappa} \frac{v^2}{v_{th}^2} \right)^{-\kappa} \quad \text{for } 3/2 < \kappa \leq \infty, \quad (1.13)$$

respectively, where here $v_{th} = (2K_B T/m)^{1/2}$ is the thermal velocity [Leubner, 2004], and T and m are the temperature and mass respectively. Unusually, Leubner [2004] also considers $\kappa < 0$. Note here that, the ‘‘thermal velocity’’, V_{th} takes the same form as the most probable speed for a Maxwellian distribution. The notation L_1 and L_3 refers to the one- and three-dimensional forms of Leubner [2002], with the latter also called the ‘‘halo’’ distribution

(see Eq. (6) of Leubner [2004]). Distributions of the form of Eq. (1.13) were used in the analysis of results from the HELIOS observations of the double humped (core-halo) solar wind proton velocity distributions [Leubner, 2004] between 0.3 and 1 a.u. Apart from the fact that Eqs. (1.12) and (1.13) are expressed in terms of the thermal velocity v_{th} (independent of κ) and not in terms of the most probable speed $\theta = \theta(\kappa, v_{th})$, (1.12) has considerable resemblance to Eq. (1.6) for the one-dimensional kappa distribution. However, for the three-dimensional case, there is a huge difference (in both the velocity and power-law terms).

In the same work of Leubner [2002] (see also Leubner [2004]), the author indicates that a conventional isotropic three-dimensional κ -distribution is represented by

$$f_L(v) = \frac{N}{\pi^{3/2} v_{th}^3} \frac{1}{\kappa^{3/2}} \frac{\Gamma(\kappa + 1)}{\Gamma(\kappa - 1/2)} \left(1 + \frac{1}{\kappa} \frac{v^2}{v_{th}^2} \right)^{-(\kappa+1)}. \quad (1.14)$$

Equation (1.14) looks similar to (1.2), the only difference here being that the distribution is expressed in terms of the ‘‘thermal velocity’’ v_{th} , and not the most probable or characteristic speed $\theta = \theta(\kappa, v_{th})$. It is then surprising that one gets the generalized form of the ‘‘thermal speed’’ $\Theta = v_{th}[(\kappa/(\kappa - 3/2))]^{1/2}$ from the second moments of the distribution function in (1.14), as Leubner [2004] puts it. Considering Eq. (1.14), the second moments of the distribution function gives

$$\langle v^2 \rangle = \frac{3}{2} \left(\frac{\kappa}{\kappa - 3/2} \right) v_{th}^2 \quad (1.15)$$

If we use $\langle v^2 \rangle = 3K_B T/m = 3v_{th}^2/2$ where here, $v_{th} = (2K_B T/m)^{1/2}$, it then follows that Eq. (1.15) can hold if and only if $\kappa \rightarrow \infty$. In other words, the expression $\Theta = v_{th}[(\kappa/(\kappa - 3/2))]^{1/2}$ as the generalized thermal velocity in the work of Leubner [2004] seems unclear.

Another form of kappa distribution is that introduced by Fu and Hau [2005] and Hau and Fu [2007], which was first applied in obtaining the Vlasov-Maxwell equilibrium solutions for the Harris sheet magnetic field. This distribution function² takes the form

$$f_H^\kappa(v) = \frac{N}{2\pi(\kappa v_\kappa^2)^{3/2}} \frac{\Gamma(\kappa + 1)}{\Gamma(\kappa - 1/2)\Gamma(3/2)} \left(1 + \frac{1}{\kappa} \frac{v^2}{v_\kappa^2} \right)^{-(\kappa+1)}, \quad (1.16)$$

²The subscript ‘H’ refers to the Hau formalism

which after using the Gamma function relation $\Gamma(\alpha + 1) = \alpha\Gamma(\alpha)$, and $\Gamma(1/2) = \pi^{1/2}$, reduces to

$$f_H^\kappa(v) = \frac{N}{(\pi\kappa v_\kappa^2)^{3/2}} \frac{\Gamma(\kappa + 1)}{\Gamma(\kappa - 1/2)} \left(1 + \frac{1}{\kappa} \frac{v^2}{v_\kappa^2}\right)^{-(\kappa+1)}. \quad (1.17)$$

In Equations (1.16) and (1.17), v_κ is defined as the thermal speed that is related to the characteristic temperature T_κ , and is given by

$$v_\kappa = \left\{ \left(\frac{2\kappa - 3}{\kappa} \right) \left(\frac{K_B T_\kappa}{m} \right) \right\}^{1/2}, \quad (1.18)$$

where T_κ is also related to the temperature T in the Maxwellian distribution, by [Fu and Hau, 2005]

$$T_\kappa = \left(\frac{\kappa - 3/2}{\kappa} \right) T \quad (1.19)$$

and [Hau and Fu, 2007]

$$T_\kappa = \left(\frac{\kappa}{\kappa - 3/2} \right) T. \quad (1.20)$$

However, we shall use Eq. (1.20) in the discussion, as (1.19) seems to have a typographical error. Otherwise, it does not make sense in that form. A simple inspection of Eqs. (1.18) and (1.20) shows that actually

$$v_\kappa = \left(\frac{2K_B T}{m} \right)^{1/2} = v_{th}. \quad (1.21)$$

In other words, Eq. (1.16) [Fu and Hau, 2005; Hau and Fu, 2007] is simply the same as Eq. (1.14), the ‘‘generalized conventional isotropic three-dimensional kappa distribution function’’ of Leubner [Leubner, 2002, 2004], but differs from Eq. (1.13) that was derived from the q -entropy statistics. Both Eqs. (1.16) and (1.14) do not give the appropriate most probable speed $\theta = \theta(\kappa, v_{th})$ that is defined, by appealing to equipartition of energy, by $\theta = v_{th}[(\kappa - 3/2)/\kappa]^{1/2}$. We point out that this approach (of Hau and Fu [2007]) has been criticized [Hellberg *et al.*, 2009]. Generally, all the different forms of κ distribution functions discussed in this Chapter have two common characteristics: (i) they all possess power law behaviour and (ii) in the limit $\kappa \rightarrow \infty$ one recovers the Maxwellian distribution function of the form of Eq. (1.5).

The relationship of the kappa distributions to the Tsallis statistical mechanics was

recently given by Livadiotis and McComas [2009], where they used the transformation $\kappa = 1/(q - 1)$ as opposed to $\kappa = 1/(1 - q)$ used by Leubner [2002]. In Tsallis statistical mechanics, there are two probability distributions that play a role in the theory: the canonical and escort probability distributions which are, respectively, given by [Livadiotis and McComas, 2009]

$$p(\epsilon; T_q; q) \sim \exp_q \left[-\frac{1}{I_q(3/2)} \frac{\epsilon}{K_B T_q} \right] \quad \text{and} \quad (1.22)$$

$$P(\epsilon; T_q; q) \sim p(\epsilon; T_q; q)^q \sim \exp_q \left[-\frac{1}{I_q(3/2)} \frac{\epsilon}{K_B T_q} \right]^q, \quad (1.23)$$

where $\epsilon = \mu u^2/2$ is the kinetic energy (μ and u are the mass and velocity, respectively), T_q is the physical temperature [Livadiotis and McComas, 2009] (see below), and q is the q index; $\exp_q(x) = [1 + (1 - q)x]^{1/(1-q)}$ is the q -deformed exponential, and $I_q(u) = 1 + (1 - q)u$ is the q -deformed ‘‘unit function’’. From (1.23), the escort probability (or escort expectation), denoted $\langle \cdot \rangle_q$, of a function of energy ϵ is given by [Livadiotis and McComas, 2009]

$$\langle f(\epsilon) \rangle_q = \frac{\int_0^\infty P(\epsilon; T_q; q) f(\epsilon) g_E(\epsilon) d\epsilon}{\int_0^\infty P(\epsilon; T_q; q) g_E(\epsilon) d\epsilon}, \quad (1.24)$$

where $g_E(\epsilon) = 2\pi(2/\mu)^{3/2} \epsilon^{1/2}$ is the density of energy states of the system. Using the escort expectation, Livadiotis and McComas [2009] showed that the internal energy U_q is estimated as the escort expectation value $\langle \epsilon \rangle_q$, that is,

$$U_q = \langle \epsilon \rangle_q = \frac{3}{2} K_B T_q, \quad (1.25)$$

where T_q is the physical temperature, not the thermodynamic temperature. Thus, Livadiotis and McComas [2009] argued that working with escort probability distributions $P(\epsilon; T_q; q)$ (in the Tsallis statistical mechanics) and not the ordinary (or canonical) probability distributions $p(\epsilon; T_q; q)$, the kinetic temperature T_K , defined by the internal energy $U_q = 3K_B T_K/2$, coincides with the physical temperature T_q in the Tsallis formalism. They further argued that since T_K is identical to T_q , the appropriate temperature in Tsallis statistics is the kinetic temperature, and not the thermodynamic temperature, that is, the appropriate definition of temperature for out-of-equilibrium systems. In other words, the system is characterized by the same internal energy (mean kinetic energy) or kinetic

temperature that is independent of the specific stationary states. To put it differently, the kinetic temperature is independent of the value of the q index (Tsallis statistics) or κ index (kappa distributions), see also Hellberg *et al.* [2009].

Apart from kappa distributions, another form of non-thermal or non-Maxwellian distribution function that is used in theoretical papers is the so-called Cairns distribution. This distribution was introduced by Cairns *et al.* [1995] as an *ad hoc* model for non-thermal velocity distributions, and takes the form

$$F_j(v) = \frac{N_{j0}}{(3\alpha + 1)} \frac{1}{\sqrt{2\pi} v_{tj}^2} \left(1 + \frac{\alpha v^4}{v_{tj}^4} \right) \exp \left(-\frac{v^2}{2v_{tj}^2} \right), \quad (1.26)$$

where α is the non-thermal parameter, N_{j0} the equilibrium number density and v_{tj} the thermal velocity of the species j . Cairns *et al.* [1995] used this distribution in explaining the electrostatic structures with density depletions observed by the Freja satellite [Dovner *et al.*, 1994], and showed that the presence of a population of energetic electrons changes the properties of ion sound waves. The distribution function (1.26) reduces to the Maxwellian distribution form when $\alpha = 0$. It is convenient to introduce the parameter $\beta = 4\alpha/(1+3\alpha)$. The normalized Cairns distribution function of (1.26) is shown in Fig. 1.2 for different values of β , and we note that for $\beta = 0$ it reduces to the Maxwellian distribution function. The figure also shows that for $\beta \geq 1/2$ (or $\alpha \geq 0.2$) the distribution function develops “wings” at high velocities, becoming multi-peaked there. In particular, beyond $\beta = 4/7$ (or $\alpha = 0.25$) [Verheest, 2010a], the distribution is triple humped, and hence could be unstable, leading to beam-instabilities. For such high values of β , the Cairns distribution function may not be good for physical applications. In other words, the Cairns distribution is appropriate for a narrow range of parameters α , or β , that produce only small deviations from the Maxwellian distribution function. As an application, a plasma model with particle species that follow the Cairns distribution given in Eq. (1.26) is discussed in Chap. 6. Since the introduction of the “Cairns non-thermal’ velocity distribution, it has not been applied extensively in the analysis of space plasma observations from satellites. However, a number of authors have used it in theoretical studies on solitary structures, for instance, Mamun [1997], Verheest and Pillay [2008a,b], Pajouh and Abbasi [2008], and Verheest [2010a], to mention a few.

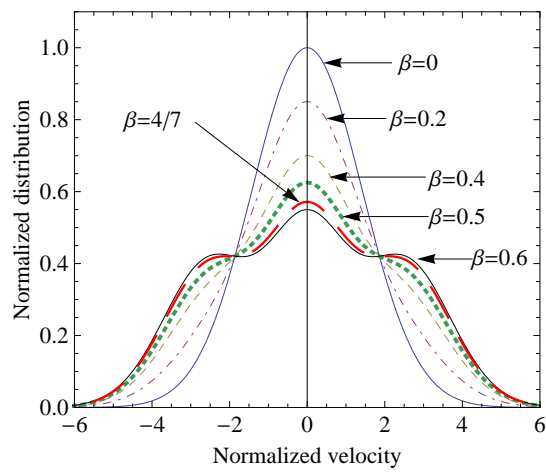


Figure 1.2: Figure showing the normalized form of Eq. (1.26) for different values of β . Note that for β values above 0.5 the distribution develops wings at high velocities, and may not be good for physical applications.

1.2 Dusty Plasmas

1.2.1 Dust and Dusty Plasmas

A dusty plasma can be defined as a collection of micro-sized electrically charged dust particles immersed in a plasma consisting of electrons, ions and neutrals [Goertz, 1989; Shukla, 1996, 2000a; Shukla and Mamun, 2002; Verheest and Cattaert, 2004].

Dust particles are very small in size, of macroscopic dimensions compared to atoms and ionized nuclei [Verheest, 2000, p. 2]). Their sizes range from nano-meters to millimeters [Shukla and Mamun, 2002, p. 2] and they have large masses. Different authors give different dust mass ranges, for example, [Verheest, 2000, p. 6] gives a range of $10^6 - 10^{18}$ times the proton mass (see also references therein) while Shukla and Mamun [2002] quotes the dust mass to be billions times the proton mass; the actual value depends on the environment of existence. Dust particles are often observed to have negative charges several times the electron charge, typically between $10^2 - 10^4 e$, where e is the electronic charge [Shukla, 1996; Verheest, 1999; Mamun and Shukla, 2005], with variations depending on the environment where they occur. On the other hand, positively charged dust particles do also occur in space, depending on the charging process in the surrounding environment. The large values of mass and charge for dust particles suggest that dust particles have significantly higher mass-to-charge ratio ($m_d/Z_d e$) than that of ions or electrons. As a result, the characteristic dust frequencies (for example, the dust plasma frequency $\omega_{pd} \propto (Z_d/m_d)^{1/2}$) are very small [Verheest, 2000, p. 7] compared to those of electrons and ions.

Due to the presence of electrons and ions in space and the ubiquitous dust, dusty plasmas exist naturally in numerous space and astrophysical environments. For example, dust is believed to occur in planetary rings, cometary tails and comae, interstellar and circumstellar clouds, Earth's mesosphere and ionosphere in the form of noctilucent clouds, the rings of Saturn (radial spokes in the B ring; braided structures in the F ring; the D ring and the narrow ringlet in the A ring near the middle of the Encke gap), and the "gossamer" ring of Jupiter (see for example, Mendis and Rosenberg [1994]; [Verheest, 2000, Chap. 3] and [Shukla and Mamun, 2002, Chap. 1], and references therein).

In laboratory experiments, dust particles are usually found in many low-temperature laboratory devices and industrial processes, such as plasma processing reactors [Shukla and

Mamun, 2002, p. 18] and etching [Verheest, 2000, p. 34], dc and rf discharges where dust particles are more abundant in electronegative gas mixtures, fusion plasma devices such as tokamaks, stellarators [Shukla and Mamun, 2002, p. 20] where the dust particles are generated as impurities through processes like desorption, arcing, sputtering, evaporation, etc.

Returning to the occurrence of dust particles in space and astrophysical environments, we list briefly some examples:

Planetary rings: In planetary rings, information obtained from Voyager 1 and 2 space missions has shown that most rings of the outer giant planets such as Jupiter, Saturn, Uranus and Neptune are made of micron- to sub-micron-sized dust particles (see [Verheest, 2000, pp. 46–56], [Shukla and Mamun, 2002, pp. 13–16], Postberg *et al.* [2006], and references therein). In particular:

(i) dust particles have been found by the Voyager 2 spacecraft to exist in a very tenuous ring [Mendis and Rosenberg, 1994], the gossamer ring of Jupiter which extends outward from the brighter thin ring to the vicinity of the satellite Thebes ($\sim 3.11R_J$), R_J being the radius of Jupiter.

(ii) The Ulysses mission to Jupiter also detected high speed streams of dust grains during its distant Jovian encounter (see Mendis and Rosenberg [1994] and references therein).

(iii) The interesting features observed in Saturn’s ring system by both Voyager 1 and 2, the nearly radial spokes [Shukla and Mamun, 2002], provided the impetus for the study of dust-plasma interactions in planetary magnetospheres.

(iv) Observations of dust in the vicinity of the moon, Rhea, whose orbital radius is approximately $9 R_s$ were reported by the Cassini team [Jones *et al.*, 2008].

Comets: Comets such as P/Halley [McDonnell *et al.*, 1987; Thomas and Keller, 1991], observed by the Giotto and Vega spacecraft, Hale-Bopp, and others have been found to have cometary dust particles (see [Verheest, 2000, pp. 58–62]; [Shukla and Mamun, 2002, pp. 9–12], and references therein). For instance, data from the Vega and Giotto spacecraft showed that the dust size distribution is well fitted by a power law distribution, $n(r) = r^{-\beta}$, with $\beta \simeq 3.3$ for Vega and 4.1 for Giotto [Verheest, 2000; Shukla and Mamun, 2002], and r being the heliocentric distance.

Earth's Atmosphere: Naturally occurring dusty plasmas have been reported in the polar mesosphere at altitudes of 80 and 90 km [Verheest, 2000, p. 43], characterized by noctilucent clouds, polar mesospheric echoes, and strong radar backscatter, observed at frequencies ranging from 50 MHz to 1.3 GHz [Verheest, 2000; Shukla and Mamun, 2002]. Large amounts of charged dust with average sizes of about $0.1\mu\text{m}$ at densities of several 10^9m^{-3} were detected during the polar mesospheric summer echoes and noctilucent clouds conditions. Both positively and negatively charged dust particles have been reported at difference altitudes in the polar mesosphere [Verheest, 2000, p. 43].

The co-existence of negative and positive dust was also found in the tropical mesopause [Gelinis *et al.*, 1998], where a thick (5 km) layer of positively charged dust was reported at an altitude of above 90 km, near both the sporadic sodium layer and sporadic E layer all of which occurred just above 90 km [Havnes, 2002]. On the other hand, negatively charged dust was reported near the bottom of the layer, covering a small part compared with the positively charged dust layer [Gelinis *et al.*, 1998; Havnes, 2002]. The presence of positive dust in the mesopause region was attributed to the difference in dust material composition from that of pure water ice [Havnes, 2002] which lowers the work function of the dust particles, and as a result, dust charging by photoelectric emission dominates. In plasma environments where both positively- and negatively charged dust particles co-exist such as comets [Horányi, 2002] and the tropical mesopause [Gelinis *et al.*, 1998; Havnes, 2002], as examples, the positively charged dust particles are small in size but numerous [Gelinis *et al.*, 1998; Shukla and Mamun, 2002] while the negatively charged dust grains are larger, enhancing coagulation [Goertz, 1989; Havnes, 2002] of dust particles in such scenarios.

1.2.2 Fundamental Length Scales

In the differentiation of dusty plasmas from other plasma systems, three essential distinct characteristic length parameters are used. These are: the *dust grain radius* (r_d), the *average inter-grain distance* a_d , and the *plasma Debye length*, λ_D . The inter-grain distance a_d is defined by $n_{d0} = 4\pi/3a_d^3$, where n_{d0} is the unperturbed dust density, though in some books [Verheest, 2000, p. 5], the factor $4\pi/3$ is neglected. The Debye length λ_D is a measure of the distance over which the electric field effect of a typical individual charged particle is felt by other surrounding charged particles in the plasmas, and is given

by [Shukla, 2000b; Shukla and Mamun, 2002] $\lambda_D^{-2} = \lambda_{De}^{-2} + \lambda_{Di}^{-2}$, where $\lambda_{De}(\lambda_{Di})$ is the electron (ion) Debye length. Since the electrons have high mobility compared to the ions, Debye shielding is mainly due to the electrons, and the Debye length expression approximates to $\lambda_D \approx \lambda_{De} = (\epsilon_0 K_B T_e / n_{e0} e^2)^{1/2}$, where T_e and n_{e0} are the electron temperature and equilibrium density, respectively. Usually the dust grain radius is much smaller than the Debye length, *i.e.*, $r_d \ll \lambda_D$, and is the smallest of the three lengths [Verheest, 2000, p. 5]. When $r_d \ll \lambda_D < a_d$, the plasma consists of isolated screened dust grains, and the system is termed “*dust-in-plasma*” [Verheest, 2000; Shukla and Mamun, 2002]. In this case the local plasma inhomogeneities need to be taken account of [Shukla and Mamun, 2002; Horányi, 2002], and the charged dust particles can be treated from a particle dynamics point of view [Shukla, 2000b, p. 2]. On the other hand, when $r_d \ll a_d < \lambda_D$, the system is called a “*dusty plasma*”. Here, the dust particles are treated as massive point particle species [Shukla, 1996; Shukla and Mamun, 2002; Horányi, 2002] similar to multiply charged (negative or positive) ions in multi-component plasmas. Therefore the charged dust particles participate in the collective behaviour of the dusty plasma.

Apart from the characteristic length parameters discussed above, other fundamental parameters for plasmas (and dusty plasma in particular) are the *plasma parameter* (some times loosely referred to as the Coulomb coupling parameter) and the *plasma beta*. The latter applies to magnetized plasmas, see for example, [Boyd and Sanderson, 2003, p.83], and will therefore not be discussed here in detail.

Plasma Parameter: In understanding the plasma parameter, we introduce two distance parameters: (i) the average distance between particles, a , given by $a = (4\pi/3n_0)^{1/3}$, where n_0 is the number density (compare with the inter-grain distance a_d), and (ii) the distance of closest approach r_c , defined as the distance at which the Coulomb energy, $U(r, v)$ vanishes, where $U(r, v) = (mv^2/2) - (e^2/4\pi\epsilon_0 r)$ is the energy of a single charged particle in the electric field of a neighbouring particle. Thus $r_c = e^2/(4\pi\epsilon_0 K_B T)$, where we have used $mv^2/2 = K_B T$. The plasma parameter, denoted by g , is a dimensionless parameter [Kivelson and Russell, 1995; Boyd and Sanderson, 2003; Parks, 2004], given by $g = 1/N_d$, where [Parks, 2004, p. 25]

$$N_d = \frac{4\pi}{3} n_0 \lambda_D^3,$$

is the number of particles in a plasma contained in a Debye sphere, and n_0 is the equilibrium number density. Note that in some books the factor $4\pi/3$ is neglected. However, in some textbooks [Miyamoto, 1997], the plasma parameter is simply given by N_d . Using $\lambda_D = (\epsilon_0 K_B T / n_0 e^2)^{1/2}$ and $n_0 = 4\pi/3 a^3$, the expression for N_d can easily be written as

$$N_d = \frac{4\pi (\epsilon_0 K_B T)^{3/2}}{3 e^3 n^{1/2}} = \frac{1}{4\pi\sqrt{3}} \left(\frac{a}{r_c} \right)^{3/2} = \frac{1}{g}.$$

From the expression above, the following is worth mentioning:

(i) When the ratio a/r_c is small, charged particles are continuously dominated by one another's electrostatic influence; their kinetic energies are small compared to the potential energies, and the Debye sphere is sparsely populated (as we have fewer particles), reminiscent of cold and dense plasmas. Such plasmas (with $g \gg 1$) are termed *strongly coupled plasmas* [Miyamoto, 1997; Shukla and Mamun, 2002].

(ii) On the other hand, when the ratio a/r_c is large, electrostatic interactions between individual particles rarely cause any sudden changes in the particle's motion. The plasma consists of a large number of hot and diffuse particles, and Debye screening becomes meaningful. Such plasmas (with $g \ll 1$) are termed *weakly coupled plasmas* [Miyamoto, 1997; Shukla and Mamun, 2002]. The condition $g \ll 1$ is also called the plasma approximation [Parks, 2004], which is taken to be a measure of the collision effects of the plasma particles; smaller g corresponds to fewer collisions, and the plasma becomes collisionless in the limit $g \rightarrow 0$ (valid in space plasma with low densities and high temperatures.)

The Coulomb coupling parameter [denoted Γ , not to be confused with the usual Gamma function used in (1.3)], is defined as the ratio of the Coulomb interaction potential energy to the mean kinetic energy of the plasma particles [Gilbert *et al.*, 1988; Melzer *et al.*, 1994; Fortov *et al.*, 1997; Shukla and Mamun, 2002]. Thus Γ is given by

$$\Gamma = \frac{\langle P.E_{\text{interaction}} \rangle}{\langle K.E \rangle}.$$

As an example, we consider a particle of charge q separated from another by a distance a . The Coulomb potential energy can be given by the Debye screening potential [Parks, 2004] $[q/(4\pi\epsilon_0 a)]\exp(-a/\lambda_D)$ while the kinetic energy is obtained from $K_B T$. Note that

the Debye screening potential reduces to the usual Coulomb potential $q/(4\pi\epsilon_0 a)$ in the limit $a \ll \lambda_D$. The Coulomb coupling parameter then becomes [Melzer *et al.*, 1994; Shukla and Mamun, 2002]

$$\Gamma = \frac{q^2}{(4\pi\epsilon_0 a)} \frac{1}{K_B T} \exp(-a/\lambda_D).$$

In the study of dusty plasmas, the value of Γ determines the possibility of formation of dusty plasma crystals [Shukla and Mamun, 2002] by the process of Wigner crystallization. This occurs for strongly coupled plasmas, with $\Gamma \gg 1$; $\Gamma \ll 1$ correspond to weakly coupled plasmas. Thus “ g ” and “ Γ ” have the same effect. In the determination of the charge on dust particles, Melzer *et al.* [1994] observed a Coulomb crystal lattice with a hexagonal structure in an rf discharge. In their experiment, they also reported that the charged dust particles form regular lattices at $\Gamma \geq \Gamma_c$, with $\Gamma_c = 170$ being the critical coupling parameter for the liquid-solid transition phase [Fortov *et al.*, 1997]. With $\Gamma_c \approx 2$, a transition from the gaseous phase to liquid phase was also predicted [Gilbert *et al.*, 1988; Dubin and O’Neil, 1988] where a liquid-like phase behaviour is exhibited by the plasma for $\Gamma_c > 2$, and a liquid-solid phase transition to a body-centered cubic (bcc) lattice occurred for $\Gamma_c \approx 178$ [Gilbert *et al.*, 1988]. The formation of dusty plasma crystals, consisting of ordered arrangements of micro-sized dust grains (or rods) in low-temperature partially ionized plasmas, was also observed experimentally in a high frequency discharge near the lower electrode in the boundary of the near-cathode regions [Chu and I, 1994; Hayashi and Tachibana, 1994; Melzer *et al.*, 1994; Thomas *et al.*, 1994].

1.2.3 Charging Process of Dust Grains

Dust particles immersed in a plasma can be charged negatively by collecting electrons or positively by emitting electrons, depending on the relative flux of electrons and ions in the system [Gelinias *et al.*, 1998; Shukla and Mamun, 2002]. The elementary processes that lead to the charging of dust grains are quite complex and depend mainly on the environment around the dust grains. Such elementary processes include interaction of dust grains with energetic particles (electrons and ions), and interaction of dust grains with photons [Shukla and Mamun, 2002]. In space, collection of electrons and plasma ions by the dust grains, and photo-ionization [Verheest, 1999] are the most common charging processes.

Negative Charge processes

In a dusty plasma, dust grains may be charged negatively by collection of charges due to thermal ions and electrons [Barkan *et al.*, 1995; Shukla and Mamun, 2002; D'Angelo, 2004], provided the photoelectric effect, secondary emission and other charging processes are negligible. The negative charge results from: (i) the higher temperature, and therefore higher thermal speed [Samarian *et al.*, 2001], and (ii) the higher mobility of the electrons, as compared to that of the ions. Thus the initial ion flux is smaller than the initial electron flux and hence it is mostly the electrons that will hit the grain [Verheest, 2000, p. 15]. As the negative dust builds up on the dust grain, the resulting electric field acts against further electron collection (electron flux decreases) and in favor of ion collection (ion flux increases). Eventually a dynamical equilibrium is reached when the sum of the plasma currents to the grain is zero.

This charging process is common in the normal glow discharge experiments, where the emission processes are insignificant [Samarian *et al.*, 2001], for example, when considering laboratory plasmas of low temperature [D'Angelo, 2004]; neglecting electron emission, the higher mobility of the electrons with respect to the ions results in negatively charged dust.

Positive Charge processes

On the other hand, dust particles can acquire appreciable positive charges by thermionic emission [Shukla, 2000b], emission of photoelectrons due to incident UV radiation, secondary electron emission due to collisions with energetic ions and electrons, and absorption of the plasma ions [Gelinis *et al.*, 1998; Shukla, 2000b; Shukla and Mamun, 2002; D'Angelo, 2004]. In this case, the electron density would be larger than that of the ions.

Thermionic emission: In this process, electrons or ions are thermally emitted from the dust grain surface when the latter is heated to a high temperature [Shukla and Mamun, 2002], leaving the dust grain positively charged. The process may be induced by laser heating, thermal infra-red heating or by hot filaments surrounding the dust grain.

Photoelectron emission: This is more common in space and astrophysical dusty plasma environments where ultraviolet radiation is abundant and results in a positive charging current, making the dust grains positively charged. During the process, photoelectrons are emitted from the dust grain surface when a flux of photons with energy larger than the

photoelectric work function of the dust grain is incident on the dust grain surface [Goertz, 1989; Shukla and Mamun, 2002].

Secondary electron emission: When energetic plasma particles (electrons and ions) are incident on a dust grain surface, they are either backscattered/reflected by the dust grain [Shukla and Mamun, 2002, p. 40] or they pass through the dust grain (through tunnelling, which is important for very small dust grains [Verheest, 2000, p. 22;23]) or releases secondary electrons. During their passage they may lose their energy partially or fully [Shukla and Mamun, 2002, p. 41]. A portion of the lost energy may excite other electrons that in turn may escape from the material, resulting in secondary electrons (emitted electrons). The release of secondary electrons from the dust grain tends to make the grain surface potential, as well as dust charge, positive [Goertz, 1989; Shukla and Mamun, 2002]. In addition, if the dust grain absorbs more of the plasma ions than the electrons, the dust grain charge as well as its surface potential becomes positive [Goertz, 1989; Shukla and Mamun, 2002]. This is because, during absorption, the electrons are attracted while the ions are repelled, thus the grain current carried by the electrons is increased and that carried by the ions is reduced [Goertz, 1989; Shukla and Mamun, 2002].

Absorption of plasma ions: In laboratory plasmas, one way of producing positively charged dust grains is by replacing the plasma electrons with negative ions whose thermal speed is smaller than the thermal speed of the positive ions [D'Angelo, 1995]. Positively charged dust grains can be produced by introducing sufficiently large amounts of SF₆ gas into a potassium (K⁺) plasma in a Q-machine. Using this approach, D'Angelo [2004] was able to experimentally investigate the excitation of dust ion-acoustic and dust acoustic waves in a plasma with positively charged dust. The SF₆ gas has a large affinity for electrons, and thus replaces the electrons with SF₆⁻ ions [D'Angelo, 2004; Kim and Merlino, 2006], taking into account the high mobility of K⁺ ions as compared to SF₆⁻ ions. In a similar method (using a Q-machine operating on potassium ions in which the highly electronegative SF₆ gas is added), Kim and Merlino [2006] experimentally investigated the charging of dust particles in a plasma consisting of positive ions, negative ions and electrons. In their experiment, the transition from negatively charged to positively charged dust required that (i) $\varepsilon = n_e/n_+$, the ratio of the electron density to positive ion density,

be sufficiently small, and (ii) the positive ion mass be smaller than the negative ion mass. In these conditions, increasing the concentration of negative ions in the plasma decreases the magnitude of the negative charge, and eventually a transition to positively charged dust is observed [Kim and Merlino, 2006].

1.2.4 Waves in Dusty Plasmas

The presence of the additional highly charged and massive dust grain species in the plasma modify the properties of the usual plasma waves [Merlino *et al.*, 1997; Shukla, 2000b; Shukla and Mamun, 2002; Hellberg *et al.*, 2006], and also leads to instabilities [Samarian *et al.*, 2001]. Unmagnetized dust plasmas support new frequency modes like the dust acoustic (DA) waves and the dust-modified ion-acoustic (DIA) waves [Merlino *et al.*, 1997; Shukla, 2000b].

The dust acoustic wave, which was first theoretically predicted by Rao *et al.* [1990] and later confirmed experimentally by Barkan *et al.* [1995], is a long-wave length, low frequency oscillation mode [Merlino *et al.*, 1997] with phase velocity that is far below the ion-acoustic velocity. In this mode, the electron and ion pressures provide the restoring force while the massive charged dust grains provide the inertia [Rao *et al.*, 1990; Merlino *et al.*, 1997; Shukla, 2000a,b; Shukla and Mamun, 2003; Hellberg *et al.*, 2006]. Thus the dust particle dynamics play an essential role where the dust behaves as a charged particle plasma species. The phase velocity of the wave is in the range $v_{td} \ll \omega/k \ll v_{ti} < v_{te}$ such that electron and ion Landau dampings are minimal.

On the other hand, the dust ion-acoustic waves, which were first predicted by Shukla and Silin [1992] and confirmed experimentally by Barkan *et al.* [1996], are ordinary fast ion-acoustic waves that are modified by the presence of charged dust. In the presence of negative dust, the phase velocity is higher than that of the usual ion-acoustic wave in an electron-ion plasma, and results in a reduction in the strength of the Landau damping [Merlino *et al.*, 1997; Shukla, 2000b]. The characteristic thermal speeds v_{tj} of electrons and ion in a DIA wave satisfy the criterion $v_{td} < v_{ti} \ll \omega/k \ll v_{te}$, that is, the phase velocity of DIA waves (ω/k) is much smaller than the electron thermal speeds (v_{te}) but much larger than the ion and dust thermal speeds (v_{td}, v_{ti}). In the DIA waves, the ion mass provides the inertia while the inertialess electrons provide the restoring force, with

the dust particles only providing a neutralizing background. Thus the ion and electron dynamics is of paramount importance in the propagation of DIA waves.

These two wave modes (DIA and DA waves) will be discussed in detail in Chapters 3 and 4 in this thesis.

1.3 Solitons and Double Layers

1.3.1 Solitons

These are special types of solitary waves (hump or dip shaped nonlinear waves of permanent profile) [Shukla and Mamun, 2002, p. 195]. They travel at constant speed and maintain a constant waveform, thus preserving their shape (see also [Baluku, 2007]. Solitons arise as a result of the balance between the effects of nonlinearity (leading to steepening) and the effects of dispersion, assuming dissipation effects are negligible.

In Fig. 1.3 we show a typical structure of a soliton, in terms of the electrostatic potential, $\phi(\xi)$, and electric field, $E = -\nabla\phi(\xi)$. The electrostatic potential soliton structure is characterized by a single hump, occurring at the origin, while the electric field structure has two humps (*i.e.*, is bipolar), equidistant from the origin. It is the double hump structures in E that are normally observed in space data.

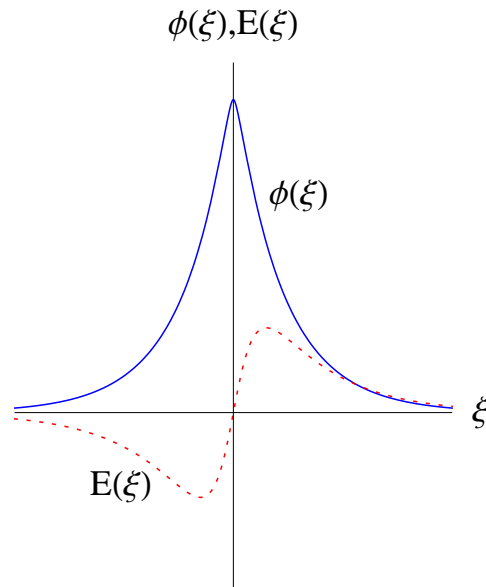


Figure 1.3: A graph showing a typical soliton structure in terms of the electrostatic potential (continuous curve) and electric field (dotted curve).

In studies of dusty plasmas, two types of acoustic solitons are commonly encountered in collisionless unmagnetized plasmas. These are dust ion-acoustic solitons (analogous to ion-acoustic solitons in pure ion-electron plasmas) and dust acoustic solitons [Shukla and Mamun, 2002, p. 94]. These solitons are correspondingly associated with different electrostatic waves, *viz.*, the dust ion-acoustic and dust acoustic waves, respectively. However,

if the plasma is magnetized we may obtain both electrostatic (acoustic) and electromagnetic (cyclotron) waves, with the acoustic wave modes propagating along the magnetic field while the cyclotron wave modes propagate (nearly but not exactly) perpendicular to the magnetic field [Merlino *et al.*, 1998]. In this thesis, however, only solitons associated with dust ion-acoustic and dust acoustic waves in various multi-component unmagnetized dusty plasmas will be investigated in Chapters 3 and 4. Besides dusty plasmas, we will also investigate ion-acoustic solitons in plasmas with two-temperature kappa electrons (Chap. 5), Cairns distributed electrons (Chap. 6) and two-temperature Boltzmann electrons (Chap. 7). Where applicable, double layers will also be discussed.

1.3.2 Double Layers

A double layer is a local region in a plasma which can sustain a potential difference or high potential drops [Block, 1978; Raadu and Carlqvist, 1981; Raadu and Rasmussen, 1981]. Double layers appear in current-carrying plasmas as nonlinear electrostatic shock-like or kink structures with potentials transiting from one value to another over a small spatial distance. They consist of two adjacent layers with equal and opposite net charge, hence the term “double layer”. One layer has an excess of positive charges and the other an excess of negative charges [Raadu and Rasmussen, 1981]. Inside the double layer the electric fields are strong but very weak outside. Thus the layer taken as a whole is practically neutral [Block, 1978; Raadu and Carlqvist, 1981; Raadu and Rasmussen, 1981].

In various energetic phenomena in space and astrophysical plasmas, double layers are considered as a possible means of accelerating particles [Smith, 1985; Raadu and Rasmussen, 1981], and have been invoked in such diverse contexts as terrestrial auroral discharges, magnetospheric substorms, solar flares, Jovian radio emission, extragalactic radio sources, etc.

A double layer is said to be strong if $e\phi_{dl}/K_B T \gg 1$, and is said to be weak if, say, $e\phi_{dl}/K_B T < 10$, where T is the temperature of the free electrons, and ϕ_{dl} the height (amplitude) of the double layer [Raadu and Carlqvist, 1981].

Strong double layers require two-sided boundary conditions [Hellberg *et al.*, 1997], with the associated particles being specified on both sides of the double layer. The particles associated with the potential variation may be conveniently divided into four classes: free

and trapped (or reflected) ions and electrons, though in principle, three of these four classes are enough to maintain a double layer (quite common with weak double layers). The free particles can pass through the double layer while the reflected/trapped particles cannot penetrate the layer because of the potential barrier. The free particles are either accelerated or decelerated depending on their direction of motion with respect to the electric field, and it is these free particles that carry the current through the layer leading to emerging beams of accelerated particles [Raadu and Rasmussen, 1981]. In this case the electric fields are strong and may lead to arbitrarily large amplitude double layers [Hellberg *et al.*, 1997]. A schematic picture showing a potential profile for a double layer as well as the free and reflected ions and electrons associated to the double layer is given in Fig. 1.4, from [Raadu and Carlqvist, 1981].

Another form of double layers is that associated with fluid acoustic models [Baboolal *et al.*, 1988; Mace and Hellberg, 1993; Hellberg *et al.*, 1997]. This is characterized by one-sided boundary conditions at infinity, and the presence of a two-temperature plasma. The result here is, in most cases, weak or small amplitude double layers, though there may be exceptions [Bharuthram and Shukla, 1992].

As we will see in the subsequent subsection, the formation of double layers requires that (i) the electric field be much stronger inside the double layer than outside. Thus the integrated positive and negative charges nearly cancel each other, leading to vanishing of the net charge of the double layer. This condition is derived from the momentum balance and Poisson's equation. (ii) Quasi-neutrality is locally violated in both space charge densities at the position of the double layer. These conditions will be discussed in detail in Sec. 1.4.2.

1.4 Methods Used in the Study of Solitary Structures

The methods used in the study of solitary structures are of two types, corresponding to small amplitude (or weak) solitons and large amplitude or arbitrary solitons. When the waves are weakly nonlinear (or quasi-linear) with acoustic-like dispersion in the low frequency regime, the *reductive perturbation analysis* is appropriate. In the case of large amplitude stationary waves, two methods are appropriate. These methods are: the *fluid-dynamic paradigm*, pioneered by McKenzie [McKenzie, 2002a,b, 2003] and co-workers [McKen-

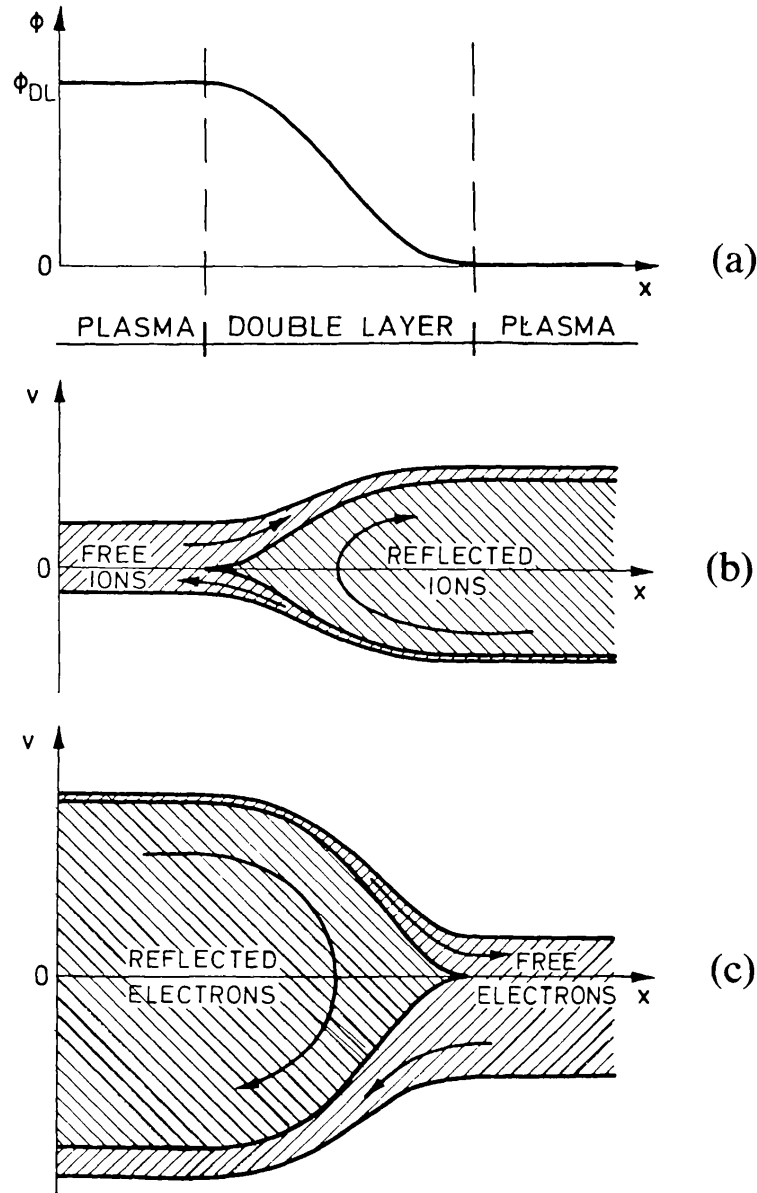


Figure 1.4: A graph showing a schematic picture of (a) potential profile, (b) phase space for the ions, and (c) phase space for the electrons, for a typical double layer structure. In the schematic diagram, both the ions and electrons consist of a combination of free particles and trapped or reflected particles; the free particles are either accelerated or decelerated depending on the direction of motion relative to the electric field. From Raadu and Carlqvist [1981].

zie and Doyle, 2003; McKenzie *et al.*, 2004b,a, 2005], and the *Sagdeev pseudopotential method* [Sagdeev, 1966]. The former (fluid-dynamic analysis) will not be discussed in detail in this thesis. It was, however, applied elsewhere [Baluku *et al.*, 2008] in the investigation of dust acoustic and dust ion-acoustic solitons in dusty plasma with positively charged

dust particles [Baluku, 2007]. Thus in the investigations of large amplitude solitons in the various multi-component plasma models that will be investigated in this thesis, we shall use the Sagdeev pseudopotential approach.

1.4.1 The Reductive Perturbation Theory

One of the commonest approaches to the reductive perturbation technique is the Korteweg-de Vries (KdV) approach. A detailed derivation of the KdV equation (and its solution), obtained for a dusty plasma model consisting of Boltzmann electrons, fluid ions and positively charged dust particles can be found in the work of Baluku [2007]. This approach has been used in obtaining the KdV equations in Chaps. 4 and 5, here involving kappa distributed electrons instead of Boltzmann electrons, and positively or negatively charged dust particles. In deriving the KdV equation, the following stretched coordinates are used [Mace *et al.*, 1991; Verheest, 2000; Shukla and Mamun, 2002]: $\zeta = \epsilon^{1/2}(x - Vt)$ and $\tau = \epsilon^{3/2}t$, where V is the phase velocity of the waves, and ϵ a smallness parameter. The KdV equation then takes the form [Swanson, 2003, p.355]

$$\frac{\partial \varphi_1}{\partial \tau} + A\varphi_1 \frac{\partial \varphi_1}{\partial \zeta} + B \frac{\partial^3 \varphi_1}{\partial \zeta^3} = 0, \quad (1.27)$$

where φ_1 is the perturbed electrostatic potential, and $A = A(V)$ and $B = B(V)$ are functions of the phase velocity V , where the latter is defined by the associated linear dispersion relation of the plasma model. The explicit form of $A(V)$ and $B(V)$ are model dependent, and have been suppressed. The equation above is used to describe one-dimensional asymptotic behaviour of small but finite amplitude waves such as shallow water waves and collisionless magnetohydrodynamic waves (see *e.g.*, [Baluku, 2007, and references therein]). The second term in Eq. (1.27), proportional to A , corresponds to the contribution of the nonlinearity effects while the third term (proportional to B) gives the dispersion term. When $B = 0$, the waves are non dispersive, resulting in a dispersion less acoustic wave relation $\omega = Ak$, where ω is the angular frequency and k is the wavenumber. Thus both the phase velocity ω/k , and the group velocity $d\omega/dk$, are equal to A [Baluku, 2007].

Solutions to Eq. (1.27) take the form of nonlinear solitary wave structures that propagate unchanged at constant speed, say V_0 , in the laboratory frame [Chen, 1984]. Transforming to a moving frame, $\chi(\zeta, \tau) = \zeta - V_0\tau = \epsilon^{1/2}(x - vt)$, where $v = V + \delta v$; with V

being the phase velocity of the solitary waves and $\delta v = \epsilon V_0$, the KdV equation in (1.27) has solution [Mace *et al.*, 1991; Verheest, 2000]

$$\varphi_1(\chi) = \left(\frac{3V_0}{A} \right) \operatorname{sech}^2 \left\{ \left(\frac{V_0}{4B} \right)^{1/2} \chi \right\}, \quad (1.28)$$

valid for $A \neq 0$ and $V_0/B > 0$, that is, both V_0 and B must be of the same sign. In this work we shall assume forward propagation ($V_0 > 0$), thus B is positive, implying that the sign of the potential φ_1 depends on the sign of A ; positive potential solitons ($\varphi_1 > 0$) require $A > 0$ while negative potential solitons ($\varphi_1 < 0$) require $A < 0$. We also point out that for given parameter values, only one sign of A is possible, implying that the KdV solution does not allow “co-existence” of negative and positive potential solitons under the same plasma parameter conditions, something that is possible in the large amplitude approach, as we will come to see. The soliton amplitude and width are given by $3V_0/A$ and $(4B/V_0)^{1/2}$, respectively. In other words, the soliton amplitude increases with increasing velocity of the solitary wave while the soliton width decreases with increasing phase speed.

For some plasma models, A is nonzero, so that both the nonlinear and dispersive terms can appropriately contribute to the formation of a solitary structure. However, as we will see in Chaps. 4 and 5, for some plasma parameters A can be equal to zero. In that case, the nonlinearity effect becomes very weak compared to the dispersion contribution. This leads to a breakdown of the KdV method, as the soliton amplitude would now go to infinity. When that is the case ($A = 0$), a more appropriate equation is the modified Korteweg-de Vries (mKdV) equation [Verheest, 2000, p. 112], which is similar to the KdV equation (1.27), but differs from it in the nonlinearity term. The mKdV equation has been derived for the plasma models described in Chaps. 4 and 5, and a detailed description is given in Appendix C.1. When $A(V) = 0$ in the KdV equation, Eq. (1.27), the soliton amplitude goes to infinity. In overcoming that scenario in the perturbation approach, we re-scale the stretched space-time variables ζ and τ . Following the approach of Baboolal *et al.* [1989], we use the stretched variables $\zeta = \epsilon(X - Vt)$ and $\tau = \epsilon^3 t$ instead of those used in the KdV approach. This approach, as can be seen in Appendix C.1, leads to the mKdV

equation of the form

$$\frac{\partial \varphi_1}{\partial \tau} + C(V) \varphi_1^2 \frac{\partial \varphi_1}{\partial \zeta} + B(V) \frac{\partial^3 \varphi_1}{\partial \zeta^3} = 0. \quad (1.29)$$

Note here that $B = B(V)$ takes the same form in equations (1.27) and (1.29). Likewise, $C(V)$ is model dependent. It also has to be noted that the mKdV approach is only valid for plasma parameters for which A is equal to or approaches zero.

Again, using the transformation $\chi(\zeta, \tau) = \zeta - u_0 \tau \equiv \epsilon(x - vt)$, where $v = V + \delta v$; $\delta v = \epsilon^2 u_0$, with u_0 being the phase velocity of the solitary wave, Eq. (1.29) takes the form of a first-order differential equation whose solution is given by [Verheest, 2000]

$$\varphi_1(\chi) = \pm \left(\frac{6u_0}{C} \right)^{1/2} \operatorname{sech} \left\{ \left(\frac{u_0}{D} \right)^{1/2} \chi \right\} \quad \text{or} \quad (1.30)$$

$$\varphi(x, t) = \pm \left(\frac{6\delta v}{C} \right)^{1/2} \operatorname{sech} \left\{ \left(\frac{\delta v}{B} \right)^{1/2} (x - vt) \right\}, \quad (1.31)$$

which is valid for $C > 0$ and $B > 0$ provided $\delta v > 0$ (forward propagation assumed). In Eq. (1.30) or (1.31), the soliton amplitude can be positive or negative due to the square root sign, thus for the same plasma parameters, the mKdV solution could result in solitons of the same amplitude (size) but opposite potential, unlike the KdV solution which gives only one sign of potential for the specific plasma parameter values.

1.4.2 The Sagdeev Pseudopotential Theory

This is the most widely used approach in the study of large (arbitrary) amplitude non-linear solitary structures (solitons and double layers). The method gives the necessary conditions for the existence of solitons and double layers, but does not describe the underlying mechanisms leading to these solitary structures as well as is the case with the fluid paradigm of McKenzie [McKenzie, 2002a,b, 2003; McKenzie and Doyle, 2003; McKenzie *et al.*, 2004a,b, 2005]. In this approach we begin with the Poisson's equation

$$\epsilon_0 \frac{\partial^2 \varphi}{\partial x^2} + \sum_j N_j q_j = 0, \quad (1.32)$$

where q_j , N_j , and φ are the charge and unnormalized density of species j , and the local electrostatic potential, respectively, where we have taken x as the unnormalized space (or position) variable. Poisson's equation (1.32) can easily be written in the form

$$\varepsilon_0 \frac{d^2\varphi}{dx^2} + \frac{dV(\varphi)}{d\varphi} = 0 \quad \text{or} \quad \frac{\varepsilon_0}{2} \left(\frac{d\varphi}{dx} \right)^2 + V(\varphi) = 0, \quad (1.33)$$

where $V(\varphi)$ is the Sagdeev (pseudo)potential. Note that here, we are still working with unnormalized quantities. In normalized form, the potential will be denoted by ϕ , and the Sagdeev potential or pseudopotential by $\Psi(\phi)$ instead of $V(\varphi)$. In Eq. (1.33), $V(\varphi) = -\int_0^\varphi G(\varphi)d\varphi$ is the pseudopotential, and $G(\varphi)$ gives the sum of the charge densities $N_j q_j$ for the plasma constituent species j . This implies that to fully have $V(\varphi)$ in terms of φ we also need the species densities $N_j = N_j(\varphi)$ for the integration to be possible. Though we have written the Sagdeev potential as $V(\varphi)$ as if it is only a function of φ , it is actually a function of more quantities such as the plasm species temperatures, densities, masses, velocities, etc.

Equation (1.33) takes the same mathematical form as Newton's law of motion, $d^2\chi/dt^2 = \mathcal{F}(\chi)/m = -d\Phi(\chi)/d\chi$, in Classical Mechanics where $\Phi(\chi)$ is the potential energy, at coordinate χ , of a particle of mass m moving under the influence of a force, $\mathcal{F}(\chi)$. Thus the second equation in (1.33) is equivalent to an energy integral of a pseudo particle of unit mass with potential energy $V(\varphi)$ (called the pseudopotential or Sagdeev potential) where φ now plays the role of particle coordinate and x the role of time.

With the Sagdeev potential defined in (1.33), it follows that at the origin ($\varphi = 0$) we have

$$V(\varphi) = \frac{dV}{d\varphi}(\varphi = 0) = 0. \quad (1.34)$$

This condition ensures that the appropriate boundary conditions used in obtaining $V(\varphi)$ are satisfied. Provided condition (1.34) is satisfied, then the existence of solitons or double layers require that [Baboolal *et al.*, 1988, 1990; Mace and Hellberg, 1993; Verheest, 2000; Verheest *et al.*, 2008]:

(i) The Sagdeev potential $V(\varphi)$ possesses a second derivative such that

$$\frac{d^2V}{d\varphi^2}(\varphi = 0) < 0. \quad (1.35)$$

Thus there is an unstable local maximum at the origin $\phi = 0$ such that the pseudo particle comes to rest at the origin when $\xi \rightarrow \pm\infty$. This condition ensures that $\Psi(\phi) < 0$ for $\phi \neq 0$ in the immediate neighbourhood of $\phi = 0$, leading to the necessary convexity at the origin [Verheest *et al.*, 2008]. Equation (1.35) is loosely referred to as the “soliton condition”, and gives the minimum (critical) value of the structure speed (from $d^2V/d\varphi^2 = 0$ at $\varphi = 0$) such that wave propagation is only possible above the critical speed. However, as we will see later in Chaps. 4, 5, 6, and 7, this applies only to plasma parameters where soliton potentials of only one sign are supported. For such solitons, their electrostatic potential goes to zero as the Mach number approaches a critical (lowest) Mach number.

In the case where solitary structures of both polarity are supported by the same plasma configuration, Eq. (1.35) takes the form

$$\frac{d^2V}{d\varphi^2}(\varphi = 0) \leq 0, \quad (1.36)$$

since in this case wave propagation may be possible even at the critical structure speed.

(ii) There exists a nonzero ϕ_m , which is a minimum potential³ (or maximum potential) for solitons or double layers, at which

$$V(0) = V(\varphi_m) = 0 \quad \text{and} \quad \frac{dV(\phi_m)}{d\varphi} \begin{cases} < 0 & \text{for } \varphi_m < 0, \\ > 0 & \text{for } \varphi_m > 0. \end{cases} \quad (1.37)$$

That is, φ_m may be the amplitude of the soliton or the potential corresponding to the higher potential side of the double layer. In the case of a double layer, the former condition, that is $V(0) = V(\varphi_m) = 0$, implies that the electric field vanishes at the edges of the double layer, with $\varphi = 0$ and $\varphi = \varphi_m$ being the potentials at the edges of the double layer. This requirement also ensures that the overall charge in the double layer vanishes, and the condition is known as the generalized Langmuir condition.

(iii) We also require

$$V(\varphi) < 0 \quad \text{for} \quad 0 < |\varphi| < |\varphi_m|. \quad (1.38)$$

This condition ensures that $(d\varphi/dx)^2$ is positive for real solutions of the potential following

³In the case of solitons, minimum potential is associated with negative potential solitons ($\varphi < 0$) while maximum potential is associated with positive potential solitons ($\varphi > 0$)

from $d\varphi/dx = (-2V(\varphi)/\varepsilon_0)^{1/2}$ in Eq. (1.33).

(iv) In the case of *double layers*, in addition to the above requirements in (1.35)–(1.38), we also require that the charge density must also vanish at the edges of the double layer. This implies that

$$\frac{dV(0)}{d\varphi} = \frac{dV(\varphi_m)}{d\varphi} = 0. \quad (1.39)$$

Thus, in particular, double layers satisfy

$$V(\varphi_m) = \frac{dV(\varphi_m)}{d\varphi} = 0. \quad (1.40)$$

It can be shown that expanding the Sagdeev potential, $V(\varphi)$ to the fourth order about $\varphi = 0$ leads to a formalism equivalent to the reductive perturbation method [Verheest, 1999]. Thus one obtains

$$\frac{\varepsilon_0}{2} \left(\frac{d\varphi}{dx} \right)^2 + C_1\varphi^2 + C_2\varphi^3 + C_3\varphi^4 = 0, \quad (1.41)$$

where the coefficients C_1 , C_2 and C_3 depend on the physical parameters, such as temperature, density etc. In the case of weak solitons, expansion of $V(\varphi)$ to third order is sufficient, and that leads to the same solution as Eq. (1.28), obtained from the KdV approach for small amplitude solitons (see also Baluku and Hellberg [2008]). Thus this approach is similar to the reductive perturbation methods for small amplitude solitons. However, for weak double layers, we need Eq. (1.41) (up to fourth order in φ). Upon applying the double layer existence conditions in Eq. (1.40), it follows that

$$C_1 = C_3\varphi_m^2 \quad \text{and} \quad C_2 = -2C_3\varphi_m, \quad (1.42)$$

and thus Eq. (1.41) takes the form

$$\frac{1}{2} \left(\frac{d\varphi}{dx} \right)^2 + \frac{C_3}{\varepsilon_0} \varphi^2 (\varphi - \varphi_m)^2 = 0. \quad (1.43)$$

A typical solution to Eq. (1.43) is given by [Verheest, 2000]

$$\phi = -\frac{\varepsilon_0 C_2}{4C_3} \left\{ 1 - \tanh \left[\left(-\frac{C_1}{2} \right)^{1/2} \xi \right] \right\}, \quad (1.44)$$

which after using Eq. (1.42) simply reduces to

$$\varphi(x) = \frac{\varepsilon_0}{2} \varphi_m \left\{ 1 - \tanh \left[\varphi_m (-C_3/2\varepsilon_0)^{1/2} x \right] \right\}; \quad (C_3 < 0). \quad (1.45)$$

In this thesis, the expanded Sagdeev potential approach is used in Chap. 3 (see also Baluku and Hellberg [2008]) in the investigation of small amplitude solitons and double layers when considering a dusty plasma with kappa distributed electrons or ions and positively charged fluid dust particles.

1.5 Outline of Thesis

In this thesis, investigations of linear and nonlinear waves in various plasma models, which may occur in some space plasma environments, are described. We first study linear electron-acoustic waves in bi-kappa plasmas, with emphasis on Saturn's magnetosphere, using a kinetic theoretical approach. We next turn to nonlinear waves, where we use a fluid approach. In the fluid models we study dusty plasmas, where we look at two cases, first, the dust acoustic waves, and second, the dust ion-acoustic waves. We extend the nonlinear studies to ion-acoustic waves and solitary structures (in the form of solitons and double layers) in bi-kappa plasmas. Finally, we deal with ion-acoustic solitary waves in two other three-component models, *viz.*, one involving an electron-ion-positron plasma, and one composed of ions and two Boltzmann-distributed electron components at different temperatures.

After this general introduction to some of the key concepts underpinning the studies in this thesis, we turn in Chapter 2 to our first research problem. It involves a discussion of linear electron-acoustic waves in bi-kappa plasmas, using kinetic theory, where the electron components are kappa distributed. We discuss specific examples relevant to the magnetosphere of Saturn, where two electron components, of different temperatures and with nonthermal distributions that deviate significantly from the Maxwellian distribution, have been reported.

In chapter 3 we investigate existence domains of dust acoustic solitons (and double layers), considering a plasma consisting of cold fluid dust grains, and kappa distributed electrons and ions. Here, we derive an expression for the density of particles (in terms of the electrostatic potential) satisfying a kappa distribution, which has also been applied to the models described in chapters 4 and 5.

Chapter 4 is a study of dust ion-acoustic waves in a three component plasma, with cold fluid ions, charged dust grains, and kappa distributed electrons. This is a considerable extension of the work of Bharuthram and Shukla [1992], who studied a plasma model consisting of Boltzmann-distributed electrons, cold ions, and negative dust. In this study, we have considered both small amplitude solitons, using the reductive perturbation technique, and arbitrary amplitude solitons, using the Sagdeev (pseudopotential) approach. In particular, we have obtained novel results, namely, finite solitons at the true acoustic speed of the DIA waves that are contrary to the KdV theory description, and also lead to a redefinition of the requirements imposed on the Sagdeev pseudopotential.

In Chapter 5 we consider ion-acoustic solitons in a plasma model consisting of cool Maxwellian ions and two (cool and hot) kappa distributed electron components. This plasma model is discussed with a view to application to the magnetosphere of Saturn, where two component electrons have been reported to be kappa distributed [Schippers *et al.*, 2008]. In this chapter, we also report results that are contrary to what is in the literature. For instance we report that, depending on the plasma configuration, solitons may be obtained even for Mach numbers greater than that at which a double layer occurs, a hitherto unreported phenomenon.

Chapter 6 describes solitary structures in an electron-positron-ion plasma, where the electrons are nonthermally distributed, obeying the Cairns distribution, the positrons are Boltzmann-distributed, while the ions are cold and fluid-like. The work described in this chapter is an extension of Pakzad [2009], however, we have provided more new results compared to what is in the literature, including showing the existence of negative solitons and double layers in this configuration.

Chapter 7 deals with an investigation of ion-acoustic solitary waves in a three-species plasma consisting of double Boltzmann electrons and cold ions. In this model solitons are also found to possess peculiar features, such as finite amplitudes at the velocity corre-

sponding to the ion-acoustic speed of the wave. In addition, positive double layers are also reported to be supported by the plasma model, for a limited parameter range, in contrast to what is reported in the literature. In this range, again, solitons are found at Mach numbers greater than that yielding a double layer.

Finally, in Chap. 8 we present a brief summary of results for all the different plasma models that are discussed in this thesis.

Electron-Acoustic Waves in Bi-kappa Plasmas

In this chapter we use kinetic theory to investigate the possible existence of electron acoustic waves in Saturn's magnetosphere.

2.1 Introduction

The co-existence of cool and hot electron populations in Saturn's magnetosphere was deduced using the Voyager PLS observations of Sittler *et al.* [1983] and later confirmed using the Cassini Plasma Spectrometer (CAPS) observations of Young *et al.* [2005]. The nonthermal nature of the electron distributions in the outer magnetosphere was also revealed by the Voyager measurements of Barbosa and Kurth [1993], who showed that the electrons possessed a superthermal tail that could be fitted by a power law function instead of a Maxwellian distribution function.

More recently, the Cassini-Huygens spacecraft orbiting Saturn carried, among others, two instruments: the Electron Spectrometer of the CAPS (CAPS/ELS) and the Low Energy Magnetospheric Measurement System of the Magnetospheric Imaging Instrument (MIMI/LEMMS). Using results from the CAPS/ELS and MIMI/LEMMS instruments, Schippers *et al.* [2008] have shown that both the cool and hot electron populations are non-Maxwellian. By fitting the Cassini data for the electron populations with (a) two Maxwellian populations, (b) Maxwellian cool electrons and κ -distributed hot electrons,

and (c) two κ -distributed electron populations, Schippers *et al.* [2008] (see their Fig. 2) showed that the double kappa distribution model fits best, with relatively low values of κ ($\kappa_c, \kappa_h \sim 2 - 4$, where subscripts “c” and “h” refer to cool and hot populations, respectively) over much of the magnetosphere.

Saturn’s magnetosphere has been categorized by many authors, using Voyager 1 and 2 [Sittler *et al.*, 1983] and Cassini data [Krimigis *et al.*, 2005; Dougherty *et al.*, 2005; Young *et al.*, 2005; Gurnett *et al.*, 2005; Schippers *et al.*, 2008; André *et al.*, 2008], as consisting of three or more regions depending on the activities taking place and the composition of the particular portion of the magnetosphere. The main three regions are the inner magnetosphere, the plasma sheet region (or loosely the middle magnetosphere), and the outer magnetosphere. The inner magnetosphere, extending to radial distances up to $(9 - 10) R_S$, where $R_S \approx 60,268$ km is the radius of Saturn, has the densest plasma in the Saturnian system, with the plasma originating from the icy moons of Rhea ($8.74 R_S$ with N^+ , O^+ and water group ions OH^+ or H_2O^+), Dione ($6.26 R_S$) and Enceladus ($3.95 R_S$), as well as neutral sources [Krupp *et al.*, 2005; André *et al.*, 2008]. Inside the inner magnetosphere lies the inner plasma torus (under $8 R_S$) which is characterized by low temperatures and high equatorial densities, and is coupled to the ring system and the icy satellites [André *et al.*, 2008]. The region lying between around $(7 - 9) R_S$ and about $(12 - 14) R_S$ corresponds to the extended plasma sheet [Krupp *et al.*, 2005; André *et al.*, 2008]. In this region, the energetic particles are confined to the equatorial plane of Saturn in a disk-like layer, and the plasma consists of a mixture of hot and cool populations resulting from transport processes [André *et al.*, 2008], where the cool plasma population dominates the density and the hot plasma population dominates the pressure. The outer region of the magnetosphere, which extends beyond $(12 - 14 R_S)$ up to the magnetopause boundary ($\sim 20 R_S$), is characterized by a low plasma density and is strongly influenced by the solar wind. The magnetopause boundary separates the solar wind plasma from that within Saturn’s magnetosphere. This outer magnetosphere consists mainly of lighter ions with masses $m_i \lesssim 10$ amu (such as H^+), a tenuous hot plasma, and a quiet magnetic field [Wahlund *et al.*, 2005; André *et al.*, 2008].

Following the analysis of the Voyager data [Gurnett *et al.*, 1981; Kurth *et al.*, 1983; Barbosa and Kurth, 1993] and recently, the Cassini data [Gurnett *et al.*, 2005; André *et al.*,

2008], a range of wave activity has been seen in the magnetosphere of Saturn. Whistler hiss and chorus were reported in the noise events at frequencies below the electron cyclotron frequency or gyrofrequency ($f_g = eB/2\pi m_e$) in the magnetosphere of Saturn [Kurth *et al.*, 1983; Barbosa and Kurth, 1993; Gurnett *et al.*, 2005]. These low frequency waves, centered at frequencies below the local electron plasma frequency (f_{pe}), were observed as electrostatic broadband bursts [Kurth *et al.*, 1983] at a radial distance of about $15.6 R_S$ (in the outer magnetosphere), and in the inner magnetosphere at about $3.1 R_S < R < 8 R_S$ [Barbosa and Kurth, 1993]. Earlier, Gurnett *et al.* [1981] had observed a strong band of noise at frequencies below 2 kHz between 3.1 and $8 R_S$ in the appropriate frequency range of whistler mode hiss and chorus emissions. At these frequencies, the emissions were found to be in resonance with low energy (1 – 5 keV) electrons.

Above f_g , electron cyclotron harmonic (ECH) waves or $(n+1/2)f_g$ bands, where n is an integer, were found to exist in the region inside $8 R_S$ provided $f_{pe} > f_g$ [Kurth *et al.*, 1983; Barbosa and Kurth, 1993] while narrow-band upper hybrid resonance (UHR) emissions at frequencies between 25 and 100 kHz (under $6.81 R_S$) were also reported by Gurnett *et al.* [2005]; the latter were said to be due to electrostatic oscillations at the UHR frequency, $f_{UHR} = (f_{pe}^2 + f_g^2)^{1/2}$. In addition, electron plasma oscillations [sometimes called Langmuir waves or electron plasma waves (EPWs)] with frequencies of about 5.6 – 10 kHz (between 13.6 and $17.7 R_S$) and 10 – 17 kHz (between 5.5 and $9.5 R_S$) [Kurth *et al.*, 1983; Barbosa and Kurth, 1993], and 10 and 17.8 kHz in the $4 R_S < R < 10 R_S$ region [Gurnett *et al.*, 1981], were also observed in the magnetosphere of Saturn.

Electromagnetic radio wave emissions at high frequencies, between about (3.6 – 5.6) kHz and 31 kHz [Gurnett *et al.*, 1981; Barbosa and Kurth, 1993], were reported in the inner magnetosphere (between 3.1 and $6 R_S$) while Gurnett *et al.* [2005] observed intense Saturn Kilometric Radiation (SKR) on both the outbound and inbound trips of the spacecraft (under $8.33 R_S$) with frequencies ranging from 100 to 400 kHz.

Apart from EPWs and whistler mode waves, which were reported in both the inner and outer magnetosphere, the majority of plasma waves were reported to have occurred in the inner magnetosphere of Saturn for radial distances less than $10 R_S$ [Gurnett *et al.*, 1981; Kurth *et al.*, 1983; Barbosa and Kurth, 1993], where (i) the magnetosphere contains icy satellites that are sources of protons and heavier ions like O^+ and water group ions OH^+ or

H_2O^+ , and (ii) the cool and hot electron population densities differ quite significantly. It should be noted that the whistler mode hiss and chorus waves, reported from the Voyager plasma wave measurements, were associated with a loss-cone pitch angle distribution based on the latitudinal dependency of the flux which decreases with latitude. In addition, Kurth *et al.* [1983] pointed out that one of the reasons why low frequency electrostatic modes may not be easily observed in the magnetosphere of Saturn is primarily due to limitations of the instrument (in the case of the Voyager plasma wave instrumentation), in that the noise spectrum that is produced by the spacecraft is most intense below frequencies of 1 kHz, and their spiky nature makes it very difficult to differentiate between true signals and interference from the instrument itself.

Bearing in mind that both cool and hot electron populations in Saturn's magnetosphere are κ -distributed [Schippers *et al.*, 2008], using a kinetic-theoretical model, we consider the possible existence of electron-acoustic waves in the magnetosphere of Saturn. Electron-acoustic waves are electrostatic waves that propagate in plasmas with two electron components having widely disparate temperatures [Watanabe and Taniuti, 1977; Gary and Tokar, 1985]. These EAWs are believed to propagate in both unmagnetized and magnetized two-temperature plasma [Tokar and Gary, 1984].

2.2 Description of Electron-Acoustic Waves

In homogeneous collisionless unmagnetized electron-ion plasmas, only two weakly damped electrostatic normal modes are possible: the electron plasma (Langmuir) wave mode, which occurs at frequencies above the electron plasma frequency (ω_{pe}), and the ion-acoustic wave, which occurs at frequencies below the ion plasma frequency (ω_{pi}). The latter requires that the ion temperature be much less than the electron temperature ($T_e/T_i \gg 1$) to avoid ion Landau damping. However, in the presence of two electron components (of similar densities but quite different temperatures), a third weakly damped electrostatic mode may propagate, and this mode has been termed the electron-acoustic wave [Watanabe and Taniuti, 1977; Tokar and Gary, 1984; Gary and Tokar, 1985; Gary, 1987]. Thus an electron-acoustic wave is considered to be a characteristic normal mode of an unmagnetized collisionless plasma in the presence of two electron components with similar densities but strongly disparate temperatures. It propagates at a phase speed satisfying $V_{tc} \ll \omega/k \ll V_{th}$, where

V_{tc} (V_{th}) is the thermal velocity of the cool (hot) electrons, given by $V_{tj} = (K_B T_j / m_e)^{1/2}$ ($j = c$ or h). The EAW frequency lies between the ion and electron plasma frequencies, though the waves are strongly damped for small k [Gary and Tokar, 1985]. In this mode, the cool electron oscillations are modified (Debye screened) by the hot electrons, while the cool ions essentially play a neutralizing role only.

Such waves have been studied in bi-Maxwellian plasmas [Watanabe and Taniuti, 1977; Gary and Tokar, 1985; Mace and Hellberg, 1990]. Gary and Tokar [1985] have shown that weak damping may be possible provided the ratio of the hot to cool electron temperature, $T_h/T_c \gg 10$, and fractional cool electron density, $n_{0c}/n_{0e} < 0.8$, where n_{0e} is the total electron density. In addition, Mace and Hellberg [1990] generated critical curves that delineate the regions in parameter space in which a higher order mode will exhibit weaker damping (smallest imaginary frequency). This approach was extended to a plasma with hot superthermal (κ -distributed) and cool Maxwellian electrons by Mace *et al.* [1999].

In such weakly damped regions it is likely that, if sufficient free energy is added (for instance, by a beam), the waves could attain observable amplitudes [Ashour-Abdalla and Okuda, 1986; Mace and Hellberg, 1993; Singh and Lakhina, 2001]. The higher-order modes referred to here are those solutions of the dispersion relation that show strong damping ($|\gamma| > \omega_r/2\pi$, where ω_r and γ are the real and imaginary parts of the complex frequency $\omega = \omega_r + i\gamma$), otherwise those with weak damping ($|\gamma| \leq \omega_r/2\pi$) are called normal modes.

While investigating wave observations in the geomagnetic tail, Ashour-Abdalla and Okuda [1986] showed that in the presence of ion beams, EAWs may be unstable if the electron Landau damping is exceeded by the inverse ion Landau damping from the beam ions, and that EAWs may exist provided $T_{ec}/T_{eh} \ll 1$, with $T_{eh} \approx 100$ eV.

Using a plasma model consisting of stationary, Maxwellian cool and hot electrons, an electron beam drifting along the magnetic field, and stationary, fluid ions, Singh and Lakhina [2001] provided analytical conditions for the generation of electron-acoustic waves in the Earth's magnetosphere, which in a sense complemented the numerical work of Tokar and Gary [1984]. They applied their results to the analysis of the dayside auroral region, where the broadband electrostatic noise (BEN) emission was observed as a common phenomenon by the Viking satellite at heights of 2 000 to 10 000 km. With parameter values typical of the auroral region they obtained unstable EAWs with frequencies between the ion

plasma frequency and the cool electron plasma frequency. In addition, Singh and Lakhina [2001] applied their results to the plasma sheet boundary layer, and the polar cusp region.

In the mid 1970's, Kawai *et al.* [1975] excited electron waves by a three-mesh exciter in a large-volume plasma in the space chamber at the Institute of Space and Aeronautical Science, University of Tokyo. In addition to the Langmuir mode, they observed the free-streaming electron mode and a new mode at frequencies less than the Langmuir frequency, which appeared to be the EAW. In their experiment, the energy distribution function of the electrons, as measured by the Faraday cup method for different anode potential, showed that the electrons consisted of a Maxwellian component and a non-Maxwellian component (modelled by a water-bag distribution function), since the tail of the energy distribution function was extended with increased anode potential.

Following on the experiment of Karlstad conducted in the Tromsø DP device [Karlstad *et al.*, 1984], Hellberg *et al.* [2000] showed that electron-acoustic waves were observed in that experiment. The plasma model involving cool Maxwellian and hot κ -distributed electrons showed minimal damping for $\kappa_h \simeq 3 - 4$, and both damping and dispersion were in good agreement with the experimental results [Hellberg *et al.*, 2000].

Electron-acoustic wave solitons have been reported in the FAST satellite data in the auroral region of the geomagnetic tail [Pottelette *et al.*, 1999], in the presence of a two-component electron plasma with one cool (< 60 eV) and a dominant hot (\sim keV) component. Mace and Hellberg [2001] used a Korteweg-de Vries–Zakharov-Kuznestov (KdV-ZK) model to study the effect of a magnetic field on such electron-acoustic solitons.

To the best of our knowledge, observations of EAWs have not yet been reported in Saturn's magnetosphere. Nonetheless, in this chapter we investigate, by using a kinetic-theoretical approach, whether they may potentially be observable. First we present a parameter survey of dispersion and damping curves for different density ratios, temperature ratios and spectral index values (κ_c and κ_h), of the two electron components. Then we consider parameter values that are representative of three regions of Saturn's magnetosphere, as illustrated in Fig. 3 of Schippers *et al.* [2008]. In particular, we show that EAWs would be weakly damped in the outer magnetosphere and hence are likely to be observable there, given a possible external source of free energy.

2.3 Theoretical Model and Basic Equations

We consider electrostatic waves in an unmagnetized, collisionless plasma consisting of kappa distributed cool and hot electrons, and singly charged cool Maxwellian ions. In the EAW, the cool electron oscillations are modified by the hot electrons, with the cool ions playing mainly a neutralizing role.

We shall use the 3-d isotropic kappa distribution, given as

$$F_\kappa(v) = \frac{1}{(\pi\kappa\theta^2)^{3/2}} \frac{\Gamma(\kappa+1)}{\Gamma(\kappa-1/2)} \left(1 + \frac{v^2}{\kappa\theta^2}\right)^{-(\kappa+1)}, \quad (2.1)$$

which is of the form of Eq. (1.2), with κ , θ and Γ taking the usual meaning as in Eq. (1.2).

The general dispersion relation for electrostatic waves in an unmagnetized plasma may be written as [Krall and Trivelpiece, 1989]

$$D(k, \omega) = 1 - \sum_\alpha \frac{\omega_{p\alpha}^2}{k^2} \int_{-\infty}^{\infty} \frac{\partial f_{\alpha 0} / \partial v_x}{v_x - \omega/k} d^3v = 0; \quad \text{Im } \omega > 0,$$

where $\omega_{p\alpha} = (n_{0\alpha}q_\alpha^2/\epsilon_0 m_\alpha)^{1/2}$ is the plasma frequency, with the parameters in $\omega_{p\alpha}$ having their usual meaning; $f_{\alpha 0}$ the unperturbed velocity distribution function of species α and the wave vector \mathbf{k} is in the $\hat{\mathbf{x}}$ - direction. For two species of κ -distributed electrons and kappa distributed ions, the dispersion relation takes the form [Hellberg and Mace, 2002; Mace and Hellberg, 2009]

$$D(k, \omega) = 1 - \frac{\omega_{pc}^2}{k^2\theta_c^2} \mathcal{Z}'(\kappa_c; \xi_c) - \frac{\omega_{ph}^2}{k^2\theta_h^2} \mathcal{Z}'(\kappa_h; \xi_h) - \frac{\omega_{pi}^2}{k^2\theta_i^2} \mathcal{Z}'(\kappa_i; \xi_i) = 0, \quad (2.2)$$

where c and h denote the cool and hot electrons, respectively, and i denotes the stationary, cold ions; $\xi_\alpha = \omega/(k\theta_\alpha) \propto \omega/(kV_{t\alpha})$ is the complex wave phase speed normalized to the most probable speed θ_α of species α , with ω being the complex angular frequency, given by $\omega = \omega_r + i\gamma = \omega_r(1 + i\gamma/\omega_r)$, and k the (magnitude of the) wave number. In particular, $\theta_\alpha^2 = [(2\kappa_\alpha - 3)/\kappa_\alpha](K_B T_\alpha/m_\alpha) = [(2\kappa_\alpha - 3)/\kappa_\alpha]V_{t\alpha}^2$, with T being the kinetic temperature [Summers and Thorne, 1991; Hellberg *et al.*, 2009; Mace and Hellberg, 2009], and $V_{t\alpha} = (K_B T_\alpha/m_\alpha)^{1/2}$ being the thermal velocity of species α .

The plasma dispersion function which we denote by $\mathcal{Z}(\kappa_\alpha; \xi_\alpha)$ is precisely the same

as $Z_{\kappa M}(\xi)$, the modified plasma dispersion function of Hellberg and Mace [2002], defined initially for a Kappa-Maxwellian velocity distribution. Hellberg and Mace [2002] also indicated that $Z_{\kappa M}(\xi)$ is related to the modified plasma dispersion function $Z_{\kappa}(\xi)$ for the isotropic three-dimensional kappa distribution [Mace and Hellberg, 1995; Hellberg and Mace, 2002] by

$$Z_{\kappa M}(\xi) = \frac{(\kappa - 1)^{3/2}}{[\kappa^{1/2}(\kappa - 3/2)]} Z_{\kappa-1} \left[\left\{ \frac{(\kappa - 1)}{\kappa} \right\}^{1/2} \xi \right],$$

and thus $Z_{\kappa M}(\xi)$ is also applicable to studies involving isotropic kappa distributions, as is the case here. Recently, Mace and Hellberg [2009] have shown that this plasma dispersion function [$\mathcal{Z}(\kappa_{\alpha}; \xi_{\alpha})$ or $Z_{\kappa M}(\xi)$], which they denoted $U_{\kappa}(\xi)$, can also be obtained starting from an isotropic kappa distribution, and therefore its application is not limited to plasmas with Kappa-Maxwellian velocity distributions. In particular, it can be applied to studies involving ordinary isotropic kappa distributions. Therefore, for general purposes we shall use the notation $\mathcal{Z}(\kappa_{\alpha}; \xi_{\alpha})$ instead of $Z_{\kappa M}(\xi)$ to refer to the plasma dispersion function for kappa velocity distributions of the form given in Eq. (1.2).

The integral and closed forms of the function $\mathcal{Z}(\kappa_{\alpha}; \xi_{\alpha})$, are given by [Hellberg and Mace, 2002; Mace and Hellberg, 2009]

$$\mathcal{Z}(\kappa_{\alpha}, \xi_{\alpha}) = \frac{1}{(\pi \kappa_{\alpha})^{1/2}} \frac{\Gamma(\kappa_{\alpha})}{\Gamma(\kappa_{\alpha} - 1/2)} \int_{-\infty}^{\infty} \frac{ds}{(s - \xi_{\alpha})(1 + s^2/\kappa_{\alpha})^{\kappa_{\alpha}}}; \quad \text{Im}(\xi_{\alpha}) > 0 \quad \text{and} \quad (2.3)$$

$$\mathcal{Z}(\kappa_{\alpha}, \xi_{\alpha}) = \frac{i(\kappa_{\alpha} - 1/2)}{\kappa_{\alpha}^{3/2}} {}_2F_1 \left[1, 2\kappa_{\alpha}, \kappa_{\alpha} + 1; \frac{1}{2} \left(1 - \frac{\xi_{\alpha}}{i\sqrt{\kappa_{\alpha}}} \right) \right], \quad (2.4)$$

respectively, where the closed form is expressed in terms of the hypergeometric function, ${}_2F_1$ [Abramowitz and Stegun, 1972, p. 556]. Though the integral expression (2.3) for $\mathcal{Z}(\kappa_{\alpha}, \xi_{\alpha})$ is defined only for $\text{Im}(\xi_{\alpha}) > 0$, its behaviour for $\text{Im}(\xi_{\alpha}) \leq 0$ is obtained through analytic continuation. In fact, Eq. (2.4) is precisely the analytic continuation of it. The function $\mathcal{Z}'(\kappa_{\alpha}, \xi_{\alpha})$, the derivative of $\mathcal{Z}(\kappa_{\alpha}, \xi_{\alpha})$ with respect to the argument ξ_{α} , takes the form [Hellberg and Mace, 2002]

$$\mathcal{Z}'(\kappa_{\alpha}, \xi_{\alpha}) = \frac{-(\kappa_{\alpha} - 1/2)}{\kappa_{\alpha}(\kappa_{\alpha} + 1)} {}_2F_1 \left[2, 2\kappa_{\alpha} + 1, \kappa_{\alpha} + 2; \frac{1}{2} \left(1 - \frac{\xi_{\alpha}}{i\sqrt{\kappa_{\alpha}}} \right) \right]. \quad (2.5)$$

Note that in the limit $\kappa_{\alpha} \rightarrow \infty$, $\mathcal{Z}(\kappa_{\alpha}, \xi_{\alpha})$ reduces to the usual plasma dispersion function

$Z(\xi)$ of Fried and Conte [Brambilla, 1989; Swanson, 1989]. For Maxwellian ions we have $\mathcal{Z}(\kappa_i; \xi_i) \rightarrow Z(\xi_i)$; where here $\xi_i = (\omega/k)/\sqrt{2}V_{ti}$, since $\theta_i \rightarrow \sqrt{2}V_{ti}$ when $\kappa_i \rightarrow \infty$. In the analytical discussion we shall use $Z(\xi)$ for the ions. However, for the numerical evaluations, we have retained the full expression $\mathcal{Z}(\kappa_\alpha; \xi_\alpha)$ in (2.2) and used a high value of κ_i (e.g., $\kappa_i = 50$) to approximate to a Maxwellian.

2.4 Analytic Solutions

On the electron-acoustic wave time scale, the phase velocity satisfies (c.f. Watanabe and Taniuti [1977]; Gary and Tokar [1985]) $V_{ti} \ll V_{tc} \ll \omega/k \ll V_{th}$. For $\xi_\alpha \propto \omega/(kV_{t\alpha})$, it follows that $|\xi_i|, |\xi_c| \gg 1$, and $|\xi_h| \ll 1$. Thus we approximate $\mathcal{Z}(\kappa_\alpha; \xi_\alpha)$ by using an asymptotic expansion for the ions and the cool electrons. On the other hand, we use a power series expansion of $\mathcal{Z}(\kappa_\alpha; \xi_\alpha)$ for the hot electrons. A detailed discussion is given in Appendix B.1.

For frequencies and wavelengths, assuming $\omega_{pi} \ll \omega_{pc}$; $|\gamma| \ll \omega_r$; $\lambda_{Dc} \ll \lambda_{\kappa h}$ (which is commonly valid); and $k\lambda_{Dc} \ll 1$, the dispersion relation [Eq. (2.2)] can be written in the approximate form [see Appendix B.1 for details],

$$\omega_r^2 = \omega_{pc}^2 \left\{ \frac{1 + 3k^2\lambda_{Dc}^2(1 + 1/k^2\lambda_{\kappa h}^2)}{(1 + 1/k^2\lambda_{\kappa h}^2)} \right\}, \quad (2.6)$$

where $\lambda_{\kappa\alpha} = [(\kappa_\alpha - 3/2)/(\kappa_\alpha - 1/2)]^{1/2} \lambda_{D\alpha}$, with $\lambda_{D\alpha} = (\varepsilon_0 K_B T_\alpha / n_{0\alpha} e^2)^{1/2}$ being the standard (Maxwellian) Debye length of species α . Here, the parameter $\lambda_{\kappa\alpha}$ is the appropriate Debye length in a kappa plasma [Bryant, 1996; Mace *et al.*, 1998, 1999], which reduces to $\lambda_{D\alpha}$ in the limit $\kappa_\alpha \rightarrow \infty$. Equation (2.6) can be written in the equivalent form

$$\omega_r^2 = k^2 \left\{ \frac{V_{s\kappa}^2}{1 + k^2\lambda_{\kappa h}^2} \right\} + 3V_{tc}^2, \quad (2.7)$$

where $V_{tc} = \omega_{pc}\lambda_{Dc}$ is the thermal velocity of the cool electrons, and $V_{s\kappa}$, the electron sound speed in a kappa plasma, is given by

$$V_{s\kappa}^2 = \omega_{pc}^2 \lambda_{\kappa h}^2 = \left(\frac{n_{0c}}{n_{0h}} \right) \left(\frac{K_B T_h}{m_e} \right) \left(\frac{\kappa_h - 3/2}{\kappa_h - 1/2} \right). \quad (2.8)$$

This expression for $V_{s\kappa}^2$ is the same as that found by Mace *et al.* [1999] for the EA speed in

a plasma with cool Maxwellian and hot kappa electrons. Indeed, we note from (2.8) that $V_{s\kappa}$ is independent of κ_c and increases with κ_h . For $\kappa_h \rightarrow \infty$, $V_{s\kappa}$ reduces to

$$C_{se} = \left(\frac{n_{0c}}{n_{0h}} \right)^{1/2} \left(\frac{K_B T_h}{m_e} \right)^{1/2}, \quad (2.9)$$

the electron-acoustic speed in the Maxwellian limit [Gary and Tokar, 1985]. Equation (2.7) is analogous to the standard ion acoustic dispersion relation in a simple electron-ion plasma (where $V_s = \omega_{pi} \lambda_{De}$) [Chen, 1984]. In that case there is an additional term associated with the ion thermal speed, which here is replaced by V_{tc} , the cool electron thermal speed. We note in passing that the adiabatic behaviour, with the ratio of the specific heat capacities, $\Upsilon = 3$, comes out naturally from the kinetic-theoretical calculation. This Υ should not be confused with the growth rate, γ , discussed in this work. Expression (2.7) also shows that the phase velocity ω/k is modified by the hot electron parameters (through the hot electron κ -dependent Debye length, $\lambda_{\kappa h}$).

We note that for typical parameters of interest below, and appropriate for much of Saturn's magnetosphere, with n_{c0} and n_{h0} of similar magnitude and $T_h \gg T_c$, it follows that $\lambda_{\kappa h} \gg \lambda_{Dc}$, and thus, while satisfying $k\lambda_{Dc} \ll 1$, it is possible to consider the effect of the additional constraints $k\lambda_{\kappa h} \ll 1$ and $k\lambda_{\kappa h} \gg 1$ on the dispersion relations (2.6) and (2.7). The latter region should possibly be more correctly designated the ‘‘intermediate wavelength’’ region, as k satisfies $k\lambda_{\kappa h} \gg 1 \gg k\lambda_{Dc}$.

We first consider the constraint $k\lambda_{\kappa h} \ll 1$ in the long wavelength regime (with $k\lambda_{Dc} \ll 1$). Here, Eq. (2.7) reduces to the form

$$\omega_r^2 = k^2(V_{s\kappa}^2 + 3V_{tc}^2), \quad \text{or} \quad \omega_r^2 = \omega_{pc}^2(k^2\lambda_{\kappa h}^2 + 3k^2\lambda_{Dc}^2). \quad (2.10)$$

In the limit $\kappa_h \rightarrow \infty$, $V_{s\kappa} \rightarrow C_{se}$, and therefore Eq. (2.10) reduces to the usual long wavelength dispersion relation for EAWs in a plasma with Maxwellian electrons [Gary and Tokar, 1985]. Equation (2.10) also indicates, significantly, that in this long wavelength regime [with $V_{tc} \ll V_{s\kappa}$ in Eq. (2.10)], the EAWs are dispersionless and all wavelengths or frequencies propagate at the same acoustic speed, $V_{s\kappa}$.

On the other hand, in the case of intermediate wavelengths, imposing the constraint

$k\lambda_{\kappa h} \gg 1$ in the numerator of Eq. (2.6), the dispersion relation yields the result of Mace *et al.* [1999]:

$$\omega_r^2 = \omega_{pc}^2 \left(\frac{1 + 3k^2\lambda_{Dc}^2}{1 + 1/k^2\lambda_{\kappa h}^2} \right), \quad (2.11)$$

which, in the limit $\kappa_h \rightarrow \infty$, reduces to the dispersion relation of Gary and Tokar [1985] for a double Maxwellian plasma (see also Mace and Hellberg [1990]). Equations (2.6) and (2.11) show that the EAW is essentially a cool electron oscillation screened by the hot electrons, with a screening factor given by $(1 + 1/[k^2\lambda_{\kappa h}^2])^{-1}$. Moreover, although we have assumed that the cool electrons are kappa-distributed, we note from (2.11) that their dynamical contribution is identical to that found in the Maxwellian case, at least within the limits of the approximations leading to Eqs. (2.6)–(2.11).

Further, if we consider even larger k values, and apply the constraint $k\lambda_{\kappa h} \gg 1$ to the denominator of Eq. (2.7) [or in both the numerator and denominator of Eq. (2.6)], then the hot electron Debye screening is eliminated, and these equations show that the EAW mode reduces to a Langmuir-like mode of the cool electrons with dispersion relation [Krall and Trivelpiece, 1989]

$$\omega_r^2 = \omega_{pc}^2 + 3k^2V_{tc}^2 \quad \text{or} \quad \omega_r^2 = \omega_{pc}^2 (1 + 3k^2\lambda_{Dc}^2), \quad (2.12)$$

Thus, in this short wavelength regime with $\lambda \ll \lambda_{\kappa h}$, the hot electron Debye shielding is insufficient, and the effects of the excess superthermal electrons associated with the κ -distributed hot and cool electrons are negligible.

In summary, we stress that the EAW branch has differing behaviour in the long wavelength regime, where it is essentially acoustic, with speed $V_{s\kappa}$ [see Eq. (2.10)], and the intermediate wavelength regime (with, $k\lambda_{\kappa h} \gg 1$, but $k\lambda_{Dc} \ll 1$) where it behaves essentially like a Langmuir mode of the cool electrons [Gary and Tokar, 1985], see Eqs. (2.11) and (2.12).

Secondly, we draw attention to the fact that the analytical theory has concentrated on finding ω_r . The complicated expression for the damping rate is not transparent even after taking approximations, but may be found in Appendix B.1.

Finally, we note that, above the EAW frequency range ($\omega_{pi} < \omega_r < \omega_{pe}$), one finds the normal electron plasma wave (EPW), in which all the electrons play a role, and satisfying

$\omega_r/k \gg V_{th} \gg V_{tc}$. It can easily be shown that the dispersion relation of the EPW in a two-electron plasma is given, using appropriate approximations, by

$$1 - \left(\frac{\omega_{pc}^2}{\omega^2} + 3k^2 \frac{V_{tc}^2 \omega_{pc}^2}{\omega^4} \right) - \left(\frac{\omega_{ph}^2}{\omega^2} + 3k^2 \frac{V_{th}^2 \omega_{ph}^2}{\omega^4} \right) = 0.$$

With $\omega_{pe}^2 = \omega_{pc}^2 + \omega_{ph}^2$, and in terms of $k\lambda_{Dc}$, the above expression becomes

$$1 - \frac{\omega_{pe}^2}{\omega^2} - 3k^2 \lambda_{Dc}^2 \frac{\omega_{pe}^2}{\omega^2} \left\{ \frac{\omega_{pc}^4}{\omega_{pe}^4} + \frac{\lambda_{Dh}^2}{\lambda_{Dc}^2} \frac{\omega_{ph}^4}{\omega_{pe}^4} \right\} = 0.$$

The term in curly brackets can be simplified to give

$$(1-f)^2 \left[1 + \frac{f\beta}{(1-f)} \right] = 1 + f[(1-f)\beta - (2-f)],$$

where $f = n_{h0}/n_{e0}$ is the fraction of the hot electron equilibrium density, and $\beta = T_h/T_c$ is the ratio of the hot to cool electron temperatures. Thus the above approximate dispersion relation for the EPWs is given by

$$\omega^2/\omega_{pe}^2 = 1 + 3k^2 \lambda_{Dc}^2 \{1 + f[(1-f)\beta - (2-f)]\} \quad \text{or}$$

$$\omega^2 = \omega_{pe}^2 (1 + 3k^2 \lambda_{Dc}^2) + 3k^2 \lambda_{Dc}^2 \omega_{pe}^2 f[(1-f)\beta - (2-f)]. \quad (2.13)$$

In terms of the cool and hot electron thermal velocities V_{tc} and V_{th} , Eq. (2.13) is simply

$$\omega_r^2 = \omega_{pe}^2 + 3(n_{c0}/n_{e0})k^2 V_{tc}^2 + 3(n_{h0}/n_{e0})k^2 V_{th}^2. \quad (2.14)$$

This approximate dispersion relation for EPW is thus independent of κ_h and κ_c , as expected from earlier studies of single-electron κ -plasmas [Mace and Hellberg, 1995].

In Fig. 2.1 we compare the analytical results following from Eqs. (2.6)–(2.13) with the analytical solution of Eq. (2.2) without approximations. The exact numerical results are depicted by solid (black) curves in the figure. We choose a plasma system with parameters $\beta = 98.04$, $f = 0.462$, $\kappa_c = 2.1$ and $\kappa_h = 4$, corresponding to a radial distance of about $13.1 R_S$ in Saturn's magnetosphere. The approximate dispersion relation for EAWs, given

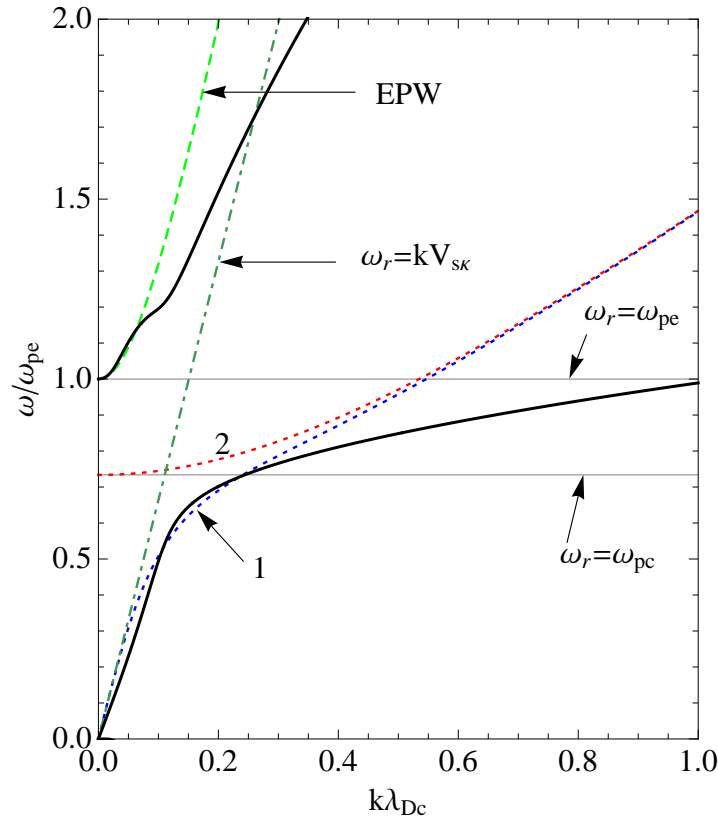


Figure 2.1: Figure showing the analytical results discussed above, applied to a plasma system with parameters $\beta = 98.04$, $f = 0.462$, $\kappa_c = 2.1$ and $\kappa_h = 4$, corresponding to a radial distance of about $13.1 R_S$ in Saturn's magnetosphere. The dotted (blue) curve, labelled 1, is given by Eq. (2.10) while the dotted (red) curve, labelled 2, which is the Langmuir-like branch of the cool electrons, is given by Eq. (2.12). The associated numerical results are shown by the solid (black) curves.

by Eq. (2.6), is indicated by the dotted blue curve, labelled 1: it is approximate to $\omega_r = kV_{s\kappa}$ (dot-dashed curve) in the small wavenumber limit [for $k\lambda_{\kappa h} \ll 1$ and $V_{tc} \ll V_{s\kappa}$ (see Eq. (2.10))], and is equivalent to the Langmuir-like branch of the cool electrons [dotted red curve (starting at ω_{pc} and labelled 2), given by Eq. (2.12)] for large wavenumbers. The approximate dispersion relation for the EPW, given by Eq. (2.13), is shown by the long dashed (green) curve. In the case of the EPW we see that the two sets of results agree well for small $k\lambda_{De}$ values only ($k\lambda_{De} < 0.1$), while for large $k\lambda_{De}$, the analytical results overestimate the frequencies. Similarly, the EAW case shows that the deviation in the frequency predicted by the analytical approximations and numerical results is minimal for low $k\lambda_{De}$ but steadily increases beyond $k\lambda_{De} \sim 0.4$.

2.5 Numerical Solutions

Here we return to the full dispersion relation, Eq. (2.2), and choose the following normalization: the density is normalized to the total electron equilibrium density n_{e0} , where the latter is equal to the sum of the hot and cool electron equilibrium densities n_{h0} and n_{c0} . The frequency ω is normalized to the electron plasma frequency $\omega_{pe} = (n_{e0}e^2/\varepsilon_0m_e)^{1/2}$, and the temperature and spatial parameter are normalized to the cool electron temperature T_c and Debye length λ_{Dc} , respectively. With this choice of normalization, we write Eq. (2.2) in the form

$$D(k, \omega) = 1 - f\mathcal{Z}'(\kappa_c; \xi_c) + (af/\beta)\mathcal{Z}'[\kappa_h; (a/\beta)^{1/2}\xi_c] + b\mathcal{Z}'[\kappa_i; (bm_i/m_e)^{1/2}\xi_c] - (1-f)(2-3/\kappa_c)k^2\lambda_{Dc}^2 = 0, \quad (2.15)$$

where $\mathcal{Z}'(\kappa_\alpha; \xi_\alpha)$ is defined by Eq. (2.5); $m_i(m_e)$ is the ion (electron) mass; $f = n_{0h}/n_{0e}$ is the fraction of the hot electron equilibrium density; $\beta = T_h/T_c$ is the fractional hot electron temperature, and the normalized complex phase velocity of the cool electrons ξ_c is related to the normalized frequency (ω/ω_{pe}) by $\omega/\omega_{pe} = [(1-f)(2-3/\kappa_c)]^{1/2}(k\lambda_{Dc})\xi_c$, using the relation $\xi_c = \omega/k\theta_c$. The constants a and b in Eq. (2.15) are given, respectively, by $a = \kappa_h(\kappa_c - 3/2)/[\kappa_c(\kappa_h - 3/2)]$ and $b = \kappa_i(\kappa_c - 3/2)/[\kappa_c(\kappa_i - 3/2)T_c/T_i]$. For numerical purposes we have assumed the mass ratio, $m_i/m_e = 1836$, the normalized ion temperature, $T_i/T_c = 10^{-3}$, and also used $\kappa_i = 50$.

We shall next describe a numerical study of Eq. (2.15) – first a parameter survey relevant to Saturn data, and then a study of wave behaviour in each of the three regions of Saturn’s magnetosphere.

In obtaining full solutions to the dispersion relation in Eq. (2.15), the following steps are followed:

- (i) We fix the spectral indices κ_c and κ_h , and the density and temperature ratios f and β , respectively.
- (ii) We then assign a non-zero value to the normalized wave number $k\lambda_{Dc}$, and solve for the complex argument $\xi_c = \xi_c(\omega)$ that satisfies the simultaneous equations $D_r(k, \omega) = 0$

and $D_i(k, \omega) = 0$, where here we have

$$\begin{aligned}
 D_r(k, \omega) &= 1 - f \mathcal{Z}'_r(\kappa_c; \xi_c) + (a f / \beta) \mathcal{Z}'_r[\kappa_h; (a/\beta)^{1/2} \xi_c] + b \mathcal{Z}'_r[\kappa_i; (b m_i / m_e)^{1/2} \xi_c] \\
 &\quad - (1 - f) (2 - 3/\kappa_c) k^2 \lambda_{Dc}^2 = 0, \quad \text{and} \\
 D_i(k, \omega) &= -f \mathcal{Z}'_i(\kappa_c; \xi_c) + (a f / \beta) \mathcal{Z}'_i[\kappa_h; (a/\beta)^{1/2} \xi_c] \\
 &\quad + b \mathcal{Z}'_i[\kappa_i; (b m_i / m_e)^{1/2} \xi_c] = 0,
 \end{aligned}$$

and subscripts r and i refer to the real part and imaginary part, respectively. Note here that ξ_h and ξ_i are expressed in terms of ξ_c as made explicit in Eq. (2.15). This process normally leads to a series of solutions of ξ_c , including the principal mode solution and high-order mode solutions. In essence we determine the zero-level contours of $D_r(k, \omega)$ and $D_i(k, \omega)$.

(iii) Each solution obtained in step (ii) is used as an initial guess for a root of the full function $D(k, \omega)$, at the same assigned value of $k\lambda_{Dc}$. A Mathematica root finder is then used to accurately obtain the root ξ_c , from which we obtain the complex frequency $\omega = k\theta_c \xi_c$. Iterating this procedure over a sequence of values of $k\lambda_{Dc}$ we obtain the dispersion relation $\omega = \omega(k)$ and the damping rate $\gamma = -\text{Im}(\omega)$.

In this model, the solutions described here are either ‘‘acoustic-like’’ (with zero frequency ω at $k\lambda_{Dc} = 0$) or ‘‘Langmuir-like’’ (with frequency $\omega = \omega_{pe}$ at $k\lambda_{Dc} = 0$). Note that we have normalized ω with the electron plasma frequency ω_{pe} . Thus, for the cool ‘‘Langmuir-like’’ wave mode the normalized frequency equals $\sqrt{n_{c0}/n_{e0}} = \sqrt{1 - f}$ at $k = 0$.

(iv) The solutions, obtained from (iii), with the least damping rate (low $|\gamma(k)|$ values) are then considered to be normal modes. Depending on the plasma composition, the value of ξ_c corresponding to the principal mode (ξ_c value with lowest imaginary term) normally gives the least damped Langmuir wave mode (or electron plasma wave) solution while one of the higher-order modes (with relatively low imaginary value) gives the least damped ‘‘acoustic-like’’ wave mode. For some plasma compositions though, the principal value of ξ_c may give the ‘‘acoustic-like’’ solution while the Langmuir wave mode solution is given by one of the higher-order modes.

An example showing the various solutions of ξ_c for a fixed $k\lambda_{Dc}$ and a given plasma composition is shown in Fig. 2.2 (left panel), obtained for the parameters: $\beta = 10$, $f =$

0.35, $\kappa_c = 1.8$, $\kappa_h = 7$ and $\kappa_i = 50$, with normalized wavenumber $k\lambda_{Dc} = 1$. The dotted (red) curves correspond to the solutions of $D_r(k, \omega) = 0$ while the continuous (blue) curves correspond to the solutions of $D_i(k, \omega) = 0$. Thus for $k\lambda_{Dc} = 1$ used here, the initial guesses of ξ_c are obtained at the points of intersection of the dotted (red) and continuous (blue) curves. In this particular example, the principal mode is labeled P while the higher-order modes are labeled 1, 2, 3 and 4, depending on how far the solutions are located from the $\text{Re}(\xi_c)$ axis, that is, as $|\text{Im}(\xi_c)|$ increases. Note that other sets of curves (or solutions) can be obtained far below $\text{Re}(\xi_c) = -30$, but these have not been considered as they lead to strongly damped wave modes.

In the right panel of Fig. 2.2 we show the full solutions to Eq. (2.15), obtained by using the ξ_c estimates in the left panel and varying $k\lambda_{Dc}$ from $1.0 \rightarrow 0.00001$, for example. The figure indicates that the principal mode is the Langmuir wave, and the higher-order modes are acoustic-like wave modes. The frequency (ω/ω_{pe}) is shown on the positive ordinate-axis while the damping rate ($\gamma/\omega_{pe} < 0$) is shown on the negative ordinate axis. Considering the steepness of the damping rate curves, one sees that the higher order modes labeled 2 – 4 show rapid increase of damping rate as $k\lambda_{Dc}$ is increased compared to the one labeled 1. Thus, if there were an external source of free energy to the plasma system, the principal mode and the first higher-order mode solutions could be possible candidates for weakly damped or growing waves for observation. In the right panel of Fig. 2.2, the dashed curves have $1/|\gamma| < 2\pi/\omega_r$ (implying strong damping) while the continuous curves have $1/|\gamma| > 2\pi/\omega_r$, the latter denoting modes that are sufficiently weakly damped to be called observable.

In order not to overcrowd the graphs for the results presented in Sections 2.6 and 2.7, we have only included the “least damped” mode solutions arising from the principal value of ξ_c and one of the higher-order mode solutions. However, for a few cases of results we have also included solutions corresponding to other higher-order modes.

2.6 Results: Effects of Density, Temperature and Spectral Index

From the analytical results in Sec. 2.4 [Eq. (2.6)], we see that the normalized frequency is affected by a number of plasma parameters, and hence it can be expressed in the form,

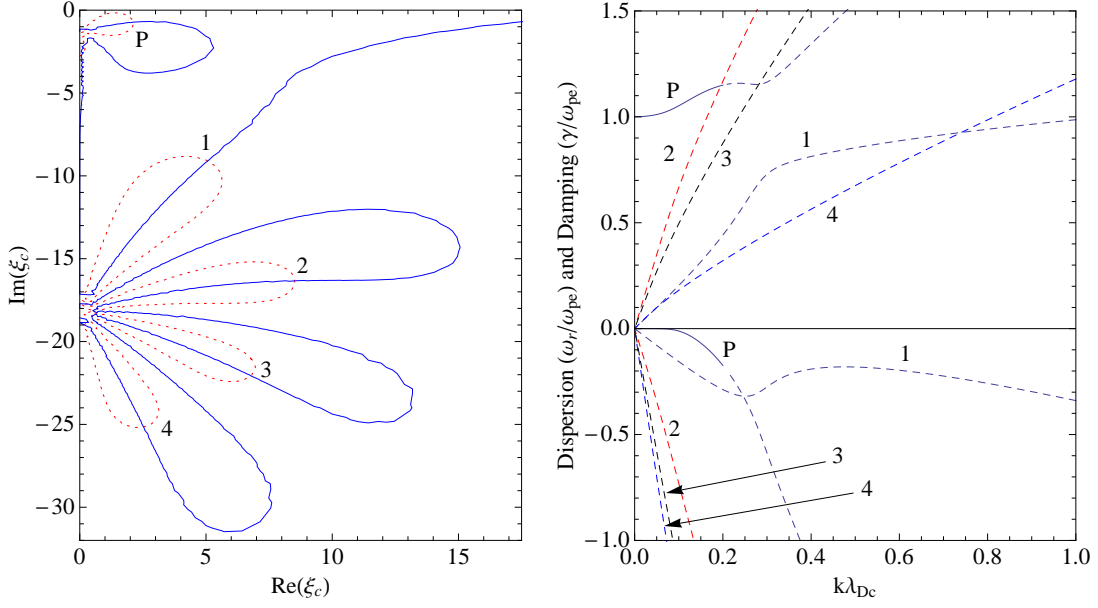


Figure 2.2: *Left panel:* A graph showing $\xi_c = \text{Re}(\xi_c) + i \text{Im}(\xi_c)$ satisfying both $D_r(k, \omega) = 0$ (dotted red curve) and $D_i(k, \omega) = 0$ (continuous blue curve) for $k\lambda_{Dc} = 1$. Other parameters used are: $\beta = 10$, $f = 0.35$, $\kappa_c = 1.8$, $\kappa_h = 7$ and $\kappa_i = 50$. The values of ξ_c are obtained from the points of intersection between the dotted (red) and continuous (blue) curves. *Right panel:* Dispersion and damping rate curves corresponding to the initial estimates of ξ_c for a plasma system with parameters as in the left panel graph. Two distinct solutions are shown: the Langmuir wave, corresponding to the principal value of ξ_c , and the “acoustic wave” modes, corresponding to the higher-order modes, which are damped. In the right panel, the dashed curves imply strong damping ($1/|\gamma| < 2\pi/\omega_r$) while the continuous curves denote modes that are sufficiently weakly damped to be called observable, since $1/|\gamma| > 2\pi/\omega_r$ in those cases.

$\omega_r/\omega_{pe} \equiv \omega_r/\omega_{pe}(k\lambda_{Dc}; \kappa_h; T_h/T_c; n_{h0}/n_{e0})$. Likewise, the normalized damping rate, from Eq. (B.16), is formally a function of

$$\frac{\gamma}{\omega_{pe}} \equiv \frac{\gamma}{\omega_{pe}} \left(k\lambda_{Dc}; \kappa_c; \kappa_h; \frac{T_h}{T_c}; \frac{T_i}{T_c}; \frac{n_{h0}}{n_{e0}}; \frac{m_i}{m_e} \right).$$

Since the ratios T_i/T_c and m_i/m_e are fixed we do not focus on the dependence of ω_r and γ on these parameters. Instead we investigate the behaviour of the EAW as the plasma parameters such as the spectral index of each of the electron components, the fractional density of electron species, and the temperature ratio of the two electron components are varied. Based on typical Saturn data, we have, in this section, carried out a parameter survey for EAWs in a plasma with a hard electron spectrum (low spectral indices) using Eq. (2.15), to investigate the effect of the parameters listed above on the resulting wave

modes supported by the plasma system.

As we have noted above, it is difficult to extract any useful information about damping rates from the approximate analytic theory, and thus the numerical solution of the full equation is vital for such studies. For the dispersion or damping curves in Figs. 2.3–2.12, dashed curves imply that the waves are strongly damped ($|\gamma| > \omega_r/2\pi$), while continuous parts indicate regions of weaker damping, with $|\gamma| < \omega_r/2\pi$, and in the presence of an external free energy source (such as a beam) the latter may grow to significant amplitudes.

In Figures 2.3–2.6, the dispersion curves (ω/ω_{pe}) are shown on the left panel while the damping rates (γ/ω_{pe}) are on the right panel of each figure, respectively, both expressed as functions of the wavenumber $k\lambda_{Dc}$. Note that the frequency ω_r and damping rate γ are normalized to the electron plasma frequency ω_{pe} while the wave number k is normalized to the reciprocal of the cool electron Debye length λ_{Dc} .

2.6.1 Effect of Electron Spectral Indices

In Figure 2.3 we illustrate the effect of varying the cool electron spectral index κ_c on the wave behaviour for fixed $\kappa_h = 4$, a temperature ratio $\beta = 100$, and a fractional hot density ratio, $f = 0.5$. We note first that the EPW solution shown in the left panel is a superposition of all the EPW solutions for the κ_c values ($2 \leq \kappa_c \leq 10$) used in this figure. Thus the figure shows that the EPW are weakly damped for small k , and their behaviour is independent of κ_c for small k , confirming the approximate solution, Eq. (2.12).

On the other hand, the electron acoustic branch is strongly damped in the low wavenumber regime (here, $k\lambda_{Dc} < 0.12$), but like the EPW, its phase velocity in this region is independent of κ_c , confirming the approximate analytic equations (2.8) and (2.10).

In contrast, for intermediate wavenumbers, the cool Langmuir region of the EA-branch is weakly damped for all κ_c , and in this range increasing κ_c slightly increases the wave frequency over which these EAWs are weakly damped above the “knee” at ω_{pc} , contrary to the analytic theory, which predicts that κ_c has no effect on the dispersion of EAWs in this range. Though this effect is significant for large wavenumbers, the EAWs are too strongly damped in that range to be observable.

In the right panel of Figure 2.3, we consider the damping rate of the weakly damped EA-branch for fixed $\kappa_h = 4$. We see that for intermediate values of wavenumbers (in the

region where the criterion $1/|\gamma| > 2\pi/\omega_r$ is satisfied), an increase in the superthermal particle excess of the cool component, *i.e.*, a decrease in the value of κ_c , gives rise to increased damping as compared to what is found for cool electron distributions closer to a Maxwellian distribution (e.g., $\kappa_c = 10$). However, the range in wavelengths that are more weakly damped is not significantly affected by κ_c . This observation also applies to Fig. 2.4 (see later), with fixed $\kappa_c = 2$ where we now vary κ_h . Therefore in the weakly damped regime (with $1/|\gamma| > 2\pi/\omega_r$), EAWs with more non-Maxwellian particles (low κ values) are more damped than those with a small proportion of non-Maxwellian particles (with relatively high κ values).

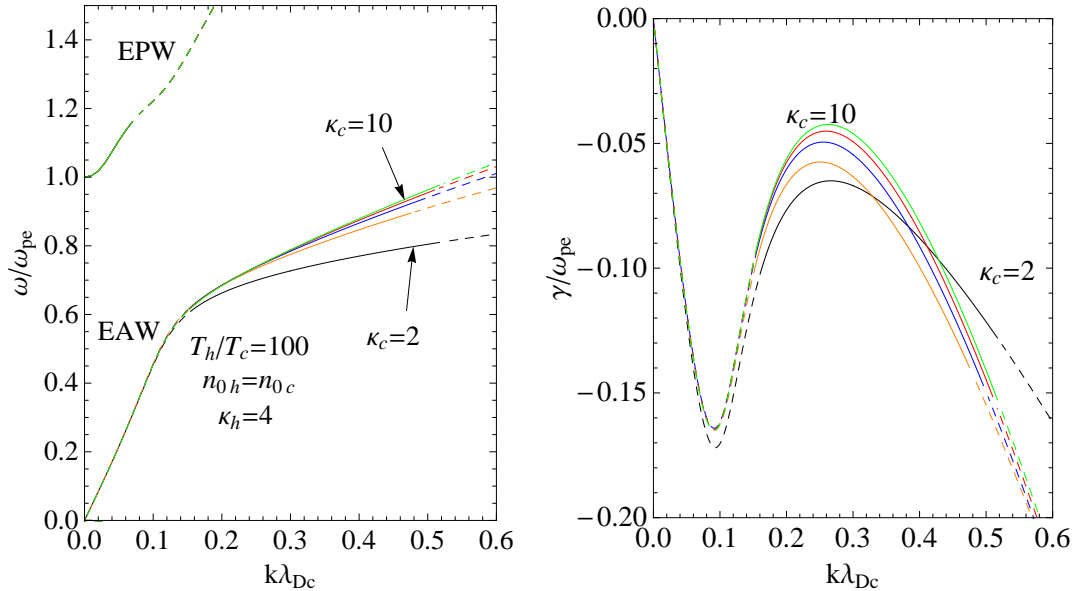


Figure 2.3: Dispersion and damping curves showing the effect of cool electron kappa indices, κ_c , for $\beta = 100$, $n_{0c} = n_{0h}$, $\kappa_h = 4$. Values of κ_c used are: $\kappa_c = 2$ (black, bottom), $\kappa_c = 4$ (orange), $\kappa_c = 6$ (blue), $\kappa_c = 8$ (red), and $\kappa_c = 10$ (green, top), respectively. As in Fig. 2.2 (right panel), the dashed curves have $1/|\gamma| < 2\pi/\omega_r$ (implying strong damping) while the continuous curves have $1/|\gamma| > 2\pi/\omega_r$, the latter denoting modes that are sufficiently weakly damped to be called observable. This (dashing) pattern also applies to Figs. 2.4–2.12. Note that for the sake of not overcrowding the graph, the damping curves (in the right panel) corresponding to the EPW modes are not shown, thus the results presented (in the right panel) are only for the EAW-like modes. This also applies to the damping curves in Figs. 2.4–2.7, unless otherwise specified.

In Fig. 2.4 we show a similar study as in Fig. 2.3, here varying κ_h , for fixed $\kappa_c = 2$. In this case we see a dependence of the frequency of the EPW mode on the hot electron κ value, which is particularly strong near $\kappa_h = 2$. This reflects the numerical results for EPW in a single-electron plasma [Mace and Hellberg, 1995], as opposed to the analytic

approximation, Eq. (2.13). In addition, the EPW branch shows coupling behaviour as κ_h becomes small, where it behaves as a Langmuir wave for low wavenumbers while for intermediate wavenumbers it shows behaviour similar to the Langmuir-like region of the EAW branch.

The phase speed of the strongly-damped acoustic region of the EAW branch shows similar κ_h dependence that is pronounced near $\kappa_h = 2$. This is to be expected because in the acoustic region $\omega_r \sim kV_{s\kappa}$ and $V_{s\kappa}$ is strongly κ_h -dependent [see Eq. (2.8)]. Varying κ_h near $\kappa_h = 2$ has a significant effect on the weakly damped range in k of the intermediate wavelength regime, which is cool Langmuir-like. In particular, one sees (see right panel of Fig. 2.4 for details) that the range $0.28 \lesssim k\lambda_{Dc} \lesssim 0.44$ is weakly damped for $\kappa_h = 2$, but that increases to $0.15 \lesssim k\lambda_{Dc} \lesssim 0.52$ for $\kappa_h = 4$ and changes little for larger κ_h values. The latter figure (Fig. 2.4) also shows that the strongly non-Maxwellian case, $\kappa_h = 2$, is much more strongly damped than one finds for large κ_h .

We then observe that for large normalized wavenumbers (where the criterion $1/|\gamma| > 2\pi/\omega_r$ is not satisfied), apart from the strongly non-Maxwellian case (with $\kappa_c = 2$, $\kappa_h = 4$, as in Fig. 2.3 or $\kappa_c = \kappa_h = 2$, as in Fig. 2.4), the variation of κ_c in Fig. 2.3 or κ_h in Fig. 2.4 has no significant effect on the damping of the resulting wave modes.

In summary then, considering the weakly-damped region of the EAW branch at intermediate wavelengths, we observe that the strongest effects of the excess superthermal particles associated with κ -distributions are centered on the extreme case $\kappa_h = 2$ of the hot electrons, where relatively large changes in damping occur. On the other hand, the increase of excess superthermal cool electrons with decreasing κ_c does have some effect on the dispersion of that EAW branch.

In all the cases the entire electron-acoustic mode (branch) shows the three distinct regimes described by Tokar and Gary [1984], and Gary and Tokar [1985]. These three regimes are:

(i) The acoustic regime which occurs for low wavenumbers (long wavelengths) with characteristic phase velocity of the order $v_\phi \approx v_{s\kappa} = \omega_{pc}\lambda_{\kappa h}$. In the case of Maxwellian electrons, the phase velocity is of the order $v_\phi \approx (n_{c0}/n_{h0})^{1/2}v_{th} = C_{se}$ [see Eq. (2.9)], where v_{th} is the thermal velocity of the hot electron component. In this regime, EAWs are strongly Landau damped by the hot electrons since $v_\phi \sim v_{th}$, as can be seen from Eq. (2.8). The

effect is most marked for low values of $\kappa_h > 3/2$. The cool electrons have no significant effect on the damping of these waves. This is illustrated by comparison of the EAW curves in Figs 2.3 and 2.4 for $k\lambda_{Dc} < 0.15$.

(ii) The second regime involves the cool Langmuir-like branch of the EAWs that are weakly damped, and occurs for intermediate values of wavenumbers ($0.15 < k\lambda_{Dc} < 0.55$). The range of wavenumbers (for weak damping) depends strongly on both the hot fraction of the total electron density ($f = n_{h0}/n_{e0}$) and the hot to cool electron temperature ratio $\beta = T_h/T_c$ [Hellberg *et al.*, 2000]. It also depends weakly on the value κ_h , essentially for low κ_h only, and does not depend on κ_c at all.

(iii) As the wavenumber increases beyond the intermediate values described in (ii) we enter a third regime where EAWs are strongly damped (by the cool electrons) as v_ϕ decreases and approaches v_{th} . Figures 2.3 and 2.4 show that in these two regimes the EAW dynamics depend more on the cool electron properties (spectral index) than on those of the hot electrons, and therefore the two regimes lie in the cold plasma region [Tokar and Gary, 1984]. In addition, the latter two regimes almost lie in the Langmuir-like region of the EAW branch, given by Eq. (2.12).

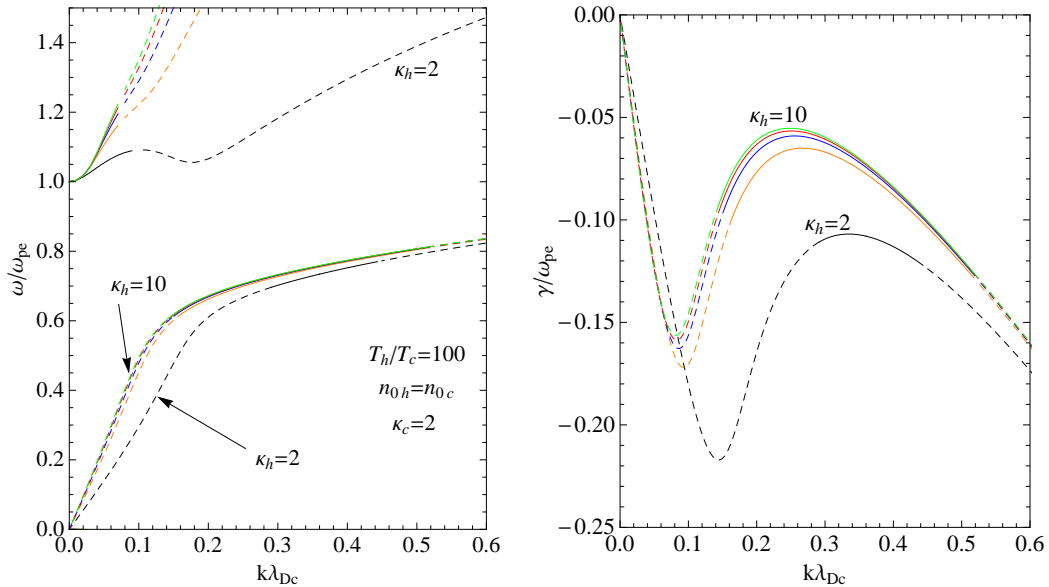


Figure 2.4: Same as in Fig. 2.3, but now for hot electron kappa indices, κ_h , with $\kappa_c = 2$.

2.6.2 Effect of Temperature Ratio

Figure 2.5 shows the effect of electron temperature ratio variation on the wave behaviour for a plasma system with fixed low kappa values ($\kappa_c = 2$ and $\kappa_h = 4$), and a density ratio of $f = 0.5$. Following from the analytical solution for the EPW [Eq. (2.13)], we see that the dispersion relation for low k depends on the temperature ratio, β . This behaviour is clearly illustrated in the left panel, where for low but fixed $k\lambda_{Dc}$, the frequency ω/ω_{pe} decreases with a decrease in β . In addition, we see that the EPWs are weakly damped over a much larger range of $k\lambda_{Dc}$ for low β values than for high β values. However, the corresponding range of frequencies over which the EPW is weakly damped remains fairly constant at $\omega_{pe} < \omega < 1.2\omega_{pe}$. We also note that for $\beta = 5$, the assumption $\lambda_{Dc} \ll \lambda_{\kappa h}$ is close to breaking down. The latter follows from the fact that $\lambda_{Dc} \ll \lambda_{\kappa h}$ requires $f \ll f_*$, where $1/f_* = 1 + [(\kappa_h - 1/2)/(\kappa_h - 3/2)]/\beta$ (see Appendix B.1), and for $\kappa_h = 4$, $\beta = 5$ we have $f_* \simeq 0.8$, which is close to $f = 0.5$ ($n_{0c} = n_{0h}$) used in Fig. 2.5.

In the case of EAWs for the fixed parameters above, the left panel of Fig. 2.5 shows that the wave frequency is strongly dependent on β , both in the long and the intermediate wavelength regimes. The waves are weakly damped for intermediate wavenumbers when $\beta > 25$ (see curves for $\beta = 50$ and 100), but are strongly damped for $\beta \leq 25$ over the entire range of wavenumbers considered. In the acoustic regime, the associated phase velocity ($\simeq V_{s\kappa}$) increases with β as predicted by Eq. (2.8). This illustrates that the first term of Eq. (2.8) is dominant. The right panel of Fig. 2.5 shows that in the “intermediate wavenumber regime”, EAWs are weakly damped for higher temperature ratios, and for a larger range of “wavenumbers” as compared to cases with low β values.

2.6.3 Effect of the Hot Electron Density Fraction

Figure 2.6 illustrates the effect of varying the hot electron density fraction, f , on the wave behaviour for a hot to cool electron temperature ratio, $\beta = 100$, and fixed indices $\kappa_c = 2$ and $\kappa_h = 4$.

The EAWs are weakly damped for intermediate wavenumbers ($k\lambda_{Dc}$) for $0.3 \leq f < 0.8$, with the potentially observable range in $k\lambda_{Dc}$ (exhibiting weak damping) decreasing as f increases. For all f , the EAW is strongly damped for low $k\lambda_{Dc}$, and the associated phase velocity ($\propto V_{s\kappa}$) decreases with increasing f , as may be expected from (2.8). However, for

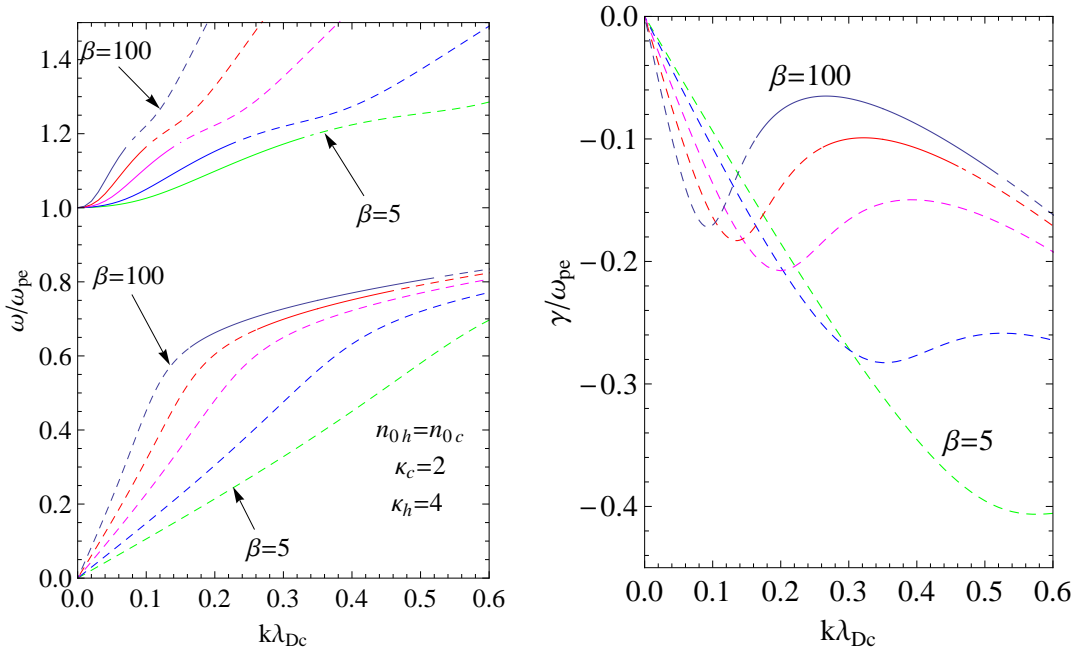


Figure 2.5: Same as in Fig. 2.3, here showing the effect of temperature ratios, $\beta = T_h/T_c$, for $n_{0c} = n_{0h}$, $\kappa_c = 2$, $\kappa_h = 4$. The parameter labeling the curves is β , which lies between $\beta = 100$ (light-blue) and $\beta = 5$ (green). Intermediate values of β are 50, 25 and 10, respectively.

$f \geq 0.8$, the EAW is strongly damped for the entire wave number range which contrasts with the Maxwellian case for the same parameters [Mace, 1991, Fig. 2.1, p18]. These results show that the behaviour of EAWs is greatly influenced by the density ratio, f .

On the other hand, the EPWs are weakly damped for low $k\lambda_{Dc}$ for all the values of f used here. The figure also shows that as f increases, the ranges of both wavenumber (in terms of $k\lambda_{Dc}$) and frequency over which the EPWs are weakly damped increases.

While the EPW and EAW are clearly two separate modes over the full range of $k\lambda_{Dc}$ for $f > 0.4$, it is seen that for the lowest values of f in this figure ($f = 0.3 - 0.4$), the EPW shows emerging signs of coupling with the cool Langmuir-like region of the EAW near the “knee”. This coupling effect is explored further in Fig. 2.7, which is an extension of Fig. 2.6, for very low hot electron fractional densities, $f = 0.1, 0.2$. In this figure there is strong coupling behaviour where the EPW makes contact with the Langmuir-like EAW at the “knee”, displaying characteristics of both EAWs and EPWs [Mace *et al.*, 1999]. The coupled EPW mode is weakly damped for a wide range of wavenumbers, from $k\lambda_{Dc} \simeq 0$ to well beyond values found for the simple EPW or EAW observed in Fig. 2.6. On the other hand, the acoustic branch of the EAW persists into the intermediate wavelength regime,

and is strongly damped for all $k\lambda_{Dc}$.

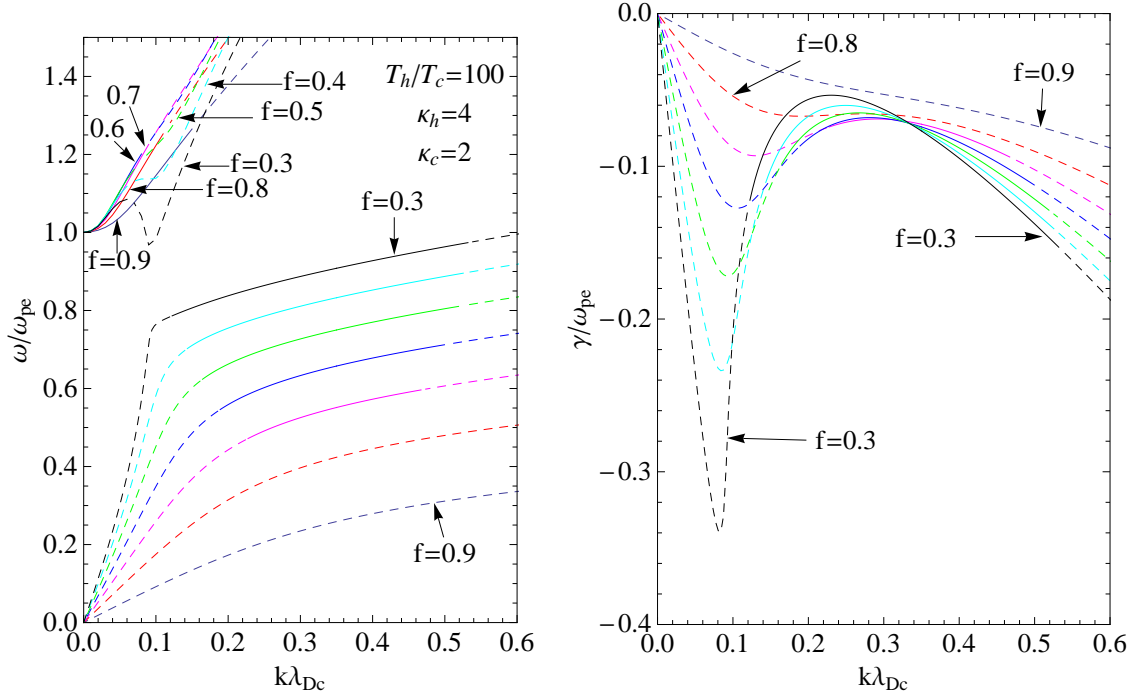


Figure 2.6: Same as in Fig. 2.3, here showing the effect of density variation, for $\beta = 100$, $\kappa_c = 2$, $\kappa_h = 4$. The parameter labeling the curves is the density ratio, $f = n_{0h}/n_{0e}$, ranging from $f = 0.9$ to $f = 0.3$, in intervals of 0.1.

2.7 Results: Application to Saturn's Magnetosphere

We solve Eq. (2.15) for parameter values which are typical of the three regions of the Saturn's magnetosphere: the inner magnetosphere (for radial distances $R \leq 9 R_S$), intermediate magnetosphere ($9 R_S < R < 13 R_S$) and the outer magnetosphere ($\geq 13 R_S$).

In Table 2.1 we list the parameter values, extracted from Fig. 3 of Schippers *et al.* [2008], where we have mainly used data values of the Cassini outbound trajectory, though similar results can be obtained using the inbound leg. We also point out that the temperatures in Table 2.1 and Figs. 2.8–2.12 are measured in energy units.

Figures 2.8–2.12 show the real frequency (ω_r/ω_{pe}) and damping rate (γ/ω_{pe}) as functions of $k\lambda_{Dc}$. The dispersion curves are those corresponding to the positive ordinate while the damping rate curves correspond to the negative ordinate. As in Figs. 2.3–2.7, the continuous (solid) lines correspond to weakly damped modes, which may be observable, since their damping time ($1/|\gamma|$) exceeds the plasma wave period ($2\pi/\omega_r$) [Mace and Hellberg, 1990]. On the other hand, the dashed curves do not satisfy this criterion, and as the waves

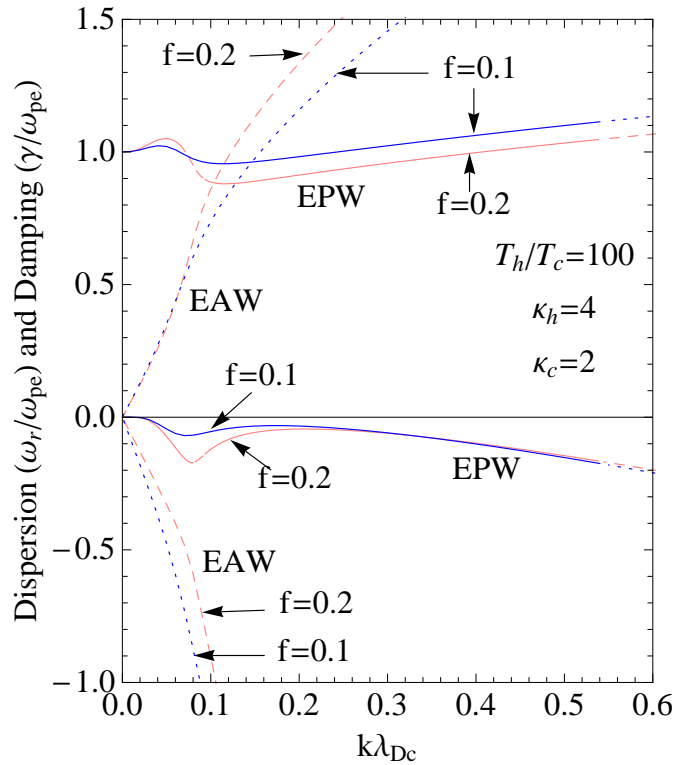


Figure 2.7: Same as in Fig. 2.6, here for $f = 0.1$ (blue) and $f = 0.2$ (red), respectively, with dispersion on the positive ordinate axis and damping on the negative ordinate axis.

are strongly damped, those modes will almost certainly not be observable.

Figure 2.8 shows the wave behaviour of both the EPW and the EAW, following from the full dispersion relation (2.2), for parameter values (see Table 2.1) corresponding to Saturn's outer magnetosphere [Schippers *et al.*, 2008] at $R = 13.1 R_S$ (left panel) and $R = 14 R_S$ (right panel), respectively. In the figure we have also included the analytical approximation, Eq. (2.6), to the EAW (dotted curves). The figure shows that in both cases ($R = 13.1 R_S$ and $14 R_S$), the EPW is weakly damped for low wavenumbers, *viz.*, $k\lambda_{Dc} \lesssim 0.08$ ($R = 13.1 R_S$) and $k\lambda_{Dc} \lesssim 0.12$ ($R = 14 R_S$), respectively. Considering the EAW, the figure shows that, as expected, the wave is weakly damped for intermediate $k\lambda_{Dc}$, but not for low or high $k\lambda_{Dc}$. In addition, the range in wavenumber over which EAWs are weakly damped is larger for data values corresponding to $R = 13.1 R_S$, where the hot fractional density and temperature ratios are significantly larger than is the case at $R = 14 R_S$. This applies particularly to the damping. Though the analytic solutions to the EAW approximate the numerical results reasonably well in the small wavenumber range, they differ quite significantly from the latter for large wavenumbers. The deviation

R (R_S)	κ values		temperatures (eV)		densities (cm^{-3})		β	f
	κ_c	κ_h	T_c	T_h	n_c	n_h		
5.4	8.0	3.0	1.8	300	10.5	0.02	166.7	0.002
6.3	2.3	3.0	2.0	400	10.5	0.01	200.0	0.001
7.0	1.8	4.0	9.0	1000	10.5	0.20	111.1	0.02
9.8	2.0	4.0	8.0	1100	2.5	0.07	137.5	0.027
11.4	2.0	3.7	8.0	1500	0.9	0.11	187.5	0.11
12.0	2.0	3.5	6.0	1200	1.00	0.11	200	0.10
12.5	1.8	4.0	20.0	1100	0.45	0.15	55.0	0.25
13.1	2.1	4.0	10.2	1000	0.21	0.18	98.0	0.46
13.8	1.6	4.0	30	900	0.40	0.15	30.0	0.27
14.0	2.1	6.0	30	900	0.15	0.10	30.0	0.40
14.3	1.8	8.0	70	800	0.30	0.20	11.4	0.40
15.0	2.0	6.0	40	1000	0.20	0.10	25.0	0.33
15.2	2.0	4.0	70	900	0.25	0.10	12.9	0.29
16.0	1.9	3.5	35	800	0.08	0.07	22.9	0.47
16.8	1.8	3.8	30	900	0.15	0.08	30.0	0.35
17.3	2.0	3.5	25	1000	0.15	0.07	40.0	0.32
17.8	1.9	3.8	28	1000	0.15	0.07	35.7	0.32

Table 2.1: Table showing parameter estimates from Fig. 3 of Schippers *et al.* [2008], corresponding to radial distances (R) in Saturn’s magnetosphere, here used in Figs. 2.8–2.12, with $\beta = T_h/T_c$ and $f = n_{h0}/n_{e0}$.

in dispersion results observed for low $k\lambda_{Dc}$ may be attributed to the fact that the analytic approximation is independent of the cool electron spectral index κ_c , which is not the case with the full solution given by the numerical approach. Results similar to those shown in Fig. 2.8 are given in Fig. 2.9, corresponding to radial distances of $15.0 R_S$ (left panel) and $17.8 R_S$ (right panel), respectively (see Table 2.1 for parameters). Here, as in Fig. 2.8, the EAWs are weakly damped for intermediate wavenumbers, and are strongly damped for low $k\lambda_{Dc}$. However, the EPW shows some coupling behaviour at these larger radial distances where the fraction of cool electrons exceeds 0.65.

In Table 2.2 below we show the wavelengths, $\lambda(\text{m})$, and frequencies, $f(\text{kHz})$, corresponding to the EAW and EPW modes for the radial distances where the former are weakly damped. The wavelengths are obtained from the expression

$$\lambda(\text{m}) = \frac{2\pi}{k\lambda_{Dc}} \left[\frac{\varepsilon_0(\text{C}^2\text{N}^{-1}\text{m}^{-2})}{e^2(\text{C}^2)} \right]^{1/2} \left[\frac{K_B T_c(\text{J})}{n_{c0}(\text{m}^{-3})} \right]^{1/2},$$

where $k\lambda_{Dc}$ is the (dimensionless) normalized wavenumber that can be read from the

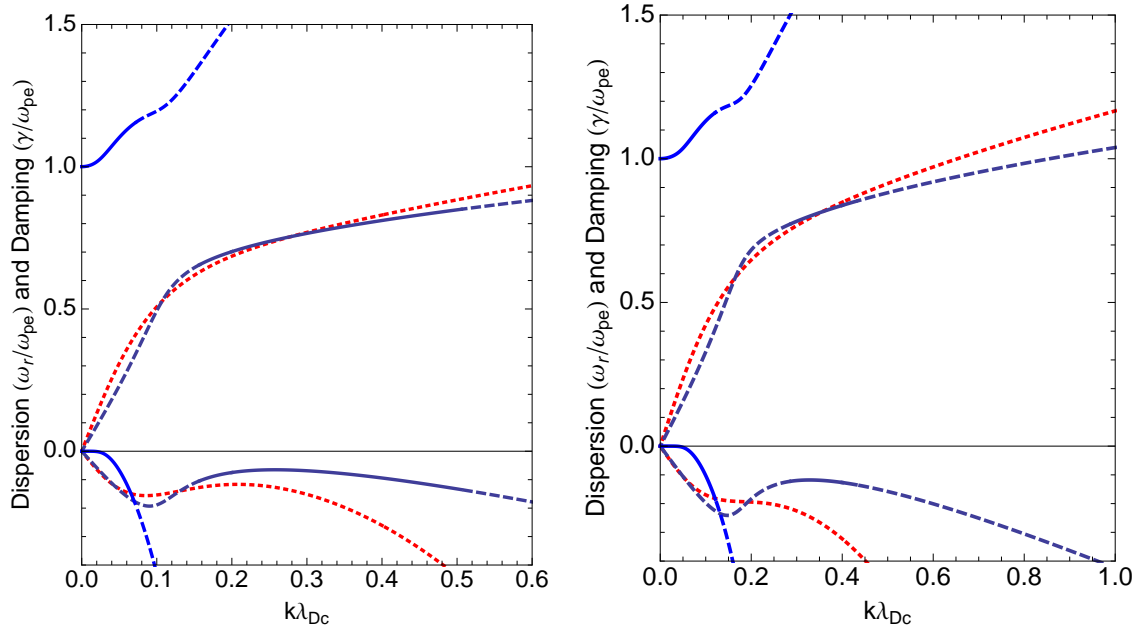


Figure 2.8: Dispersion (ω_r/ω_{pe}) and damping (γ/ω_{pe}) versus $k\lambda_{Dc}$ for parameters corresponding to the Saturnian magnetosphere. *Left panel:* at about $13.1 R_S$, with parameters $n_{0c} = 0.21 \text{ cm}^{-3}$, $n_{0h} = 0.18 \text{ cm}^{-3}$, $T_c = 10.2 \text{ eV}$, $T_h = 1000 \text{ eV}$, $\kappa_c = 2.1$, $\kappa_h = 4$. *Right panel:* at about $14 R_S$, with parameters $n_{0c} = 0.15 \text{ cm}^{-3}$, $n_{0h} = 0.1 \text{ cm}^{-3}$, $T_c = 30 \text{ eV}$, $T_h = 900 \text{ eV}$, $\kappa_c = 2.1$, $\kappa_h = 6$. Analytical results [from Eq. (2.6) and (B.16)] are shown in red, which for small $k\lambda_{Dc}$ agree with the numerical solution to some extent.

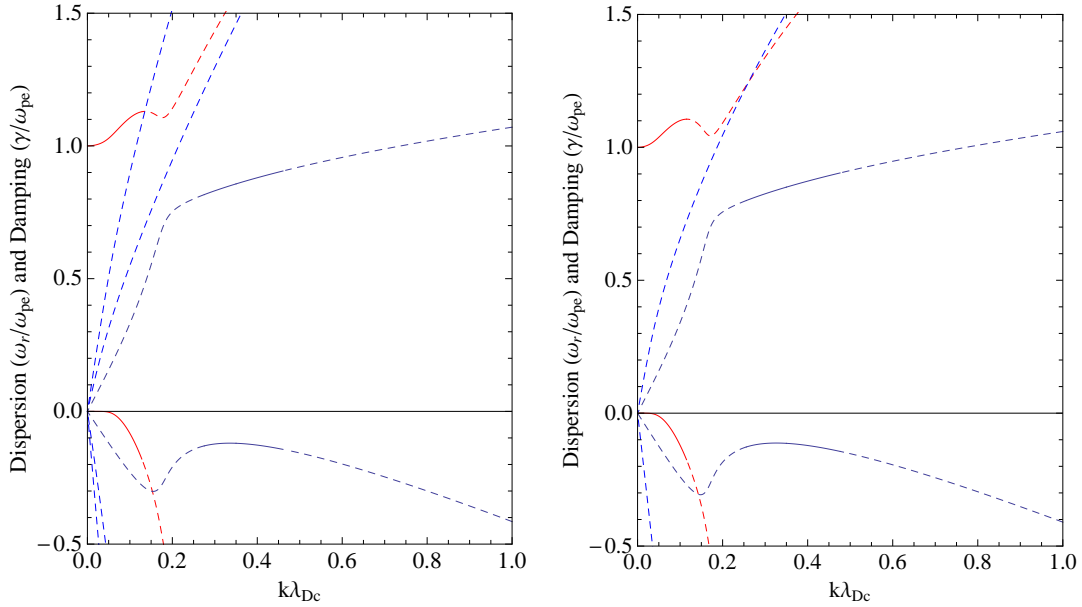


Figure 2.9: Same as in Fig. 2.8, *Left panel:* at about $15 R_S$ with parameters, $n_{0c} = 0.2 \text{ cm}^{-3}$, $n_{0h} = 0.1 \text{ cm}^{-3}$, $T_c = 40 \text{ eV}$, $T_h = 1000 \text{ eV}$, $\kappa_c = 2.0$, $\kappa_h = 6.0$. *Right panel:* at about $17.8 R_S$, with parameters: $n_{0c} = 0.15 \text{ cm}^{-3}$, $n_{0h} = 0.08 \text{ cm}^{-3}$, $T_c = 28 \text{ eV}$, $T_h = 950 \text{ eV}$, $\kappa_c = 2.0$; $\kappa_h = 3.8$. Here, we have also included the high-order mode solutions, which are strongly damped.

graphs. These results show that weakly damped EAWs have frequencies in the range (3.33–4.81) kHz, and wavelengths approximately in the range (640–2580) m.

R (R_S)	Wavelength, λ (km)		Frequency, f (kHz)	
	EAW	EPW	EAW	EPW
13.1	0.64–2.21	$\lambda > 4.15$	3.61–4.81	5.61–6.60
14.0	1.54–2.47	$\lambda > 5.55$	3.43–3.85	4.49–5.24
15.0	1.38–2.58	$\lambda > 4.43$	3.98–4.53	4.92–5.54
17.8	1.27–2.51	$\lambda > 4.66$	3.33–3.79	4.21–4.64

Table 2.2: Table showing the range of wavelength, λ (m), and frequency, f (kHz), of the EPW and EAW modes, corresponding to the particular (four) radial distances in Saturn’s magnetosphere, discussed in this work, where the waves are weakly damped.

In summary, in the outer magnetosphere ($13 R_S < R < 18 R_S$) the Langmuir (EPW) wave is weakly damped ($1/|\gamma| > \omega_r/2\pi$) for small wave numbers $k\lambda_{Dc}$; the EAW is weakly damped for intermediate $k\lambda_{Dc}$, where it exhibits Langmuir-like behaviour in the vicinity of ω_{pc} , but not for low or high $k\lambda_{Dc}$.

Figure 2.10 shows examples of wave behaviour in the intermediate region of Saturn’s magnetosphere ($9 R_S < R < 13 R_S$), here for radial distances $R = 12 R_S$ (left panel) and $R = 9.8 R_S$ (right panel), respectively. The EPW exhibit strong coupling behaviour with the Langmuir-like region of the EAW branch. This coupled mode is weakly damped for a wide range of wavenumbers ($k\lambda_{Dc} \lesssim 0.56$). We note that in the intermediate magnetosphere of Saturn, the hot fractional density ratio is very small, implying that ω_{pc} is very close to ω_{pe} . Thus the Langmuir-like region of the EAW branch (which is near ω_{pc}) is close to the conventional EPW, inducing coupling. However, the acoustic region of the EAW mode is strongly damped in this case (see dashed curves). We point out that similar coupling behaviour is also sometimes observed in the outer magnetosphere ($R > 13 R_S$), in cases where the density ratio n_{0h}/n_{0e} is very small, and thus ω_{pc} approaches ω_{pe} . An example here is shown in Fig. 2.11 which correspond to data values at about $15.2 R_S$ (left panel) and $16 R_S$ (right panel). Here, the associated higher order modes, though acoustic-like, do not satisfy the damping criterion $1/|\gamma| > 2\pi/\omega_r$, and are therefore strongly damped, as can be seen from the dashed curves of Fig. 2.10. The coupled-EPW is weakly damped for a wide range of normalized wavenumber $k\lambda_{Dc} \lesssim 0.56$. Finally we consider the inner magnetosphere ($R < 9 R_S$), for example, as shown in Fig. 2.12, corresponding to radial dis-

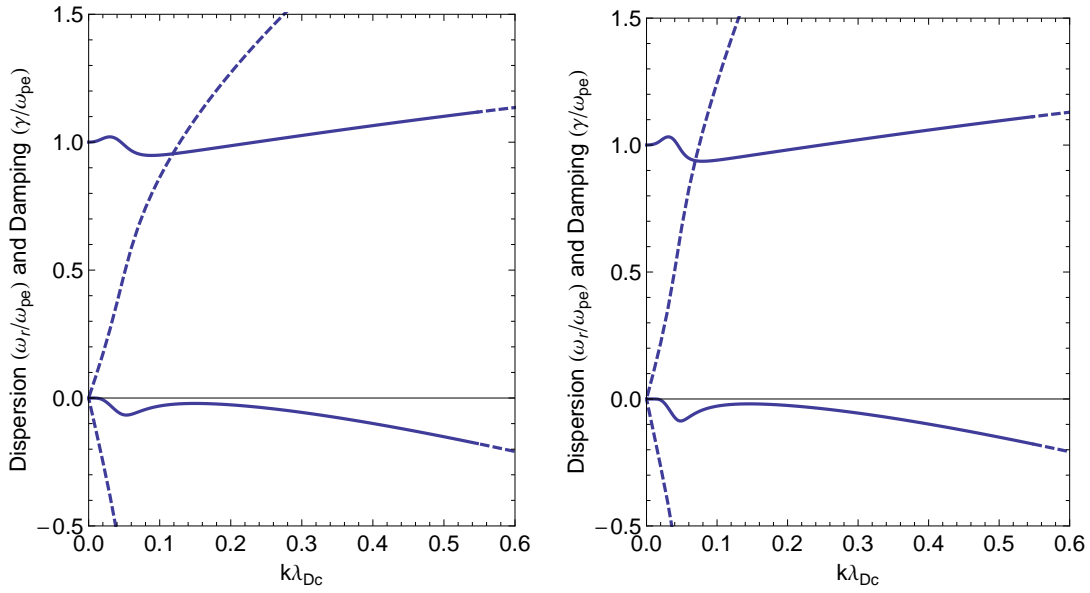


Figure 2.10: Same as in Fig. 2.8, *Left panel*: at about $12 R_S$ with parameters, $n_{0c} = 1.0 \text{ cm}^{-3}$, $n_{0h} = 0.11 \text{ cm}^{-3}$, $T_c = 6 \text{ eV}$, $T_h = 1200 \text{ eV}$, $\kappa_c = 2.0$, $\kappa_h = 3.5$. *Right panel*: at about $9.8 R_S$, with parameters: $n_{0c} = 10.9 \text{ cm}^{-3}$, $n_{0h} = 0.11 \text{ cm}^{-3}$, $T_c = 8 \text{ eV}$, $T_h = 1500 \text{ eV}$, $\kappa_c = 2$; $\kappa_h = 4$.

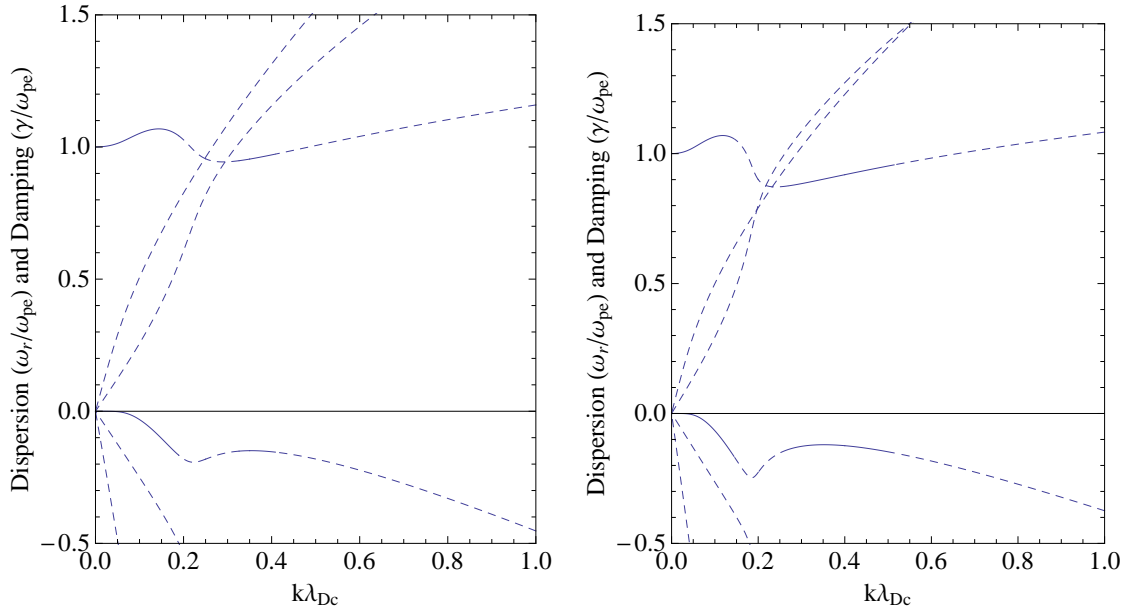


Figure 2.11: Same as in Fig. 2.10, *Left panel*: at about $15.2 R_S$ with parameters, $n_{0c} = 0.25 \text{ cm}^{-3}$, $n_{0h} = 0.07 \text{ cm}^{-3}$, $T_c = 70 \text{ eV}$, $T_h = 1000 \text{ eV}$, $\kappa_c = 2$, $\kappa_h = 4$. *Right panel*: at about $16.0 R_S$, with parameters: $n_{0c} = 0.2 \text{ cm}^{-3}$, $n_{0h} = 0.07 \text{ cm}^{-3}$, $T_c = 35 \text{ eV}$, $T_h = 800 \text{ eV}$, $\kappa_c = 1.85$; $\kappa_h = 3.5$. The “acoustic-like” modes, given by the high-order mode solutions of the dispersion relation, are strongly damped.

tances of $R = 5.4 R_S$ (left panel) and $R = 6.5 R_S$ (right panel), respectively. In these two cases, the density of the high-temperature component is typically very small, and therefore

values of f are small too, that is, 0.001 and 0.002, respectively (see Table 2.1). Here only the EPW is weakly damped while the “acoustic modes” are too strongly damped to be observable. In the case of $R = 5.4 R_S$ we have also included the analytic approximations to the EPW mode (dotted green curve) and the Langmuir-like branch of the EAW given by Eq. (2.12) (solid red curve). The figure shows that in this case, with $f \ll 1$ and $\beta \gg 1$, the EPW and the Langmuir-like branch of the EAW are close to each other for low normalized wavenumbers. In addition, the numerical and analytic results for the EPW agree well in this range.

Mace and Hellberg [1990], for a bi-Maxwellian electron distribution, and Mace *et al.* [1999], for a hot-kappa/cool-Maxwellian plasma mix, showed that electron-acoustic waves can be weakly damped only for relatively high hot fractional densities (n_{0h}/n_{0e}) and relatively high hot-to-cool electron temperatures, above the threshold values. From the Voyager 1 and 2 inbound results of the PLS observations, Sittler *et al.* [1983] showed that between $15 R_S$ and $20 R_S$ for Voyager 1, and between about $13 R_S$ and $20 R_S$ for Voyager 2 observations, the outer magnetosphere of Saturn has relatively high superthermal fractional densities and pressure (see their Fig. 10). This trend is confirmed by the Cassini results of Schippers *et al.* [2008], where beyond $13 R_S$, the densities of the two electron components are similar within an order of magnitude. However, for radial distances below $13 R_S$, though the temperature ratio T_h/T_c is in some instances large enough (~ 100) to support EAWs, the cool and hot electron densities are so disparate (orders of magnitudes apart), that the ratio n_{0h}/n_{0e} becomes too small. Our results show that “weakly damped” electron-acoustic waves require relatively high hot-to-cool temperature ratios, and hot-to-total electron density ratios that are well above 0.2.

2.8 Conclusions and Chapter Summary

Using kinetic theory, we have carried out a study of electron-acoustic waves in a plasma with two kappa-distributed electron components, having different temperatures. Based on data obtained from Saturn’s magnetosphere [Schippers *et al.*, 2008], we have carried out a parameter survey of dispersion and damping of the waves, for a variety of values of the hot and cool electron κ values (κ_h, κ_c), with an emphasis on low κ values, the hot electron density fraction f , and the hot to cool electron temperature ratio $\beta = T_h/T_c$.

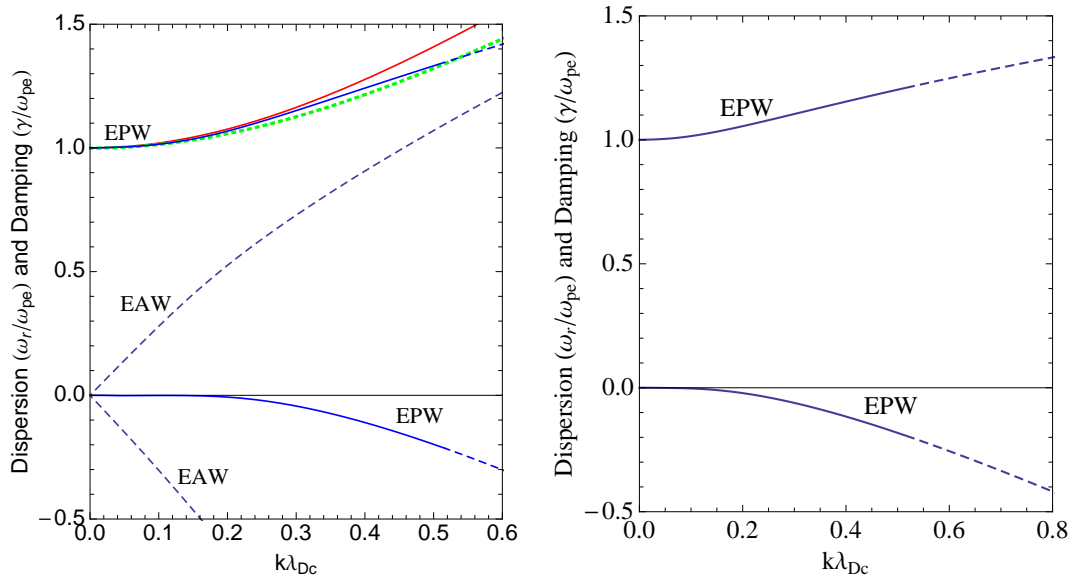


Figure 2.12: Same as in Fig. 2.8: *Left panel:* at about $5.4 R_S$, with parameters: $n_{0c} = 10.5 \text{ cm}^{-3}$, $n_{0h} = 0.02 \text{ cm}^{-3}$, $T_c = 1.8 \text{ eV}$, $T_h = 300 \text{ eV}$, $\kappa_c = \kappa_h = 5.0$. *Right panel:* at about $6.3 R_S$ with parameters, $n_{0c} = 10.5 \text{ cm}^{-3}$, $n_{0h} = 0.01 \text{ cm}^{-3}$, $T_c = 2 \text{ eV}$, $T_h = 400 \text{ eV}$, $\kappa_c = 2.3$, $\kappa_h = 3.0$. In the left panel, the analytic solution for the EPW [from Eq. (2.13)] is also shown in red, which agrees with the numerical solution for small wavenumbers (here $k\lambda_{DC} < 0.2$). In addition, we have included the analytical Langmuir-like solution from Eq. (2.12) (dotted, green curve). Thus for small $k\lambda_{DC}$, Eqs. (2.13) and (2.12) are equivalent when $\beta \gg 1$ and $f \ll 1$.

Our results show that even in the presence of two strongly non-Maxwellian electron components, it is essentially the dependence of the damping rate on the hot-to-cool electron temperature ratio $\beta = T_h/T_c$ and the fractional hot electron component density $f = n_{h0}/n_{e0}$ that determines the range in wavenumber (in terms of $k\lambda_{DC}$) over which EAWs are weakly damped; κ_h plays a weaker, albeit significant role, particularly for low values (~ 2), while the effect of κ_c , even for strongly non-Maxwellian values, is weak but not negligible. In our studies we differentiate between wave ranges that are strongly damped ($|\gamma| > \omega_r/2\pi$), and thus will definitely not be observable, and those that are potentially observable, either as a result of random thermal fluctuations or a given source of free energy. These results are then applied to three regions of Saturn's magnetosphere.

In the outer magnetosphere, our results suggest that weakly damped electron-acoustic waves may occur at radial distances in the range $13 - 18 R_S$ where

- (i) the densities of the hot and cool electron populations are of the same order of magnitude;
- (ii) the temperatures differ by about two orders of magnitude, that is $T_h/T_c \sim 100$, and

(iii) the kappa index values are more or less constant around $\kappa_c \simeq 2$ and $\kappa_h \simeq 4$.

It is thus likely that EAWs should be observable in this outer region. In terms of frequencies and wavelengths, our results suggest that the weakly damped EAWs have frequencies in the range (3.33–4.81) kHz, and wavelengths approximately in the range (640–2580) m.

In the intermediate magnetosphere, $f = n_{h0}/n_{e0}$ is very small, and thus $\omega_{pc} \sim \omega_{pe}$. The strong coupling between the cool Langmuir-like branch of the EAW (near ω_{pc}) and the EPW yields potentially observable waves that are Langmuir-like. This pattern is also obtained, for some cases, in the $R > 13 R_S$ region, in cases where the density ratio n_{h0}/n_{e0} is very small, and hence the cool electron component density $n_{c0} \simeq n_{e0}$.

Finally, in the inner magnetosphere ($R < 9 R_S$), EAWs are strongly damped and are highly unlikely to be observed in the absence of a source of free energy; only the EPW is weakly damped. This may be attributed to the fact that the fractional hot electron density is very small.

Dust Acoustic Solitons in Plasmas with Kappa-Distributed Electrons
and/or Ions

In this Chapter, we investigate the existence conditions for dust acoustic (DA) solitons and double layers in a dusty plasma in which the electrons and/or ions have a kappa distribution, and the dust grains are modelled as a cold, inertial fluid. This work enables one to undertake a direct comparison between the effects of the Cairns and the kappa distribution, as examples of two nonthermal distributions, on DA solitary wave existence in dusty plasmas. Unlike the situation found for the Cairns distribution, we will show that electrostatic solitary structures are restricted to negative (positive) potential solitons if the dust is made up of negatively (positively) charged grains.

*The results presented in this Chapter have been published as T. K. Baluku and M. A. Hellberg, *Physics of Plasmas*, 15, 123705 (2008)*

3.1 Introduction

In Sec. 1.2, we discussed the main properties of dust particles, and the various areas where they can exist in space, astrophysical and laboratory environments.

In studies of dust acoustic waves in space, the electrons or ions are quite often modelled by the Boltzmann distribution, and the dust treated as a cold fluid due to the great inertia

provided by its mass. Using such a model, for example, Mamun [1996] found that a dusty plasma with cold negatively charged inertial dust fluid and (Boltzmann distributed) thermal ions, with background (Boltzmann) electrons would admit negative potentials associated with small amplitude dust acoustic solitary waves.

In explaining the electrostatic structures with density depletions observed by the Freja satellite [Dovner *et al.*, 1994], using a nonthermal velocity distribution function, Eq. (1.26), often referred to as the Cairns distribution, Cairns *et al.* [1995] showed that the presence of a population of energetic electrons changes the properties of ion sound waves.

Based on the Cairns distribution function in Eq. (1.26), a number of authors [Mamun, 1997; Verheest and Pillay, 2008a,b], to mention a few, have studied the behaviour of solitary structures in nonthermal plasmas. Recently, Verheest and Pillay [2008a] investigated the existence of large amplitude dust acoustic solitary waves in plasmas consisting of negatively charged dust in the presence of either nonthermally distributed ions or electrons using the Cairns distribution. In their study, it was found that nonthermal electrons support only negative potential solitary waves, while, for a limited range of f and α , nonthermal ions admit both positive and negative potential solitons, with $f = N_{e0}/N_{i0}$ being the ratio of the equilibrium electron number density to that of the ions. Positive double layers were also found under related conditions. For the case of positive dust they [Verheest and Pillay, 2008b] found equivalent results, the only differences being a change of sign of soliton potential and of the light species (ions versus electrons) governing the process.

Here, we thus investigate the effect of using a different nonthermal distribution for the electrons or the ions on the resulting DA wave structures, *viz.* the kappa distribution.

3.2 Model and Basic Equations

We consider a three component, homogeneous, unmagnetized dusty plasma comprising electrons, singly charged ions and negatively charged dust particles, the latter satisfying the continuity and momentum equations. In view of the typical charging timescales, it is expected that charge fluctuations would have a minimal effect on dust acoustic modes [Shukla and Mamun, 2002], and so we assume that the dust charge is constant. Both the ions and electrons of mass m_i (m_e) and temperature T_i (T_e) follow a generalized three dimensional

kappa distribution given by

$$F_\kappa(v_j) = \frac{N_{j0}}{(\pi\kappa_j\theta_j^2)^{3/2}} \frac{\Gamma(\kappa_j+1)}{\Gamma(\kappa_j-1/2)} \left[1 + \frac{v_j^2 + 2q_j\varphi/m_j}{\kappa_j\theta_j^2} \right]^{-(\kappa_j+1)}, \quad (3.1)$$

where q_j is the species charge of the electrons ($j = e$) or ions ($j = i$); φ the local electrostatic potential, v_j and N_{j0} the ion (electron) species velocity and equilibrium number density, respectively; other parameters are as defined in Eq. (1.3). The gamma function, $\Gamma(a)$, is related to the beta function, $B(a, b)$, where the latter arises from the normalization of $F_\kappa(v_j)$ such that $\int F_\kappa(v_j) d^3v_j = N_{j0}$, that is, from computing the statistical (velocity) moments $\langle v^n \rangle$ of the distribution, with the integer $n = 0$. To obtain Eq. (3.1) from (1.2), we have taken into account the energy associated with the position of the particle species [Goldston and Rutherford, 1995], and thus used the energy conservation relation: $m_j v_j^2/2 + q_j\varphi = m_j V^2/2$, where $q_j\varphi$ is the increase in potential energy and V is the velocity of the particles in the initial equilibrium state (*i.e.*, $m_j V^2/2 = W_r$ gives the total energy in the system). This family of velocity distribution functions includes the Maxwell-Boltzmann distribution for $\kappa_i, \kappa_e \rightarrow \infty$.

Integrating the kappa distribution over velocity space, one obtains the number density for the ions ($j = i$) and the electrons ($j = e$), respectively, as

$$N_j(\varphi) = N_{j0} \left(1 + \frac{2q_j\varphi}{m_j\kappa_j\theta_j^2} \right)^{-(\kappa_j-1/2)}, \quad (3.2)$$

where q_j is the charge of species j . Note that $q_j\varphi = e\varphi$ for positive ions of single charge, and $-e\varphi$ for electrons, respectively. A full derivation is given in Appendix A.1.2. In the limit $e\varphi \ll \kappa_j m_j \theta_j^2/2$, Eq. (3.2) reduces to Eq. (15) of Bryant [1996], with $E_\kappa = m\theta^2/2$, and is similar (for small perturbations) to Eq. (80) of Treumann [1999], which follows from his distribution function (78) with $\phi \rightarrow -e\phi$ for electrons instead of our Eq. (3.1). In addition, we point out that using the one dimensional κ -distribution [with the power in Eq. (3.1) being $-\kappa$ instead of $-(\kappa+1)$] leads to the same expressions in Eq. (3.2).

For simplicity, we choose the following normalizations: the local electrostatic potential is normalized to $K_B T_i/e$, number density to the ion number density, N_{i0} , and velocity to the dust acoustic speed, $C_d = (Z_d K_B T_i/m_d)^{1/2}$, where m_d (Z_d) is the dust grain mass

(number of electronic charges residing on the dust grain surface of arbitrary charge q_d , *i.e.*, $Z_d = |q_d/e|$). For completeness, in one-dimensional geometry, the space and time variables are normalized to the “dust Debye length”, $\lambda_{Dd} = (\varepsilon_0 K_B T_i / Z_d N_{d0} e^2)^{1/2}$ and dust plasma period, $\omega_{pd}^{-1} = [(Z_d^2 e^2 N_{d0} / \varepsilon_0 m_d)]^{-1/2}$, respectively.

The normalized ion and electron number densities are thus given by

$$n_i(\phi) = \left(1 + \frac{\phi}{\kappa_i - 3/2}\right)^{-(\kappa_i - 1/2)} \quad (3.3)$$

and

$$n_e(\phi) = f \left(1 - \frac{\sigma \phi}{\kappa_e - 3/2}\right)^{-(\kappa_e - 1/2)}, \quad (3.4)$$

respectively, where $\sigma = T_i/T_e$ is the ratio of the ion temperature to that of electrons, $f = N_{e0}/N_{i0}$ the ratio of the equilibrium number density of electrons to ions, and ϕ the normalized potential. In the limit $\kappa_i, \kappa_e \rightarrow \infty$, Eqs. (3.3) and (3.4) reduce to $n_i(\phi) = \exp(-\phi)$ and $n_e(\phi) = f \exp(\sigma \phi)$, the Maxwellian distributions for the ions and electrons, respectively.

On the other hand, the fluid of cold, negatively charged dust particles, characterized by the normalized density n_d and velocity u_d , satisfies the continuity and momentum equations (in the absence of pressure, since we assume the dust temperature, $T_d = 0$):

$$\frac{\partial n_d}{\partial t} + \frac{\partial}{\partial x}(n_d u_d) = 0 \quad (3.5)$$

and

$$\frac{\partial u_d}{\partial t} + u_d \frac{\partial u_d}{\partial x} - \frac{\partial \phi}{\partial x} = 0. \quad (3.6)$$

The species' densities are coupled by Poisson's equation

$$\frac{\partial^2 \phi}{\partial x^2} + \frac{N_{i0}}{Z_d N_{d0}} (n_i - n_e - Z_d n_d) = 0. \quad (3.7)$$

In transforming to a stationary frame, we assume that all quantities depend on $\xi = x - M t$, where the Mach number M gives the velocity of the solitary wave normalized to the dust acoustic speed C_d , *i.e.*, it is equivalent to the normalized speed of the dust particles in the stationary frame. With this transformation we have, $\partial/\partial x \rightarrow \partial/\partial \xi$ and $\partial/\partial t \rightarrow -M \partial/\partial \xi$.

By imposing the appropriate boundary conditions for localized disturbances, that is, $n_d \rightarrow N_{d0}/N_{i0}$, and $\phi, d\phi/d\xi \rightarrow 0$ as $\xi \rightarrow \pm\infty$, equations (3.5) and (3.6) can be solved to get

$$n_d(\phi) = \left(\frac{N_{d0}}{N_{i0}} \right) \left(1 + \frac{2\phi}{M^2} \right)^{-1/2}. \quad (3.8)$$

From Eqs. (3.3), (3.4) and (3.8) we observe that when $f = 0$, $n_e \rightarrow 0$ while n_d is finite, and similarly, when $f = 1$, $n_d \rightarrow 0$ while n_e is finite. Thus at these extreme values of f , the model reduces to a two-component plasma: an electron-ion plasma for $f = 1$ and an ion-dust plasma for $f = 0$.

Also, with the transformation $\xi = x - Mt$, Poisson's equation becomes

$$\frac{\partial^2 \phi}{\partial \xi^2} + \frac{N_{i0}}{Z_d N_{d0}} (n_i - n_e - Z_d n_d) = 0. \quad (3.9)$$

In the unperturbed initial state, $\sum q_j N_{j0} = 0$, and with $f = N_{e0}/N_{i0}$ we obtain $Z_d N_{d0}/N_{i0} = 1 - f$, where $f < 1$ for negatively charged dust particles.

Substitution of the density expressions into Poisson's equation leads to

$$\begin{aligned} \frac{d^2 \phi}{d\xi^2} = & \frac{f}{1-f} \left(1 - \frac{\phi \sigma}{\kappa_e - 3/2} \right)^{-(\kappa_e - 1/2)} \\ & - \frac{1}{1-f} \left(1 + \frac{\phi}{\kappa_i - 3/2} \right)^{-(\kappa_i - 1/2)} + \left(1 + \frac{2\phi}{M^2} \right)^{-1/2}. \end{aligned} \quad (3.10)$$

Equation (3.10) can be written in the "energy integral" form

$$\frac{1}{2} \left(\frac{d\phi}{d\xi} \right)^2 + \Psi(\phi) = 0, \quad (3.11)$$

where

$$\begin{aligned} \Psi(\phi) = & \frac{f}{(1-f)\sigma} \left[1 - \left(1 - \frac{\phi \sigma}{\kappa_e - 3/2} \right)^{-(\kappa_e - 3/2)} \right] \\ & + \frac{1}{1-f} \left[1 - \left(1 + \frac{\phi}{\kappa_i - 3/2} \right)^{-(\kappa_i - 3/2)} \right] \\ & + M^2 \left[1 - \left(1 + \frac{2\phi}{M^2} \right)^{1/2} \right] \end{aligned} \quad (3.12)$$

is the Sagdeev (pseudo)potential of the plasma system with ϕ the “coordinate” (pseudo position) and ξ the “time”. Note that $d^2\phi/d\xi^2 = -\Psi'(\phi)$, the prime denoting the derivative with respect to ϕ . Equation (3.12) has the property that at the origin ($\phi = 0$), $\Psi(\phi) = \Psi'(\phi) = 0$, thus by imposing the solitary structure requirements discussed in Sec. 1.4 for the Sagdeev pseudopotential theory, we are in a position to obtain existence domains of the DA solitons or double layers supported by the plasma model. These requirements are summarized as follows:

- (i) $\Psi''(\phi = 0) < 0$ such that there is a maximum at the origin (*i.e.*, the fixed point at the origin is unstable);
- (ii) there exists a nonzero ϕ_m , which is a minimum (or maximum) value of ϕ , at which $\Psi(\phi_m) = 0$;
- (iii) $\Psi(\phi) < 0$ for $0 < |\phi| < |\phi_m|$, and
- (iv) in the case of double layers, both $\Psi(\phi_m)$ and $\Psi'(\phi_m)$ must be zero.

The requirement in (i) leads to the “soliton condition”,

$$M > M_s, \tag{3.13}$$

where

$$M_s = \left\{ \frac{f\sigma}{1-f} \left(\frac{2\kappa_e - 1}{2\kappa_e - 3} \right) + \frac{1}{1-f} \left(\frac{2\kappa_i - 1}{2\kappa_i - 3} \right) \right\}^{-1/2} \tag{3.14}$$

is the lower Mach number limit below which no solitons (or double layers) can exist. For $\kappa_e, \kappa_i \rightarrow \infty$ this reduces to the familiar expression obtained for Boltzmann electrons and ions [Verheest *et al.*, 2005], *i.e.*, $M_s^2 = (1-f)/(1+f\sigma) < 1$.

Solitons are inherently super acoustic, but the “Mach number” referred to here is based on a specific normalization, and hence one may have $M < 1$. Whereas we have used an approximate dust acoustic speed $C_d = (Z_d K_B T_i / m_d)^{1/2}$ for the normalization, the actual dust acoustic speed in the plasma under consideration can be shown to be $C_{d\kappa} = \omega_{pd} \lambda_{D\kappa}$, where the global Debye length $\lambda_{D\kappa}$ [Bryant, 1996; Mace *et al.*, 1998, 1999] is given by

$$\frac{1}{\lambda_{D\kappa}^2} = \frac{e^2}{\varepsilon_0 K_B} \left\{ \frac{N_{e0}}{T_e} \left(\frac{2\kappa_e - 1}{2\kappa_e - 3} \right) + \frac{N_{i0}}{T_i} \left(\frac{2\kappa_i - 1}{2\kappa_i - 3} \right) \right\},$$

which reduces to the usual expression for λ_D when $\kappa_e, \kappa_i \rightarrow \infty$. It can also be written as

$$\frac{1}{\lambda_{D\kappa}^2} = \frac{Z_d N_{d0} e^2}{\epsilon_0 K_B T_{\text{eff}}},$$

where the effective temperature T_{eff} is given by

$$\frac{T_i}{T_{\text{eff}}} = \frac{1}{(1-f)} \left\{ f \sigma \left(\frac{2\kappa_e - 1}{2\kappa_e - 3} \right) + \left(\frac{2\kappa_i - 1}{2\kappa_i - 3} \right) \right\}.$$

Thus we can see that

$$M_{d\kappa}^2 = \frac{V^2}{C_{d\kappa}^2} = \frac{M^2 C_d^2}{C_{d\kappa}^2} = \frac{M^2 T_i}{T_{\text{eff}}} = \frac{M^2}{M_s^2},$$

where we have used the definitions of M , M_s , $M_{d\kappa}$, C_d , $C_{d\kappa}$ and $\lambda_{D\kappa}$. It follows that if $M > M_s$, the “true” Mach number $M_{d\kappa} > 1$, and the structures are truly super acoustic, as expected.

It is seen that in the absence of electrons, when $f \rightarrow 0$, the soliton condition (3.14) is obviously independent of both σ and κ_e , both of which are electron-related. On the other hand, for $f = 1$, the number densities of ions and electrons are equal, there is no dust, and $M_s \rightarrow 0$.

3.3 Small Amplitude Dust Acoustic Solitons (DAS) and Double Layers

To study small amplitude solitary wave structures, we shall use an expanded Sagdeev potential approach, and thus carry out a series expansion of $\Psi(\phi)$ about the origin ($\phi = 0$). As we require $\Psi(0) = \Psi'(0) = 0$, the constant term and linear term vanish. To fourth order this gives

$$\frac{1}{2} \left(\frac{d\phi}{d\xi} \right)^2 + A \phi^2 + B \phi^3 + C \phi^4 = 0, \quad (3.15)$$

where

$$A = \frac{-(\kappa_i - 1/2)}{2(1-f)(\kappa_i - 3/2)} - \frac{f \sigma (\kappa_e - 1/2)}{2(1-f)(\kappa_e - 3/2)} + \frac{1}{2M^2}, \quad (3.16)$$

$$B = \frac{(\kappa_i - 1/2)(\kappa_i + 1/2)}{6(1-f)(\kappa_i - 3/2)^2} - \frac{f \sigma^2 (\kappa_e - 1/2)(\kappa_e + 1/2)}{6(1-f)(\kappa_e - 3/2)^2} - \frac{1}{2M^4} \quad (3.17)$$

and

$$C = \frac{5}{8M^6} - \frac{(\kappa_i - 1/2)(\kappa_i + 1/2)(\kappa_i + 3/2)}{24(1-f)(\kappa_i - 3/2)^3} - \frac{f\sigma^3(\kappa_e - 1/2)(\kappa_e + 1/2)(\kappa_e + 3/2)}{24(1-f)(\kappa_e - 3/2)^3}. \quad (3.18)$$

3.3.1 Small Amplitude Solitons

In investigating small amplitude solitons, we first assume that the fourth order term in (3.15) is small enough to be neglected [Verheest and Hellberg, 1997] and only consider

$$\frac{1}{2} \left(\frac{d\phi}{d\xi} \right)^2 + A\phi^2 + B\phi^3 = 0. \quad (3.19)$$

The solution to Eq. (3.19) is the usual Korteweg-de Vries (KdV)-type solution

$$\phi(\xi) = -\frac{A}{B} \operatorname{sech}^2 \left[(-A/2)^{1/2} \xi \right]. \quad (3.20)$$

The maximum soliton potential and width are given by $|A/B|$ and $\sqrt{-2/A}$, respectively. Thus, for the soliton width to be real we require $A < 0$ in (3.20), and B must be non-zero, since we require $\phi \rightarrow 0$ as $\xi \rightarrow \pm\infty$. The sign of the potential thus depends on the sign of B : ϕ is positive when $B > 0$ and negative when $B < 0$. In other words, the sign of the coefficient of ϕ^3 in the Taylor expansion of $\Psi(\phi)$ about $\phi = 0$ determines the sign of the potential of the small amplitude solitons that exist in the plasma model. This also applies to small amplitude double layers, if they exist, as discussed below in this section. As other plasma models will show, these small amplitude solitons have the property that their amplitudes go to zero as M approaches M_s . Such solitons will be termed ‘‘KdV-like’’ solitons in this thesis.

This approach, which is valid for weak (small amplitude) solitons, is similar to the reductive perturbation technique that results in the Korteweg-de Vries equation of the form of Eq. (3.19).

Small Amplitude Negative Potential Solitons:

Considering the case of small amplitude negative potential solitons, we require $B < 0$ in (3.17), which leads to a constraint on the Mach number, *viz.*

$$M < \left\{ \frac{(\kappa_i - 1/2)(\kappa_i + 1/2)}{3(1-f)(\kappa_i - 3/2)^2} - \frac{f\sigma^2(\kappa_e - 1/2)(\kappa_e + 1/2)}{3(1-f)(\kappa_e - 3/2)^2} \right\}^{-1/4} \equiv M_\beta, \quad (3.21)$$

provided the expression in brackets is positive, *i.e.*,

$$f \leq \frac{1}{\sigma^2} \left(\frac{\kappa_i + 1/2}{\kappa_e + 1/2} \right) \left(\frac{\kappa_i - 1/2}{\kappa_e - 1/2} \right) \left(\frac{\kappa_e - 3/2}{\kappa_i - 3/2} \right)^2, \quad (3.22)$$

for real M_β (and $f < 1$ and $\kappa_e, \kappa_i > 3/2$). Here M_β is the upper Mach number limit above which small amplitude negative potential solitons cannot exist. That is, the existence domain is restricted to the range $M_s < M < M_\beta$. When $\kappa_i = \kappa_e = \kappa$, M_β in Eq. (3.21) reduces to

$$M_\beta = \left[\frac{3(1-f)(\kappa - 3/2)^2}{(1-f\sigma^2)(\kappa - 1/2)(\kappa + 1/2)} \right]^{1/4}, \quad (3.23)$$

which at $f \rightarrow 0$ is independent of σ , and goes to zero for $f = 1$ as long as $\sigma \neq 1$. The case $\sigma = 1$ (*i.e.*, $T_i = T_e$) is a singular case, in which the ‘‘upper limit’’ M_β is seen to be independent of f . We shall return to this case in our numerical evaluations. In addition, for $\kappa_i = \kappa_e$, Eq. (3.22) reduces to $f \leq 1/\sigma^2$. Then the entire range of f , *viz.*, $0 < f < 1$, is covered for $\sigma \leq 1$, but for $\sigma > 1$, the expression is valid for only a limited range.

Small Amplitude Positive Potential Solitons:

Next, we turn to the possible existence of positive potential solitons. We see from Eq. (3.20) that with $A < 0$, positive potential solitons ($\phi > 0$) would require $B > 0$, that is, $M > M_\beta$. This condition dominates the soliton condition, $M > M_s$, and leads to unbounded values of M . One of the less stringent conditions for the existence of solitons is that the Sagdeev potential $\Psi(\phi)$ must have at least one charge neutral point, that is $\Psi'(\phi)$ must change sign in the range $0 < \phi < \phi_m$, where ϕ_m satisfies $\Psi(\phi_m) = 0$. However, as will be discussed for the arbitrary amplitude case in Section IV, numerical investigations show that $\Psi'(\phi)$ is never zero for any $\phi > 0$ and $M > M_s$. That is, no charge neutral point outside the origin is found, and thus neither positive solitons nor double layers can

be formed. Thus we shall not discuss further the case of $B > 0$ in this section.

3.3.2 Small Amplitude Double Layers

We consider the possible existence of small amplitude negative potential double layers. In a number of plasma models, double layers may act as limits of a sequence of solitons, and can thus give rise to a limit of an existence domain for solitons [Baboolal *et al.*, 1990]. The existence of double layers requires $\Psi(\phi_m) = \Psi'(\phi_m) = 0$, at a possible root $\phi = \phi_m \neq 0$. Applying this double layer condition to Eq. (3.15), one obtains $\phi_m^2 = A/C$ and $\phi_m = -B/2C$, *i.e.*, $B^2 = 4AC$. Using this transformation, (3.15) can then be written in the form [Verheest and Hellberg, 1997]

$$\frac{1}{2} \left(\frac{d\phi}{d\xi} \right)^2 + C \phi^2 (\phi - \phi_m)^2 = 0, \quad (3.24)$$

which has a solution

$$\phi = -\frac{B}{4C} \left\{ 1 - \tanh \left[\left(-\frac{A}{2} \right)^{1/2} \xi \right] \right\}, \quad (3.25)$$

provided $A < 0$. Also, using $\phi_m^2 = A/C$ it implies that C must be negative for real values of ϕ_m . Therefore the sign of the double layer given by (3.25) depends solely on whether B is negative or positive. Here, $C < 0$ yields $M > M_\alpha$ where

$$M_\alpha = \left\{ \frac{(\kappa_i - 1/2)(\kappa_i + 1/2)(\kappa_i + 3/2)}{15(1-f)(\kappa_i - 3/2)^3} + \frac{f \sigma^3 (\kappa_e - 1/2)(\kappa_e + 1/2)(\kappa_e + 3/2)}{15(1-f)(\kappa_e - 3/2)^3} \right\}^{-1/6}. \quad (3.26)$$

As was found to be the case for both M_s and M_β , we see that $M_\alpha \rightarrow 0$ for $f \rightarrow 1$, while at $f = 0$, of course, only the ions play a role.

In general, the existence of (small amplitude) negative potential double layers thus requires $\text{Max}(M_s, M_\alpha) < M < M_\beta$, provided the constants A , B and C in Eqs. (3.15)-(3.18) satisfy the constraint $B^2 = 4AC$.

Figures 3.1 and 3.2 show the behaviour of M_s , M_α and M_β as functions of f for particular values of σ , κ_e and κ_i . In Fig. 3.1 we have chosen $\sigma = T_i/T_e = 0.5$. In the left panel both species have a low spectral index ($\kappa_i = \kappa_e = 2$), while the right panel illustrates a case in which the electrons and ions are essentially quasi-Maxwellian ($\kappa_i = \kappa_e = 25$).

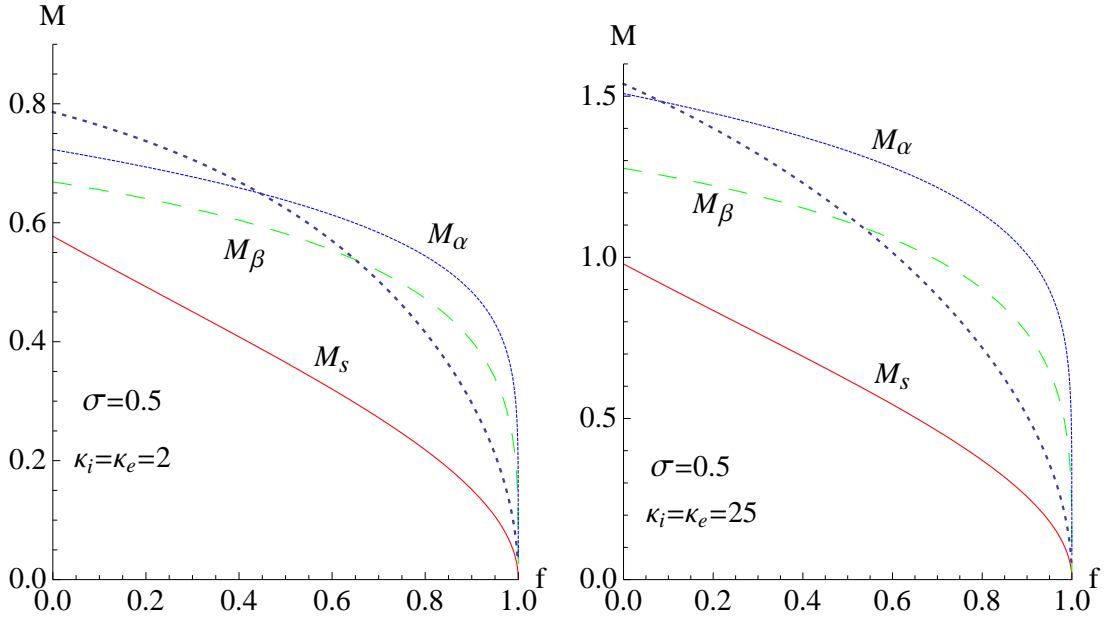


Figure 3.1: Existence domain for weak negative potential dust acoustic solitary waves, from the small amplitude theory (M_s , M_β , M_α), for $\sigma = 0.5$ and $\kappa_e = \kappa_i = 2$ (left panel) and $\kappa_e = \kappa_i = 25$ (right panel). Solitons, satisfying Eq. (3.20), occur in the region $M_s < M < M_\beta$, but no double layers exist since $M_\alpha > M_\beta$. The dotted (light-blue) curves correspond to the upper Mach number limit, from the arbitrary amplitude (Sagdeev potential) theory, limiting the existence of negative solitons. This will be discussed further in Sec. 3.4.3.

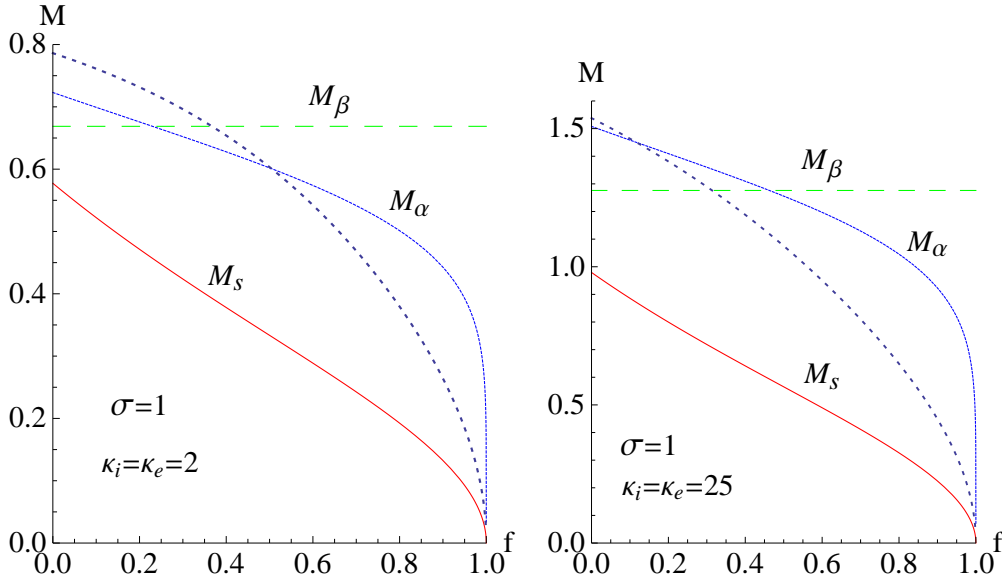


Figure 3.2: Same as Fig. 3.1 but for $\sigma = 1$. Here, for a range of f we have $M_\alpha < M_\beta$, implying that double layers can apparently exist, but critical analysis shows this to be wrong.

In both figures, small amplitude negative potential solitons are confined to the region between M_s and M_β . The qualitative similarity between the two figures indicates that the

enhanced superthermal electron and ion components associated with a kappa distribution with low κ have quantitative effects only - the values and ranges of Mach numbers that support solitons are different in the two cases. Further, as $M_\alpha > M_\beta$ over the full range of possible number density ratios, f , it follows that small amplitude double layers cannot exist. Similar results to those shown in Fig. 3.1 can be obtained for $0 < \sigma < 0.5$.

On the other hand, retaining the same spectral indices, but considering different temperature ratios as shown, for example, in Fig. 3.2 (where $T_i = T_e$), we can find a region in parameter space of (f, M) where $M_s < M_\alpha < M_\beta$ is satisfied for some values of f [$f > 0.23$ (left panel) and $f > 0.463$ (right panel), respectively]. Note that for $\kappa_i = \kappa_e = \kappa$ and $\sigma = 1$, Eq. (3.23) gives $M_\beta = M_\beta(\kappa)$, which is independent of f , and only depending on the spectral index κ of the ions or electrons. Thus, we get the constant curves, parallel to the f -axis in Fig. 3.2. Considering the fact that for some values of f we can have $M_s < M_\alpha < M_\beta$, a cursory interpretation of this figure may then lead one to suggest that both double layers and solitons may exist in such a region of parameter space for $\phi < 0$, as one of the required double layer conditions is satisfied. Similar apparent “existence domains” in the parameter space of (f, M) can be obtained for other values of κ_e , κ_i and σ .

However, a more careful study of these cases indicates that although $M_\alpha < M_\beta$ in some regions, the further double layer requirement $B^2 = 4AC$, and in particular, $\phi_m = -\sqrt{A/C} = -B/2C$, for $\phi < 0$, is violated. This is illustrated in Table 3.1 for the parameter values $\kappa_i = \kappa_e = 2$ and $\sigma = 1$ for the density ratio $f = 0.8$. For this case, we have listed examples of Mach numbers lying in the range $M_s < M_\alpha < M < M_\beta$, which should apparently support double layers. For each such value, we have listed the corresponding values of $4AC$ and B^2 (which are clearly far from equal), and also the values of the root, ϕ_m , that may be calculated from the above two relations. The table shows that for the given parameter values, no second double root exists. A similar approach for other parameter values (of κ_e , κ_i and σ) that are admissible to the current plasma model leads to the same conclusion. This appears to rule out the existence of negative potential double layers and therefore, only negative potential solitons can exist in such plasmas. As we shall see below, these results also agree with those obtained from the large amplitude treatment.

M	4AC	B^2	ϕ_{m1}	ϕ_{m2}
0.52	128.739	18.82	-0.785	-1.634
0.53	289.558	14.72	-0.311	-1.748
0.54	432.201	11.43	-0.184	-1.867
0.55	558.996	8.786	-0.126	-2.000
0.56	671.941	6.678	-0.092	-2.146
0.57	772.758	5.003	-0.069	-2.313
0.58	862.933	3.680	-0.053	-2.503
0.59	943.749	2.645	-0.042	-2.724
0.60	1016.320	1.844	-0.032	-2.986
0.61	1081.611	1.235	-0.025	-3.308
0.62	1140.460	0.781	-0.019	-3.715
0.63	1193.607	0.454	-0.014	-4.262
0.64	1241.690	0.231	-0.009	-5.057
0.65	1285.256	0.091	-0.006	-6.397
0.66	1324.810	0.018	-0.003	-9.562
0.67	1360.781	3.5×10^{-4}	3.4×10^{-4}	$-25.703i$

Table 3.1: Table showing the double layer conditions arising from Eq. (3.15) for $\kappa_i = \kappa_e = 2$, $\sigma = 1$ and $f = 0.8$; $M_s = 0.19245$, $M_\alpha = 0.51279$ and $M_\beta = 0.66874$. Here $\phi_{m1} = -B/2C$ and $\phi_{m2} = -(A/C)^{1/2}$.

3.4 Arbitrary Amplitude DAS and Double Layers

3.4.1 Positive Potential Solitons

From Eqs. (3.3) and (3.4) it follows that for positive potentials, the limitation on ϕ would in principle be provided by the electrons at the critical potential $\phi_{ce} = (\kappa_e - 3/2)/\sigma$, where $\kappa_e > 3/2$, beyond which the electron density is complex. At this limiting potential, we require $\Psi(\phi_{ce}) > 0$, a condition that is essential for obtaining the upper limit to the Mach number for positive dust acoustic solitons to exist. However, substitution in Eq. (3.12) shows that for $\kappa_e > 3/2$, $\Psi(\phi_{ce}) = -\infty < 0$, and thus this requirement is not satisfied. It follows that this ‘‘electron density limit’’ cannot provide an upper limit on M for positive potential solitons. Any such upper limit on M , should it exist, then needs to be given by the value of M at which a double layer occurs for particular values of κ_i , κ_e , σ and f , provided positive potential solitons and/or double layers exist in the model under consideration.

Generally, for solitons or double layers to exist, it is imperative that there exists a charge neutral point (CNP) for some $\phi_{CNP} > 0$ between the origin and the potential

corresponding to the upper Mach number limit, which here would occur for $\phi = \phi_{ce}$, *i.e.*, there exists an accessible value ϕ_{CNP} at which the curve of $\Psi(\phi)$ against ϕ has zero slope, before a root of $\Psi(\phi)$ is encountered. We have carried out a numerical investigation over a wide range of parameter values and have not been able to find a position of charge equilibrium outside the unperturbed state for positive ϕ , as $\Psi'(\phi) < 0$ always, implying that $n_e + Z_d n_d > n_i$. Thus it appears that neither positive solitons nor double layers can be obtained with a dusty plasma model with κ -distributed ions and/or electrons.

ϕ	$\Psi'(\phi, M)$			
	$M = 0.34$	$M = 0.35$	$M = 0.36$	$M = 0.37$
-0.0700	1.69+2.18 <i>i</i>	1.69+2.65 <i>i</i>	1.69+3.53 <i>i</i>	1.69+6.65 <i>i</i>
-0.0675	1.66+2.44 <i>i</i>	1.66+3.13 <i>i</i>	1.66+4.90 <i>i</i>	-6.830
-0.0650	1.63+2.83 <i>i</i>	1.63+4.04 <i>i</i>	1.63+18 <i>i</i>	-2.822
-0.0625	1.61+3.51 <i>i</i>	1.61+7 <i>i</i>	-3.702	-1.786
-0.0600	1.58+5.13 <i>i</i>	-5.4209	-2.095	-1.267
⋮	⋮	⋮	⋮	⋮
-0.0200	-0.0531	-0.0351	-0.0192	-0.0052
-0.0175	-0.0375	-0.0231	-0.0104	0.0010
-0.0150	-0.0252	-0.0139	-0.0038	0.0052
-0.0125	-0.0158	-0.0071	0.0007	0.0077
-0.0100	-0.0088	-0.0024	0.0034	0.0086
-0.0075	-0.0040	0.0006	0.0045	0.0082
-0.0050	-0.0011	0.0017	0.0042	0.0065
-0.0025	0.0002	0.0015	0.0027	0.0038
0	0	0	0	0
0.0025	-0.0015	-0.0027	-0.0037	-0.0047
0.0050	-0.0042	-0.0063	-0.0083	-0.0102
0.0075	-0.0079	-0.0110	-0.0138	-0.0164
0.0100	-0.0126	-0.0165	-0.0201	-0.0234
0.0125	-0.0182	-0.0228	-0.0270	-0.0310
0.0150	-0.0245	-0.0297	-0.0346	-0.0392
0.0175	-0.0316	-0.0374	-0.0428	-0.0479
0.0200	-0.0394	-0.0457	-0.0516	-0.0571
⋮	⋮	⋮	⋮	⋮
0.400	-10.7075	-10.7166	-10.7255	-10.7344
0.425	-16.7644	-16.7733	-16.7822	-16.7909
0.450	-31.1965	-31.2052	-31.2139	-31.2225
0.475	-89.0376	-89.0462	-89.0547	-89.0631
0.500	<i>i</i> ∞	<i>i</i> ∞	<i>i</i> ∞	<i>i</i> ∞

Table 3.2: Table showing the behaviour of $\Psi'(\phi)$ for $\kappa_i = \kappa_e = 2$, $\sigma = 1$, $f = 0.5$, and $M > M_s = 0.33$ for both $\phi < 0$ and $\phi > 0$.

A simple illustration is shown in Table 3.2, which shows some results for the parameter values $\kappa_i = \kappa_e = 2$, $\sigma = 1$ and $f = 0.5$. For each value of M shown, we observe that there is no change of sign of $\Psi'(\phi)$ for $\phi > 0$, while for negative potentials a zero does occur until complex values of $\Psi'(\phi, M)$ are encountered. The table also shows that for values of positive ϕ , $\Psi'(\phi, M)$ remains negative but finite up to $\phi = 0.5$, where it becomes infinite and complex.

In addition to the above, recent investigations [Baluku *et al.*, 2010a,b; Verheest and Hellberg, 2010; Verheest, 2010a] have shown that if $\Psi'''(\phi = 0, M_s) \neq 0$, then for the parameters of the plasma system, the sign of $\Psi'''(\phi = 0, M_s)$ corresponds to the sign of the soliton potential whose amplitude goes to zero as $M \rightarrow M_s$. Otherwise for the same plasma parameters, solitons with the sign opposite to that of $\Psi'''(\phi = 0, M_s)$, if they exist, must have finite amplitudes at M_s . With this approach, we can, for a given σ , obtain critical density ratios f , for corresponding κ ($\kappa_e = \kappa_i = \kappa$), such that $\Psi'''(\phi = 0, M_s) = 0$. However, for all values of σ , $\Psi'''(\phi = 0, M_s) = 0$ gives values of $f < 0$, which are unphysical. In other words, for the physical f domain $[0, 1]$ in the case of negative dust, $\Psi'''(\phi = 0, M_s)$ does not change sign, implying that only one potential sign (in this case, negative) may be supported. This also rules out the possibility of positive potential solitons (or double layers) for this plasma model.

3.4.2 Negative Potential Solitons

As shown in the example above, for $\phi < 0$ a charge neutral point is often found for negative potential. The existence of a charge neutral point is necessary but not sufficient for soliton existence. Thus negative solitons may exist, but only if the Sagdeev pseudopotential has a root for an admissible value of ϕ before the cutoff imposed by a physical limit. In this case the limitations on ϕ are in principle provided by the ion and dust grain species with limiting potentials $\phi_{ci} = -(\kappa_i - 3/2)$ and $\phi_{cd} = -M^2/2$, respectively, where $\kappa_i > 3/2$. As discussed earlier, at these limiting potentials we require $\Psi(\phi_{ci} \text{ or } \phi_{cd}) > 0$ to ensure existence of a root. However, for $\kappa_i > 3/2$, $\Psi(\phi_{ci}) = -\infty < 0$; the ion limit condition $\Psi(\phi_{ci}) > 0$ is thus meaningless, just as an “electron limit” was found to be inadmissible for possible positive solitons. Therefore only the dust limit condition, $\Psi(\phi_{cd}) > 0$, is necessary to find the upper limit on M for the existence of negative potential dust acoustic solitons

in the (f, M) space. This case is discussed further in the next section. In principle, negative double layers could provide a limit on ϕ that is smaller in magnitude than $|\phi_{cd}|$. In addition to the general soliton condition [Eq. (3.13)], the existence of double layers requires $\Psi(\phi_m, M) = \Psi'(\phi_m, M) = 0$ and $\Psi''(\phi_m, M) < 0$, where ϕ_m is the amplitude (see Sec. 1.4). We have sought values of ϕ_m and M that satisfy the double layer conditions, over a wide range of values of the parameters $\kappa_e, \kappa_i, \sigma$ and f , but our numerical exploration has not yielded any arbitrary amplitude double layers based on this requirement.

The Sagdeev potential for a soliton possesses a single charge neutral point lying between the origin and the soliton amplitude while double layers have a charge neutral point between two double roots, one of which is at the origin - at the second double root the slope of the pseudopotential is again zero. In our experience, when $\phi < 0$ and $M > M_s$, $\Psi'(\phi)$ remains negative after the first charge neutral point outside the origin. That is, it changes sign only once as seen, for instance, in Table 3.2. Note that for $\phi < 0$, $\Psi'(\phi)$ remains negative, until it becomes complex for relatively small $|\phi|$, in this case for $0.06 < |\phi| < 0.07$ when M is in the range 0.34–0.37, typically after $\Psi(\phi)$ has passed through a zero. Similar results were obtained for other values for the key parameters, *viz.*, $\kappa_i, \kappa_e > 3/2$, $\sigma >$ or < 1 and $0 < f < 1$.

We thus believe that it is highly unlikely that double layers are supported by a dusty plasma with kappa-distributed electrons and/or ions, and thus the upper limit on M is based on ϕ_{cd} .

3.4.3 Numerical Results and Discussion

In this section we discuss numerical results related to the existence of negative potential solitons.

Effect of Spectral Index Variation

In Figure 3.3(a) we show the effect on the negative soliton existence domain, of varying the spectral index of the electron distribution, in association with effectively Maxwellian (high- κ) ions, for equal ion and electron temperatures ($\sigma = 1$). The lower curves represent the lower Mach number limit, M_s [obtained from Eq. (3.13)]. The upper set of curves corresponds to the upper limit of M , obtained from the condition $\Psi(-M^2/2) = 0$, using (3.12).

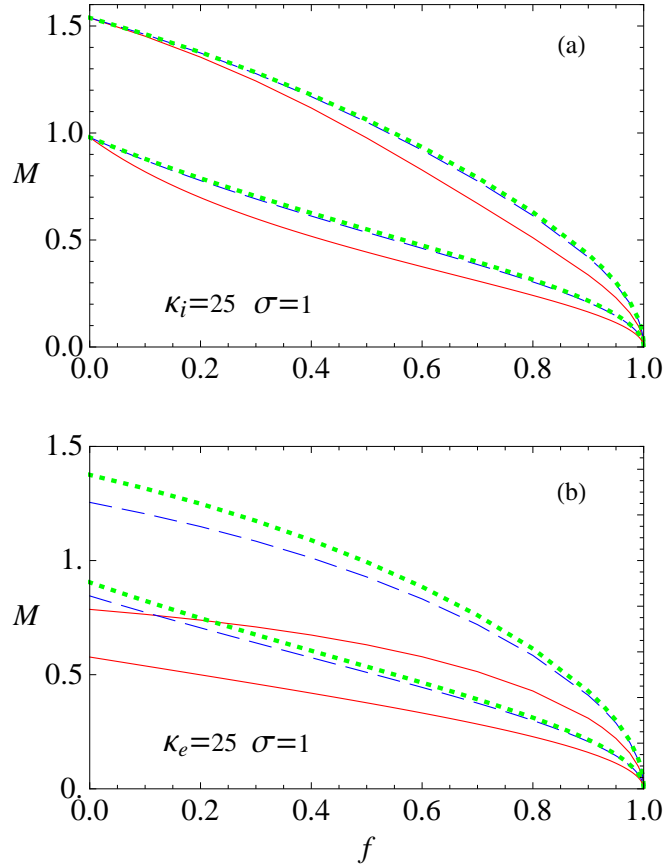


Figure 3.3: Existence domains for negative potential solitons for $\sigma = 1$ and varying κ values. (a) *Upper panel*: $\kappa_i = 25$; $\kappa_e = 2$ (solid, red curves), $\kappa_e = 4$ (dashed, blue curves) and $\kappa_e = 6$ (dotted, green curves), respectively. (b) *Lower panel*: $\kappa_e = 25$; $\kappa_i = 2$ (solid, red curves), $\kappa_i = 4$ (dashed, blue curves) and $\kappa_i = 6$ (dotted, green curves), respectively.

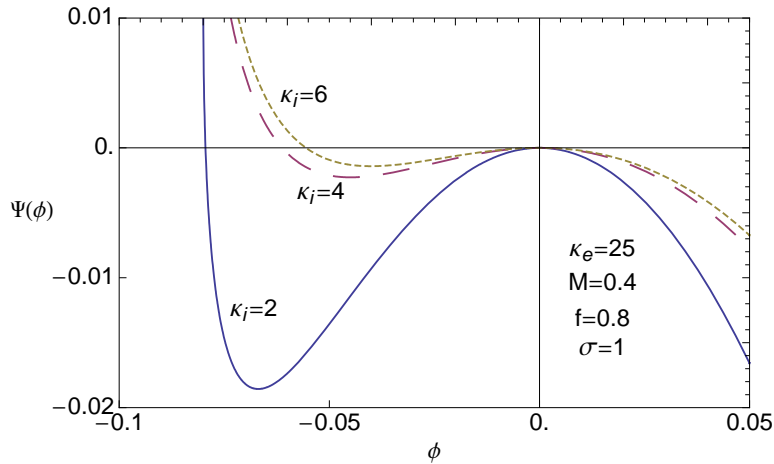


Figure 3.4: Typical Sagdeev potentials for the case of Fig 3.3(b). The pairing $f = 0.8$, $M = 0.4$ lies within the expected existence domain for all three values of κ_i . For larger values of κ_i , fixed M is closer to the lower soliton limit, M_s , and thus the amplitude is smaller.

Thus, for a given electron spectral index value, κ_e , solitons may exist between the two curves. It is seen that for all cases, $M_s \rightarrow 1$ for $f \rightarrow 0$ (ion-dust plasma), and $\rightarrow 0$ for $f \rightarrow 1$ (electron-ion plasma). This agrees with our earlier analytical comments on the form of M_s . The upper limits, too, are the same for all κ_e values for $f \rightarrow 0$ and $f \rightarrow 1$. Further, all curves are qualitatively the same, and the difference between the curves (for both upper and lower limits) corresponding to $\kappa_e = 4$ and $\kappa_e = 6$ is insignificant. From this one may deduce that Maxwellian electrons would yield a similar curve, and that only very low κ values are differentiated from the rest.

The lower panel of Figure 3.3 illustrates the effects of varying κ_i with quasi-Maxwellian electrons. As in the upper panel, both sets of curves converge to $M = 0$ for $f \rightarrow 1$, but unlike the earlier case, both upper and lower limits increase with increasing κ_i as $f \rightarrow 0$. Again, the difference between the curves for $\kappa_i = 4$ and 6 is significantly smaller than that between $\kappa_i = 2$ and 4. Importantly, an increase in the superthermal ion component (*e.g.*, $\kappa_i = 2$) results in a reduction in the range of Mach numbers for which solitons may exist. This appears to be the largest difference from the case in which both electrons and ions have Boltzmann distributions.

Typical Sagdeev potential plots are shown in Fig. 3.4, where we have chosen near-Maxwellian electrons ($\kappa_e = 25$), with $f = 0.8$, *i.e.*, a plasma with 80% of the negative charge carried by the electrons, equal ion and electron temperatures ($\sigma = 1$) and a Mach number $M = 0.4$, which lies in the range for which solitons would be expected for all three values of κ_i used. As one might expect from Fig. 3.3(b), the soliton amplitudes decrease as κ_i is increased, as the chosen value of M is increasingly close to the lower limit, M_s .

Comparison with Small Amplitude Theory

In Figures 3.1 and 3.2 we indicated that the dotted (light-blue) curves correspond to the numerical solutions for the existence of arbitrary amplitude *negative solitary structures*, using Eq. (3.12), as compared to the M_β limit, from the small amplitude approach. In the case of $\kappa_i = \kappa_e = 2$ (left panel of Fig. 3.1), comparing the analytical (M_β) and numerical solutions (dotted, light-blue curve) for the upper limit of M on the existence domain of negative solitons, we see that M_β underestimates the range in M for $f < 0.65$ while for $f > 0.65$, it is overestimated. In fact, no solitons exist above the dotted curve for $f > 0.65$.

The same applies to the right panel of Fig. 3.1 for approximately $f > 0.3$, and also to Fig. 3.2 with $\sigma = 1$. Thus the results in Figs. 3.1 and 3.2 show that when $\kappa_i = \kappa_e$, the upper limit on M for the existence of negative potential solitons from the analytic solution (KdV approach) does not agree with the numerical results to a great extent. Here, in Fig. 3.5, we consider the case of $\kappa_i \neq \kappa_e$, $\sigma = 1$, and compare the existence domains of negative solitons from the KdV theory (or Expanded Sagdeev potential approach) and the full Sagdeev approach. As was the case of $\kappa_i = \kappa_e$, M_β does not give a better approximation to the upper limit of M for the existence of solitons. In the case of quasi-Maxwellian ions and hard spectrum for electrons (high κ_i and low κ_e , as in the left panel of Fig. 3.5), M_β diverges far away from the numerical solutions for $f \gtrsim 0.18$. On the other hand, in the case of quasi-Maxwellian electrons ($\kappa_e = 25$) and strongly non-Maxwellian ions ($\kappa_i = 4$), as shown in the right panel of Fig. 3.5, M_β overestimates the upper limit on M for $f > 0.6$.

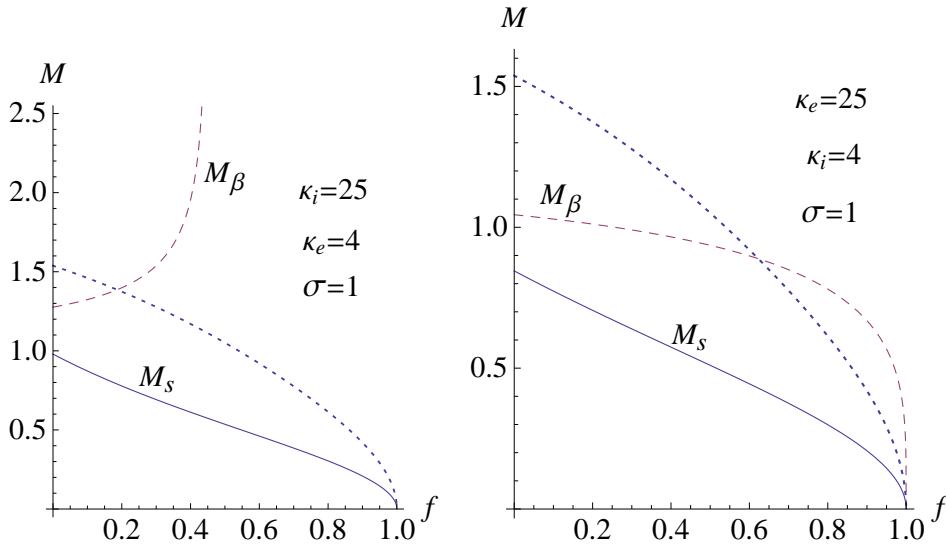


Figure 3.5: Same as Fig. 3.3 but for $\kappa_i = 25$; $\kappa_e = 4$ (*left panel*) and $\kappa_i = 4$; $\kappa_e = 25$ (*right panel*). In both cases, the analytic approximation to the upper limit of M for the existence of negative solitons is the dashed curve labeled M_β , while the numerical solution (obtained by solving $\Psi(-M^2/2) = 0$) is given by the dotted curve.

Effect of Temperature Variation

Having explored the effect of varying κ_e and κ_i on the soliton existence domains for equal ion and electron temperatures, we consider next the effect of varying the temperature ratio for a plasma with significant excess superthermal electrons and ions (small spectral indices). The results are shown in Figure 3.6.

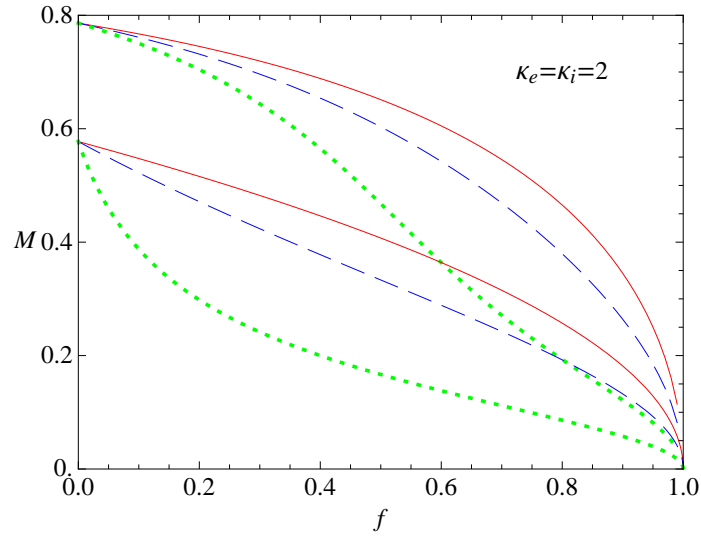


Figure 3.6: Existence domains for negative potential solitons for $\kappa_e = \kappa_i = 2$, with $\sigma = 0.01$ (solid, red curves), $\sigma = 1$ (dashed, blue curves) and $\sigma = 10$ (dotted, green curves).

As was shown in Fig. 3.3(a) when varying κ_e , we find that σ , too, has no effect on M_s and the upper limit of M for $f \rightarrow 0$ and $f \rightarrow 1$. As already indicated, at the extreme values of f the model reduces to a two-component plasma; an electron-ion plasma for $f = 1$ and an ion-dust plasma for $f = 0$. Thus the behaviour of the solitary structures at the extreme f values is not of physical significance for our model but can be used to compare with other simpler plasma models. Varying σ does, however, have a significant effect on the shape of the limiting curves. We note that the drop in M_s as f increases from zero (*i.e.*, increasing electron fraction) is much larger for $\sigma > 1$ (*i.e.*, $T_i > T_e$) than for $\sigma \leq 1$. As a result, the existence domain has a slightly large range in Mach number for this case than for the other two.

3.5 Dust Acoustic Structures with Positive Dust

In the previous section, the discussion has been based on the dust being negatively charged, which is generally regarded as the more common situation. In this section we consider positively charged dust instead of negatively charged dust, where we show that in the presence of positive dust only positive potential solitons are supported.

In this case the dust density expression analogous to that found in Eq. (3.8) is

$$n_{d+}(\phi) = \left(\frac{N_{d0}}{N_{i0}} \right) \left(1 - \frac{2\phi}{M^2} \right)^{-1/2}, \quad (3.27)$$

and substitution into the appropriate form of Poisson's equation leads to expressions for the pseudopotential and soliton condition [cf. Eqs. (3.12) and (3.14)] taking the form

$$\begin{aligned} \Psi_+(\phi) = & \frac{f}{(f-1)\sigma} \left[1 - \left(1 - \frac{\phi\sigma}{\kappa_e - 3/2} \right)^{-(\kappa_e - 3/2)} \right] \\ & + \frac{1}{f-1} \left[1 - \left(1 + \frac{\phi}{\kappa_i - 3/2} \right)^{-(\kappa_i - 3/2)} \right] \\ & + M^2 \left[1 - \left(1 - \frac{2\phi}{M^2} \right)^{1/2} \right] \end{aligned} \quad (3.28)$$

and

$$M_{s+} = \left\{ \frac{f\sigma}{f-1} \left(\frac{2\kappa_e - 1}{2\kappa_e - 3} \right) + \frac{1}{f-1} \left(\frac{2\kappa_i - 1}{2\kappa_i - 3} \right) \right\}^{-1/2}, \quad (3.29)$$

respectively, where $f > 1$, with $f = N_{e0}/N_{i0}$ as before.

Following the same approach as used for the case of negatively charged dust one finds that solitary structures in the presence of positively charged dust are restricted to positive potentials, and that only solitons (no double layers) are supported. These positive potential dust acoustic solitons are bounded from below by M_{s+} [defined in Eq. (3.29)] and from above by M_γ , where the latter is obtained from $\Psi_+(\phi = M^2/2) = 0$ at $M = M_\gamma$ in Eq. (3.28). These results are illustrated in Fig. 3.7, equivalent to Figs. 3.3(a) and 3.6, respectively, but now with $f > 1$.

On the other hand, if we normalize the densities with respect to the electron density, instead of retaining our earlier definition of the density ratio f , we can rewrite the expressions for the pseudopotential (3.28) and soliton condition (3.14) in terms of an appropriate alternative fractional density variable, $g = N_{i0}/N_{e0} < 1$, obtaining

$$\begin{aligned} \Psi_+(\phi) = & \frac{1}{(1-g)\sigma} \left[1 - \left(1 - \frac{\phi\sigma}{\kappa_e - 3/2} \right)^{-(\kappa_e - 3/2)} \right] \\ & + \frac{g}{1-g} \left[1 - \left(1 + \frac{\phi}{\kappa_i - 3/2} \right)^{-(\kappa_i - 3/2)} \right] \\ & + M^2 \left[1 - \left(1 - \frac{2\phi}{M^2} \right)^{1/2} \right] \end{aligned} \quad (3.30)$$

and

$$M_{s+} = \left\{ \frac{\sigma}{1-g} \left(\frac{2\kappa_e - 1}{2\kappa_e - 3} \right) + \frac{g}{1-g} \left(\frac{2\kappa_i - 1}{2\kappa_i - 3} \right) \right\}^{-1/2}.$$

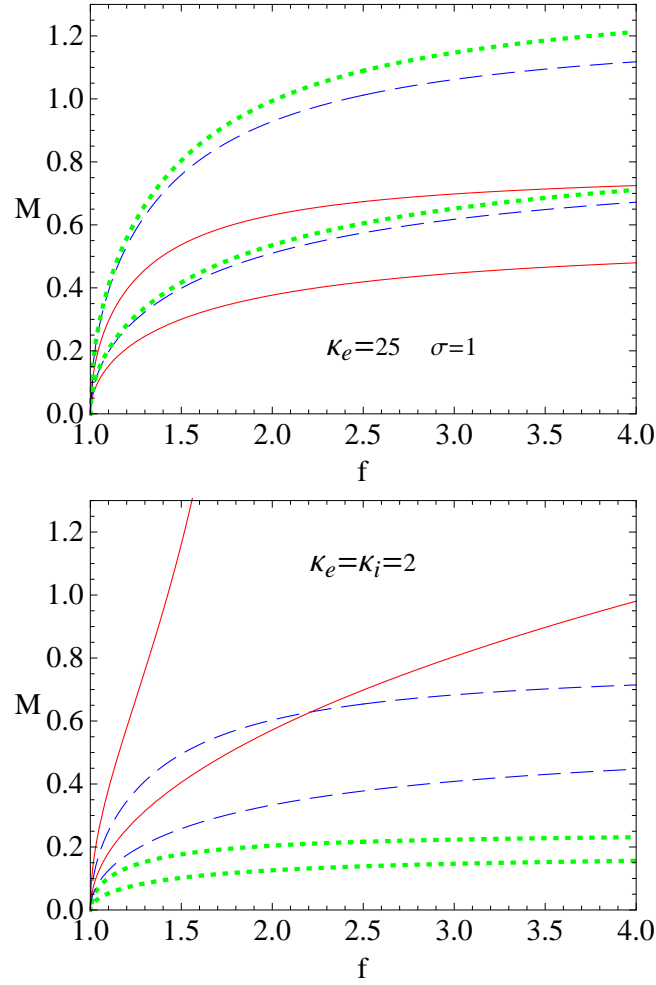


Figure 3.7: *Upper panel:* Existence domains for positive potential solitons in the presence of positive dust for near-Maxwellian ions and varying κ_e , analogously to Fig. 3.3(a), but with $f > 1$; $\sigma = 1$, $\kappa_i = 25$ and $\kappa_e = 2$ (solid, red curves), $\kappa_e = 4$ (dashed, blue curves) and $\kappa_e = 6$ (dotted, green curves), respectively. *Lower panel:* Similar to upper panel, now for $\kappa_e = \kappa_i = 2$, showing the variation with temperature ratio, $\sigma = 0.01$ (solid, red curves), $\sigma = 1$ (dashed, blue curves) and $\sigma = 10$ (dotted, green curves), respectively. This is analogous to Fig. 3.6, but with $f > 1$.

In that case we see that for $\sigma = 1$, the expression is identical to that found in (3.12), apart from a simple reversal of the sign of the potential. Thus, for $T_i = T_e$, the results are identical to those for negative dust, apart from a change of the soliton polarity.

However, for $\sigma \neq 1$ there can be significant differences between the two cases. These are illustrated with the aid of Fig. 3.8, which shows the variation of the existence domains with σ in a plasma with significant superthermal contributions for both the electrons and the ions. It is seen, in particular, that for $\sigma = 0.01$ (*i.e.*, $T_e \gg T_i$), the Mach number range

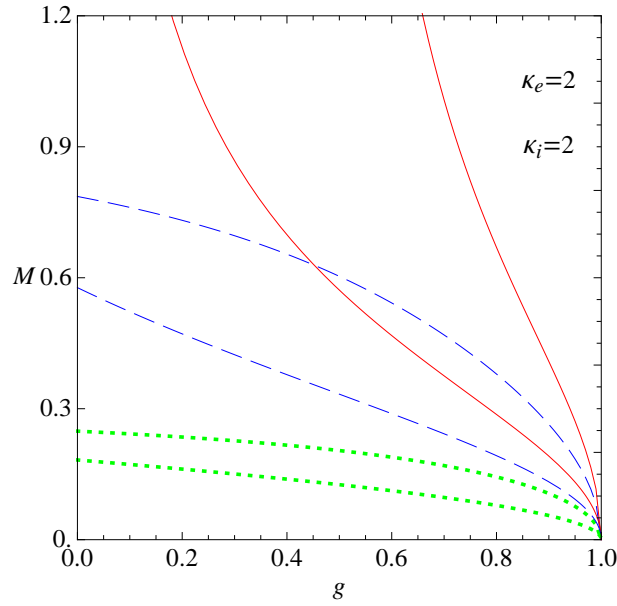


Figure 3.8: Existence domains for positive potential solitons in a positive dusty plasma, plotted as a function of the alternative fractional density variable, $g = N_{i0}/N_{e0}$ for $\kappa_e = \kappa_i = 2$, with $\sigma = 0.01$ (solid, red curves), $\sigma = 1$ (dashed, blue curves) and $\sigma = 10$ (dotted, green curves), respectively. This is analogous to Fig. 3.6.

increases rapidly as the normalized ion density, g , is decreased, *i.e.*, the ions are replaced by positive dust grains. To understand that, let us consider $g \rightarrow 0$, in which case the upper limiting condition $\Psi_+(M^2/2) = 0$ gives

$$(1 + M^2\sigma) \left(1 - \frac{M^2\sigma}{2\kappa_e - 3}\right)^{\kappa_e - 3/2} = 1,$$

which for $\kappa_e = \kappa_i = 2$, as in Fig. 3.8, and $M^2 > 0$, reduces to $M = \sqrt{(1 + \sqrt{5})/\sigma}$. Likewise, the lower Mach number limit, M_s , varies as $\sqrt{(2\kappa_e - 3)/[\sigma(2\kappa_e - 1)]}$, as $g \rightarrow 0$. Thus, as $g \rightarrow 0$, both the lower and upper Mach number limits will vary inversely as the square root of the temperature ratio, hence leading to the shapes exhibited in the figure for $\sigma = 0.01$. Both these expressions are independent of κ_i .

Thus it is clear that while for $\sigma = 1$, the positive dust case is directly analogous to that with negative dust, with a change of soliton potential sign, a slightly more complicated set of differences appears when one considers a case in which the two hot species have temperatures that are significantly different from one another.

3.6 Chapter Summary

We have investigated the existence of dust acoustic solitons in dusty plasmas with κ -distributed ions and/or electrons, and found that only negative potential solitons exist when the dust is negative. Reducing the spectral indices (κ_e, κ_i) only affects the existence domains of the solitons quantitatively.

In the presence of positively charged dust, only positive potential solitons are found, but the ion to electron temperature ratio has significant quantitative effects: particularly for $T_e \gg T_i$ the results are very different from those for $T_e = T_i$. In both cases we find that the soliton polarity agrees with the sign of the charge of the inertial species (dust), as observed in a number of other plasma models, albeit not universally so. For instance, this characteristic was also observed previously for positive dust in a plasma with polytropic or Boltzmann electrons and ions [Baluku *et al.*, 2008]. However there are quantitative differences, arising from the functional form of the number density for a κ -distribution as in Eq. (3.2).

Although the κ -distribution is nonthermal, the results reveal important differences from those found when one of the hot plasma species has a different nonthermal distribution, *viz.*, the Cairns distribution [Verheest and Pillay, 2008a,b]. They showed that for negative (positive) dust, positive (negative) solitons could also be found, limited by double layers, for sufficient nonthermality of the ions (electrons) and sufficiently low electron (ion) density. For nonthermal electrons (ions) only negative (positive) potential solitons were found, as in our case. This difference in results could be due to the fact that for the κ distribution the main change from a Maxwellian lies in the ‘tail’ region, unlike the case of the Cairns distribution.

Comparing results from the small amplitude expansion (by expanding the Sagdeev potential) with those from the arbitrary amplitude approach, our results show that the existence domains for negative solitons from the former approach include a range in (f, M) space that is unphysical, that is, lying in a region where no solitons can be obtained, following the arbitrary amplitude approach. This difference in results shows that small amplitude approaches should not be relied on too much when, for example, interpreting observational data for solitary structures.

In view of the observations of both kappa-distributed ions and electrons in Saturn's magnetosphere [Krimigis *et al.*, 1983; Schippers *et al.*, 2008], as well as dust [Jones *et al.*, 2008], the results of this work can assist in the interpretation of nonlinear electrostatic solitary waves that may be observed in that region.

Dust Ion-Acoustic Solitons in a Plasma with Kappa-Distributed Electrons

In this chapter we investigate solitary structures that may be supported by dusty plasmas consisting of kappa distributed electrons, fluid adiabatic ions and dust particles. As dust particles are usually negatively charged (in most dust plasma environments), we discuss our results mainly with negatively charged dust. However, we also discuss, briefly, the case for positively charged dust.

The results presented in this Chapter have been published as Baluku et al., Physics of Plasmas, 17, 053702 (2010)

4.1 Introduction

Dust ion-acoustic (DIA) waves in unmagnetized plasmas are low frequency waves with phase velocity lying between the electron and ion thermal velocities ($V_{tj} = (K_B T_j / m_j)^{1/2}$; $j = e, i$), that is, $V_{ti} < \omega/k < V_{te}$ to avoid Landau damping. They were first studied theoretically by Shukla and Silin [1992] and later confirmed experimentally by Barkan *et al.* [1996].

Dust ion-acoustic waves are basically ion-acoustic waves whose wave behaviour is modified by the presence of dust grains. It has earlier been shown [Verheest *et al.*, 2005; Baluku and Hellberg, 2008], using a fluid dynamic paradigm, that the (normalized) phase velocity, here denoted $v_\phi = (\omega/k)/C_s$, of the DIA wave can be expressed as $v_\phi^2 = [1 + (f - 1)z]/f$,

where $C_s = (K_B T_e / m_i)^{1/2}$ is the ion-acoustic speed in the absence of dust, $f = N_{e0} / N_{i0}$ is the ratio of the electron to ion equilibrium densities, with $f < 1$ ($f > 1$) for negatively (positively) charged dust grains; $z = Z_d m_i / m_d$ is the ratio of the charge-to-mass ratio of the ions to the dust particles, with the ions assumed singly charged. Thus the phase velocity of linear DIA wave is increased (reduced) when the dust is negatively (positively) charged.

Nonlinear DIA waves have been studied by a number of authors [Bharuthram and Shukla, 1992; Mamun and Shukla, 2002; McKenzie *et al.*, 2005; Verheest *et al.*, 2005; Hellberg *et al.*, 2006; Mamun and Jahan, 2008; Sayed *et al.*, 2008]. However, most nonlinear studies [Mamun and Shukla, 2002; Mamun and Jahan, 2008; Sayed *et al.*, 2008] used Reductive Perturbation Theory or equivalent expansions), to study various aspects of small amplitude solitons and/or double layers while others [Bharuthram and Shukla, 1992; Verheest *et al.*, 2005; McKenzie *et al.*, 2005; Hellberg *et al.*, 2006] considered arbitrary amplitude DIA structures, using the Sagdeev pseudopotential approach [Sagdeev, 1966]. In particular, Bharuthram and Shukla [1992] considered a plasma model consisting of Boltzmann-distributed electrons, cold ions and immobile negative dust. They sought positive potential solitons, and found existence ranges of both normalized soliton speed (M) and amplitude ϕ as a function of the fraction of negative charge residing on the dust. In addition, they considered negative potential solitons. However, they only presented Sagdeev potential curves for two values of M and two values of mobility. In addition to studying dust-acoustic solitons, Verheest *et al.* [2005] examined DIA solitons in a plasma model which allowed for arbitrary values of the polytropic index (γ_e) for the electrons, cold ions and mobile dust. Numerical evaluation of existence diagrams was carried out for two values of γ_e , *viz.*, $\gamma_e = 1$ (isothermal, *i.e.*, Boltzmann) and $3/2$.

While most authors have discussed dust ion-acoustic waves and solitons, with Maxwellian electrons or ions theoretically [Bharuthram and Shukla, 1992; Ghosh *et al.*, 2000a,b; Mamun and Shukla, 2002; Rahman *et al.*, 2007; Mamun and Jahan, 2008; Pajouh and Abbasi, 2008; Sayed *et al.*, 2008] and experimentally [Barkan *et al.*, 1996], space plasmas are observed to possess non-Maxwellian distributions [Krimigis *et al.*, 1983; Hasegawa *et al.*, 1985; Christon *et al.*, 1988; Pierrard and Lemaire, 1996; Maksimovic *et al.*, 1997; Pierrard *et al.*, 2004] as we mentioned in Sec. 1. These non-Maxwellian distributions can be modelled

accurately by a kappa (or generalized Lorentzian) distribution [Olbert, 1968; Vasyliunas, 1968], like the one given by Eq. (1.2).

In this work we thus study the behaviour of and existence domains for dust ion acoustic solitons that may be supported by a plasma in which the electrons are non-Maxwellian and following a kappa-distribution. Small amplitude structures are investigated using the reductive perturbation technique, while the Sagdeev pseudopotential approach is used for arbitrary amplitude soliton studies. While most of the investigation deals with the more interesting and relevant case of negative dust, we also consider positive dust. In particular we draw attention to the occurrence of finite amplitude solitary waves at the dust ion-acoustic speed in a negative dust plasma, and explore some of the characteristics of this phenomenon.

4.2 Basic Equations

We consider a plasma with kappa distributed electrons of temperature T_e and density N_e , fluid adiabatic ions of temperature T_i and density N_i , and cold dust particles. The charge quasi-neutrality condition for the system is

$$N_{e0} = N_{i0} + sZ_d N_{d0}, \quad (4.1)$$

where N_{j0} is the equilibrium density of species j , ($j = e, i, d$ for electrons, ions and dust, respectively); Z_d is the size of the dust charge, and $s = \pm 1$ is the sign of the dust charge (for positive or negative dust particles). The ions are assumed to be singly charged, like protons, and therefore, throughout the discussion we shall take $Z_i = 1$ in this plasma model.

In the presence of an electrostatic potential, the κ -distributed electrons have normalized density $n_e = N_e/N_{i0}$ given by [Baluku and Hellberg, 2008]

$$n_e(\phi) = f \left(1 - \frac{\phi}{\kappa - 3/2} \right)^{-(\kappa-1/2)}, \quad (4.2)$$

where ϕ is the electrostatic potential, here normalized with respect to the electron thermal energy ($K_B T_e/e$); $f = N_{e0}/N_{i0} = 1 + sZ_d N_{d0}/N_{i0}$ defines the fraction of electron equilibrium density with respect to the ion equilibrium density. The density expres-

sion given above is only valid for $\kappa > 3/2$, and it reduces to the usual Maxwellian form $f n_e(\phi) = \exp(-\phi)$ when $\kappa \rightarrow \infty$. In unnormalized form, the electron density expression in Eq. (4.2) is obtained from $N_e(\varphi) = \iiint F_\kappa(v) d^3v$ where $F_\kappa(v)$ is the velocity distribution function defined in Eq.(1.2) with the transformation [Baluku and Hellberg, 2008] $v^2 \rightarrow v^2 + 2q_e\varphi/m_e$, see Appendix. A.1 for details.

The density of the ions ($j = i$) and dust particles ($j = d$) are obtained from the continuity, momentum and pressure equations

$$\frac{\partial n_j}{\partial t} + \frac{\partial}{\partial x}(n_j u_j) = 0, \quad (4.3)$$

$$\frac{\partial u_j}{\partial t} + u_j \frac{\partial u_j}{\partial x} + \frac{m_i}{m_j} \frac{\sigma}{n_j} \frac{\partial p_j}{\partial x} + \frac{m_i}{m_j} \frac{q_j}{e} \frac{\partial \phi}{\partial x} = 0, \quad \text{and} \quad (4.4)$$

$$\frac{\partial p_j}{\partial t} + u_j \frac{\partial p_j}{\partial x} + 3p_j \frac{\partial u_j}{\partial x} = 0, \quad (4.5)$$

respectively, where $\sigma = T_i/T_e$; u_j , n_j and p_j are the normalized ion velocity, density and pressure, of species j , respectively, and ϕ the electrostatic potential.

The independent variables, x and t , are normalized to an effective Debye length $\lambda_{D\text{eff}} = (\varepsilon_0 K_B T_e / N_{i0} e^2)^{1/2}$ and the inverse ion plasma frequency $\omega_{pi}^{-1} = (N_{i0} e^2 / \varepsilon_0 m_i)^{-1/2}$, respectively; the dependent variables, u_j , n_j , p_j and ϕ , are normalized to $C_s = (K_B T_e / m_i)^{1/2}$, N_{i0} , $P_{i0} = N_{i0} K_B T_i$ and $K_B T_e / e$, respectively.

The macroscopic variables, n_j , p_j , u_j and ϕ satisfy the boundary conditions $\phi, \partial\phi/\partial x, u_j \rightarrow 0; n_j \rightarrow N_{j0}/N_{i0}$, and $p_j \rightarrow P_{j0}/P_{i0}$, as $x \rightarrow \pm\infty$.

From Eqs. (4.3)–(4.5), and after transforming to a stationary frame where all quantities depend on $\xi = x - Mt$, the normalized ion density is thus obtained as [Ghosh *et al.*, 1996; Verheest *et al.*, 2008]

$$n_i(\phi) = \frac{1}{2\sqrt{3\sigma}} \left\{ \left[\left(M + \sqrt{3\sigma} \right)^2 - 2\phi \right]^{1/2} \pm \left[\left(M - \sqrt{3\sigma} \right)^2 - 2\phi \right]^{1/2} \right\}, \quad (4.6)$$

where M is the soliton speed or Mach number in the stationary frame of reference with position $\xi = x - Mt$. From the boundary conditions, we have $n_i \rightarrow 1$ for $\phi \rightarrow 0$. This is only true if we take the minus sign in Eq. (4.6), and that will give us the appropriate expression for $n_i(\phi)$ that will be used in the discussion which will follow. In the limit $\sigma \rightarrow 0$ (cold ions), $n_i(\phi) = (1 - 2\phi/M^2)^{-1/2}$. This means that when $\phi = M^2/2$, $n_i \rightarrow \infty$, and the

ions are infinitely compressed.

Similarly the normalized density of the dust particles is given by

$$n_d(\phi) = \frac{N_{d0}/N_{i0}}{2\sqrt{3}\sigma_D} \left\{ \left[(M + \sqrt{3}\sigma_D)^2 - 2sz\phi \right]^{1/2} \pm \left[(M - \sqrt{3}\sigma_D)^2 - 2sz\phi \right]^{1/2} \right\}. \quad (4.7)$$

where $z = m_i(Z_d/m_d)$ is the fraction of the the charge-to-mass ratio of dust to that of ions (with $Z_i = 1$); $\sigma_D = (m_i T_d / m_d T_e) = \sigma \sigma_d$ with $\sigma_d = V_{id}^2 / V_{ti}^2$. Here, $V_{ti}(V_{td})$ is the ion(dust) thermal velocity. Again, for the \pm sign, we shall use the minus sign in our calculations as that gives the appropriate boundary conditions as $\xi \rightarrow \infty$.

Since we shall consider cold dust particles ($\sigma = 0$) in the model, the density of the dust particles takes the form

$$n_d(\phi) = \frac{(f-1)}{sZ_d} (1 - 2sz\phi/M^2)^{-1/2}. \quad (4.8)$$

However, if the dust motion is not included, $n_d \rightarrow N_{d0}/N_{i0} = (f-1)/sZ_d$, since the immobile dust particles then only provide neutralization in the background. This will be the case when discussing small amplitude solitons using the reductive perturbation technique, but we shall allow for dust mobility in the pseudopotential calculations.

The species' densities, given by equations (4.2), (4.6) and (4.8), are coupled by Poisson's equation

$$\frac{\partial^2 \phi}{\partial \xi^2} + n_i(\phi) - n_e(\phi) + sZ_d n_d(\phi) = 0. \quad (4.9)$$

4.3 Linear Dispersion Relation

In linearized form, the electron density takes the form

$$n_{e1} \simeq f \left(\frac{\kappa - 1/2}{\kappa - 3/2} \right) \phi_1. \quad (4.10)$$

Next we Fourier analyze the continuity, pressure and momentum equations in terms of normalized angular frequency ω and wavenumber k , and expand them to linear order. For

the ions, this gives

$$n_{i1} = \frac{k^2}{\omega^2 - 3\sigma k^2} \phi_1. \quad (4.11)$$

Alternatively, we can rewrite M as $M = M_0 + \delta M$, where M_0 and δM are the equilibrium (unperturbed) and perturbed values of Mach number. The unperturbed Mach number coincides with the lowest Mach number value, below which no solitons can be supported by the plasma model, and also defines the phase velocity of the propagating waves, as we will see later. If we assume that the perturbations in M are so small that they can be neglected ($\delta M \ll 1$), then $M \sim M_0 = \omega/k$. Thus letting $\phi \simeq \phi_1$ and $n_i(\phi) \simeq 1 + n_{i1}(\phi_1)$, the series expansion of Eq. (4.6) about $\phi = 0$ leads to $n_{i1}(\phi_1) \simeq \phi_1/(M_0^2 - 3\sigma)$, such that with the substitution $M_0 = \omega/k$ we recover Eq. (4.11).

Similarly,

$$n_{d1} \simeq \frac{z(f-1)k^2}{Z_d \omega^2} \phi_1. \quad (4.12)$$

In terms of ϕ_1 , Poisson's equation, (4.9), becomes

$$\frac{\partial^2 \phi_1}{\partial \xi^2} + n_{i1}(\phi_1) - n_{e1}(\phi_1) + s Z_d n_{d1}(\phi_1) = 0, \quad (4.13)$$

which upon substitution of Eqs. (4.10)–(4.12) into (4.13), with $\partial/\partial \xi = \partial/\partial x \rightarrow ik$, leads to

$$k^2 \phi_1 \left\{ 1 - \frac{1}{\omega^2 - 3\sigma k^2} + \frac{f}{k^2} \left(\frac{\kappa - 1/2}{\kappa - 3/2} \right) - \frac{s(f-1)z}{\omega^2} \right\} = 0.$$

The non-trivial solution gives the linear dispersion relation as

$$1 - \frac{1}{\omega^2 - 3\sigma k^2} + \frac{f}{k^2} \left(\frac{\kappa - 1/2}{\kappa - 3/2} \right) + \frac{s(1-f)z}{\omega^2} = 0. \quad (4.14)$$

We see that for the typical situation ($z \ll 1$), Eq. (4.14) becomes

$$1 - \frac{1}{\omega^2 - 3\sigma k^2} + \frac{1}{k^2 V_{s0}^2} = 0, \quad (4.15)$$

where the effective DIA speed V_{s0} is given by

$$V_{s0}^2 = \frac{1}{f} \left(\frac{\kappa - 3/2}{\kappa - 1/2} \right) = \left(\frac{N_{i0}}{N_{e0}} \right) \left(\frac{\kappa - 3/2}{\kappa - 1/2} \right), \quad (4.16)$$

yielding $1/f$ in the limit $\kappa \rightarrow \infty$. In the long wavelength limit, $k \ll 1$, one then obtains

$$\omega^2 = k^2(V_{s0}^2 + 3\sigma). \quad (4.17)$$

However, in the long wavelength limit ($k \rightarrow 0$, that is $k \ll 1$) and $z \neq 0$ (not negligibly small), the dispersion relation (4.14) yields

$$\frac{\omega^2}{k^2} = \frac{b}{2a} \left[1 \pm \left(1 - \frac{4ac}{b^2} \right)^{1/2} \right], \quad (4.18)$$

provided $b^2 - 4ac \geq 0$ for non-complex values of the phase velocity, and the constants a , b , and c are, respectively, given by

$$a = f \left(\frac{\kappa - 1/2}{\kappa - 3/2} \right), \quad b = 1 + sz(f - 1) + 3\sigma a, \quad \text{and} \quad c = 3\sigma sz(f - 1). \quad (4.19)$$

Of course when $z \ll 1$, we have $c \rightarrow 0$ and $b \rightarrow 1 + 3\sigma a$, and therefore the effective phase velocity takes the form $\omega/k = (b/a)^{1/2}$.

Since the phase velocity ω/k is normalized to the ion sound speed $C_s = (K_B T_e / m_i)^{1/2}$, for a plasma system with cold ions ($\sigma \rightarrow 0$), immobile dust ($z \rightarrow 0$) and Maxwellian electrons ($\kappa \rightarrow \infty$) we get $a \rightarrow f$ and $b \rightarrow 1$. Therefore we recover the dispersion relation $\omega^2 \simeq (N_{i0}/N_{e0})k^2 C_s^2$ of Shukla and Silin [1992] with $Z_i = 1$.

4.4 Small Amplitude Solitons: Reductive Perturbation Technique

In the reductive perturbation method, the electron density is obtained from

$$\begin{aligned} n_e(\phi) &= f \left(1 - \frac{\phi}{\kappa - 3/2} \right)^{-(\kappa-1/2)} \\ &\simeq f + c_1 \phi + c_2 \phi^2 + c_3 \phi^3 + \dots, \end{aligned} \quad (4.20)$$

where

$$\begin{aligned}
 c_1 &= f \left(\frac{\kappa - 1/2}{\kappa - 3/2} \right), \\
 c_2 &= \frac{f(\kappa - 1/2)(\kappa + 1/2)}{2!(\kappa - 3/2)^2}, \\
 c_3 &= \frac{f(\kappa - 1/2)(\kappa + 1/2)(\kappa + 3/2)}{3!(\kappa - 3/2)^3}, \dots \\
 &\text{etc}
 \end{aligned} \tag{4.21}$$

A word of caution here is that the expansion of Eq. (4.2) [leading to Eq. (4.21)] is only valid for $\kappa > 3$. For $1.5 < \kappa \lesssim 3$ the higher order terms are large compared to those of lower order, and therefore cannot be neglected. This comparison is shown in Table 4.1, where we show values of the coefficients c_j/f for few values of $\kappa \leq 4$. The table shows that for $\kappa = 2$ and 2.5, the values in the fourth and fifth columns are higher than the third column values. In the case of $\kappa = 2.9$ and 3, although the fourth column values are less than the third column values, they are nevertheless not negligible. Thus when one uses the reductive perturbation method for plasmas involving κ -distributed particles, the range of κ values for which it is valid imposes an important constraint.

κ	c_1/f	c_2/f	c_3/f	c_4/f	c_5/f
2.0	3.000	7.500	17.50	39.38	86.63
2.5	2.000	3.000	4.000	5.000	6.000
2.9	1.714	2.082	2.181	2.103	1.923
3.0	1.667	1.944	1.944	1.782	1.545
3.1	1.625	1.828	1.752	1.533	1.265
3.2	1.588	1.728	1.593	1.335	1.052
3.5	1.500	1.500	1.250	0.934	0.656
4.0	1.400	1.260	0.924	0.601	0.360

Table 4.1: Table showing the the coefficients, c_j/f in Eq. (4.21) for some values of κ . For $\kappa \geq 3$ the fourth order terms (c_4/f) are smaller than the third order terms (c_3/f) and therefore can be neglected in the expansion. However, for $\kappa < 3$, c_4/f is greater than c_3/f , provided κ is not very close to 3.

In addition, we assume that the dust particles are cold and that they only provide neutralization in the background ($n_d \rightarrow N_{d0}/N_{i0}$), since for DIAW, it is the ion and electron dynamics that are more important. Thus Poisson's equation (4.9) may be written

as

$$\frac{\partial^2 \phi}{\partial \xi^2} + n_i(\phi) - n_e(\phi) + f - 1 \approx 0, \quad (4.22)$$

where $\xi = x - Mt$ in the wave frame, and the ion density $n_i(\phi)$ is obtained from the perturbation expansion of the ion fluid equations (4.3)–(4.5).

4.4.1 Korteweg-de Vries (KdV) Equation

In deriving the KdV equation we use the usual stretched coordinates [Mace *et al.*, 1991; Verheest, 2000; Shukla and Mamun, 2002] $\chi = \epsilon^{1/2}(x - M_a t)$ and $\tau = \epsilon^{3/2}t$, where M_a is the phase velocity normalized to the fixed acoustic speed in the absence of dust, and ϵ a smallness parameter. We then arrive at the KdV equation [Mace *et al.*, 1991; Verheest, 2000; Mamun and Shukla, 2002; Shukla and Mamun, 2002]:

$$\frac{\partial \phi_1}{\partial \tau} + A \phi_1 \frac{\partial \phi_1}{\partial \chi} + B \frac{\partial^3 \phi_1}{\partial \chi^3} = 0, \quad (4.23)$$

where the constants A and B are obtained from

$$A = B(12\sigma c_1^3 + 3c_1^2 - 2c_2); \quad B(2c_1^2 M_a) = 1; \quad M_a = (3\sigma + 1/c_1)^{1/2}, \quad (4.24)$$

and c_1 and c_2 are defined in Eq. (4.21).

We use the transformation $\eta = \chi - M_0 \tau = \epsilon \xi$; $\xi = x - Mt$, where M_0 is the speed of the solitary wave in the stationary frame, and M is the Mach number, given by $M = M_a + \epsilon M_0$, equivalent to the normalized speed of the solitary waves in the laboratory frame. We then obtain the solution to Eq. (4.23) as [Washimi and Taniuti, 1966; Mace *et al.*, 1991; Verheest, 2000; Mamun and Shukla, 2002; Shukla and Mamun, 2002]

$$\phi_1(\eta) = \frac{3M_0}{A} \operatorname{sech}^2 \left\{ \left(\frac{M_0}{4B} \right)^{1/2} \eta \right\}. \quad (4.25)$$

Finally, transforming back to the laboratory frame [with coordinates (x, t)] we get [Mace *et al.*, 1991; Verheest, 2000]

$$\phi(x, t) \sim \epsilon \phi_1(x, t) = \frac{3\delta M}{A} \operatorname{sech}^2 \left\{ \left(\frac{\delta M}{4B} \right)^{1/2} [x - Mt] \right\}, \quad (4.26)$$

where $\delta M = \epsilon M_0 = M - M_a$. The amplitude and width of the soliton are given by $3\delta M/A$ and $(4B/\delta M)^{1/2}$, respectively. Thus Eq. (4.26) shows that the KdV soliton has zero amplitude when $M = M_a$ (or $\delta M = 0$), and the amplitude increases with δM . Since B is always positive (from the definition of B in (4.24), and $M_a > 0$ for forward propagation), the validity of Eq. (4.26) requires $\delta M > 0$, that is, $M > M_a$, as both B and δM must have the same sign for real soliton width. Therefore the dust ion-acoustic solitons that exist in this model are super-acoustic – and we shall see that it also follows from the standard arbitrary amplitude approach. It will be shown later (cf. (4.38) in the limit $z \rightarrow 0$) that $M_a = M_s$, where M_s is the lowest Mach number below which solitons cannot exist. Also, with $\delta M > 0$, the sign of the potential solitons will depend on whether A is positive or negative.

Since B is always positive for $\kappa > 3/2$, then from the expression of A in Eq. (4.24) one can, for given κ , find a critical plasma composition, *i.e.*, a critical value of f , here denoted f_c , for which the coefficient, A , of the nonlinear term ($\phi \partial\phi/\partial\chi$) in the KdV equation [Eq. (4.23)] is zero, and the amplitude ($3\delta M/A$) in Eq. (4.26) goes to infinity, and therefore the KdV approach breaks down. The critical value of f_c will be seen to play a significant role in determining the soliton characteristics in the arbitrary amplitude, pseudopotential study that will follow in the subsequent section. It is worth noting that for f close to f_c , the arbitrary soliton amplitudes (obtained from the Sagdeev approach in the next section) show surprising behaviour in that the soliton amplitude at $M = M_s$ is nonzero, and that in the neighbourhood of M_s solitons already possess large amplitudes. Such a scenario is shown in Fig. 4.8, for $f = 0.5$ ($\phi > 0$, with $\kappa = 2$) and $f = 0.9$ ($\phi < 0$).

In Fig. 4.1 the continuous (red) curve shows the variation, with κ , of f_c , the solution of the equation $A \equiv A(f, \kappa) = 0$, for fixed σ and z . From the sign of A one can show that positive (negative) small amplitude potential solitons are obtained for $f > f_c$ ($f < f_c$), *i.e.*, above (below) the continuous red curve in Fig. 4.1. Therefore, solitons with either polarity are in principle supported by the plasma model. However, for fixed values of f , κ , and σ , and hence of c_1 and c_2 , the sign of A and thus the soliton polarity, are uniquely defined, *i.e.*, for a given plasma configuration, only a single sign of soliton potential is permitted. This figure also yields a further interesting physical result (I. Kourakis, 2009,

pers. comm.¹) : for a plasma with, say, $f = 0.4$, the figure shows that a Maxwellian-like distribution ($\kappa \geq 10$) supports positive KdV solitons ($f > f_c$), while for $\kappa \approx 4$, the KdV solitons would be negative ($f < f_c$).

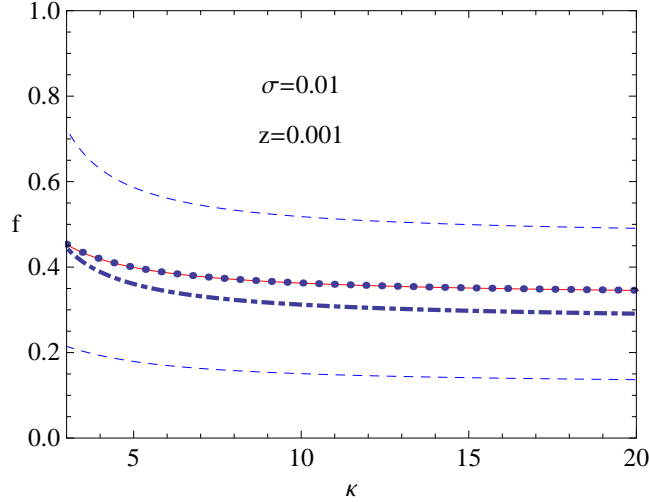


Figure 4.1: *Continuous (red) curve*: Variation of the critical density fraction, f_c (where the KdV coefficient $A = 0$) with κ for $\sigma = 0.01$ and $z = 0.001$. *Dashed (light blue) curves*: These represent the region in f over which the mKdV coefficient, C , is positive. *Dotted (dark blue) curve*: This coincides with the continuous (red) curve for f_c , and represents values of f obtained from $\Psi'''(f, M = M_s, \phi = 0) = 0$, in the arbitrary amplitude case (see next section). *Dot-dashed (dark blue) curve*: This maximizes the parameter C in the mKdV equation for small amplitude solutions in Eq. (4.29). For discussion purposes κ values take the range 2 – 20, though we have indicated that for expansion of kappa distributed physical quantities κ must exceed 3.

4.4.2 Modified Korteweg-de Vries (mKdV) Equation

We have already indicated that the KdV method is invalid close to the critical composition, f_c , since the soliton amplitude goes to infinity when $A(f, \kappa) = 0$. In overcoming that scenario we have to turn to the modified KdV (mKdV) approach in that neighbourhood. In the mKdV approach we use the stretched coordinates $\chi = \epsilon(x - M_a t)$ and $\tau = \epsilon^3 t$, and thus obtain the mKdV equation [Verheest, 2000]:

$$\frac{\partial \phi_1}{\partial \tau} + C \phi_1^2 \frac{\partial \phi_1}{\partial \chi} + B \frac{\partial^3 \phi_1}{\partial \chi^3} = 0, \quad (4.27)$$

where the quadratic nonlinear term of the KdV equation is now replaced by a cubic non-linearity. Here, in Eq. (4.27), B takes the same form as defined in the KdV equation while

¹Dr. I. Kourakis, Queen's University Belfast, Belfast BT7 1NN, Northern Ireland, U. K.

C is given by

$$C = B \left\{ 36\sigma c_1^2(c_2 - c_1^2) + 2c_1c_2(5 + 2c_1) - c_1^3(2c_1 + 19/2) - 3c_3 \right\},$$

with c_1 , c_2 and c_3 defined in Eq. (4.21). Using the transformation $\eta = \chi - M_0\tau$, it can easily be shown that Eq. (4.27) has (the standard) solution [Mace *et al.*, 1991; Verheest, 2000],

$$\phi_1(\eta) = \pm(6M_0/C)^{1/2} \operatorname{sech} \left\{ (M_0/B)^{1/2} \eta \right\}. \quad (4.28)$$

Details for the derivation of Eq. (4.28) are given in Appendix C.2. Equation (4.28) can also be written as

$$\phi(\xi) \sim \epsilon \phi_1(x, t) = \pm(6\delta M/C)^{1/2} \operatorname{sech} \left\{ \left(\frac{\delta M}{B} \right)^{1/2} (x - Mt) \right\}, \quad (4.29)$$

where $\xi = x - Mt = (\chi - M_0\tau)/\epsilon$; $\delta M = \epsilon^2 M_0 = M - M_a$, with parameters M , M_0 and M_a , as well as B defined as in the KdV expressions.

The validity of Eq. (4.29) requires that all B , C and δM are of the same sign for real soliton width and potential amplitude. However, for all $\kappa > 3/2$, B is always positive, therefore $\delta M > 0$, or $M > M_a$, which gives the lower Mach number as M_a , and the only other restriction on the existence of small amplitude potential solitons (from the mKdV solution) will be given by the condition $C > 0$, which imposes restrictions on the range of f . From the form of Eq. (4.29), it follows that the polarity of mKdV solitons is not specified.

In Fig. 4.1 the range of validity for different spectral indices κ lies between the two dashed (light blue) curves, corresponding to $C = 0$. Although the range of f over which $C > 0$ appears quite large in Fig. 4.1, the mKdV equation, like the KdV equation, applies only to small amplitude solitary waves. From Eq. (4.29) it is clear that small amplitude solitons require C as large as possible. One can show that C peaks at $f \sim (f_c - 0.1)$ for all $\kappa \geq 4$, with typical maxima ≤ 0.5 , see dot-dashed curve in Fig. 4.1.

4.5 Arbitrary Amplitude Solitons: Pseudopotential Approach

We now substitute Eqs. (4.2), (4.6) and (4.8) in Poisson's equation, Eq. (4.9). After an integration, we get the usual energy equation [Sagdeev, 1966; Verheest, 2000]

$$\frac{1}{2} \left(\frac{\partial \phi}{\partial \xi} \right)^2 + \Psi(\phi, M) = 0,$$

where the pseudopotential $\Psi(\phi, M)$ is given by

$$\begin{aligned} \Psi(\phi, M) = & f \left[1 - \left(1 - \frac{\phi}{\kappa - 3/2} \right)^{3/2 - \kappa} \right] - (1 - f) \frac{M^2}{s z} \left[1 - \left(1 - \frac{2s z \phi}{M^2} \right)^{1/2} \right] \\ & + \left(\frac{1}{6\sqrt{3}\sigma} \left[\left\{ (M - \sqrt{3}\sigma)^2 - 2\phi \right\}^{3/2} - \left\{ (M + \sqrt{3}\sigma)^2 - 2\phi \right\}^{3/2} \right] \right. \\ & \left. + M^2 + \sigma \right), \end{aligned} \quad (4.30)$$

and the boundary conditions $\phi, \partial\phi/\partial\xi \rightarrow 0$ as $\xi \rightarrow \pm\infty$ have been used. Equation (4.30) satisfies $\Psi(0, M) = 0$ and $\Psi'(0, M) = 0$, with the prime denoting derivative with respect to ϕ . The three terms in Eq. (4.30) represent the contributions to the pseudopotential, of the κ -distributed electrons, cold mobile dust, and warm fluid ions, respectively.

In the limit $z \rightarrow 0$, the cold dust particles contribution to Eq. (4.30) [the second term in Eq. (4.30)] becomes $(1 - f)\phi$. Thus, in the presence of cool moving ions and immobile dust particles, $\Psi(\phi, M)$ takes the form

$$\begin{aligned} \Psi(\phi, M) \approx & f \left[1 - \left(1 - \frac{\phi}{\kappa - 3/2} \right)^{3/2 - \kappa} \right] - (1 - f)\phi + M^2 + \sigma \\ & + \frac{1}{6\sqrt{3}\sigma} \left[\left\{ (M - \sqrt{3}\sigma)^2 - 2\phi \right\}^{3/2} - \left\{ (M + \sqrt{3}\sigma)^2 - 2\phi \right\}^{3/2} \right]. \end{aligned} \quad (4.31)$$

Results from Eq. (4.31) will be compared with the small amplitude solitons results for a dusty plasma with cool moving ions, with the cold dust particles only providing a neutralizing background.

In the presence of stationary negatively charged dust particles, cold ions [$\sigma = 0$, and

$n_i = (1 - 2\phi/M^2)^{-1/2}$], and Boltzmann electrons ($\kappa \rightarrow \infty$), Eq. (4.30) reduces to

$$\Psi(\phi, M) = f \left(1 - e^\phi \right) - (1 - f)\phi + M^2[1 - (1 - 2\phi/M^2)^{1/2}], \quad (4.32)$$

which is essentially Eq. (8) of Bharuthram and Shukla [1992], with $N_e = f$ and $N_d = (1 - f)$ in their notations. Similarly, in the presence of cold ions, cold moving dust and Boltzmann electrons we recover their Eq. (19). In addition, we also observe that when $f = 1$, the plasma system is completely without dust, and therefore in the case of cold ions ($\tau = 0$), we recover Eq. (19) of Saini *et al.* [2009], that is, the model reduces to a cold-ion/kappa-electron plasma.

It is easy to see that $\Psi'(\phi, M)$ gives the sum of the charge densities in the plasma system. Thus $\Psi'(0, M) = 0$ gives the charge neutrality condition (4.1). In order to ensure that the origin ($\phi = 0$) is (locally) unstable for the propagating waves, we need $\Psi''(0, M) < 0$. This requirement, which is sometimes referred to as the soliton condition by some authors leads to

$$\Psi''(\phi = 0, M) \equiv \frac{1}{M^2 - 3\sigma} + (f - 1)\frac{sz}{M^2} - f \left(\frac{\kappa - 1/2}{\kappa - 3/2} \right) < 0. \quad (4.33)$$

Equation (4.33) can be simplified and written as

$$M^2 > 3\sigma + \mathcal{V}_{s0}^2, \quad (4.34)$$

where

$$\frac{1}{\mathcal{V}_{s0}^2} = f \left(\frac{\kappa - 1/2}{\kappa - 3/2} \right) - (f - 1)\frac{sz}{M^2}. \quad (4.35)$$

For clarity, one can see that in the limit $z \ll 1$ (such that the last term in (4.35) is neglected),

$$\mathcal{V}_{s0}^2 \approx V_{s0}^2 = \frac{N_{i0}}{N_{e0}} \left(\frac{\kappa - 3/2}{\kappa - 1/2} \right),$$

and therefore (4.34) gives $M^2 > 3\sigma + V_{s0}^2$, where the right hand side of the inequality gives the phase velocity of the linear dust ion-acoustic waves defined in Eq. (4.17).

Note that Eq. (4.34) is not fully transparent in M as \mathcal{V}_{s0}^2 is itself a function of M . By

treating (4.33) as a quadratic in M^2 we can instead write (4.34) as

$$M^2 > M_s^2 \equiv \frac{b}{2a} \left[1 \pm \left(1 - \frac{4ac}{b^2} \right)^{1/2} \right], \quad (4.36)$$

provided $b^2 - 4ac \geq 0$ for non-complex values of M_s^2 , where the latter is evaluated at $\Psi''(\phi = 0, M) = 0$. The constants a , b , and c are, respectively, given by

$$a = f \left(\frac{\kappa - 1/2}{\kappa - 3/2} \right), \quad b = 1 + s(f - 1)z + 3\sigma a, \quad \text{and} \quad c = 3\sigma sz(f - 1), \quad (4.37)$$

as in Eq. (4.19).

Equation (4.36) represents the lower limit of the soliton existence domain in the (f, M) space, and is the actual true speed of the dust ion-acoustic waves in the plasma model under investigation. Also note that M_s^2 , in Eq. (4.36), is equivalent to the right-hand-side of the linear phase velocity expression in Eq. (4.18).

We have already stated that DIA waves require that the thermal velocities of the ions and electrons satisfy (in unnormalized form) $V_{ti} < \omega/k < V_{te}$, where ω/k is the unnormalized phase velocity of the DIA waves, and $V_{tj} = (K_B T_j / m_j)^{1/2}$ is the thermal velocity for electrons ($j = e$) and ions ($j = i$). Suppose we denote the normalized thermal velocity (with respect to the ion-acoustic speed $C_s = (K_B T_e / m_i)^{1/2}$) by U_{tj} , that is, $U_{tj} = V_{tj} / C_s$. It then follows that $U_{ti} = \sqrt{\sigma}$ and $U_{te} = \sqrt{m_i / m_e} \gg 1$, assuming $m_i \sim 1836 m_e$ for protons. In other words, the electron thermal speed varies proportionally with the square root of the ion-electron temperature ratio, σ . Similarly, the electron thermal velocity is proportional to the square root of the ion-electron mass ratio, m_i / m_e . Representing the normalized phase velocity by M_s , it then implies that propagation of DIA waves require $U_{ti} < M_s < U_{te}$. Since U_{te} is very large (in this model), we can make a comparison of U_{ti} and M_s , with the latter defined in Eq. (4.36). We can also observe that when $\sigma = 0$ (cold ions) or $z = 0$ (immobile dust), then $c = 0$ in (4.36), and therefore for the allowable values of $M_s > 0$ we can only use the plus sign in (4.36). For example, with $\tau = 0$, $\kappa \rightarrow \infty$, we get $M_s^2 = [1 + sz(f - 1)] / f$, which reduces to $M_s^2 = 1 / f$ for $z \ll 1$. Thus one recovers the usual $M_s = 1$ lower Mach number limit for ion-acoustic solitons in electron-ion plasmas with cold ions and Maxwell-Boltzmann electrons [Chen, 1984] or polytropic

electrons [McKenzie *et al.*, 2004a; Verheest *et al.*, 2005]. The question then remains: what sign do we have to consider as appropriate and physical in cases where $\sigma \neq 0$ or $z \neq 0$? In this case we consider the ratio U_{ti}/M_s , which may not give us any insight unless we make many assumptions. However, numerical results show that with the minus sign in (4.36), the ratio U_{ti}/M_s exceeds unity. In other words, the phase velocity of the wave is less than the thermal velocity of the plasma ion species, leading to a breakdown of the model. For discussion purposes we choose a dusty plasma with negatively charged dust grains ($s = -1$ or $f < 1$) with fixed parameters $\sigma = 0.01$ and $z = 0.001$. Provided $\sigma < 1$ (ions assumed to be cooler than the electrons) and $z < 1$, the general trend here is obtained for other values of σ and z .

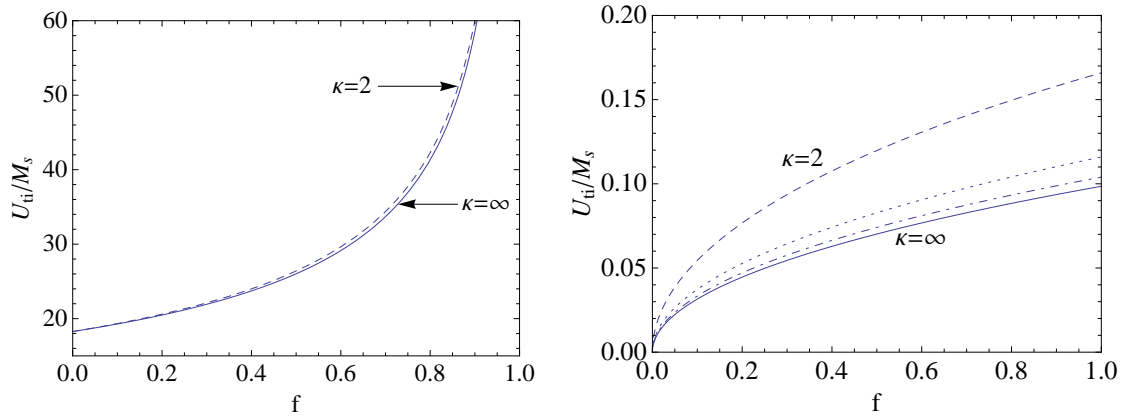


Figure 4.2: Variation of the thermal velocity-to-phase speed ratio, U_{ti}/M_s with fractional density, $f = N_{i0}/N_{e0}$ for a dusty plasma with negatively charged warm dust grains ($z = 0.001$), warm ions ($\sigma = 0.01$) and kappa electrons: $\kappa = 2$ (dashed), $\kappa = 4$ (dotted), $\kappa = 10$ (dot-dashed), and $\kappa = \infty$ (continuous). *Left panel:* Results correspond to M_s in Eq. (4.36) with the minus sign. *Right panel:* Results correspond to M_s in Eq. (4.36) with the plus sign.

In Fig. 4.2 we show curves corresponding to the ratio U_{ti}/M_s as a function of fractional density f for different values of κ . In the left panel, where we have considered the minus sign in (4.36), results show that there is no significant difference between low kappa values (with many superthermal particles in the distribution tail) and high kappa values (approximating a Maxwellian case), with the main result being that $U_{ti} \gg M_s$. Here, U_{ti} is over 18 times M_s for $0 < f < 1$. On the other hand, in the right panel where we have used the plus sign in the expression of M_s , results show that $U_{ti} < M_s$ for the full range of $0 < f < 1$, with the Maxwellian case ($\kappa \rightarrow \infty$) giving much lower ratios compared to the cases with low

κ values. Therefore in this work we shall use the expression of M_s in Eq. (4.36) with the plus sign and neglect the inappropriate negative square root.

In (4.36) we have expressed the Mach number in terms of the fractional density of the electrons, f . However, it is sometimes preferable to consider the constraint on the fractional density at fixed Mach number. Thus we rewrite Eq. (4.33) or (4.36) in the form [McKenzie *et al.*, 2005; Verheest *et al.*, 2008]

$$f > f_s(M) \equiv \frac{1/(M^2 - 3\sigma) - sz/M^2}{\beta_1 - sz/M^2}, \quad (4.38)$$

where M is the Mach number at the soliton condition, implying that solitons or double layers will exist for all $f > f_s(M)$.

4.5.1 Electrostatic potential limitations

In the existence domains of solitons, soliton regions may be bounded by a number of possible physical constraints, *e.g.*, (i) the occurrence of a double layer, (ii) when one of the species reaches a sonic point (for simpler models that implies infinite rarefaction or compression of the species), or (iii) a density takes on a complex value [McKenzie *et al.*, 2005; Verheest *et al.*, 2005; Cattaert *et al.*, 2005; Hellberg and Verheest, 2008]. It is usual for the density limit arising from a species of a given charge sign to lead to limitation of that sign of potential, *i.e.*, positive particles provide positive potential limits and vice versa [McKenzie *et al.*, 2005; Verheest *et al.*, 2005]. However, it is easily seen from Eq. (4.2) that κ -distributed electrons are well-behaved for all $\phi < 0$. Although, clearly, $n_e(\phi) \rightarrow \infty$ at $\phi \rightarrow (\kappa - 3/2)$, closer examination shows that the pseudopotential $\Psi[(\kappa - 3/2), M] \rightarrow -\infty$ [Baluku and Hellberg, 2008]. Thus the Sagdeev potential $\Psi(\phi, M)$ does not satisfy the requirement for limiting the potential, [McKenzie *et al.*, 2005; Cattaert *et al.*, 2005; Baluku *et al.*, 2008; Saini *et al.*, 2009] *viz.*, $\Psi[(\kappa - 3/2), M] > 0$.

It follows that in the case of *negative dust*, the positive ion and negative dust densities will limit the electrostatic potential for positive and negative potential solitary waves, respectively. On the other hand, for the case of *positive dust*, positive potential solitons will be limited typically by the ions, which have the smaller limiting potential because of their much smaller mass. The limiting (maximum possible) potentials ϕ_{lj} ($j = e, i, d$) are obtained from the density expressions of ions or dust particles when the species densities

either become non-real or when the species are infinitely compressed [$n_j(\phi) \rightarrow \infty$] or rarefied [$n_j(\phi) \rightarrow 0$]. In addition, $\Psi(\phi, M)$ must remain positive and finite close to the limiting potentials ϕ_{lj} . Since the soliton amplitude [root of $\Psi(\phi, M)$ other than at the origin] increases with Mach number M , it follows that the maximum soliton Mach number occurs for a soliton with amplitude $\phi = \phi_{lj}$. Thus the upper limit on M is given by $\Psi(\phi_{lj}, M) = 0$. Alternatively, the limitation on ϕ may be caused by the occurrence of double layers [Baboolal *et al.*, 1988], in which case the condition $\Psi(\phi_m, M) = \Psi'(\phi_m, M) = 0$ must be satisfied.

The description above agrees with the fluid paradigm for dust ion-acoustic solitons [Verheest *et al.*, 2005; Baluku *et al.*, 2008] where, in the presence of negative dust, for $\phi < 0$ the (subsonic) electrons, with velocity u_e , are rarefied ($u_e > 1$) and move towards their sonic point; the (supersonic) dust particles, with velocity u_d , are compressed ($u_d < 1$) and also move towards their sonic point while the ions (also supersonic) are rarefied and move away from their sonic point. Similarly for $\phi > 0$, the electrons are compressed and move away from their sonic point; the ions are compressed and move towards their sonic point while the dust particles are rarefied and move away from their sonic point. However, it is only the supersonic species, which move towards their sonic point, that contribute in limiting the potential, based on the density or velocity dynamics of the plasma species. An illustration is given in Fig. 4.3 showing the Bernoulli relation $\epsilon_j(u_j)$ as a function of the species velocity u_j for adiabatic electrons [McKenzie, 2002a,b; Verheest *et al.*, 2005; Baluku, 2007], given by

$$\epsilon_j(u_j) = \frac{1}{2}(u_j^2 - 1) + \frac{1}{(\gamma_j - 1)M_j^2} \left(\frac{1}{u_j^{\gamma_j - 1}} - 1 \right) = -\phi \equiv q_j \varphi / m_j V^2; \quad \text{for } \gamma_j \neq 1, \quad (4.39)$$

where $(\varphi)\phi$ is the (un)normalized electrostatic potential; V the velocity of the wave in the reference frame; m_j the species mass; M_j the species Mach number, and $q_j = Z_j e$ the species charge, with Z_j being the charge on the species, j , which can be positive or negative depending on whether the individual species are positively or negatively charged, respectively, and e being the charge of an electron. Here, $\gamma_j = 3/2$ for adiabatic species.

In the case of positive dust, when $\phi < 0$ all the species are rarefied, with the supersonic species moving away from their sonic points while the subsonic electrons move towards

their sonic points; for $\phi > 0$, all the species are compressed, with the supersonic species moving towards their sonic points while the electrons move away from their sonic points.

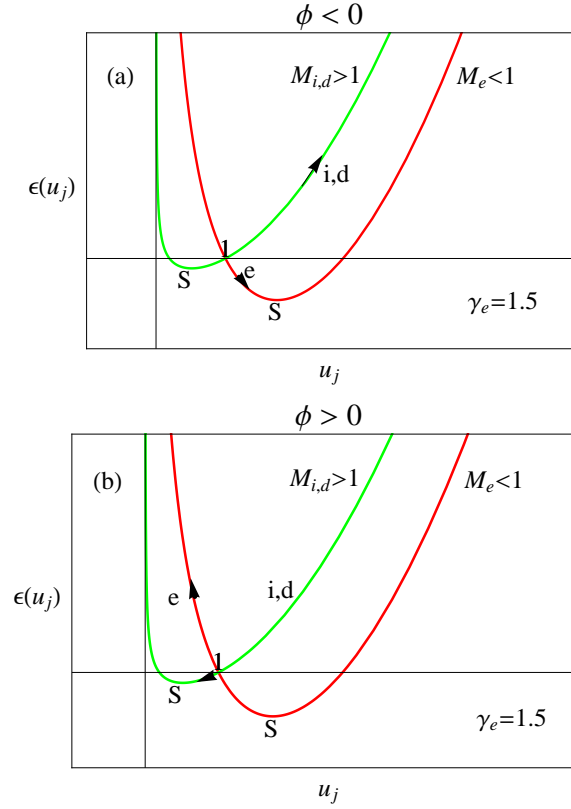


Figure 4.3: Schematic representation of Bernoulli integrals for cool, supersonic ($M_j > 1$) and hot, subsonic ($M_j < 1$) species, having a minimum at their respective sonic points, S , for adiabatic electrons ($\gamma_e = 3/2$). In a *potential hill* ($\phi > 0$), positively charged particles (with $q_j > 0$) are decelerated ($u_j < 1$) and driven towards their sonic points if the flow is supersonic ($M_j > 1$) while negatively charged particles (with $q_j < 0$) are accelerated ($u_j > 1$) and driven away from their sonic points if the flow is subsonic ($M_j < 1$). The reverse is true in a *potential dip* ($\phi < 0$): positively charged particles are accelerated and driven away from their sonic points if the flow is subsonic ($M_j < 1$) while negatively charged particles are decelerated and driven towards their sonic points if the flow is supersonic. Here M_j is the species Mach number. From [Baluku, 2007]

Limitations on Positive Potential Solitons

As observed earlier [Baluku and Hellberg, 2008], whereas $n_e(\phi) \rightarrow \infty$ at $\phi = \phi_{le} \equiv (\kappa - 3/2) > 0$, the pseudopotential $\Psi[\phi_{le}, M] \rightarrow -\infty$, which is not finite (and not a positive quantity). In other words, the condition $\Psi[\phi_{le}, M] > 0$ is meaningless, and therefore if positive solitons exist, they must be limited by either the ions only (in the case of a plasma with negatively charged dust), or limited by the ions or positively charged dust (in the case of a plasma with positively charged dust), or limited by a double layer, but not by

infinite compression of electrons.

Now, in the case of double layers, we expect to get at least two roots of $\Psi(\phi, M)$ outside the origin (with the root close to the origin giving the amplitude of the soliton); the roots coalesce into a double root when a double layer occurs. However, the behaviour of $\Psi(\phi, M)$ as ϕ becomes large indicates that $\Psi(\phi, M) \rightarrow \infty (i\infty)$ as $\phi \rightarrow \infty$ in the case of negative dust (positive dust). This implies that in this plasma model $\Psi(\phi, M)$ can have at most one root (other than at the origin), essentially ruling out the occurrence of double layers for positive potentials. Thus positive potential solitons will be limited by the positively charged ions only (in the case of a plasma with negatively charged dust) and positively charged ions or dust (when considering a plasma with positively charged dust).

The restriction on M or f for positive potential solitons associated with the ion density is given by $\Psi(\phi_{li}, M) > 0$, since for $\phi > \phi_{li} = (M - \sqrt{3\sigma})^2/2$ the ion density, $n_i(\phi)$, is complex. One can easily see that $n_i(\phi)$ is also complex for $\phi \geq (M + \sqrt{3\sigma})^2/2$, but, as that potential exceeds ϕ_{li} , it follows that $\Psi(\phi_{li}, M) > 0$ will be the practical constraint limiting positive potential solitons. The condition $\Psi(\phi_{li}, M) > 0$ leads to an upper limit on f , viz.,

$$f < f_{li}(M) \equiv \frac{f_A(M)}{f_B(M)}, \quad \text{where} \quad (4.40)$$

$$f_A(M) = \frac{M^2}{sz} \left\{ \left[1 - \frac{sz}{M^2} (M - \sqrt{3\sigma})^2 \right]^{1/2} - 1 \right\} + M^2 + \sigma - 4M^{3/2} \left(\frac{\sigma}{27} \right)^{1/4}$$

and

$$f_B(M) = \left[1 - \frac{(M - \sqrt{3\sigma})^2}{(2\kappa - 3)} \right]^{3/2 - \kappa} + \frac{M^2}{sz} \left\{ \left[1 - \frac{sz}{M^2} (M - \sqrt{3\sigma})^2 \right]^{1/2} - 1 \right\} - 1.$$

Limitations on Negative Potential Solitons

From the density expressions of the plasma constituents, in the presence of negatively charged dust, negative potential solitons are limited by the negative dust while in the presence of positively charged dust, negative potential solitons appear not to be limited by any of the plasma species.

However, considering the behaviour of $\Psi(\phi, M)$ as $\phi \rightarrow -\infty$ we see that $\Psi(\phi, M) \rightarrow +i\infty (-\infty)$ for a plasma with negatively (positively) charged dust, respectively. Therefore,

in the case of negative dust, you can have at most one root of $\Psi(\phi, M)$ outside the origin, implying that double layers may not be supported in such a plasma model.

In this case, the necessary condition that will yield a constraint on the range of M or f over which negative potential solitons can exist will then be given by $\Psi(\phi_{ld}, M) > 0$, which upon using Eq. (4.30) leads to

$$f < f_{ld}(M) \equiv \frac{f_D(M)}{f_E(M)}, \quad (4.41)$$

where

$$f_D(M) = \frac{1}{6\sqrt{3\sigma}} \left\{ \left[(M + \sqrt{3\sigma})^2 - \frac{M^2}{sz} \right]^{3/2} - \left[(M - \sqrt{3\sigma})^2 - \frac{M^2}{sz} \right]^{3/2} \right\} + M^2 \left(1 - \frac{1}{sz} \right) + \sigma$$

and

$$f_E(M) = \left[1 - \frac{M^2}{sz(2\kappa - 3)} \right]^{3/2 - \kappa} - \frac{M^2}{sz} - 1.$$

Equations (4.38)–(4.41) imply that in the case of *negative* dust, for given parameters κ , σ and M , positive potential solitons will exist in a region of parameter space (M, f) satisfying $f_s(M) < f < f_{li}(M)$ while negative solitons will be bounded by $f_s(M) < f < f_{ld}(M)$. Note that the value of M corresponding to $f_s(M)$ gives the lower Mach number below which no solitons exist, that is, the value of M at the soliton condition, M_s . Likewise, the values of M associated with f_{li} and f_{ld} will give the upper Mach number limits for positive potential (M_{li}) and negative potential (M_{ld}) solitons, respectively, at given f .

The curves representing the lower and upper limits intersect at a critical value of f , where, for positive solitons, f_p occurs for $f_s = f_{li}$, *i.e.*, f_p is defined by $f_p = f_{li}(M_s)$. For negative solitons, the critical value is $f_n = f_{ld}(M_s)$. These two critical values provide cutoffs in f below (above) which, no positive (negative) solitons are supported in a plasma with negative dust grains. Similarly, in the case of positive dust, no positive solitons are supported below f_p .

In general, it follows that for negative dust, (i) only negative solitons are observed for $0 < f < f_p$, (ii) solitons of both polarities are supported for $f_p < f < f_n$, and (iii) only

positive solitons are found for $f > f_n$. When $f \rightarrow f_p$, $\phi \rightarrow \phi_{\ell i} = (M - \sqrt{3\sigma})^2/2$ and $n_i(\phi)$ becomes complex, yielding a cutoff for the existence domain. Similarly, when $f \rightarrow f_n$, $\phi \rightarrow \phi_{\ell d} = M^2/2z$ and $n_d(\phi) \rightarrow \infty$.

4.6 Negative Dust

4.6.1 Effect of Dust Grain Mass–Charge Ratio (through z)

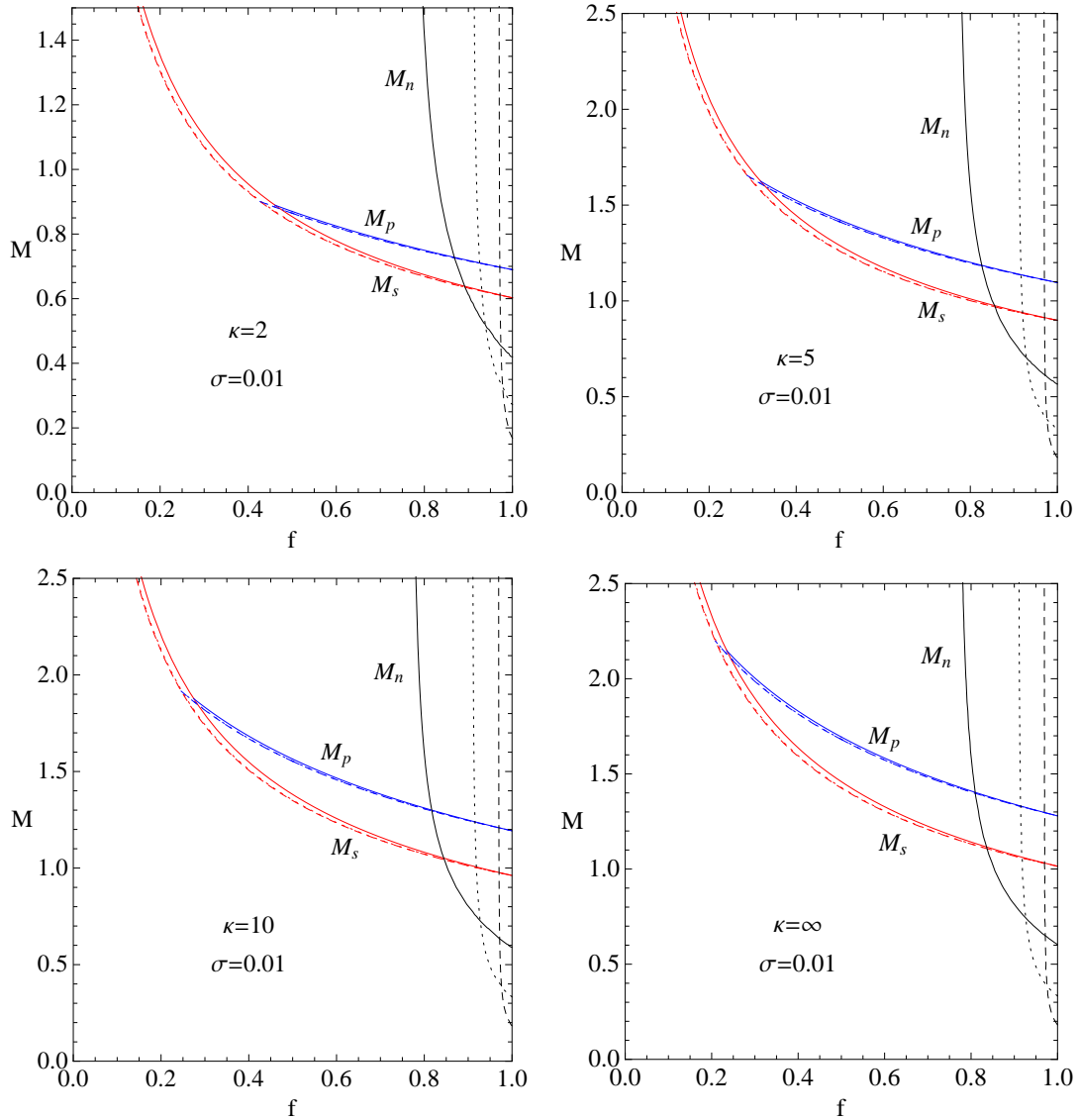


Figure 4.4: Existence domain for dust ion-acoustic solitons with varying z for fixed $\sigma = 0.01$, and for the spectral indices κ as indicated on the graphs. The dashed curves are for $z = 0.001$, the dotted ones for $z = 0.01$, and the continuous curves for $z = 0.1$, respectively. As in Fig. 4.6, positive potential solitons are bounded by the red and blue curves while negative potential solitons are bounded by the red and dark blue curves.

Figure 4.4 shows the effect of varying $z = Z_d m_i / m_d$ on the existence domain of solitons,

for different values of κ ($\kappa = 2, 5, 10$ and ∞), for a fixed temperature ratio, $\sigma = 0.01$. In each case, dashed curves correspond to $z = 0.001$, dotted curves to $z = 0.01$ and solid (continuous) curves to $z = 0.1$, respectively. In these figures, positive solitons are bounded by curves labeled M_s (red) and M_p (blue) while negative solitons are bounded by curves M_s and M_n (dark blue). The results in Fig. 4.4 show that the variation of z has an insignificant effect on both the lower and upper Mach numbers bounding positive potential solitons for fixed κ . On the other hand, different κ values have a quantitative effect on the range of M over which positive solitons exist. However, for negative potential solitons, the more massive the dust particles (smaller the value of z) the larger the range of f over which solitons will exist. For example, when $\kappa = 2$ and $\sigma = 0.01$, negative potential solitons will exist for $f < 0.89$ ($z = 0.1$), $f < 0.93$ ($z = 0.01$) and $f < 0.97$ ($z = 0.001$), respectively. Other upper limits of f , denoted f_n , for different spectral indices κ are shown in Table 4.2, where we see that for $z \lesssim 0.001$ and $\kappa > 3/2$ negative solitons exist for almost the entire range of f , *i.e.*, $0 < f < 1$.

κ	f_n					
	$z = 10^{-1}$	$z = 10^{-2}$	$z = 10^{-3}$	$z = 10^{-4}$	$z = 10^{-5}$	$z = 10^{-6}$
2	0.891	0.929	0.972	0.990	0.997	0.999
5	0.854	0.920	0.971	0.990	0.997	0.999
10	0.844	0.919	0.970	0.990	0.997	0.999
50	0.837	0.918	0.970	0.990	0.997	0.999
100	0.837	0.918	0.970	0.990	0.997	0.999
∞	0.836	0.918	0.970	0.990	0.997	0.999

Table 4.2: Table showing the upper limit of fractional density, f below which both positive and negative potential solitons can be obtained for different values of z and spectral indices κ . The ion temperature σ has been fixed at $\sigma = 0.01$. For $f > f_n$ we have positive potential solitons only

4.6.2 Effect of Ion Temperature (through σ)

Figure 4.5, which is similar to Fig. 4.4, shows the effect of normalized ion temperature (σ) on the existence domain of dust ion-acoustic solitons for a dusty plasma with kappa distributed electrons, here with $\kappa = 2$ and $\kappa = \infty$ (Maxwellian case). Dashed curves are for $\sigma = 0.001$, dotted curves for $\sigma = 0.01$ and solid (continuous) curves for $\sigma = 0.1$, respectively. Thus positive solitons are bounded by the pair of dashed, dotted or solid curves, for each case ($\sigma = 0.001, 0.01, \text{ or } 0.1$).

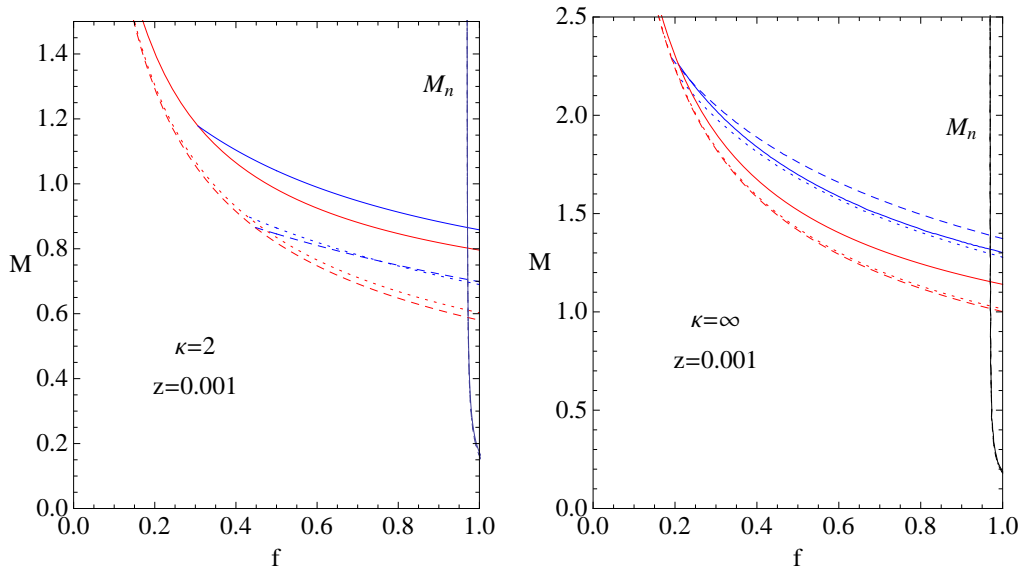


Figure 4.5: Existence domain for dust ion-acoustic solitons with varying σ for fixed $z = 0.001$, and $\kappa = 2$ (left panel) and $\kappa = \infty$ (right panel), respectively. The dashed curves are for $\sigma = 0.001$, the dotted curves for $\sigma = 0.01$, and the continuous curves for $\sigma = 0.1$, respectively. As in Fig. 4.6, positive potential solitons are bounded by the red and blue curves while negative potential solitons are bounded by the red and dark blue curves.

The graphs show that the warmer the ions (the higher the value of σ), the bigger the range in (f, M) space over which solitons can be obtained, with the region of existence of solitons decreasing with increasing excess superthermality of the electrons (lower κ). We have chosen $z = 0.001$ for illustrative purposes as a typical value with $z \ll 1$, and therefore the dust grains may be regarded as immobile in most cases. The assumption of $z \ll 1$ is due to the high dust charge z_d (of the order $\simeq 10^2 - 10^4$), and high m_d/m_i ratio (of the order $\simeq 10^6 - 10^{12}$) depending on the dust environment. This value of z will also be used in the subsequent results discussed below.

However, in the case of negative solitons, the variation of σ , for fixed z and κ , has no effect on the upper limit of M in the existence domain. Thus the almost vertical curve (labeled M_n) shown in the graphs is a superposition of curves corresponding to the three values of σ used in this figure.

4.7 Results and Discussion

In Fig. 4.6 we discuss existence domains, delineated by Eqs. (4.38)–(4.41), of dust ion-acoustic solitons in the parameter space of Mach number (M) and fractional electron density (f). In the left panel, we consider the case studied by Bharuthram and Shukla

[1992], of positive solitons in a plasma composed of Maxwellian electrons ($\kappa = \infty$), cold ions ($\sigma = 0$), and immobile dust ($z = 0$). The continuous curves (which appear to be superimposed on other curves) essentially reproduce the results of Bharuthram and Shukla [1992], where positive solitons are supported in the domain bounded by the two curves, *i.e.*, the lower, red (soliton existence) curve (f_s or M_s), and the upper, blue curve ($f_{\ell i}$ or $M_{\ell i}$). Thus positive solitons may exist for $f > f_p = 0.16$, where f_p is the lower cutoff of f defined by $f_p = f_{\ell i}(M_s)$. At that value of f , one finds the highest Mach number at which positive solitons can be supported, to be $M \simeq 2.5$. As expected, for $f = 1$ the system reduces to ion-acoustic solitons in a simple electron-ion plasma, and we observe the usual range [Chen, 1984] of Mach numbers, *viz.*, $1.0 < M < 1.6$.

In this figure (Fig. 4.6) we also consider the effects of dust mobility, by including curves for four other values of z , *viz.*, $z = 0.001$ (dotted), 0.01 (dashed), 0.1 (dot-dashed) and 1 (continuous and marked with $z = 1$). Both the M_s curve and, for positive solitons, the $M_{\ell i}$ curve for the mobile cases are virtually indistinguishable from the case $z = 0$. However, for the case $z = 1$ (valid for a negative ion plasma, but not for dust) mobility does affect M_s significantly and increases the lower cutoff to $f_p \simeq 0.34$ and decreases the highest accessible value of M (at $f = f_p$) to $\simeq 2.2$.

For negative solitons to exist, the structure must have a speed exceeding M_s , but there is effectively no upper limit in M for $z \ll 1$, though the same cannot be said for $z = 1$, and for the immobile dust model they can exist over the full range $0 < f < 1$. In the second part of Bharuthram and Shukla [1992], they considered mobility briefly (using $z = 0.1$), but only presented examples of Sagdeev potentials for two values of M . From their results it is clear that mobility has a large effect on the amplitudes of negative solitons [Bharuthram and Shukla, 1992]. Our results in the left panel of our Figure 4.6 show that the almost vertical (black) curves for $f_{\ell d}$ or $M_{\ell d}$ are affected significantly by the value of the mobility parameter, z , thereby introducing a nontrivial upper cutoff in f for negative solitons. Thus the existence domains for negative solitons are found to be smaller for mobile dust grains than for immobile dust. The upper limit f_n decreases for increasing mobility from 1.0 ($z = 0$), through 0.97 ($z = 0.001$) and 0.93 ($z = 0.01$) to 0.89 ($z = 0.1$), see Table 4.2. As seen, mobility causes a small shift in relevant M_s . In the case of negative ions ($z = 1$), the pattern is different, here f_n increases to 0.95 , in contrast to the decreasing pattern

observed for $z = 0.01$ and $z = 0.1$, and the bounding curve shows f_n varying significantly with M .

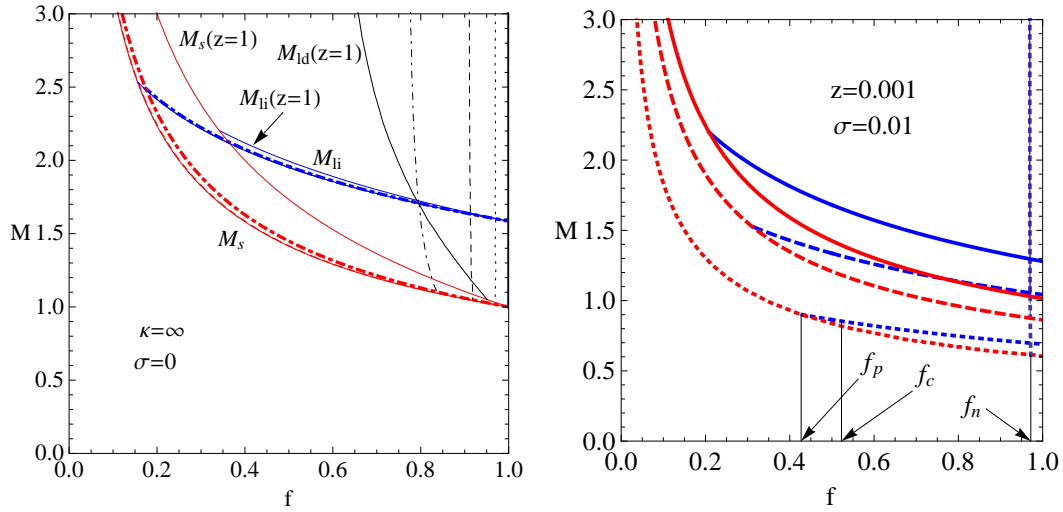


Figure 4.6: Existence domain for DIA solitons. *Left panel:* Maxwellian electrons, cold ions ($\sigma = 0$): immobile dust ($z = 0$, continuous curves), after Bharuthram and Shukla [1992]; and mobile dust [$z = 0.001$ (dotted curves), $z = 0.01$ (dashed curves), $z = 0.1$ (dot-dashed curves)]. Positive solitons have a lower cutoff at $f \simeq 0.16$. Negative solitons have a z -dependent upper cutoff at $f \simeq 0.85 - 1$. *Right panel:* Cool ions ($\sigma = 0.01$), mobile dust ($z = 0.001$); continuous curves ($\kappa = \infty$), dotted curves ($\kappa = 4$), dashed curves ($\kappa = 2$), respectively. Positive solitons are bounded at low f while negative solitons have a κ -independent upper bound close to $f = 1$. We also show the values f_p , f_c and f_n explicitly for $\kappa = 2$.

In the right panel of Figure 4.6 we investigate the effects of excess super-thermal electrons (through choice of the parameter κ) on the range of existence of DIA solitons, for mobile dust ($z = 0.001$) and an ion-electron temperature ratio of $\sigma = 0.01$. The continuous curves represent a Maxwellian electron distribution ($\kappa = \infty$), a typical space plasma ($\kappa = 4$) is given by dotted curves, and the dashed curves are for a strongly non-Maxwellian plasma with $\kappa = 2$. The ranges in both f and M that can support positive potential solitons are seen to decrease with increased excess superthermality (decreasing κ). The figure also shows that, as above, negative potential solitons exist for unbounded Mach numbers, $M > M_s$ over a large range of f , with the cutoff being virtually independent of κ ($f_n \simeq 0.97$). In addition we point out that, although not shown explicitly in this figure, the precise value of σ , within the range of appropriate values, has little effect on the existence domains.

From Fig. 4.6 one sees that for the chosen parameter values, both positive and negative

potential solitons are supported in the range (0.21, 0.97) in a Maxwellian plasma. For $\kappa = 4$, the range is reduced to (0.31, 0.97) and in a strongly non-Maxwellian plasma with $\kappa = 2$, the range supporting both polarities is (0.43, 0.97). Thus decreasing the spectral index κ from a Maxwellian to a hard spectrum has a significant effect on the range of f (through f_p) and of M , over which solitons of both polarities may exist.

As we shall show below, the critical values of the fractional electron density f that have been introduced above, *viz.*, f_c, f_p and f_n , play an important role in providing a better understanding of the soliton characteristics in a three-component plasma for which there is a range in f in which both positive and negative potential solitons are supported. We shall later consider in Fig. 4.9 a plasma with $\kappa = 2$, $\sigma = 0.01$, and $z = 0.001$. From $A(f_c) = 0$ or $\Psi'''(\phi = 0, M_s, f_c) = 0$, and (4.38)–(4.41), one finds that for these parameters $f_c \simeq 0.523$, $f_p \simeq 0.428$ and $f_n \simeq 0.97$. We show the values f_p, f_c and f_n explicitly in the existence diagram for this case in Fig. 4.6.

In Fig. 4.7 we show the effect of the spectral index κ on soliton amplitude for *fixed* Mach number M and f , and $z = 0.001$, $\sigma = 0.01$. For illustrative purposes, we have chosen a region in parameter space (f, M) for two different values of f : $f = 0.2$ (left panel) and $f = 0.5$ (right panel), respectively, where negative potential solitons are expected to occur for all spectral indices $\kappa > 1.5$, as seen in Fig. 4.6. Note that the limitations for positive potential solitons for the allowable values of f and M do not allow such comparison of ϕ_m with κ for $\kappa > 1.5$, for the ion and dust parameters used in this plasma model. The graphs show that the soliton amplitude $|\phi_m|$ increases with decreasing κ , that is, the more super-thermal particles are in the high energy tail of the distribution, the higher the amplitude of the associated solitons at fixed soliton speed. In the case of higher κ values, the amplitudes remain almost constant. However, as κ is decreased, the minimum soliton speed M_s is also decreased, and so the speed relative to the DIA speed is increased, thus explaining the higher amplitude [Saini *et al.*, 2009], Hence in Fig. 4.8, we prefer to show the effect of κ on the soliton amplitude as a function of the soliton speed normalized to the true acoustic speed (M/M_s).

In Fig. 4.8 we show the effect of κ on the soliton amplitude as we vary the Mach number (in terms of M/M_s). Contrary to the results of Fig. 4.6 for fixed M , we now see that soliton amplitudes increase as κ increases for a particular Mach number ratio M/M_s . Note that

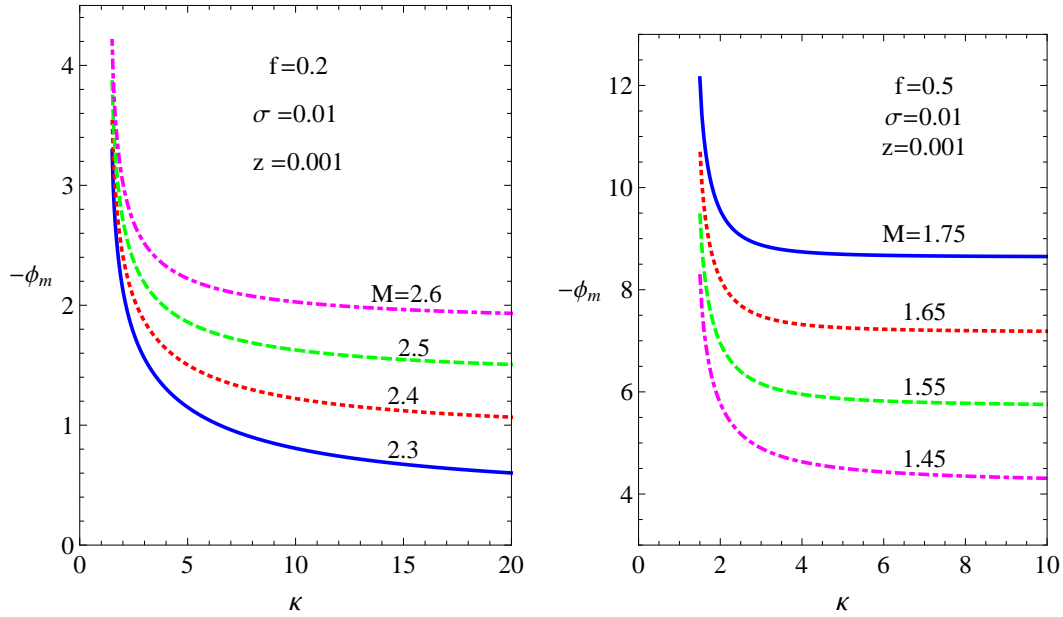


Figure 4.7: Variation of potential amplitude, ϕ_m with κ for $\sigma = 0.01$, $z = 0.001$ and different values of M (labeled on the graphs), with $f = 0.2$ (*left panel*) and $f = 0.5$ (*right panel*), respectively.

$M_s = M_s(\kappa)$, thus a fixed value of the ratio M/M_s corresponds to varying values of M_s for different values of κ .

In the upper left panel of Fig. 4.8, we consider positive potential solitons in plasmas with different κ values, for the case $f = 1$, *i.e.*, for ion-acoustic solitons in a pure electron plasma, as discussed in detail previously [Saini *et al.*, 2009]. However, whereas in the latter paper the plot was made against $M - M_s$, we have here used M/M_s . As found earlier, the “ $\phi_m - M$ ” curves decrease monotonically with decreasing κ , *i.e.*, with increasing excess superthermal electrons. The upper limit in M for positive solitons also decreases with decreasing κ , as found for IA solitons by Saini *et al.* [2009]. While for $\kappa = 2$ one has small amplitude solitons over the full existence range, they go beyond the KdV range for higher κ [Saini *et al.*, 2009]. The upper right panel of Fig. 4.8 shows that when some dust is included ($f = 0.9$) the results for positive solitons are very similar to those for IA solitons, but with slightly larger amplitudes.

Considering a case with a larger dust charge density ($f = 0.5$), the amplitudes increase even further, although they are still of order one in normalized magnitude, as seen in the lower left panel of Fig. 4.8. In addition, however, two important changes are observed. First, the curves no longer vary monotonically – they cross each other. Secondly, we find

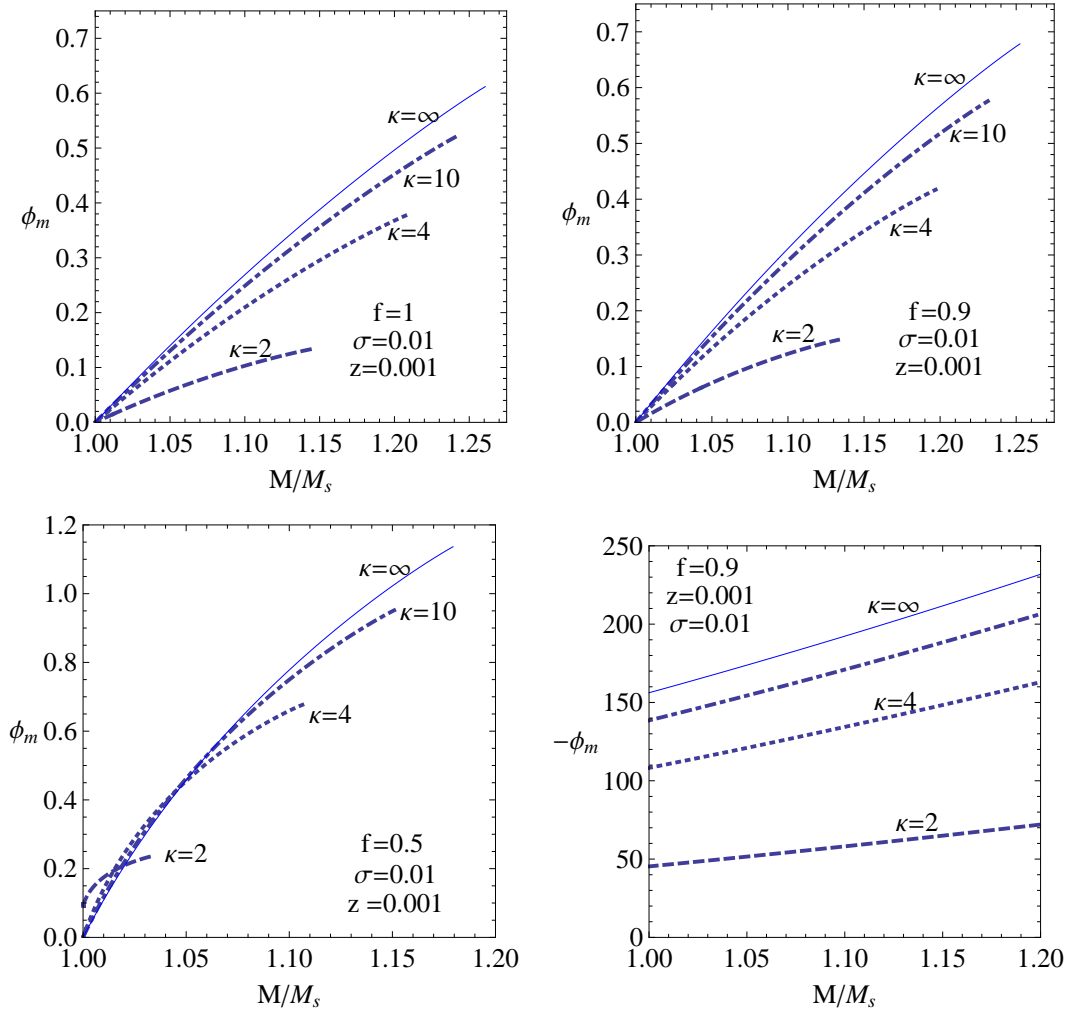


Figure 4.8: Variation of potential amplitude ϕ_m with the ratio M/M_s for $\sigma = 0.01$, $z = 0.001$, and various values of κ ; positive solitons ($f = 1, 0.9$ and 0.5); and (lower right panel) negative solitons ($f = 0.9$). The curves represent $\kappa = 2$ (dashed), 4 (dotted), 10 (dot-dashed), and ∞ (continuous), respectively. The negative solitons have large amplitude at $M = M_s$: $|\phi_m| \simeq 45.3, 108.2, 138.5$ and 156 for $\kappa = 2, 4, 10$, and ∞ , respectively. As they are unbounded in M , they have extremely large amplitudes for $M \gg M_s$.

the surprising result that for $\kappa = 2$ the amplitude ϕ_m is nonzero for $M/M_s = 1$, *i.e.*, a nonzero soliton exists at the acoustic speed, something that goes completely against KdV theory for small amplitude solitary waves.

Finally, in the lower right panel of Fig. 4.8 we show negative potential solitons for $f = 0.9$ (*i.e.*, the companion figure to the upper right panel). In this case, we find that the curves again vary monotonically with κ , but for all κ , negative solitons with finite amplitude are found at the acoustic speed. These solitons are orders of magnitude larger than the positive solitons for the same plasma configuration, *e.g.*, at the lowest Mach number supporting

solitons, $M/M_s = 1$, solitons have amplitudes $|\phi_m| \simeq 45$ ($\kappa = 2$), 108 ($\kappa = 4$), 138 ($\kappa = 10$) and 156 ($\kappa = \infty$, *i.e.*, Maxwellian), respectively. Furthermore, as negative solitons are effectively unbounded in Mach number, increasing M can yield extremely large amplitudes. Large amplitude negative solitons were also reported by Bharuthram and Shukla [1992] with Maxwellian electrons, $z = 0.1$, $\sigma = 0$ and $f = 0.7$ (see their Fig. 4). However, they did not examine the peculiar behaviour at the lowest Mach numbers.

To examine further these large amplitude negative potential solitons, we carried out calculations for different parameters, as shown in Table 4.3. For comparison, the results of Bharuthram and Shukla [1992] for $M = 1.75$ are incorporated in the Table and marked with an asterisk. The two sets of calculations are consistent with one another; the amplitudes are virtually independent of the normalized ion temperature, σ , but they do depend strongly on mobility, particularly over the range $0.01 \leq z \leq 0.1$.

z	ϕ_m		
	$\sigma = 0$	$\sigma = 10^{-2}$	$\sigma = 10^{-1}$
10^{-1}	-13.1*	-13.1	-13.0
10^{-2}	-35.1	-35.1	-34.6
10^{-3}	-41.0	-40.9	-40.3
10^{-4}	-41.6	-41.6	-41.0
10^{-5}	-41.7*	-41.6	-41.0

Table 4.3: Table showing the soliton amplitude ϕ_m for the particular parameters, $f = 0.7$ and $M = 1.75$, with Maxwellian electrons, where the values with asterisks are from Bharuthram and Shukla [1992].

Using a specific case study, *viz.*, a plasma with $\kappa = 2$, $\sigma = 0.01$, and $z = 0.001$, we next examine in Fig. 4.9 the role of f_c and its neighbourhood. Specifically, we consider the dependence of soliton amplitude on the Mach number (in terms of M/M_s) for f in the range (f_p, f_n) . We recall that for these parameter values, solitons of both polarities are found in the range $(0.43, 0.97)$, while $f_c \simeq 0.52$

In the upper left panel we present the amplitudes of positive solitons as a function of M/M_s for some values of f . First, we note that for $f_c \leq f < f_n$ (for instance, $f = f_c$, 0.55 and 0.6), the amplitudes of positive solitons vanish for $M/M_s = 1$, and they increase monotonically as f approaches f_c . In addition, the range of M/M_s that supports solitons becomes narrower. Turning next to $f < f_c$ (*e.g.*, $f = 0.48$ and 0.5), we see that, although the trends of increasing ϕ_m and decreasing range in M , with decreasing f , persists, one

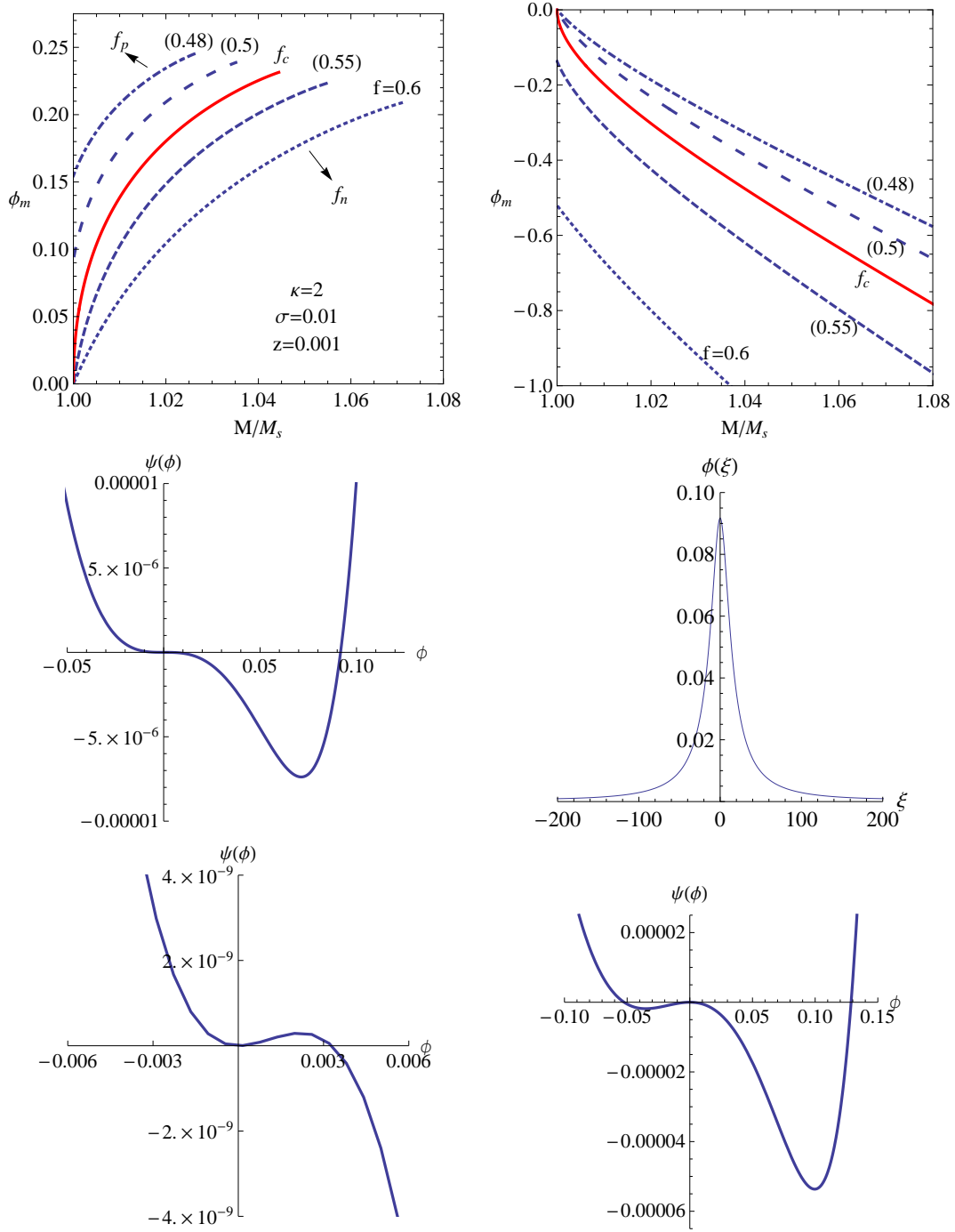


Figure 4.9: *Upper panel:* Plot of ϕ_m vs. M/M_s for positive (left) and negative (right) solitons, for different f in the range ($f_p; f_n$). Note the two different scales for ϕ_m . Parameter values: $\kappa = 2$, $\sigma = 0.01$ and $z = 0.001$. *Middle panel:* Pseudopotential plot at $f = 0.5, M = M_s \simeq 0.835$, and the associated potential profile of the soliton. *Lower panel:* Pseudopotential plots at $M_s - 0.0001$ (left) and $M_s + 0.0023$ (right).

now finds that the amplitude of positive solitons is not zero at $M = M_s$.

In the upper right panel we present similar curves for negative solitons for the same val-

ues of f (please note the change of scale of ϕ_m). Again the amplitudes vary monotonically with f , but the solitons have zero amplitude for $f_p < f \leq f_c$ at $M/M_s = 1$, while in the range $f_c < f < f_n$ amplitudes are nonzero at $M = M_s$. The negative solitons in general have larger amplitudes than their positive counterparts. In the middle left panel of Fig. 4.9 we show the pseudopotential plot for a case with nonzero positive amplitude at $M = M_s$, *viz.*, with $f = 0.5$, $M = M_s$, $\phi_m \simeq 0.09$. Although we find that $\phi_m \neq 0$ at the DIA speed for this example in the range $f_p < f < f_c$, we see that the usual requirement of a maximum of the pseudopotential at the origin [$\Psi''(\phi = 0, M) < 0$] is not satisfied. Instead, the function $\Psi(\phi, M)$ has a point of inflexion at the origin, with $\Psi''(\phi = 0, M_s) = 0$, while the convexity requirement at the origin is provided by the third derivative, $\Psi'''(\phi = 0, M_s) < 0$. We point out that a finite amplitude soliton at the acoustic speed has recently been found in a study of dust-acoustic solitons in another three-component plasma, *viz.*, one composed of negatively charged fluid dust and two positive ion species, a cooler Boltzmann and a hotter nonthermal Cairns distribution [Verheest and Hellberg, 2010]. In that case, too, it was found to occur in conjunction with a point of inflexion in the pseudopotential at the origin [Verheest and Hellberg, 2010], rather than a maximum, as is normally required for a soliton.

We emphasize that these structures obtained at the acoustic speed are indeed typical solitons, as may be seen from the potential profile in the middle right panel, and also reported recently by Verheest and Hellberg [2010]. This interesting result implies that the usual convexity requirement at the origin [$\Psi''(\phi = 0, M) < 0$] is a necessary but not a sufficient condition for the existence of solitons, specifically for models that support existence of solitons of both polarities. Furthermore, these finite amplitude solitary waves cannot be found by a KdV approach, as the latter solitons have $\phi_m = 0$ for $M = M_s$, as discussed for small amplitude solitons in Sec. 4.4.1.

In the lower left panel of Fig. 4.9 we show the pseudopotential for a marginally sub-acoustic structure speed ($M = M_s - 0.0001$). Clearly, the positive pulse seen in the middle left panel disappears for $M < M_s$, however small the reduction below the DIA speed – the pseudopotential has no well, and no soliton is found. On the other hand, for $M > M_s$ ($M = M_s + 0.0023$) one sees that the positive soliton has a slightly increased amplitude ($\phi_m \approx 0.13$), while a smaller amplitude negative soliton ($|\phi_m| \approx 0.05$), which vanished at

$M = M_s$, is observed.

This phenomenon is explored further in Fig. 4.10, which shows soliton amplitudes at the DIA speed, M_s , as a function of f , in the range (f_p, f_n) , for different values of κ . Clearly the points of intersection with the line $\phi = 0$ define critical values of f – they occur where $\Psi'''(\phi = 0, M = M_s, f, \kappa) = 0$. These values are plotted as a dotted curve in Fig. 4.1 and are seen to be the same as the value f_c defined in Sec. 4.4.1 as the solution to the equation $A(f; \kappa) = 0$. Here $f_c \approx 0.523, 0.419, 0.365$, and 0.329 for $\kappa = 2, 4, 10$, and ∞ , respectively. At f_c , the amplitudes of both polarities of soliton vanish at the DIA speed², and, as we have seen in Sec. 4.4.1, KdV theory has to be replaced by the mKdV approach. As seen in Fig. 4.10, for each value of κ , *positive potential solitons* have $\phi_m \neq 0$ at $M = M_s$ for $f_p < f < f_c$, increasing with $|f - f_c|$ as one approaches f_p , but (not shown in figure) we find that the amplitudes vanish at the acoustic speed for $f > f_c$. For $M > M_s$, however, these solitons have finite amplitude. On the other hand, *negative solitons* have zero amplitude at M_s for $f < f_c$ (not shown in figure; again, with nonzero amplitudes for $M > M_s$), and take on finite values at M_s for $f_c < f < f_n$, increasing with $|f - f_c|$ as $f \rightarrow f_n$. The largest positive and negative soliton amplitudes at the acoustic speed occur for $f = f_p$ and $f = f_n$, respectively. In summary, as f is varied, the solitons of either polarity switch at f_c from

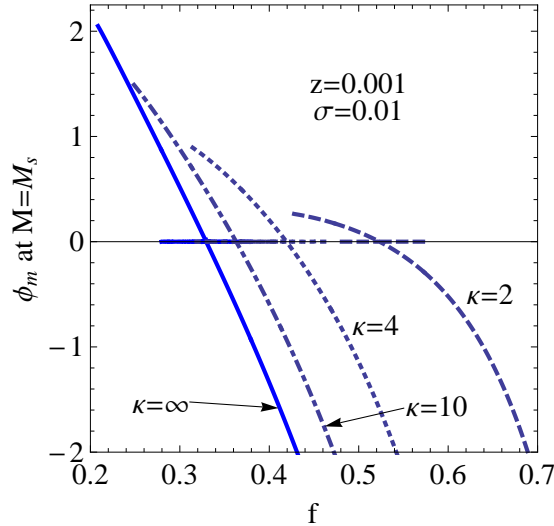


Figure 4.10: Soliton amplitudes obtained at $M = M_s$ for $z = 0.001$ and $\sigma = 0.01$, f in the range (f_p, f_n) ; and $\kappa = 2$ (dashed curve), 4 (dotted), 10 (dot-dashed), and ∞ (continuous).

“KdV-like” behaviour (vanishing at $M = M_s$), to a “nonKdV-like” form with $\phi_m \neq 0$ at

²Below (above) f_c we get “nonKdV-like” (“KdV-like”) positive potential solitons and “KdV-like” (“nonKdV-like”) negative potential solitons, respectively.

the DIA speed. Equivalently, as f is increased through f_c , the “KdV-like” solitons change sign from negative to positive, while the “nonKdV-like” structures switch from positive to negative potential. Of course, negative solitons are effectively unbounded in M for $z \ll 1$ and can thus have very large amplitudes, but in Fig. 4.10 we have shown the amplitudes only up to 2, although $|\phi_{\ell d}|$ can be very large. For this model in particular, since negative solitons are limited by the negatively charged dust, the resulting solitons must be less than the critical potential amplitude $\phi_{ld} = M^2/2z$, which is 500 times M^2 for $z = 0.001$ as used in the discussion. This shows that the size of the possible solitons greatly depends on the value of $z = (Z_d/m_d)/(Z_i/m_i)$, and therefore on the mass and size of charge on the dust particles. The maximum potential amplitudes at $f = f_n$ or f_p for the parameters shown in Fig. 4.10 are shown in Table. 4.4 below. The table shows that for $z = 0.001$ and $\sigma = 0.01$, f_p decreases with increasing superthermality (increasing κ) while f_n is almost constant at $f \simeq 0.97$. The amplitude of the associated maximum potentials also increases slightly with increasing κ , but lie below 2.1 for positive potential solitons. In the case of negative solitons, these maximum amplitudes are huge ($|\phi_{dl}|$ is over 100 for all $\kappa > 3/2$).

κ	f_p	M_s	ϕ_{li1}	f_n	M_s	ϕ_{ld}
2	0.426955	0.90064	0.264581	0.971858	0.610733	-186.497
4	0.309592	1.52930	0.919495	0.970641	0.875164	-382.956
10	0.245913	1.91603	1.518710	0.970391	0.975738	-476.032
50	0.215603	2.13963	1.933410	0.970304	1.019710	-519.907
∞	0.208418	2.19814	2.050180	0.970285	1.029880	-530.327

Table 4.4: Table showing the maximum potential amplitudes, $\phi_{li1} = (M_s^2 - \sqrt{3\sigma})^2/2$ and $\phi_{ld} = M_s^2/2z$ at $f = f_p$ and f_n , respectively, for the parameters in Fig. 4.10, that is, for $\sigma = 0.01$ and $z = 0.001$.

4.8 Positive Dust

We have already seen that in the case of positive dust grains, positive solitons are limited by ion compression (as $\phi_{li} \ll \phi_{\ell d}$), while negative solitons, if they exist, would be limited by the occurrence of double layers, if the latter are supported by this plasma model [Baluku and Hellberg, 2008], see also Chapter 3. However, the double layer requirements [$\Psi(\phi_m, M) = \Psi'(\phi_m, M) = 0$] are not met for this model. Both the pseudopotential, $\Psi(\phi, M)$, and its derivative, $\Psi'(\phi, M)$, go to $-\infty$ as $\phi \rightarrow -\infty$, so no double layers can form. This observation agrees, for the Maxwellian case, with earlier work [Baluku *et al.*,

2008]. More insight into the existence of negative solitons can be obtained from the sign of $\Psi'''(\phi = 0; M = M_s)$. We saw in Sec. 4.4.1 that small amplitude negative solitons can be obtained only for $f < f_c$. As seen in Fig. 4.1, $f_c < 1$ for all κ . This means that for positive dust ($f > 1$) only one sign of potential can be supported. Thus only positive potential dust ion-acoustic solitons can occur in dusty plasmas with positive dust, kappa electrons and fluid ions. On the other hand, comparison of the dust and ion limiting potentials, $\phi_{ld} = M^2/2z$ and $\phi_{li1} = (M - \sqrt{3\sigma})^2/2$, respectively, shows that $\phi_{ld}/\phi_{li1} \gg 1$, thus the ion limit will be met before the dust ion limit can be invoked. Therefore, in the presence of positively charged dust, positive potential solitons are limited only by the positive ions.

The existence domains for positive solitons, bounded by the continuous (lower Mach number) and dotted (upper Mach number) curves, respectively, are shown in Fig. 4.11 (left panel) for $\kappa = 2, 4$ and ∞ , and (for $\kappa = 2$) over an extended range in positive dust charge density in the right panel. These solitons all have amplitudes that are less than ϕ_{li1} . We see that the existence domains are extensions of those seen for $f < 1$, and that they appear similar to each other, but for decreasing κ both the typical values of M and the accessible ranges in M are reduced.

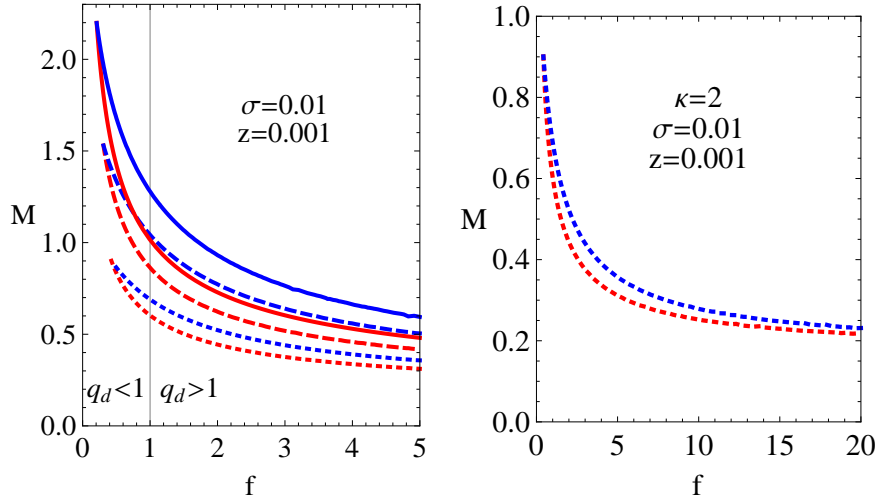


Figure 4.11: Existence domains for positive potential DIA solitons for $\sigma = 0.01$, $z = 0.001$, and $\kappa = \infty$ (continuous curve), 4 (dashed) and 2 (dotted), covering both negatively charged dust ($f < 1$) and positive dust ($f > 1$). The right panel shows the results over a larger range of positive dust charge density for $\kappa = 2$.

4.9 Comment

In a number of papers, such as [Mendoza-Briceño *et al.*, 2000; Mamun and Shukla, 2002; Shukla and Mamun, 2002; Mamun and Shukla, 2008], Mamun and co-workers have suggested that if one expands the Sagdeev potential $\Psi(\phi)$ around $\phi = 0$, say up to the third order in ϕ , then the sign of the coefficient of ϕ^3 in the expansion gives the appropriate sign of the potential solitons supported by the plasma model at hand. Indeed such formalism holds for small amplitude solitons only, that is, solitons whose amplitudes tend to zero as $M \rightarrow M_s$. In other words, the sign of the coefficient of ϕ^3 in the expansion of $\Psi(\phi)$ is only associated with the sign of the KdV-like solitons (with amplitudes that vanish at M_s) that can exist in the plasma model. However, for plasma situations where both positive and negative potential solitons can be supported, this formalism (Mamun approach), if applied to the large amplitude (normally referred to as the arbitrary amplitude) methods, misses solitons of the opposite sign to the KdV-like solitons.

In understanding this, we shall look at the case of dust ion-acoustic solitary waves in an unmagnetized dusty plasma in which the fluid ions are treated as cold, the electrons are Boltzmann distributed, and the dust particles are stationary and therefore only provide a neutralizing background. This particular plasma model was discussed by Mamun [Mamun and Shukla, 2008] in the work he presented at the “2007 ICTP Summer College on Plasma Physics”. The Sagdeev potential is now given by Eq. (4.32), here rewritten as:

$$\Psi(\phi, M) = f \left(1 - e^\phi\right) - (1 - f)\phi + M^2[1 - (1 - 2\phi/M^2)^{1/2}], \quad (4.42)$$

where we have used f for μ and Ψ for V in their notation, but the meaning remains the same. The critical Mach number “above which solitary wave solutions exist” is now given by $M_c = 1/\sqrt{f}$, and the critical value of f , here denoted f_c evaluated at $\Psi'''(\phi = 0, M = M_c) = 0$ now becomes $f_c = 1/3$ such that above or below f_c , $\Psi'''(\phi = 0, M)$ changes sign. In their study of the properties of arbitrary amplitude DIA solitary waves, following from Eq. (4.42), the authors indicated that for any dusty plasma parameters satisfying $M > 1/\sqrt{f}$ and $f < f_c$, DIA solitary waves with both $\phi > 0$ and $\phi < 0$ exist while for $M > 1/\sqrt{f}$ and $f > f_c$, only DIA solitary waves with $\phi > 0$ can exist. This is, however,

not quite correct. We emphasize that in the neighbourhood of f_c one gets solitons with both positive and negative potential signs, but the KdV approach or the expanded Sagdeev potential only gives solitons associated with the sign of $\Psi'''(\phi = 0, M_s)$ while that of the opposite sign is inaccessible. For this case we show Sagdeev potential profiles for two cases; $f < f_c$ and $f > f_c$, in particular, $f = f_c - 0.001$ with $M = M_c + 0.0001$ and $f = f_c + 0.001$ with $M = M_c + 0.001$, respectively. Though not indicated here, provided one is in the f -region where both positive and negative potential solitons exist, one gets finite positive (negative) amplitude solitons at $M = M_c$ for $f < f_c$ ($f > f_c$), similar to the one shown in Fig. (4.9) (middle left panel) for $f < f_c$.

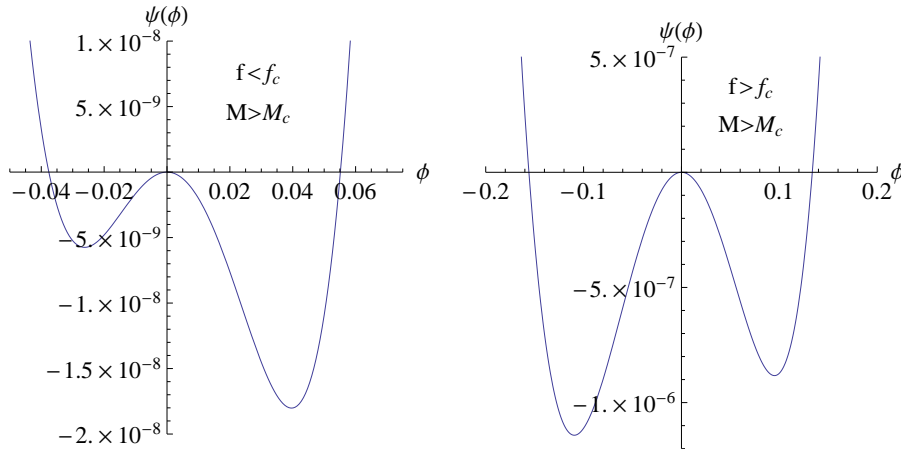


Figure 4.12: Sagdeev potential for $f < f_c$ (left panel) and $f > f_c$ (right panel) for dust ion acoustic solitons in a plasma with static dust, cold fluid ions and Maxwellian electrons, after Mamun and Shukla [2008].

4.10 Discussion and Chapter Summary

Using the pseudopotential approach, we have studied arbitrary amplitude dust ion-acoustic solitons in a plasma of positive ions, κ -distributed electrons and charged dust grains. This represents a considerable extension of the work of Bharuthram and Shukla [1992], who studied a plasma model consisting of Boltzmann-distributed electrons, cold ions, and immobile negative dust in one case, and mobile negative dust in another case.

For the case of negative dust, we have shown that for all κ the model supports both positive and negative potential solitons, where the Mach number for positive (negative) potential solitons is limited from above by the condition at which the ion density becomes complex (the dust is infinitely compressed). This agrees with the analysis of Verheest *et*

al. [2005] for polytropic electrons, where following a fluid dynamic paradigm, proposed by McKenzie [McKenzie, 2002a,b, 2003] and co-workers [McKenzie and Doyle, 2003; McKenzie *et al.*, 2004b,a, 2005], that emphasizes the hydrodynamic rather than the electrostatic properties of the plasma system, it was found that both negative and positive potential dust-ion-acoustic solitons may exist in a dusty plasma with negatively charged dust, positively charged ions and polytropic electrons. We prefer not to use the commonly used word “coexist” in this context, as coexistence seems to imply that in a specific plasma configuration, both polarities can exist at the same time, whereas in fact only one will occur, and which of the two polarities will be observed depends on details of the initial disturbance.

Positive potential DIA solitons experience a low- f cutoff (f_p) which decreases with increasing κ (*i.e.*, with a decrease in excess super-thermal particles), and hence this increases the range in (f, M) space over which positive solitons exist. Allowing for finite dust grain mobility has little or no effect on the existence domain for positive solitons. On the other hand, the smaller the value of z , that is the heavier the dust particles (assuming constant dust charge), the larger the domain in (f, M) space over which negative potential solitons can be obtained. Also, the variation of the ion temperature (through σ) has a weak effect, increasing the size of the existence domain as σ is increased. That is, the warmer the ions (the larger the value of σ) the larger the existence domain for solitons, with the region of existence decreasing as κ decreases.

Negative potential solitons do not exist above a κ -independent cutoff f_n lying approximately in the range 0.9–1, the exact value of which depends significantly on the magnitude of the dust mobility factor $z = Z_d m_i / m_d$. They are effectively not subject to an upper limit in M as $z \ll 1$ implies that $\phi_{ld} \gg 1$, and thus negative solitons may be very large.

A surprising result is that over the range of fractional electron density f in which solitons of both polarities are supported, finite amplitude solitary structures occur even at the DIA speed – behaviour which contradicts KdV theory. Recently a similar result was found in another three-component plasma [Verheest and Hellberg, 2010], where, as here, the phenomenon is associated with a point of inflexion of the pseudopotential at $\phi = 0$ and $M = M_s$, rather than the usual maximum. The sign of $\Psi'''(\phi = 0; M = M_s; f)$ then designates the polarity of the KdV-like soliton that vanishes at $M = M_s$.

A critical role is played by f_c , the value of f at which the KdV coefficient $A = 0$,

which also satisfies the constraint $\Psi'''(\phi = 0; M = M_s; f_c) = 0$. In particular, as f is varied, solitons of each polarity switch at $f = f_c$ from a “KdV-like” form to “nonKdV-like” behaviour. For $f_p < f < f_c$, positive solitons at $M = M_s$ have finite amplitude, increasing in size with $|f - f_c|$ as f approaches f_p , while negative solitons have zero magnitude at $M = M_s$, as expected from KdV theory. This situation reverses in polarity for solitons found for $f_c < f < f_n$.

On the other hand, in a plasma with positive dust grains, only positive potential (“KdV-like”) solitons are supported by the plasma model, with the upper limit on M provided by infinite compression of the ions, and the positively charged dust particles only contribute in neutralizing the electrons in the background. The Maxwellian case agrees with earlier results, using the fluid dynamic paradigm with polytropic electrons [Baluku *et al.*, 2008]. Decreasing κ leads to small reductions in both the accessible M and the existence range in M . The dusty plasma model with positive dust is similar to a two component ion-electron plasma, with modifications to the dynamics due to the presence of weakly mobile dust. The results are reminiscent of those found for ion-acoustic solitons in a two-ion plasma [McKenzie *et al.*, 2005], but for a much heavier second “positive ion”.

Ion-Acoustic Solitons in a Plasma with Two-Temperature κ -distributed Electrons

In this chapter we investigate, and discuss existence domains of ion-acoustic solitons in plasmas composed of two electron components (of different temperatures) that are kappa-distributed, and a singly charged adiabatic fluid ion species (protons). Such plasmas are of interest in the Saturnian magnetosphere where bi-kappa-distributed electrons are reported to exist [Schippers *et al.*, 2008].

5.1 Introduction

In Chap. 2 we indicated that both cool and hot electron populations that are non-Maxwellian have been inferred to exist in Saturn's magnetosphere using the Voyager PLS observations [Sittler *et al.*, 1983; Barbosa and Kurth, 1993] and the Cassini CAPS observations [Young *et al.*, 2005]. By fitting the CAPS/ELS and MIMI/LEMMS data from the Cassini spacecraft orbiting Saturn over a range of $5.4 - 20 R_S$ where $R_S \approx 60,268$ km is the radius of Saturn, Schippers *et al.* [2008] have shown that both the cool and hot electron populations are κ -distributed.

Ion-acoustic solitons in a plasma with two electron components have been studied by many authors in different plasma environments, both theoretically [Nishihara and Tajiri,

1981; Baboolal *et al.*, 1990; Rice *et al.*, 1993; Ghosh *et al.*, 1996; Ghosh and Iyengar, 1997] and experimentally [Nakamura *et al.*, 1996]. However, most of the studies have been centered on Maxwellian plasmas. Since plasmas in space and astrophysical plasmas, as well as in laboratory environments, possess non-Maxwellian distributions, studies on ion-acoustic waves and solitary structures have to be extended to non-Maxwellian cases to incorporate the deviation from the Maxwellian form in the analysis. Ion-acoustic solitons in non-Maxwellian plasmas (either in the form of the Cairns distribution [Cairns *et al.*, 1995] or kappa-distribution [Abbasi and Pajouh, 2007; Chuang and Hau, 2009]) with only one electron component have been studied in the past.

In this chapter we study a three component plasma comprising adiabatic fluid ions that are singly positively charged like protons, and two electron components, one cool and the other hot, that are kappa-distributed, to explore existence domains of ion-acoustic solitons, using both the reductive perturbation analysis and arbitrary amplitude (Sagdeev potential) approach. These results can be applied to the plasma system in the Saturnian magnetosphere [Schippers *et al.*, 2008] where the low energy (cool) and high energy (hot) electron components are both kappa-distributed.

Our results show that both compressive (with a hump in the density as well as the electrostatic potential) and rarefactive (with a dip in the density and electrostatic potential) can be supported by the model. However, a peculiar behaviour of soliton amplitudes occurs for density ratios that support coexistence of both hump ($\phi > 0$) and dip ($\phi < 0$) solitons. There exists a critical fractional cool electron density ratio, f_c , below which negative solitons have *finite* (nonzero) amplitudes (nonKdV-like) at the lower Mach number cutoff while positive solitons have zero amplitudes (KdV-like) at the lower Mach number. The situation reverses when $f > f_c$; positive solitons are nonKdV-like while negative solitons are KdV-like.

Comparison between the perturbation theory and the large amplitude techniques show that whereas the perturbation technique seem to be accurate for very small amplitudes, especially for structures that move with velocities close to the phase velocity of the wave, the method becomes less reliable for velocities far from the phase velocity, especially in cases where both signs of potential solitons exist. Thus the arbitrary amplitude approach, such as the pseudopotential/Sagdeev method (which we will discuss in detail) is indispensable.

5.2 Model and Basic Equations

We consider an infinite, collisionless and unmagnetized plasma comprising cool adiabatic fluid ions (with a single positive charge) that propagate only along the x -axis, and a mixture of both hot and cool κ -distributed electrons.

The kappa-distributed electrons have unnormalized densities given by [Baluku *et al.*, 2008]

$$N_s(\varphi) = N_{s0} \left[1 + \frac{1}{(\kappa_s - 3/2)} \frac{q_s \varphi}{K_B T_s} \right]^{-(\kappa_s - 1/2)}, \quad (5.1)$$

where N_{s0} and T_s are the equilibrium number density and temperature of species s ($s = c$ for cool electrons and h for hot electrons); K_B is the Boltzmann constant, φ is the local electrostatic potential, and κ_s is the spectral index of species s , which must be greater than $3/2$ for non complex characteristic thermal velocities (most probable speeds) associated with the kappa-distributed electron components [Baluku *et al.*, 2008]. For this plasma model, $q_s = -e$, the charge of the electrons.

We assume that the ions are adiabatic ($P_i \propto N_i^{\gamma_i}$, where $\gamma_i = 3$), with the ion density having both inertial and pressure contributions. Thus the ions satisfy the continuity and momentum equations (in unnormalized form):

$$\frac{\partial N_i}{\partial t'} + \frac{\partial}{\partial X}(N_i V_i) = 0, \quad (5.2)$$

$$\frac{\partial V_i}{\partial t'} + V_i \frac{\partial V_i}{\partial X} + \frac{C_{ti}^2}{N_{i0}^2} N_i \frac{\partial N_i}{\partial X} + \frac{q_i}{m_i} \frac{\partial \varphi}{\partial X} = 0, \quad (5.3)$$

and the species' densities are coupled by Poisson's equation

$$\varepsilon_0 \frac{\partial^2 \varphi}{\partial X^2} + \sum_{j=c,h,i} N_j q_j = 0, \quad (5.4)$$

with boundary conditions φ , $\partial\varphi/\partial X$ and $V_i \rightarrow 0$, and $N_i \rightarrow N_{i0}$ as $X \rightarrow \pm\infty$. In equations (5.2)–(5.4), $C_{ti} = (\gamma_i P_{i0}/m_i N_{i0})^{1/2} = (3K_B T_i/m_i)^{1/2}$ is the thermal velocity of the adiabatic ions; N_i , V_i , P_i , and φ are the unnormalized density, velocity and pressure of the ions, and local electrostatic potential, respectively, while X and t' are the spatial and temporal unnormalized variables.

5.3 The Linear Dispersion Relation

In the linearization process we make the following substitutions:

$$\begin{aligned}
 N_j &= N_{j0} + N_{j1} \\
 P_j &= P_{j0} + P_{j1} \\
 V_j &= V_{j1} \\
 \varphi &= \varphi_1 \\
 \partial N_{j0}/\partial X &= \partial P_{j0}/\partial X = 0 \\
 \partial N_{j0}/\partial t' &= \partial P_{j0}/\partial t' = 0,
 \end{aligned} \tag{5.5}$$

where N_{j0} , P_{j0} are the unperturbed density and pressure quantities describing the equilibrium state, and N_{j1} , P_{j1} , V_{j1} and φ_1 are the small perturbations in these quantities. The unperturbed velocity is zero and we have chosen $\varphi_0 = 0$ (since we have zero electric field for the unperturbed states).

Since the electrons are kappa-distributed, the first order perturbations in density of the electrons is obtained from Eq. (5.1), and is given by

$$N_{s1} = -N_{s0} \left(\frac{\kappa_s - 1/2}{\kappa_s - 3/2} \right) \frac{q_s \varphi_1}{K_B T_s}. \tag{5.6}$$

The perturbed system of the positively charged ions is governed by the fluid continuity and momentum equations (in linearized form). Then assuming a steady-state harmonic time-dependent perturbation solution for the oscillating quantities of the form N_{i1} , V_{i1} , P_{i1} , $\varphi_1 \propto \exp\{i(kX - \omega t')\}$, the time-derivative and gradient can be replaced, by $\partial/\partial t' \rightarrow -i\omega$, and $\partial/\partial X \rightarrow ik$, respectively. This process gives

$$V_{i1} = \frac{k\omega q_i/m_i}{(\omega^2 - k^2 C_{ti}^2)} \varphi_1, \tag{5.7}$$

$$N_{i1} = \frac{k^2 N_{i0} q_i/m_i}{(\omega^2 - k^2 C_{ti}^2)} \varphi_1 \tag{5.8}$$

and hence

$$\left[-\varepsilon_0 k^2 - \sum_{s=c,h} \frac{N_{s0} q_s^2}{K_B T_s} \left(\frac{\kappa_s - 1/2}{\kappa_s - 3/2} \right) + k^2 \frac{N_{i0} q_i^2 / m_i}{\omega^2 - k^2 C_{ti}^2} \right] \varphi_1 = 0. \quad (5.9)$$

Using the definition of the ion plasma frequency, $\omega_{pi} = (N_{i0} q_i^2 / \varepsilon_0 m_i)^{1/2}$, Eq. (5.9) can be written as

$$\left[1 + \frac{1}{k^2 \lambda_{D\kappa}^2} - \frac{\omega_{pi}^2}{\omega^2 - k^2 C_{ti}^2} \right] \varphi_1 = 0, \quad (5.10)$$

which for $\varphi_1 \neq 0$ gives the linear dispersion relation for a plasma comprising κ -distributed hot and cool electrons, and adiabatic positively charged ions. That is,

$$\frac{\omega_{pi}^2}{\omega^2 - k^2 C_{ti}^2} - \frac{1}{k^2 \lambda_{D\kappa}^2} = 1. \quad (5.11)$$

The associated kappa dependent Debye length $\lambda_{D\kappa}$ is given by

$$\frac{1}{\lambda_{D\kappa}^2} = \sum_{s=c,h} \frac{N_{s0} q_s^2}{\varepsilon_0 K_B T_s} \left(\frac{\kappa_s - 1/2}{\kappa_s - 3/2} \right), \quad (5.12)$$

which is an extension of the Debye length in kappa-plasmas [Chateau and Meyer-Vernet, 1991; Bryant, 1996; Mace *et al.*, 1998] to bi-kappa plasmas. When $\kappa_s \rightarrow \infty$ ($s = c, h$), equation (5.12) reduces to $1/\lambda_D^2 = 1/\lambda_{Dc}^2 + 1/\lambda_{Dh}^2$, where λ_{Dc} and λ_{Dh} are the Debye lengths of the cool and hot electrons, respectively. In the long wavelength limit ($k \rightarrow 0$) we have $k\lambda_{D\kappa} \ll 1$, and Eq. (5.11) becomes

$$\omega^2 = k^2 C_{i\kappa}^2 + k^2 C_{ti}^2, \quad (5.13)$$

where $C_{i\kappa} = \omega_{pi} \lambda_{D\kappa}$ is the ion-acoustic sound speed of the plasma model comprising of cool and hot kappa-distributed electrons and fluid ions. Thus the phase velocity of the propagating structures is greater than the thermal velocity of the ions. In the limit $\kappa \rightarrow \infty$,

$$C_{i\kappa} \rightarrow C_{ia} = \omega_{pi} \lambda_{De},$$

where C_{ia} is the ion-acoustic sound speed [Chen, 1984] for a plasma with cool and hot Maxwellian electrons; $\lambda_{De} = (\varepsilon_0 K_B T_e / N_{e0} e^2)^{1/2}$, and $N_{e0} / T_e = N_{c0} / T_c + N_{h0} / T_h$; $N_{e0} =$

$N_{e0} + N_{h0}$. Thus N_{e0} and T_e are the effective (total) electron density and temperature, respectively. Hence in the limit $\kappa \rightarrow \infty$ and $k\lambda_{De} \ll 1$, Eq. (5.11) gives the Maxwellian form [Chen, 1984]

$$\omega^2 = k^2 \left(\frac{K_B T_e}{m_i} + \frac{\gamma_i K_B T_i}{m_i} \right).$$

5.4 Small Amplitude Solitons

5.4.1 The Korteweg-de Vries (KdV) Equation

The density of the κ -distributed cool and hot electrons in Eq. (5.1) can be expanded to give

$$N_s(\varphi) = N_{s0} \sum_{r=0}^{\infty} (-1)^r \nu_{sr} \varphi^r, \quad (5.14)$$

where

$$\begin{aligned} \nu_{s0} &= 1, \\ \nu_{s1} &= \left(\frac{\kappa_s - 1/2}{\kappa_s - 3/2} \right) \frac{q_s}{K_B T_s}, \end{aligned} \quad (5.15)$$

$$\nu_{s2} = \frac{1}{2!} \frac{(\kappa_s - 1/2)(\kappa_s + 1/2)}{(\kappa_s - 3/2)^2} \left(\frac{q_s}{K_B T_s} \right)^2, \quad (5.16)$$

$$\nu_{s3} = \frac{1}{3!} \frac{(\kappa_s - 1/2)(\kappa_s + 1/2)(\kappa_s + 3/2)}{(\kappa_s - 3/2)^3} \left(\frac{q_s}{K_B T_s} \right)^3, \quad (5.17)$$

\dots

etc.

Note that for fixed $q_s/K_B T_s$ and φ , the series expansion in Eq. (5.14) is valid only for $\kappa_s > 3$ since for $1.5 < \kappa_s \lesssim 3$, higher order terms (ν_{s4}, \dots) are large compared to the lower order ones, and therefore cannot be neglected (see also Sec. 4.4). This implies that the reductive perturbation method will not be appropriate for determination of small amplitude solitons for κ_s values in the range $1.5 < \kappa_s < 3$.

The positively charged ions are described by the fluid continuity and momentum equations (5.2) and (5.3), respectively.

Applying the reductive perturbation technique, we use the stretched coordinates [Nishihara and Tajiri, 1981; Mace *et al.*, 1991; Verheest, 2000] $\zeta = \epsilon^{1/2}(X - V t')$ and $\mathcal{T} = \epsilon^{3/2} t'$ which correspond to the spatial and temporal coordinates, with $\epsilon \ll 1$ being a smallness

parameter that measures the strength of the wave amplitude and V is the soliton speed (which is equivalent to the phase velocity of the wave in the long wavelength limit). The varying parameters, N_j , V_j and φ are expressed in terms of ϵ using the expansions [Nishihara and Tajiri, 1981; Mace *et al.*, 1991]:

$$\begin{aligned} N_j &= N_{j0} + \epsilon N_{j1} + \epsilon^2 N_{j2} + \dots \\ V_j &= \epsilon V_{j1} + \epsilon^2 V_{j2} + \dots \\ \varphi &= \epsilon \varphi_1 + \epsilon^2 \varphi_2 + \dots \end{aligned} \quad (5.18)$$

Thus Poisson's equation now becomes

$$\epsilon \varepsilon_0 \frac{\partial^2 \varphi}{\partial \zeta^2} + N_i q_i + \sum_{s=c,h} N_{s0} \sum_{r=0}^{\infty} (-1)^r \nu_{sr} \varphi^r q_s = 0, \quad (5.19)$$

where N_i , V_i and φ are defined in Eq. (5.18). Equation (5.19) can be expanded to obtain the following equations

$$\bigcirc (\epsilon^0) : \sum_{s=c,h} N_{s0} q_s + N_{i0} q_i = 0, \quad (5.20)$$

$$\bigcirc (\epsilon^1) : N_{i1} q_i - \sum_{s=c,h} q_s N_{s0} \nu_{s1} \varphi_1 = 0, \quad (5.21)$$

$$\bigcirc (\epsilon^2) : \varepsilon_0 \frac{\partial^2 \varphi_1}{\partial \zeta^2} + N_{i2} q_i - \sum_{s=c,h} q_s N_{s0} \nu_{s1} \varphi_2 + \sum_{s=c,h} q_s N_{s0} \nu_{s2} \varphi_1^2 = 0, \quad (5.22)$$

where Eq. (5.20) can be recognized as the charge neutrality condition of the unperturbed plasma constituents at equilibrium.

Following from the continuity and momentum equations, the first-order perturbed velocity V_{i1} and density N_{i1} (in terms of φ_1) are again given by Eqs. (5.7) and (5.8). Thus Eq. (5.21) leads to the linear dispersion relation of the plasma model given in Eq. (5.13) in the long wavelength limit ($k\lambda_{D\kappa} \ll 1$ or $k \rightarrow 0$), that is, $\omega^2 = k^2 C_{i\kappa}^2 + k^2 C_{ti}^2$.

Also, differentiating equation (5.22) once with respect to ζ gives

$$\varepsilon_0 \frac{\partial^3 \varphi_1}{\partial \zeta^3} + q_i \frac{\partial N_{i2}}{\partial \zeta} - \sum_{s=c,h} q_s N_{s0} \nu_{s1} \frac{\partial \varphi_2}{\partial \zeta} + 2 \sum_{s=c,h} q_s N_{s0} \nu_{s2} \varphi_1 \frac{\partial \varphi_1}{\partial \zeta} = 0, \quad (5.23)$$

where the second-order perturbed density N_{i2} can easily be obtained from the continuity

and momentum expressions (details not shown here) to give

$$\begin{aligned} \frac{\partial N_{i2}}{\partial \zeta} &= \left\{ \frac{2N_{i0}Vq_i/m_i}{(V^2 - C_{ti}^2)^2} \right\} \frac{\partial \varphi_1}{\partial \mathcal{T}} + \left(\frac{N_{i0}q_i/m_i}{V^2 - C_{ti}^2} \right) \frac{\partial \varphi_2}{\partial \zeta} \\ &+ \left\{ \frac{N_{i0}q_i^2/m_i^2(3V^2 + (\gamma_i - 2)C_{ti}^2)}{(V^2 - C_{ti}^2)^3} \right\} \varphi_1 \frac{\partial \varphi_1}{\partial \zeta}. \end{aligned} \quad (5.24)$$

Combining equations (5.23) and (5.24) we get

$$\begin{aligned} \varepsilon_0 \frac{\partial^3 \varphi_1}{\partial \zeta^3} + 2V \frac{N_{i0}q_i^2/m_i}{(V^2 - C_{ti}^2)^2} \frac{\partial \varphi_1}{\partial \mathcal{T}} + \left(\frac{N_{i0}q_i^2/m_i}{V^2 - C_{ti}^2} - \sum_{s=c,h} q_s N_{s0} \nu_{s1} \right) \frac{\partial \varphi_2}{\partial \zeta} \\ + \left\{ 2 \sum_{s=c,h} q_s N_{s0} \nu_{s2} + \frac{N_{i0}q_i^3/m_i^2[3V^2 + (\gamma_i - 2)C_{ti}^2]}{(V^2 - C_{ti}^2)^3} \right\} \varphi_1 \frac{\partial \varphi_1}{\partial \zeta} = 0. \end{aligned} \quad (5.25)$$

However, the nontrivial ($\varphi_1 \neq 0$) solution of equation (5.25) requires that the coefficient of the term involving the second-order perturbed potential, φ_2 , must be zero. Clearly, with the phase velocity $V = \omega/k$, this follows from Eqs. (5.8) and (5.21) for $\varphi_1 \neq 0$. Equation (5.25) then becomes

$$\begin{aligned} \frac{\partial^3 \varphi_1}{\partial \zeta^3} + \frac{2V \omega_{pi}^2}{(V^2 - C_{ti}^2)^2} \frac{\partial \varphi_1}{\partial \mathcal{T}} \\ + \left[2 \sum_{s=c,h} \frac{q_s N_{s0}}{\varepsilon_0} \nu_{s2} + \frac{(3V^2 + (\gamma_i - 2)C_{ti}^2) \omega_{pi}^2 q_i/m_i}{(V^2 - C_{ti}^2)^3} \right] \varphi_1 \frac{\partial \varphi_1}{\partial \zeta} = 0. \end{aligned} \quad (5.26)$$

In terms of the first order-perturbed potential, φ_1 , Eq. (5.23) leads to the well known KdV equation [Mace *et al.*, 1991; Verheest, 2000]

$$\frac{\partial \varphi_1}{\partial \mathcal{T}} + A \varphi_1 \frac{\partial \varphi_1}{\partial \zeta} + B \frac{\partial^3 \varphi_1}{\partial \zeta^3} = 0, \quad (5.27)$$

where

$$A = \frac{A_2}{A_1} \quad \text{and} \quad B = \frac{1}{A_1}; \quad (5.28)$$

$$A_1 = \frac{2V \omega_{pi}^2}{(V^2 - C_{ti}^2)^2} \quad \text{and} \quad (5.29)$$

$$A_2 = 2 \sum_{s=c,h} \frac{q_s N_{s0}}{\epsilon_0} \nu_{s2} + \frac{[3V^2 + (\gamma_i - 2)C_{ti}^2] \omega_{pi}^2 q_i / m_i}{(V^2 - C_{ti}^2)^3}, \quad (5.30)$$

with $\gamma_i = 3$ since we consider the ions to be adiabatic. The phase velocity V in Eqs. (5.29) and (5.30) is obtained from the linear dispersion relation given in Eq. (5.13).

In getting solutions to Eq. (5.27), we seek nonlinear solitary wave structures that propagate unchanged at constant speed V_0 in the laboratory frame [Chen, 1984]. Thus, we seek stationary solutions in a moving frame, $\chi(\zeta, \mathcal{T}) = \zeta - V_0 \mathcal{T} = \epsilon^{1/2}(X - vt')$, with boundary conditions

$$\varphi_1, \frac{\partial \varphi_1}{\partial \zeta}, \frac{\partial^2 \varphi_1}{\partial \zeta^2} \rightarrow 0 \quad \text{as} \quad \zeta \rightarrow \pm \infty.$$

Here, $v = V + \delta v$, where V is the phase velocity of the solitary waves and $\delta v = \epsilon V_0$. Upon using the transformation $\chi(\zeta, \mathcal{T}) = \zeta - V_0 \mathcal{T} = \epsilon^{1/2}(X - vt')$, the solution of the resulting differential equation becomes [Mace *et al.*, 1991; Verheest, 2000]

$$\varphi_1(\chi) = \left(\frac{3V_0}{A} \right) \text{sech}^2 \left\{ \left(\frac{V_0}{4B} \right)^{1/2} \chi \right\}. \quad (5.31)$$

In terms of the laboratory frame coordinates (X, t') , the solution becomes

$$\varphi(X, t') \sim \epsilon \varphi_1(X, t') = \frac{3\delta v A_1(V)}{A_2(V)} \text{sech}^2 \left\{ \left(\frac{\delta v A_1(V)}{4} \right)^{1/2} (X - vt') \right\}. \quad (5.32)$$

Equation (5.31) is valid for $A \neq 0$ and $V_0/B > 0$, where the constants A and B are defined in Eq. (5.28). Note that for $V_0 > 0$, the condition $B > 0$ implies $V > C_{ti}$, that is, supersonic ions, which justifies the need of a sluggish species (cooler or massive species) that will provide inertia in the system for the generation of oscillations [Verheest, 2000, p. 110].

We now take the following normalization (as will be used in the arbitrary amplitude

approach): temperature is normalized to the cool electron temperature T_c ; local potential to $K_B T_c/e$; number density to N_{e0} , where $N_{e0} = N_{c0} + N_{h0} = Z_i N_{i0}$ is the total electron equilibrium density with N_{c0} , N_{h0} and N_{i0} being the cool electrons, hot electrons and cool ions equilibrium density. Here, Z_i is the size of charge residing on the ions, which is +1 for singly charged ions (protons in this case). The velocity is normalized to the acoustic speed $C_s = (Z_i K_B T_c/m_i)^{1/2}$; the spatial and time variables to the inverse ion plasma frequency $\omega_{pi}^{-1} = (\epsilon_0 m_i/N_{i0} q_i^2)^{1/2} = (\epsilon_0 m_i/Z_i N_{e0} e^2)^{1/2}$ and effective Debye length $\lambda_{Deff} = (N_{c0}/N_{e0})^{1/2} \lambda_{Dc} = \epsilon_0 K_B T_c/N_{e0} e^2)^{1/2}$.

The constants A_1 and A_2 in Eq. (5.29) and (5.30) can then be written in the form:

$$A_1 = \frac{2}{C_s} \frac{1}{\lambda_{Deff}^2} \alpha_{s1}^{3/2} (1 + 3\tau \alpha_{s1})^{1/2} \quad \text{and} \quad (5.33)$$

$$A_2 = \frac{\phi(\xi)/\varphi(\chi)}{\lambda_{Deff}^2} \alpha_{s1}^2 \left[3(1 + 4\tau \alpha_{s1}) - \frac{\alpha_{s2}}{\alpha_{s1}^2} \right], \quad (5.34)$$

where ϕ is the normalized electrostatic potential, and $\tau = (T_i/T_c)/Z_i$, which simply becomes T_i/T_c (the normalized ion temperature with $Z_i = 1$), respectively; $\xi = x - M t = \chi/\lambda_{Deff}$, where $M = v/C_s$ is the Mach number, and x and t are the normalized spatial and time variables, respectively. Here, $M = M_s + \delta M$ where $M_s = V/C_s = (3\tau + 1/\alpha_{s1})^{1/2}$ is the phase velocity normalized to the effective sound speed, which is equivalent to the lower Mach number, and $\delta M = \epsilon M_0 = \epsilon(V_0/C_s)$. The constants α_{s1} and α_{s2} are given, respectively, by

$$\alpha_{s1} = \sum \beta_s \frac{N_{s0} \kappa_s - 1/2}{N_{e0} \kappa_s - 3/2} \quad \text{and} \quad (5.35)$$

$$\alpha_{s2} = \sum \beta_s^2 \frac{N_{s0} (\kappa_s - 1/2)(\kappa_s + 1/2)}{N_{e0} (\kappa_s - 3/2)^2}, \quad (5.36)$$

with $s = c(h)$ for cool (hot) electrons, and $\beta_s = T_c/T_s$ is the reciprocal of the normalized temperature. For simplicity, $\beta = \beta_h = T_c/T_h$.

Note that $\varphi(\chi) \sim \epsilon \varphi_1(\chi)$ and $\phi(\xi) \sim \epsilon \phi_1(\xi)$, thus to first order in ϵ , Eq. (5.32) can be written as

$$\phi(\xi) = \phi_0 \operatorname{sech}^2(\xi/\Delta), \quad (5.37)$$

where ϕ_0 and Δ are the soliton amplitude and width, respectively, given by

$$\phi_0 = 6\delta M(M_s/Q) = \frac{12/\alpha_{s1}^2}{Q\Delta^2} \text{ and} \quad (5.38)$$

$$\frac{1}{\Delta} = \left(\frac{\delta M}{2}\right)^{1/2} \alpha_{s1}^{3/4} (1 + 3\tau \alpha_{s1})^{1/4}, \quad (5.39)$$

where $Q = 3(1 + 4\tau\alpha_{s1}) - \alpha_{s2}/\alpha_{s1}^2$. Equation (5.37) is valid (i) for $\delta M > 0$, leading to $M > M_s$, and (ii) for $Q \neq 0$, that is, $A_2 \neq 0$, and therefore the sign of the potential depends on whether Q is positive or negative. Also, Eqs. (5.38) and (5.39) imply that $\phi_0 \propto 1/\Delta^2 \propto \delta M$, thus as δM (or M) increases the soliton amplitude (ϕ_0) increases while the soliton width (Δ) decreases.

In getting the appropriate sign of the soliton potential, we determine a critical density ratio f_c , corresponding to $Q = 0$, at which ϕ_0 [from (5.38)] goes to infinity. When $f < f_c$ we get positive potential (compressive) solitons while the reverse gives negative potential (rarefactive) solitons. For example, when $\kappa_c = 2$, $\kappa_h = 3$, $\tau \simeq 1/300$, $\beta = 3/100$, which are typical parameter values for Saturn's outer magnetosphere [Schippers *et al.*, 2008] at about $16 R_S$, we have $f_c \simeq 0.472$. In the presence of Maxwellian cool and hot electrons ($\kappa_c = \kappa_h = \infty$) and $\tau \simeq 1/300$, $\beta = 3/100$, we have $f_c \simeq 0.704$. Positive (negative) potential solitons will exist for $f < (>)f_c$. These critical density ratios will be referred to in the discussion of numerical results in the subsequent sections. For $Q = 0$ we have $A_2(V) = 0$ in Eq. (5.27), and therefore the soliton amplitude goes to infinity. For values of f for which the nonlinearity term in the KdV equation vanishes, that is $A_2(V) = 0$, the mKdV approach may be appropriate [Nishihara and Tajiri, 1981; Baboolal *et al.*, 1989]. We briefly look at this approach in the subsequent subsection.

5.4.2 The Modified Korteweg-de Vries (mKdV) Equation

We have already seen that when $A_2(V) = 0$ in Eq. (5.27), the soliton amplitude goes to infinity. In dealing with that scenario in the perturbation approach, we re-scale the stretched space-time variables ζ and \mathcal{T} . Following the approaches of Baboolal *et al.* [1989] and Roy Chowdhury *et al.* [1994], we use the stretched variables $\zeta = \epsilon(X - Vt')$ and $\mathcal{T} = \epsilon^3 t'$. With this scaling, and proceeding as in the KdV case above, the modified KdV

equation takes the form (see Appendix C.1 for details)

$$\frac{\partial \varphi_1}{\partial \mathcal{T}} + C(V) \varphi_1^2 \frac{\partial \varphi_1}{\partial \zeta} + D(V) \frac{\partial^3 \varphi_1}{\partial \zeta^3} = 0, \quad (5.40)$$

where again the phase velocity V is obtained from $V^2 = C_{ti}^2 + C_{i\kappa}^2$, and

$$\begin{aligned} C(V) &= -A_3/A_1; \quad D(V) = B(V) = 1/A_1; \\ A_1 &= \frac{2V \omega_{pi}^2}{(V^2 - C_{ti}^2)^2} \quad \text{and} \\ A_3 &= \frac{3 \omega_{pi}^2 V^2 q_i^2 / m_i^2}{2 (V^2 - C_{ti}^2)^4} + 3 \sum_{s=c,h} \frac{q_s N_{s0}}{\epsilon_0} \nu_{s3} \\ &\quad + \frac{\omega_{pi}^2 [4V^2 + (3\gamma_i - 4)c_{ti}^2]}{(V^2 - C_{ti}^2)^2} \sum_{s=c,h} \frac{q_s N_{s0}}{q_i N_{i0}} \nu_{s2}. \end{aligned} \quad (5.41)$$

Using the transformation, $\chi(\zeta, \mathcal{T}) = \zeta - u_0 \mathcal{T} \equiv \epsilon(X - vt')$, where $v = V + \delta v$; $\delta v = \epsilon^2 u_0$, Eq. (5.40) then takes the form of a first-order differential equation whose solution is given by (see Appendix C.2 for details)

$$\varphi_1(\chi) = \left(\frac{6u_0}{C} \right)^{1/2} \text{sech} \left\{ \left(\frac{u_0}{D} \right)^{1/2} \chi \right\} \quad \text{or} \quad (5.42)$$

$$\varphi(X, t') = \left(\frac{6\delta v}{C} \right)^{1/2} \text{sech} \left\{ \left(\frac{\delta v}{D} \right)^{1/2} (X - vt') \right\}, \quad (5.43)$$

which is valid for $C > 0$ and $D > 0$ provided $\delta v > 0$.

Again, with our chosen normalization, the constant A_1 is given by Eq. (5.29), while A_3 is given by

$$A_3 = - \frac{\phi^2(\xi)/\varphi^2(\chi)}{2\lambda_{D\text{eff}}^2} \left\{ \alpha_{s1} \alpha_{s2} (4 + 9\gamma_i \tau \alpha_{s1}) - \left[3(1 + 3\tau \alpha_{s1}) \alpha_{s1}^3 + \alpha_{s3} \right] \right\}, \quad (5.44)$$

where α_{s1} and α_{s2} are defined in Eqs. (5.35) and (5.36), respectively, and α_{s3} is given by

$$\alpha_{s3} = \sum \beta_s^3 \frac{N_{s0}}{N_{e0}} \frac{(\kappa_s - 1/2)(\kappa_s + 1/2)(\kappa_s + 3/2)}{(\kappa_s - 3/2)^3}. \quad (5.45)$$

It should be noted that the mKdV equation (or solution) is relevant only when the coefficient of $\partial \phi_1^2 / \partial \chi$ in the KdV equation is negligible. In this case, that occurs when

$A_2(V) = 0$. We have already shown in the previous section that A_2 vanishes when $Q = 3(1 + 4\tau\alpha_{s1}) - \alpha_{s2}/\alpha_{s1}^2 = 0$. Thus the mKdV solution will only be valid for $\alpha_{s4} = \alpha_{s2} - 3\alpha_{s1}^2(1 + 4\tau\alpha_{s1}) = 0$.

With $\xi = x - Mt = \chi/\lambda_{D\text{eff}}$, where $M = v/C_s = M_s + \delta M$; $M_s = V/C_s = (3\tau + 1/\alpha_{s1})^{1/2}$; $\delta M = \delta v/C_s$, Eq. (5.43) then becomes

$$\phi(\xi) = \phi_{0s} \text{sech}(\xi/\Delta_w), \quad (5.46)$$

where ϕ_{0s} and Δ_w are the soliton amplitude and width, respectively, given by

$$\phi_{0s} = (24\delta M/\alpha_{s5})^{1/2} [\alpha_{s1}^3(1 + 3\tau\alpha_{s1})]^{1/4} = \frac{2\sqrt{3}}{\Delta_w\sqrt{\alpha_{s5}}}; \quad (5.47)$$

$$\frac{1}{\Delta_w} = (2\delta M)^{1/2} [\alpha_{s1}^3(1 + 3\tau\alpha_{s1})]^{1/4}; \quad (5.48)$$

$$\alpha_{s5} = \alpha_{s1}\alpha_{s2}(4 + 9\gamma_i\tau\alpha_{s1}) - [3(1 + 3\tau\alpha_{s1})\alpha_{s1}^3 + \alpha_{s3}],$$

provided $\alpha_{s4} = 0$, $\alpha_{s5} > 0$, and $\delta M > 0$. Equations (5.47) and (5.48) imply that $\phi_{0s} \propto 1/\Delta_w \propto \delta M^{1/2}$, thus ‘‘faster’’ solitons (with increasing δM) have *large* amplitudes, and are *thin* in width. The expressions for α_{sl} where $l = (1 - 5)$ can be written in terms of the hot electrons fractional density $f = N_{h0}/N_{e0}$. If we denote f_1 and f_2 as the solutions of $\alpha_{s4}(f) = 0$ and $\alpha_{s5}(f) = 0$, respectively, then $\alpha_{s5}(f) > 0$ requires $f < f_2$, that is, $f_1 < f_2$ for the mKdV to be meaningful.

In Fig. 5.1 we show the variation of f with κ (with $\kappa = \kappa_c = \kappa_h$) for which the nonlinear coefficient A in the KdV equation (5.27) goes to zero (blue solid curve), which simply corresponds to the solutions of $\alpha_{s4}(f) = 0$. The dotted (blue) curve, superimposed on the continuous curve, corresponds to the critical values of f , denoted, f_c , for which $\Psi'''(\phi, M, f) = 0$ at $M = M_s$, that we will discuss in detail in the arbitrary amplitude approach. In addition, the dashed (light-blue) curve in Fig. 5.1, labelled f_2 gives the values of f for which $\alpha_{s5}(f) = 0$. Thus for $f > f_2$, the mKdV solution (5.46) is complex. We therefore note that for the parameters in Fig. 5.1, for all values of $\kappa_c = \kappa_h$ we have $f_1 > f_2$, and thus at $f = f_1$, $\alpha_{s5}(f) < 0$, leading to complex solutions of the soliton amplitude.

Also, numerical results show that the variation of f_1 and f_2 with $\beta = T_c/T_h$ for $\tau =$

$T_i/T_c = 1/300$ and constant spectral indices ($\kappa_c = \kappa_h = 5$ and ∞ , as shown in Fig. 5.2 as examples) shows that $f_1 > f_2$, implying that $\alpha_{s5}(f) < 0$ and hence the soliton amplitude at $f = f_1$ is complex. These results indicate that the modified KdV solution is not appropriate for small amplitude solitons with the parameters described above. Similar results with $\tau = 1/300$, $\beta = 3/100$ are obtained for both $\kappa_c > \kappa_h$, and $\kappa_c < \kappa_h$ (not shown here). However, when keeping the spectral indices and electron temperatures fixed, the

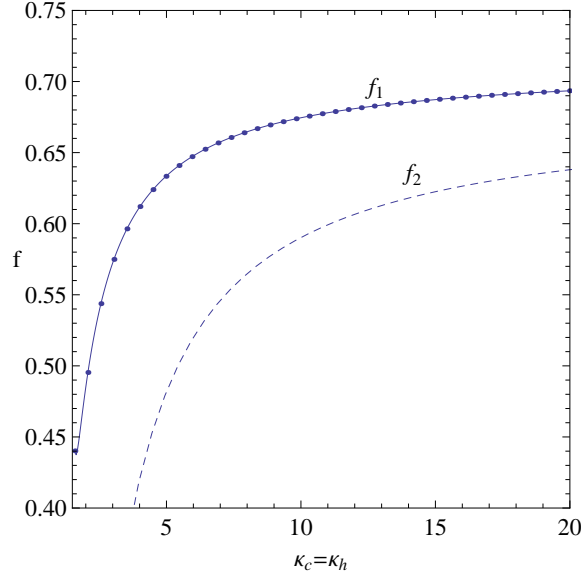


Figure 5.1: f -solutions of $\alpha_{s4}(f) = 0$ (dashed) and $\alpha_{s5}(f) = 0$ (dotted) as functions of τ for $\tau = 1/300$, $\beta = 3/100$, and $\kappa_c = \kappa_h$. For all values of $\kappa_c = \kappa_h$, we have $f_1 > f_2$, and thus at $f = f_1$, $\alpha_{s5} < 0$ and therefore will lead to complex solutions of soliton potential amplitudes.

variation of f_1 and f_2 with the normalized ion temperature $\tau = T_i/T_c$ gives a different picture. For example, in Fig. 5.3 (left panel) we take $\beta = 1/10$. Here, the results are similar to those obtained in the case of Fig. 5.2, that is, f_2 is less than f_1 for all τ . When we reduce β to $3/100$, as shown in Fig. 5.3 (right panel), we see that $f_2 > f_1$ for some values of τ : with $\beta = 3/100$ and $\kappa_c = \kappa_h = \infty$, we get $f_2 > f_1$ provided $0.052 < \tau < 8.143$, and with $\kappa_c = \kappa_h = 5$ we get $f_2 > f_1$ for $0.164 < \tau < 6.813$, implying that the mKdV approach may be valid for that range of parameters. Note that Fig. 5.3 has been plotted only up to $\tau = 1$. These results (for the variation of ion temperature) also suggest that the ion dynamics may be essential when using the mKdV approach.

While the perturbation technique seems to be accurate for very small amplitudes, especially for Mach numbers very close to M_s , that is, for structures that move with

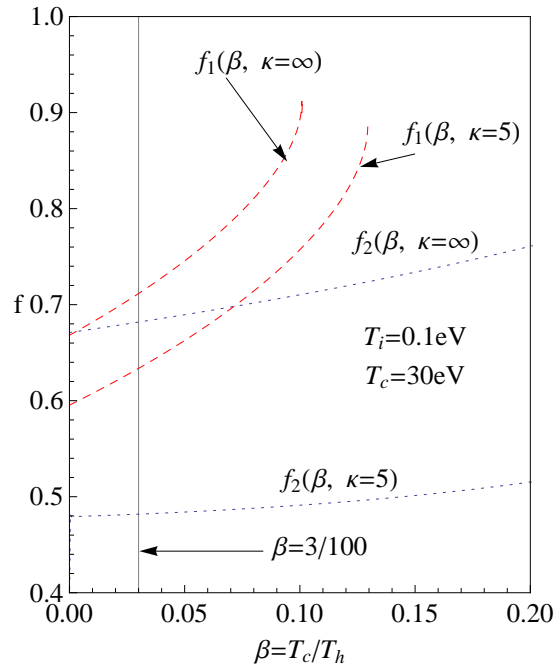


Figure 5.2: f -solutions of $\alpha_{s4} = 0$ (dashed) and $\alpha_{s5} = 0$ (dotted) as functions of β for $\tau = 1/300$, and $\kappa_c = \kappa_h = \kappa$, with $\kappa = 5$ and ∞ . Again, we have $f_1 > f_2$; thus at $f = f_1$, $\alpha_{s5} < 0$ and therefore will lead to complex solutions of soliton potential amplitudes.

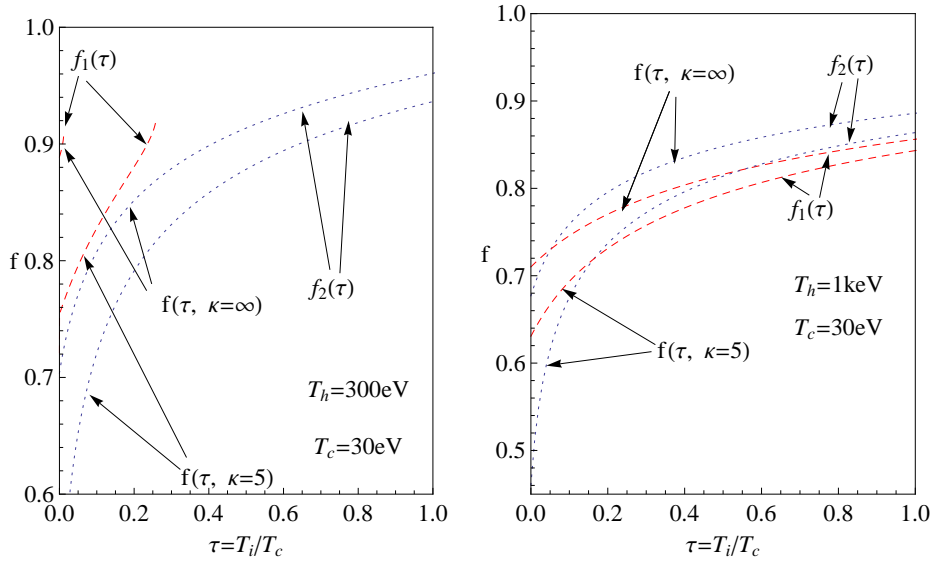


Figure 5.3: f -solutions of $\alpha_{s4} = 0$ (dashed) and $\alpha_{s5} = 0$ (dotted) for $\beta = 1/10$ (left panel) and $\beta = 3/100$ (right panel), and for $\kappa_c = \kappa_h = \kappa$, with $\kappa = 5$ and 50 . Here, we see that for β small, as in the right panel, we have $f_1 < f_2$ for some values of τ . Therefore for the parameters in the right panel graph, the mKdV approach may be used.

velocities close to the phase velocity of the wave. As will be shown in Fig. 5.11, the method becomes less reliable for Mach numbers far from M_s in cases where solitons of both polarity exist. For such cases, there exists a density ratio $f = N_{h0}/N_{e0}$ for which

the nonlinear term in the KdV equation ($\propto \phi \partial \phi / \partial \xi$) vanishes and therefore the balance between the nonlinear term and the dispersive term ($\propto \partial^3 \phi / \partial \xi^3$) is no longer attainable for propagation of solitary structures. Even applying the modified KdV solutions does not seem fruitful in resolving this problem. Thus for such cases, the arbitrary amplitude approach like the pseudopotential/Sagdeev method (which we discuss below) is vital. We will show soliton potential structures in Fig. 5.10 that cannot be obtained from the KdV solution for this particular model.

5.5 Arbitrary Amplitude IA Solitons

With the chosen normalization, as used in the perturbation theory, equations (5.2)–(5.4) take the form:

$$\frac{\partial n_i}{\partial t} + \frac{\partial}{\partial x}(n_i u_i) = 0, \quad (5.49)$$

$$\frac{\partial u_i}{\partial t} + u_i \frac{\partial u_i}{\partial x} + 3\tau n_i \frac{\partial n_i}{\partial x} + \frac{\partial \phi}{\partial x} = 0, \quad (5.50)$$

and

$$\frac{\partial^2 \phi}{\partial x^2} + n_i(\phi) - n_c(\phi) - n_h(\phi) = 0, \quad (5.51)$$

respectively, where again $\tau = (T_i/T_c)/Z_i$, which simply becomes T_i/T_c with $Z_i = 1$; n_c and n_h are the normalized density of the cool and hot electrons, respectively; $n_i(u_i)$ are the normalized ion density (velocity) of the cool ions; x and t are the normalized spatial and temporal variables, and ϕ the electrostatic potential, respectively. The corresponding boundary conditions are ϕ , $\partial \phi / \partial x$ and $u_i \rightarrow 0$, and, $n_i \rightarrow 1$ as $x \rightarrow \pm \infty$.

We seek simple traveling wave solutions of Eqs. (5.49)–(5.51) that are stationary in a frame moving with velocity M . Thus we transform to a stationary state, where we assume that all the quantities depend on $\xi = x - Mt$; M being the Mach number, equivalent to the velocity of the solitary wave normalized to the acoustic speed $C_s = (Z_i K_B T_c / m_i)^{1/2}$. With the boundary conditions stated above, Eqs. (5.49) and (5.50) can be solved for $n_i(\phi)$, giving [Baboolal *et al.*, 1989, 1990; Ghosh *et al.*, 1996; Verheest *et al.*, 2008]

$$M^2 \left(\frac{1}{n_i^2} - 1 \right) + 3\tau (n_i^2 - 1) + 2\phi = 0, \quad (5.52)$$

which is quadratic in n_i^2 with solution

$$n_i^2 = \frac{1}{6\tau} \left\{ M^2 + 3\tau - 2\phi \pm \left[(M^2 + 3\tau - 2\phi)^2 - 12M^2\tau \right]^{1/2} \right\}. \quad (5.53)$$

The first term of the left-hand side of Eq. (5.52) is the inertial contribution to the restoring force while the second term is the pressure contribution. In the absence of pressure ($\tau \rightarrow 0$), the restoring force is solely due to inertia and Eq. (5.52) gives $n_i(\phi) = (1 - 2\phi/M^2)^{-1/2}$, which can also be obtained by taking the limit, as $\tau \rightarrow 0$, of Eq. (5.53) with the minus sign of the term under square brackets.

Following the approaches of Ghosh *et al.* [1996] and Verheest *et al.* [2008], we rewrite the ion density in the form

$$n_i(\phi) = a(\sqrt{A} \pm \sqrt{B}),$$

where a , A and B are constants to be determined, and only the negative sign is physically relevant. This gives

$$n_i = \frac{1}{2\sqrt{3\tau}} \left\{ \left[(M + \sqrt{3\tau})^2 - 2\phi \right]^{1/2} - \left[(M - \sqrt{3\tau})^2 - 2\phi \right]^{1/2} \right\}. \quad (5.54)$$

Note that the boundary conditions $\phi \rightarrow 0$, $n_i(\phi) \rightarrow 1$ as $\xi \rightarrow \pm\infty$ are satisfied in Eq. (5.54) only when $M > \sqrt{3\tau}$, that is, $V > C_{ti}$ as required for ion acoustic structures.

With the transformation $\xi = x - Mt$, Poisson's equation is now given by

$$\frac{\partial^2 \phi}{\partial \xi^2} = n_c(\phi) + n_h(\phi) - n_i(\phi) \equiv G(\phi), \quad (5.55)$$

where $n_i(\phi)$ is obtained from Eq. (5.54), and $n_c(\phi)$ and $n_h(\phi)$ are obtained from Eq. 5.1, after normalization, as

$$n_s(\phi) = \frac{N_{s0}}{N_{e0}} \left(1 - \frac{\beta_s \phi}{\kappa_s - 3/2} \right)^{-(\kappa_s - 1/2)}, \quad (5.56)$$

with $s = c(h)$ for cool (hot) electrons, and $\beta_s = T_c/T_s$ is the reciprocal of the normalized temperature.

Poisson's equation [Eq. (5.55)] can then easily be written in the form

$$\frac{d^2\phi}{d\xi^2} + \frac{d\Psi(\phi)}{d\phi} = 0 \quad \text{or} \quad \frac{1}{2} \left(\frac{d\phi}{d\xi} \right)^2 + \Psi(\phi) = 0, \quad (5.57)$$

where $\Psi(\phi) = -\int_0^\phi G(\phi)d\phi$ is the pseudopotential of the plasma system and $G(\phi) = n_c(\phi) + n_h(\phi) - n_i(\phi)$. The boundary conditions $\phi, \partial\phi/\partial\xi \rightarrow 0$ as $\xi \rightarrow \pm\infty$ have been used.

5.5.1 Pseudopotential Approach

Now in seeking soliton solutions of Eq. (5.57), we need to confirm that the pseudopotential $\Psi(\phi)$ satisfies $\Psi(\phi) = \Psi'(\phi) = 0$ at $\phi = 0$ for all M as a first requirement (see Sec. 1.4.2). This procedure leads to the pseudopotential expression of the plasma system as

$$\begin{aligned} \Psi(\phi) = & \frac{f}{\beta} \left[1 - \left(1 - \frac{\beta\phi}{\kappa_h - 3/2} \right)^{(3/2-\kappa_h)} \right] + (1-f) \left[1 - \left(1 - \frac{\phi}{\kappa_c - 3/2} \right)^{(3/2-\kappa_c)} \right] \\ & + \frac{1}{6\sqrt{3\tau}} \left\{ \left[(M - \sqrt{3\tau})^2 - 2\phi \right]^{3/2} - \left[(M + \sqrt{3\tau})^2 - 2\phi \right]^{3/2} \right\} \\ & + M^2 + \tau. \end{aligned} \quad (5.58)$$

Here, $f = N_{h0}/N_{e0}$ is the fractional density of hot electrons and $\beta = \beta_h = T_c/T_h$ is the ratio of the cool to hot electron temperatures.

In investigating the existence domain for solitary structures, solitons or double layers we require $M > M_s$, where

$$M_s = \left\{ 3\tau + \left[\frac{(1-f)(\kappa_c - 1/2)}{(\kappa_c - 3/2)} + \frac{\beta f(\kappa_h - 1/2)}{(\kappa_h - 3/2)} \right]^{-1} \right\}^{1/2} \quad (5.59)$$

is the lower limit of M restricting the existence of solitons, obtained at $\Psi''(\phi = 0) = 0$. The usual soliton condition $M > M_s$ implies that $V^2 > C_{ii}^2 + C_{i\kappa}^2$, where $C_{i\kappa} = \omega_{pi}\lambda_{D\kappa}$ is the κ -dependent ion acoustic speed. If we define the "true" Mach number of the solitary waves by $M_{i\kappa} = V/C_{i\kappa}$, then $M_{i\kappa}^2 > 1 + C_{ii}^2/C_{i\kappa}^2$, which is always greater than unity for all temperatures, resulting in superacoustic structures as pointed out earlier.

Further, with our choice of normalization, the normalized phase velocity following from

Eq. (5.13) is given by

$$V_{ph}^2 \equiv \frac{\omega^2/k^2}{C_s^2} = \frac{\omega_{pi}^2 \lambda_{D\kappa}^2}{C_s^2} + \frac{C_{ti}^2}{C_s^2},$$

which can easily be written as

$$V_{ph}^2 = 3\tau + \left[\frac{(1-f)(\kappa_c - 1/2)}{(\kappa_c - 3/2)} + \frac{\beta f(\kappa_h - 1/2)}{(\kappa_h - 3/2)} \right]^{-1} \equiv M_s^2. \quad (5.60)$$

Equations (5.59) and (5.60) imply that the existence of solitary structures (solitons or double layers) require the resulting structures to move with velocities exceeding the phase velocity of the associated waves. However, as our results will show, it turns out that solitons can have a velocity equal to the phase velocity of the wave, that is, with Mach numbers, $M = M_s$. *This peculiar scenario occurs in situations where both positive and negative potential solitons can be supported by the plasma system under consideration.*

5.5.2 Potential Limitations

Firstly, in the case of positive potential solitons we observe from Eq. (5.54) that finite non-negative values of $n_i(\phi)$ require $\phi \leq (M - \sqrt{3\tau})^2/2 \equiv \phi_{i1}$ and $\phi < (M + \sqrt{3\tau})^2/2 \equiv \phi_{i2}$, since at $\phi = \phi_{i1}$, $n_i = (M/\sqrt{3\tau})^{1/2}$, which is finite, and at $\phi = \phi_{i2}$, $n_i = i(M/\sqrt{3\tau})^{1/2}$, which is complex. The expression $\Psi(\phi_{i1}) > 0$ or $\Psi(\phi_{i2}) > 0$ will provide the upper limit on M for the existence of positive potential solitons (since both ϕ_{i1} and ϕ_{i2} give positive real values for all M and f). However, ϕ_{i1} being less than ϕ_{i2} for all M and f implies that the limiting condition $\Psi(\phi_{i1}) > 0$ dominates $\Psi(\phi_{i2}) > 0$, and the former will be used here. That is, we consider $\phi \leq \phi_{i1}$ so that the ion density is real and finite to prevent wave breaking [Baboolal *et al.*, 1990].

We also observe from Eq. (5.58) that $\Psi(\phi) \rightarrow +\infty$ when $\phi \rightarrow +\infty$, and as we require $\Psi(\phi)$ to be negative in the vicinity of the origin ($\phi = 0$) and before a second root (ϕ_m) is encountered, that is, $\Psi(\phi) < 0$ for $0 < \phi < \phi_m$, it follows that we can have at most one single root before we approach the limiting potential ϕ_{i1} on the positive potential side [Verheest *et al.*, 2008]. In addition, since soliton amplitudes increase with increasing Mach number or soliton speed (see perturbation theory), it implies that the Mach number corresponding to $\Psi(\phi_{i1}) = 0$ must be the upper limit of M for $\phi > 0$. Therefore the upper limit of M for the existence of positive potential solitons is obtained from $\Psi(\phi_{i1}) = 0$.

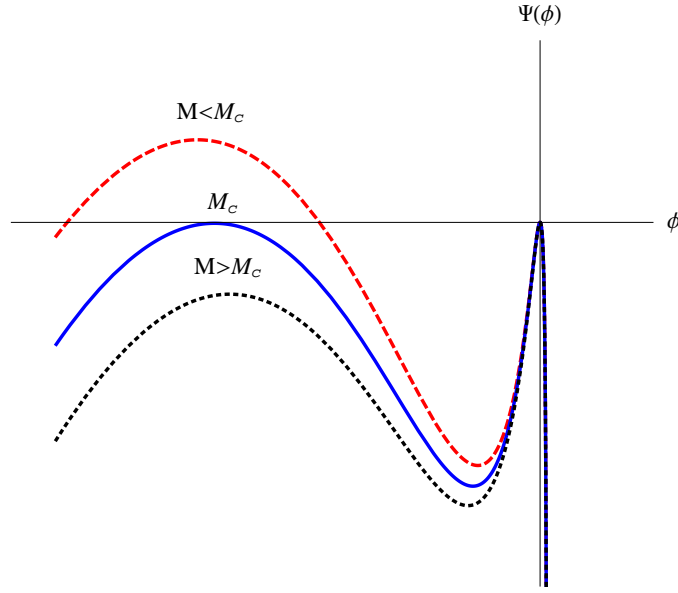


Figure 5.4: Restriction of solitons by double layers, obtained for the parameters: $T_i = 0.1$ eV, $T_c = 30$ eV, $T_h = 1$ keV, $\kappa_c = 2.0$, $\kappa_h = 3.0$, $f = 0.5$, typical for Saturn's outer magnetosphere [Schippers *et al.*, 2008] at about $16 R_S$, where R_S is the radius of Saturn. The double layer is obtained for $M_c \simeq 1.38097$, and has amplitude $|\phi_m| \simeq 21.55$. Thus solitons will have amplitudes less than ϕ_m .

Secondly, negative potential solitons in the plasma model are restricted from below by the soliton condition and from above by the double layer limit, where the latter occurs for Mach numbers, M satisfying the double layer condition $\Psi(\phi_m) = \Psi'(\phi_m) = 0$ for particular values of f , τ , β , and spectral indices κ_c and κ_h . As we argued in the positive potential case, this follows from the following description: firstly, other than at the origin $\phi = 0$, we also require $\Psi(\phi) < 0$ before we encounter another zero of $\Psi(\phi)$ on the negative potential side. Secondly, since the electron contributions in Eq. (5.58) remain finite [scaling as $(1 - f) + f/\beta$] as $\phi \rightarrow -\infty$, we get $\Psi(\phi) \rightarrow -\infty$ as $\phi \rightarrow -\infty$. These two conditions imply that in the interval $[0, -\infty]$ there exists is a root ϕ_d , satisfying $\Psi(\phi_d) = \Psi'(\phi_d) = 0$, and hence leading to double layers.

As soliton amplitudes increase with increasing Mach number, in a number of plasma models the existence of a double layer brings an end to the existence of solitons [Baboolal *et al.*, 1988]. Thus the Mach number corresponding to the second double root (*i.e.*, other than at the origin) provides the upper limit on the Mach number for the existence of negative potential solitons. A typical example is shown in Fig. 5.4, where solitons will occur for Mach numbers, $M < M_c$; M_c is the solution of the double layer condition, and

no soliton-like structures will be obtained for $M > M_c$. However, we point out that the occurrence of a double layer does not always provide an upper cutoff for the existence of solitons of a particular potential sign. Our results in Chapter 7 (Fig. 7.4) show that solitons can be obtained even beyond a double layer, if the pseudopotential function has sufficient local minima.

5.5.3 Existence Domain for Ion-Acoustic Solitons and Double Layers

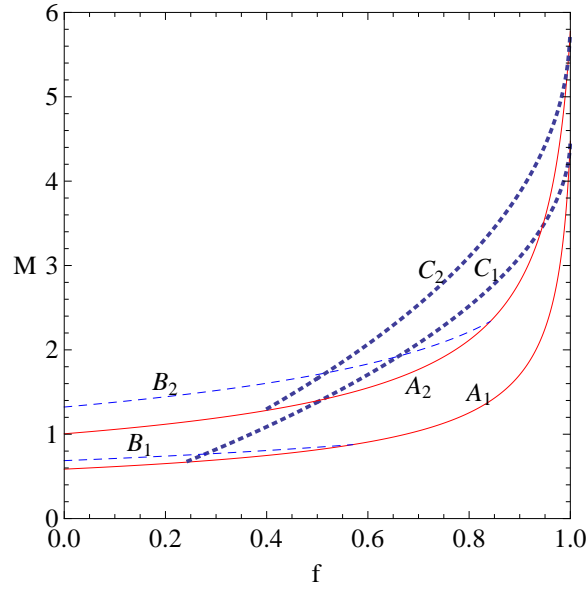


Figure 5.5: Existence domain for ion-acoustic solitons for the parameters: $T_i = 0.1$ eV, $T_c = 30$ eV, $T_h = 1$ keV. For $\kappa_c = 2.0$, $\kappa_h = 3.0$, positive, and negative potential solitons are bounded by curves A_1 and B_1 , and A_1 and C_1 , respectively. Similarly, for $\kappa_c = \kappa_h = \infty$ (Maxwellian case), positive, and negative potential solitons are bounded by curves A_2 and B_2 , and A_2 and C_2 , respectively.

Figure 5.5 shows the existence domain of ion-acoustic solitons for a plasma with both cool and hot electrons having a considerable excess of superthermal particles in both electron components, as seen in Saturn's magnetosphere [Schippers *et al.*, 2008] (curves A_1 , B_1 , C_1 , with $\kappa_c = 2$, $\kappa_h = 3$), and the Maxwellian equivalent (curves A_2 , B_2 , C_2 , with $\kappa_c = \kappa_h = \infty$). Here, we introduce the notations f_n and f_p , defined by the values of f such that below f_n you don't get negative potential solitons limited by the existence of double layers while above f_p you don't get positive potential solitons limited by the ions. Thus the figure shows that compressive (positive potential) solitons will occur for $f < f_p \simeq 0.57$ (curves A_1 and B_1) when $\kappa_c = 2$, $\kappa_h = 3$, and for $f < f_p \simeq 0.842$ (curves A_2 and B_2) for the Maxwellian cool and hot electrons, respectively. Thus the range in f is considerably

reduced for Saturnian parameter values than would be predicted by a double-Maxwellian model. On the other hand, rarefactive (negative potential) solitons are expected to occur over a wider range of f for Saturnian than for Maxwellian electrons. Specifically, they occur for $f > f_n \simeq 0.239$ (curves A_1 and C_1) in the case of $\kappa_c = 2$, $\kappa_h = 3$, and $f > f_n \simeq 0.393$ (curves A_2 and C_2) in the case of Maxwellian electrons, respectively. Both positive and negative potential solitons can “co-exist” for $f_n < f < f_p$, that is, $0.239 < f < 0.57$ for $\kappa_c = 2$, $\kappa_h = 3$, and $0.393 < f < 0.842$ for the Maxwellian case, respectively. The graphs also show that for $f = 1$, that is, $n_{c0} \rightarrow 0$, the lower and upper limits on the Mach number coalesce at $M \approx 4.43628$ for low kappa values ($\kappa_c = 2$, $\kappa_h = 3$) compared to $M \approx 5.5793$ for the case of Maxwellian electrons.

The resulting effect of spectral index κ on the existence domain of solitons (or double layers) is that in comparison to Maxwellian particles, low kappa values (increased superthermal particles in the high energy tail of the distribution) reduce the existence domain in the parameter space of Mach number M and density ratio $f = N_{h0}/N_{e0}$ over which compressive solitons or both compressive and rarefactive solitons can exist. However, for constant species temperatures, densities and speed (in terms of Mach number), the variation of soliton amplitude with the spectral index κ shows that low values of κ result into large amplitudes compared with the Maxwellian case. This variation is illustrated in Fig. 5.6 where the values of f and M used correspond to a region in (f, M) parameter space shown in Fig. 5.5 where rarefactive (negative potential) solitons can be supported for both low ($\kappa_c = 2$, $\kappa_c = 3$) and high ($\kappa_c = \kappa_c = \infty$) kappa values.

5.5.4 Variation of Soliton Potential Amplitude (ϕ_m) with Mach Number

In Figures 5.7 and 5.8, we plot the soliton potential amplitudes for different values of $\delta M = M - M_s$, where M is the Mach number satisfying the soliton conditions and M_s is given in Eq. (5.59). The end points of the curves correspond to the upper limit in M , which for example, in the case of negative potential solitons occur when a double layer is met. We have already seen from Fig. 5.5 that when $\kappa_c = 2$, $\kappa_h = 3$, for example, positive potential solitons occur for $f < f_p \simeq 0.57$ while negative potential solitons occur for $f > f_n \simeq 0.24$.

From the (small amplitude) KdV approach we defined f_c as being the density ratio at

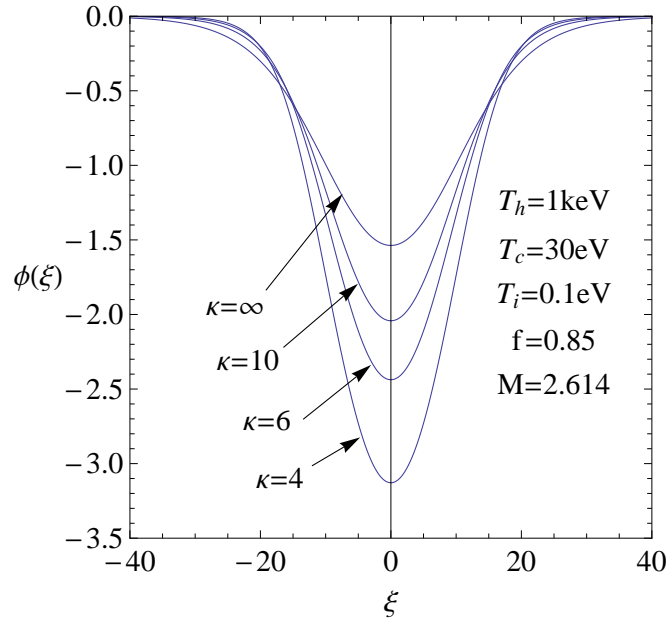


Figure 5.6: Variation of soliton amplitude for different spectral index values $\kappa = \kappa_c = \kappa_h$, for the temperature values in Fig. 5.5, with $f = 0.85$ and $M = 2.614$.

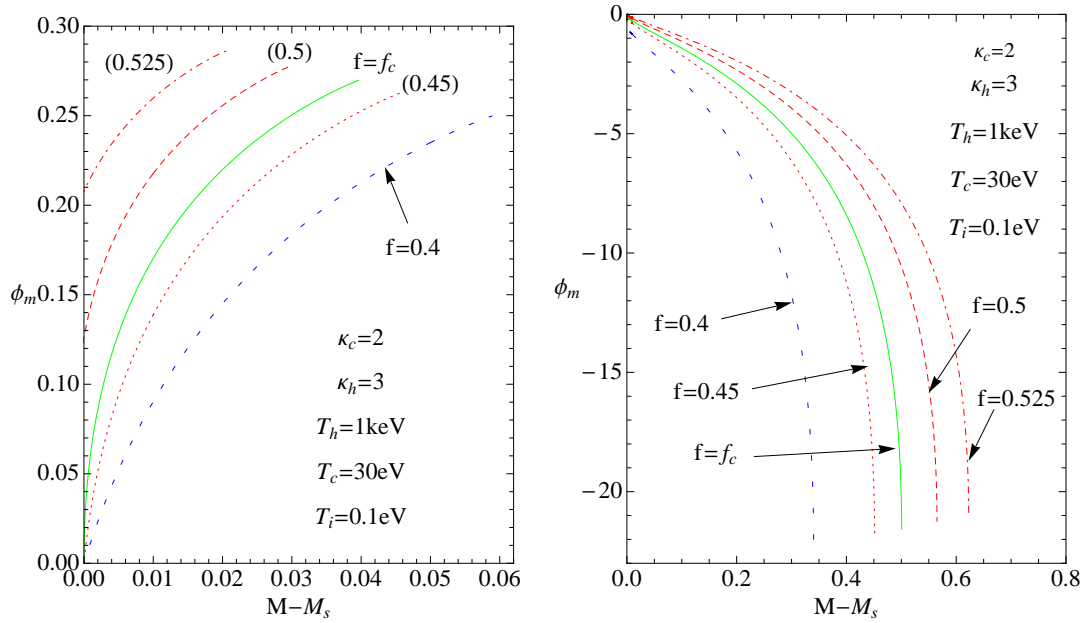


Figure 5.7: Variation of soliton potential amplitude with $\delta M = M - M_s$ for a 'hard' electron spectrum (low κ values) with spectral indices and temperature values as in the figure, *Left panel*: ($\phi > 0$) and *Right panel*: ($\phi < 0$). The parameter labeling the curves is the density ratio $f = n_{h0}/n_{e0}$. The solid (continuous) green curves correspond to the critical density ratio $f = f_c \simeq 0.472$ at which the soliton amplitudes from the KdV (small amplitude) method goes to infinity (see discussion of the subsequent section). Note the change of scale for ϕ between the two figures.

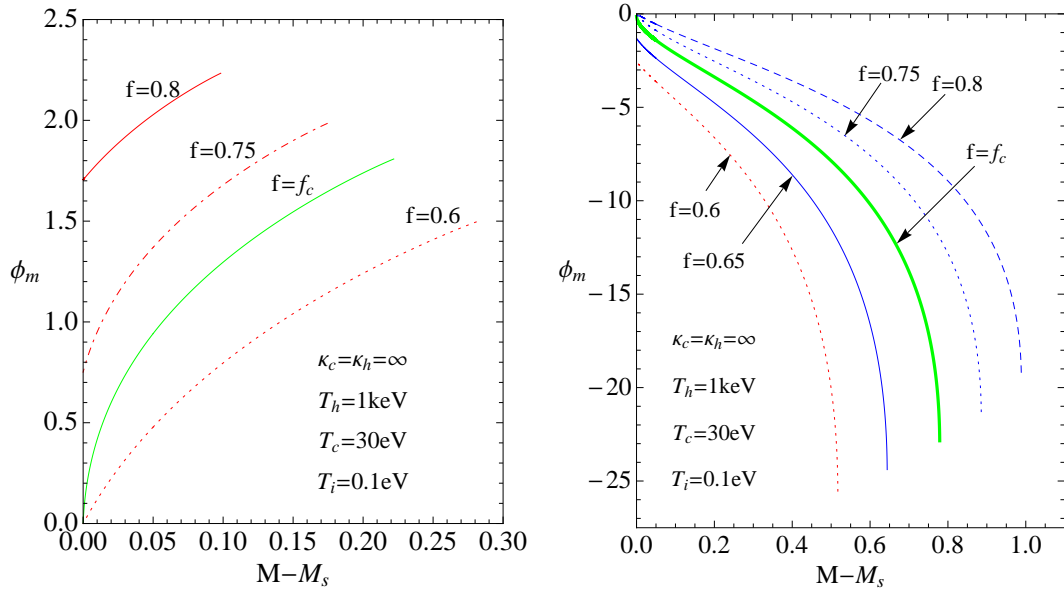


Figure 5.8: Same as in Fig. 5.7, now for the Maxwellian equivalent ($\kappa_c = \kappa_h = \infty$), with $f_c \simeq 0.704$.

which the nonlinearity term in the KdV equation vanishes, and hence the soliton amplitude goes to infinity such that for $f < (>)f_c$ the potential is positive (negative). In the arbitrary amplitude approach, f_c can also be obtained by finding a value of f that satisfies $\Psi'''(\phi = 0, M = M_s, f) = 0$ [Baluku *et al.*, 2010a], see also Chap. 4. Thus Fig. 5.1 clearly shows that the nonlinear term in the KdV equation vanishes at the same density fraction, f_1 , as that at which the third derivative of the Sagdeev potential, evaluated at the origin for a structure moving at the minimum soliton speed, $M = M_s$, becomes zero.

Figures 5.7 and 5.8 show that for some density ratios in the range $f_c < f < f_p$ (for $\phi > 0$) or $f_n < f < f_c$ (for $\phi < 0$), the soliton amplitude at $M = M_s$ is nonzero, and thus solitons exist even at the lowest Mach number M_s ($\delta M = M - M_s = 0$). We also see that for a very small increment in M , the amplitude is large compared to cases of f far from the critical f values (for which only one potential sign can be supported). Note that the negative solitons have much greater amplitude than the positive potential solitons.

Soliton amplitudes obtained at $M = M_s$, for f values in the region where both polarities are supported for the parameter values used in Fig. 5.5, are shown in Fig. 5.9. For each case, f_c corresponds to the value of f for which $\phi_m = 0$. that is, $f_c \simeq 0.472$, and 0.712 , respectively. The graph shows that for a particular potential sign, the soliton amplitude at $M = M_s$ increases monotonically as you move away from f_c , with larger amplitudes

obtained in the case of Maxwellian electrons ($\kappa = \infty$) than for the hard spectrum Saturnian case with low κ values. As shown in Fig. 5.9, finite positive solitons exist at M_s for $f_c < f < f_p \simeq 0.57$ (in the case of low kappa values shown on the graph) and for $f_c < f < f_p \simeq 0.84$ (in the case of Maxwellian electrons), with the maximum amplitudes for these critical values being $\phi_m = 0.30$ and 2.5, respectively. Similarly, finite negative solitons at M_s exist for $f_c > f > f_n \simeq 0.24$ (in the case of low kappa values) and for $f_c > f > f_n \simeq 0.4$ (Maxwellian case), with the maximum amplitudes at $M = M_s$ for these critical values (not shown on graph) being $|\phi_m| = 20.7$ and 28.8, respectively.

We also point out that if one chooses the normalized density ratio to be $f = N_{c0}/N_{e0}$ instead of $f = N_{h0}/N_{e0}$ as used in this work, then for the Maxwellian case one arrives at a similar pattern of results to those shown in Chapter 7, Fig. 7.3 for the double Maxwellian electrons case.

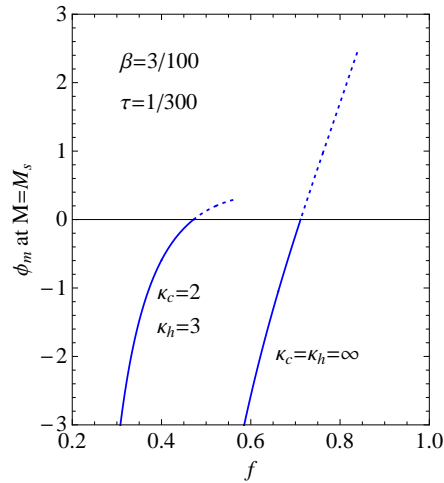


Figure 5.9: Finite solitons at $M = M_s$ in the “coexistence” region: Above f_c the amplitude at M_s is finite for $\phi < 0$ and goes to zero for $\phi > 0$. The reverse is true for $f < f_c$.

Since $\Psi''(\phi = 0) = 0$ at the lowest Mach number $M = M_s$, that is, $\Psi''(\phi)$ has a double root, and $\Psi(\phi)$ has a triple root at the origin ($\phi = 0$) when $M = M_s$, it implies that in these peculiar cases the convexity condition $\Psi''(\phi = 0) < 0$ is now taken over by $\Psi'''(\phi = 0, M = M_s) < 0$, which ensures that the origin remains unstable for $\phi < 0$ [Verheest and Hellberg, 2010]. This phenomenon is quite surprising but it brings out the point why small amplitude (perturbation) techniques may not be appropriate in analyzing experimental or observational results, especially in the case of plasmas whose density ratios (here, $f = N_{h0}/N_{e0}$) allow the coexistence of both positive and negative potential solitons.

The perturbation methods fail to pick up the “already large amplitude” solitons in the vicinity of M_s and thus can only be obtained numerically from large amplitude methods like the pseudopotential/Sagdeev approach employed in this work. The unreliability of the perturbation theory was also pointed out in the experiments of Nakamura *et al.* [1996], where, using negative ions (argon) and two Boltzmann electrons in a multi-dipole plasma machine experiment, they showed that the velocity and width of solitons from the KdV approach deviated significantly from the pseudopotential and experimental results.

In Fig. 5.10 we plot typical potential profiles for two values of f ($f = 0.75$ and $f = 0.65$) which are close to $f_c \approx 0.704$ for the Maxwellian case shown in Fig. 5.8. For example, for $f = 0.75$ (left panel) the graph shows that a positive potential soliton can occur at the lowest Mach number M_s (that is, for $\delta M = 0$) with quite a large amplitude of about 0.75 in addition to both positive and negative potential solitons for $M > M_s$ or $\delta M > 0$. A similar behaviour occurs as f is lowered, say to $f = 0.65$ (right panel) in this case, where now the solitary structure at M_s is negative and is of amplitude more than unity (with $|\phi_0| \simeq 1.312$). The soliton potentials shown in Fig. 5.10 also show that as the Mach number increases, the soliton potential amplitudes increase, accompanied by a reduction in the soliton width.

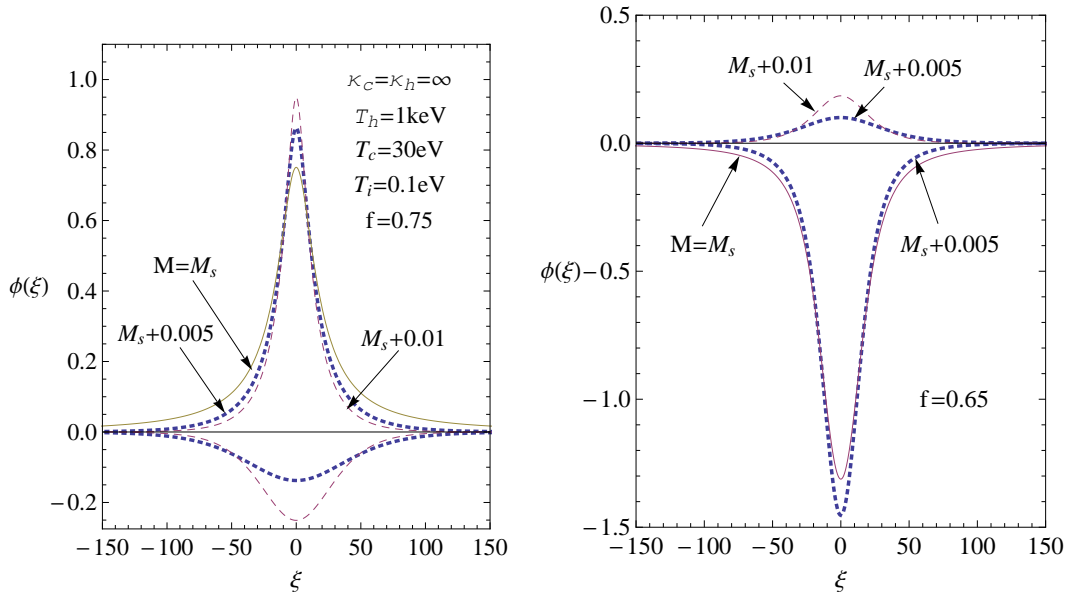


Figure 5.10: Typical soliton profiles at the lowest Mach number M_s shown (corresponding to $\delta M = 0$) for $f = 0.75 > f_c$ (left panel) and $f = 0.65 < f_c$ (right panel). The parameters, as shown on the figure, are the same as those of Fig. 5.8.

5.5.5 Sagdeev (Pseudopotential) Approach vs. Perturbation Technique

A comparison between the large amplitude approach and the perturbation technique is shown in Fig. 5.11 for $\tau = 1/300$, $\beta = 3/100$, and $\kappa_c = 2$, $\kappa_h = 3$ (left panel, plotted for $f > f_c$ in the case of negative potential solitons, and $\kappa_c = \kappa_h = \infty$ (right panel, plotted for $f < f_c$ in the case of positive potential solitons), respectively). In both cases the numerical results are shown by the continuous lines. In comparison with results from the arbitrary amplitude approach, we observe from Fig. 5.5 that for $\kappa_c = 2$, $\kappa_h = 3$, $\tau = 1/300$, $\beta = 3/100$, positive potential solitons will exist for $f < f_p = 0.56$ while negative potential solitons will occur for $f > f_n = 0.24$. This means that the small amplitude (KdV) method breaks down for $f_c < f < f_p$ (for $\phi > 0$) and $f_n < f < f_c$ (for $\phi < 0$), respectively. Though we expect both methods to be in agreement to some extent [*i.e.*, for Mach numbers close to M_s with $f \gg f_c$ ($\phi < 0$) and $f \ll f_c$ ($\phi > 0$)], we point out that for values of f close to f_c in this case, results deviate quite significantly even for very small values of δM , for example, as low as 0.0007 with $f = 0.5$ (red curves) compared with $f = 0.6$ (light-blue curves) where the ϕ_m versus δM plots remain linear up to about 0.013 in Fig. 5.11, left panel. A similar trend is observed in the right panel graphs as f gets close to f_c .

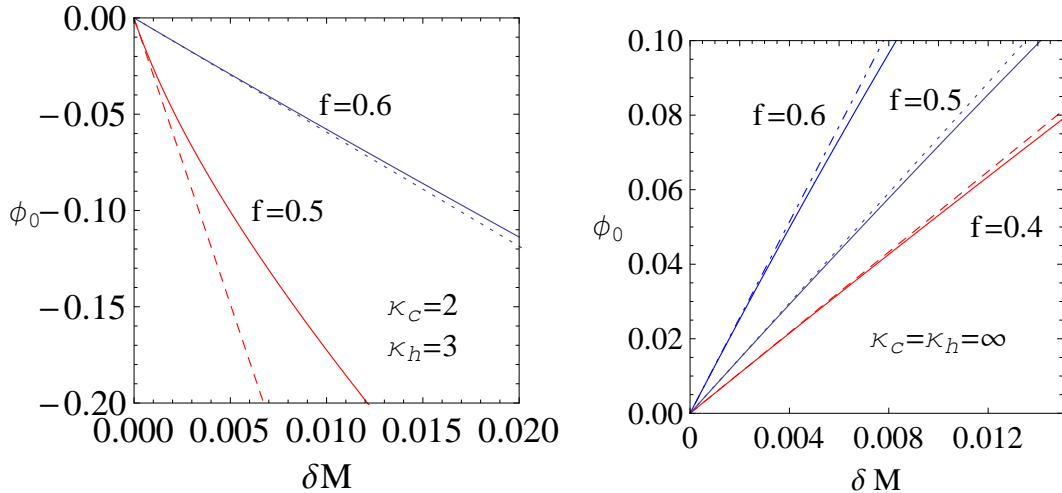


Figure 5.11: Soliton amplitude (ϕ_0) as a function of Mach number, M , for $\tau = 1/300$, $\beta = 3/100$; *Left panel*: $\kappa_c = 2$, $\kappa_h = 3$, $f = 0.5$ (red) and $f = 0.6$ (light blue), both greater than $f_c \sim 0.47$, *Right panel*: $\kappa_c = \kappa_h = \infty$, $f = 0.4$ (red), $f = 0.5$ (light blue), and $f = 0.6$ (blue), all less than $f_c \simeq 0.7$. The continuous curves are the numerical solutions (from the pseudopotential method) while the broken curves follow from Eq. (5.38).

5.6 Positive Potential Double Layers

First of all, in this work we have used values of temperature ratio $\beta = T_c/T_h$ that are typical of a particular region in Saturn's magnetosphere. However, if we choose β values that are quite large, as we will see in this section, then there are possibilities of getting positive double layers. Such positive double layers are also discussed in Chapter 7 when considering a plasma with Maxwellian electron components and cold ions. To investigate the existence of positive double layers in plasmas with κ -distributed electron components, we consider two cases, *viz.*, cold ions ($\tau = 0$) and cool ions ($\tau = 1/300$).

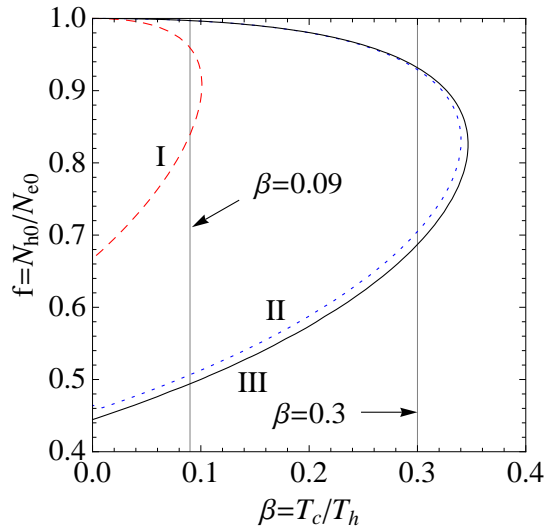


Figure 5.12: Variation of f_c with temperature ratio, β . The parameters corresponding to the curves are: Curve I: $\kappa_c = \kappa_h = \infty$, $\tau = T_i/T_c = 0$, curve II: $\kappa_c = 2$; $\kappa_h = 3$, $\tau = 0$, and curve III: $\kappa_c = 2$; $\kappa_h = 3$, $\tau = 1/300$, respectively.

In Fig. 5.12 we show a plot of density ratio, $f = N_{h0}/N_{e0}$ versus temperature ratio $\beta = T_c/T_h$ at which the third derivative of the pseudopotential, $\Psi(\phi, M)$, changes sign when $\phi = 0$ and $M = M_s$. The curve labeled I depicts a plasma with Maxwellian cool and hot electron components in the presence of cold ions. This figure is essentially the same as Fig. 1(a) of Baluku *et al.* [2010b] (see also Fig. 7.1 in Chapter 7), only that here we have defined the density ratio in terms of the fraction of hot electron density. In curves II and III we look at a plasma with a large excess of superthermal electrons (with a hard spectrum or low κ values) in the presence of cold ions ($\tau = 0$, curve II) and cool ions ($\tau = 1/300$, curve III), respectively. Figure 5.12 shows that the critical temperature ratio, β_c , above which $\Psi(\phi = 0, M_s)$ does not change sign, increases in the presence of non-Maxwellian

electrons. For curve I, $\beta_c \simeq 0.101021$, compared to $\beta_c \simeq 0.3406$ and $\beta_c \simeq 0.3468$ for curves II and III, respectively. Thus cool ions increase β_c only marginally above the value found for cold ions.

In the search for positive double layers for this plasma model we shall consider two β values: $\beta = 0.09$, that is also discussed in Fig. 3 of Baluku *et al.* [2010b] and Fig. 7.1 in Chapter 7, and corresponds to Maxwellian electron components, and $\beta = 0.3$, corresponding to non-Maxwellian electron components. The case for $\beta = 0.09$ is shown in Fig. 5.13. Here, we recover the results of Baluku *et al.* [2010b], that is, we get both positive and negative double layers that are separated by one of the critical values of f_c . Negative solitons are bounded by double layers [the dotted (light-blue) curve for $0.75 < f < 0.95$] while positive solitons, limited by the ion limit constraint, are bounded by the continuous (blue) curve. For $f > f_{c2}$, we get positive double layers along the dashed light-blue curve. Thus, for some range of f positive solitons exist even after a double layer has occurred, as will be discussed in Chapter 7.

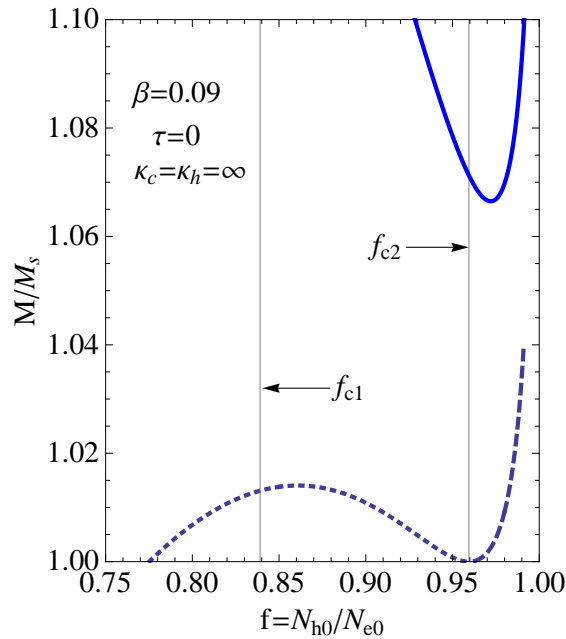


Figure 5.13: Existence domain for positive double layers for a plasma with Maxwellian electron components and cold ions, with $\beta = 0.09$. The critical values of f_c are $f_{c1} \simeq 0.8391$ and $f_{c2} \simeq 0.9595$.

However, with $\beta = 0.3$ (in the presence of non-Maxwellian electrons), as in Figure 5.14 (left panel), though we get solitons limited by the positive double layers, we don't

get solitons beyond the positive double layers as was the case in Fig. 5.13 for Maxwellian electrons. Here, the positive solitons limited by the ions (shown by the continuous blue curve) occur for $f < 0.753$ far from the values of f for which positive potential double layers can be supported. This also applies to $\tau \neq 0$, here with $\tau = 1/300$ as shown in the right panel of Fig. 5.14, where positive solitons limited by the ion limitation exist only for $f < 0.738$. This effect appears to be related to the dip in the ion cut-off curve of Fig. 5.13, which for smaller κ values is lowered, and cuts the critical axis $M = M_s$ at some value of f , above which it no longer plays a role.

Figure 5.14 also shows that the narrow region, where solitons of both potential signs can be supported (under the dotted and continuous curves), is bounded from below by the critical value of f , f_{c1} . Recall from Fig. 5.12 that for $\beta = 0.3$ we have $\Psi(\phi = 0, M_s) < 0$. Thus in the region $f_{c1} < f < f_{c2}$, if positive potential solitons exist, they will have finite amplitude solitons at $M = M_s$ while for negative potential solitons, $\phi \rightarrow 0$ as $M \rightarrow M_s$. Below f_{c1} (and above f_{c2}) we have $\Psi(\phi = 0, M_s) > 0$, thus the positive potential solitons that exist in those regions have amplitudes which go to zero as $M \rightarrow M_s$.

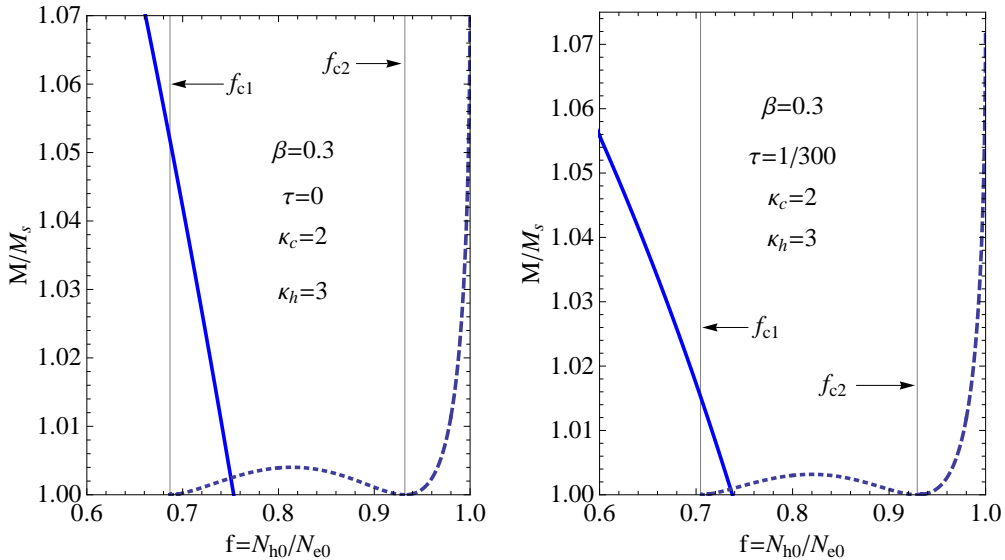


Figure 5.14: Same as in Fig. 5.13, now with $\beta = 0.3$. *Left panel:* $\tau = 0$, the lower value of f_c is $f_{c1} \simeq 0.6868$ while the upper value is $f_{c2} \simeq 0.9319$. *Right panel:* $\tau = 1/300$, the lower value of f_c is $f_{c1} \simeq 0.7046$ while the upper value is $f_{c2} \simeq 0.9292$.

5.7 Conclusions and Chapter Summary

In this chapter we have investigated in some details solitons supported by plasmas with fluid ions and kappa-distributed two temperature electrons. Our results reveal the following main features:

(i) Both compressive and rarefactive solitons can be supported by the model. The former are characterized by a hump in the density as well as the electrostatic potential ($\phi > 0$) while the latter have a dip in the density and electrostatic potential ($\phi < 0$).

(ii) The effect of spectral index κ on the existence domain of solitons (or double layers) is that, compared to high values of kappa (which represent Maxwellian particles), low kappa values, which indicate increased superthermal particles in the high energy tail of the distribution, reduces the existence domain in the parameter space of (f, M) over which compressive solitons or both polarities can exist.

(iii) A peculiar behaviour occurs for density ratios that support coexistence of both hump ($\phi > 0$) and dip ($\phi < 0$) solitons. Here we have obtained a critical density ratio, f_c , which in the KdV approach is associated with the vanishing of the coefficient of the nonlinear term in the KdV equation, and in the arbitrary amplitude approach is associated with $\Psi'''(\phi = 0, M_s) = 0$. Below f_c , solitons which have the same sign as $\Psi'''(\phi = 0, M_s)$, in this case positive, are KdV-like, with vanishing amplitudes as M approaches M_s . However, for the same plasma configuration, with $f < f_c$, we also obtain solitons with the sign opposite to that of $\Psi'''(\phi = 0, M_s)$ that are nonKdV-like, with finite (nonzero) amplitudes at M_s . The reverse is true for $f > f_c$.

(iv) Comparison between the perturbation theory and the large amplitude technique shows that whereas the perturbation technique seem to be accurate for very small amplitudes, especially for Mach numbers close to M_s , that is, for structures that move with velocities close to the phase velocity of the wave, the method becomes less reliable for velocities far from the phase velocity, especially in cases where solitons of both polarities exist. Thus the arbitrary amplitude approach like the pseudopotential method is more useful. We have shown soliton potential structures from the pseudopotential method that cannot be obtained from the perturbation theory, even for $\phi \ll 1$, for this particular model in Fig. 5.10, *viz.*, those that are finite at $M = M_s$.

(v) The large rarefactive potential solitons ($\phi < 0$) reported for this plasma model may be attributed to the fact that the small but finite electron mass, which is a measure of the electron inertia, is neglected in the electron density expression. In the parameter space of amplitude and cool electron density for a two electron temperature plasma, Rice *et al.* [1993] showed that whereas the inclusion of the electron inertia in the plasma model has negligible effect on the existence domain of compressive ($\phi > 0$) ion-acoustic solitons it does reduce the range of density and amplitude over which rarefactive solitons exist. In this model such a scheme would now require getting the electron density expression from the fluid equations of motion, with the associated kappa-distributed pressure term incorporated. The pressure expression associated with a kappa-distribution function has been derived in Appendix A.1.2, though it has not been applied to this model. This is open for further investigation.

(vi) We have shown that positive double layers may be found over a narrow range of fractional cool electron density ($< 10\%$), for both Maxwellian and low- κ distributions, the range being larger for the latter case.

(vii) Whereas for Maxwellian electrons, one value of the critical density fraction, f_{c1} , lies in the region where solitons of both polarities are supported (in this case, the existence domain for negative potential double layers), it is seen that for low- κ electrons, both critical density fractions, f_{c1} and f_{c2} , may lie at the boundary of the existence domain for negative potential double layers.

Ion-Acoustic Solitary Waves in an Electron-Positron-Ion (e-p-i) Plasma

In this chapter we consider ion-acoustic solitary waves in a fluid plasma model consisting of nonthermal electrons, which are described by the Cairns distribution function [Cairns *et al.*, 1995], Boltzmann positrons and singly charged positive cold fluid ions. This work follows on a recent article by Pakzad [2009].

6.1 Introduction

Electron-positron plasmas are characterized as fully ionized gases, consisting of electrons and positrons of equal mass. They are believed to exist in the active galactic nuclei and in the pulsar magnetospheres [Popel *et al.*, 1995; Moslem *et al.*, 2007]. They were also considered to have appeared in the early universe (see Popel *et al.* [1995], and references therein), solar atmosphere, and in the inertial confinement fusion schemes using ultra-intense lasers [Liang *et al.*, 1998], see also Moslem *et al.* [2007], and references therein. Due to the abundant nature of ions in many astrophysical plasmas, the study of electron-positron-ion plasmas has been of interest to many authors [Berezhiani *et al.*, 1994; Popel *et al.*, 1995; Nejoh, 1997; Saleem *et al.*, 2003; Haque and Saleem, 2003; Moslem *et al.*, 2007; Pakzad, 2009], and others. Popel *et al.* [1995] studied arbitrary amplitude ion-acoustic solitons in a three-component plasma consisting of Boltzmann electrons and positrons, and singly charged positive fluid ions. They reported the existence of positive potential

solitons, and showed that the presence of the positron component reduces the propagation speed of the solitons. The larger the fraction of positron density the lower the Mach number for a soliton of fixed amplitude to propagate. In addition, they showed that the amplitude of the solitons drops off drastically in the presence of a significant fraction of positrons. However, Popel *et al.* [1995] could not obtain double layers.

Kakati and Goswami [2000] investigated the existence of small amplitude double layers associated with kinetic Alfvén waves in a magnetized electron-positron-ion plasma. Here, it was shown that small-amplitude double layers can be supported by a plasma model with Boltzmann electrons and positrons independently of the electron-positron temperature ratio. Haque and Saleem [2003] studied large amplitude two-dimensional ion-acoustic and drift wave vortices in magnetized electron-positron-ion plasmas, where the electrons and positrons were also assumed to be Boltzmann distributed.

In studying two-dimensional propagation of nonlinear acoustic excitations in e-p-i plasmas, Moslem *et al.* [2007] applied their studies to the accretion disks of the active galactic nuclei, where the ion temperatures are (3–300) times higher than those of the electrons. However, due to the very high ion temperatures in the accretion disc, the ions were modelled by the Boltzmann distribution while the electrons and positrons were governed by the fluid equations. Thus Moslem’s model [Moslem *et al.*, 2007] was quite different from that used by Popel *et al.* [1995].

Using a nonthermal distribution function for electrons in a simple electron-ion plasma, Cairns *et al.* [1995] showed that the presence of nonthermal particles modifies the type of solitary waves obtained. They reported both positive and negative potential solitons coexisting, that could not be obtained with thermal or Boltzmann electrons. Thus it could be of interest to consider an e-p-i plasma in which at least one of the leptons is modelled by a Cairns distribution.

Pakzad [2009] recently discussed ion-acoustic solitons propagating in a plasma with nonthermal electrons, Boltzmann positrons and fluid ions, and reported that positive potential solitons are supported by the plasma model.

In this work, we show that in addition to the positive solitons reported by Pakzad [2009], negative potential solitons and double layers can also be supported by the plasma model, though for a limited range of positron-to-electron temperature ratios.

6.1.1 Nonthermal Distributions: The Cairns Distribution

In the context of interpreting results from the Freja satellite, the Cairns distribution was introduced in Ref. [Cairns *et al.*, 1995] as an *ad hoc* model for a population with excess fast particles, in the analysis of the effect of such particles on solitary waves. In unnormalized form, the nonthermal Cairns distribution function is given by Eq. (1.26), rewritten here, for clarity, as

$$F_j(v) = \frac{N_{j0}}{(2\pi v_{tj}^2)^{1/2}} \frac{[1 + \alpha(v/v_{tj})^4]}{(3\alpha + 1)} \exp\left[-\frac{(v/v_{tj})^2}{2}\right], \quad (6.1)$$

where α is a parameter characterizing the nonthermality of the individual particles, and $v_{tj} = (K_B T_j / m_j)^{1/2}$ is the species thermal velocity.

In the case of electrons, using the normalization $u \rightarrow v/v_{te}$; $n_e \rightarrow N_e/N_{e0}$, the normalized distribution function $F_*(u) \equiv v_{te} F_e(v) / N_{e0}$ can be written as

$$F_*(u) = \frac{1}{\sqrt{2\pi}} \frac{n_{e0}}{(3\alpha + 1)} (1 + \alpha u^4) \exp\left(-\frac{u^2}{2}\right). \quad (6.2)$$

Using the transformation $u^2 \rightarrow u^2 - 2\phi$, where ϕ is the normalized electrostatic potential (with respect to $K_B T_e / e$), the normalized electron density can be obtained as [Cairns *et al.*, 1995]

$$n_e(\phi) = n_{e0}(1 - \beta\phi + \beta\phi^2)\exp(\phi), \quad (6.3)$$

where we have used the standard notation for this distribution. Note that with the choice of normalization we have $n_{e0} = 1$. Also, if we normalize the velocities in (6.1) with respect to $C_s = (K_B T_e / m_i)^{1/2}$, the ion-acoustic speed (in the absence of positrons), instead of v_{te} , we arrive at the same expression for the normalized electron density as that in Eq. (6.3). The parameter¹ β is defined by $\beta = 4\alpha / (1 + 3\alpha)$: $\beta = 0$ (or $\alpha = 0$) leads to the Boltzmann-Maxwellian density $n_e(\phi) = n_{e0} \exp(\phi)$. Allowing α to run from 0 to ∞ , one sees that β is restricted to $0 \leq \beta \leq 4/3$.

For different values of β , the normalized Cairns distribution, as a function of normalized velocity, is shown in Fig. 1.2. The figure shows that for $\beta \geq 0.5$ (or $\alpha \geq 0.2$) the distribution

¹This parameter β should not be confused with the temperature ratio $\beta = T_c / T_h$ used in Chapters 4 and 5

function develops wings at high velocities, becoming multi-peaked. For such high values of β , the Cairns distribution function may not be good for physical applications, as it may be unstable. In particular, Verheest and Pillay [2008a] put the limit on β (above which the Cairns distribution ceases to be monotonically decreasing) at $\beta = 4/7 \simeq 0.571$, which corresponds to $\alpha = 1/4$. In other words, the Cairns distribution is appropriate only for a narrow range of the parameter α deviating from the Maxwellian distribution function [Verheest and Pillay, 2008a; Verheest, 2010a].

6.2 Plasma Model and Basic Equations

The plasma model consists of cool nonthermal electrons (temperature T_e and density n_e , given in (6.3)), Boltzmann distributed positrons (temperature T_p and density n_p), and cold inertial ions (density n_i).

The densities of the positrons and ions are given by

$$n_p(\phi) = n_{p0} \exp(-\sigma \phi); \quad \sigma = T_e/T_p, \quad (6.4)$$

and

$$n_i(\phi) = n_{i0} \left(1 - \frac{2\phi}{M^2} \right)^{-1/2}, \quad (6.5)$$

respectively, where we have used the transformation $\xi = x - Mt$ to a moving frame with velocity M , the latter being normalized with respect to C_s . That is, normalization is with respect to the ion sound speed, C_s , the reciprocal of the ion plasma frequency, $\omega_{pi}^{-1} = (\varepsilon_0 m_i / N_{i0} e^2)^{1/2}$, and a mixed Debye length $\lambda_{Deff} = (\varepsilon_0 K_B T_e / e^2 N_{i0})^{1/2}$; the densities N_j to N_{e0} , and electric potential ϕ to $K_B T_e / e$. Recall also that the equilibrium densities n_{j0} are normalized quantities with respect to N_{e0} , that is, $n_{p0} = N_{p0} / N_{e0}$ and $n_{i0} = N_{i0} / N_{e0}$. In obtaining Eq. (6.5) we have used the boundary conditions ϕ and $u \rightarrow 0$, and $n_i \rightarrow n_{i0}$ as $\xi \rightarrow \pm\infty$.

We point out that the normalized ion density can take several forms depending on the choice of normalization used, provided consistency is maintained. For example, if normalization is with respect to the electron parameters, that is, the equilibrium electron density N_{e0} , the electron thermal velocity, v_{te} , the electron Debye length $\lambda_{De} = (\varepsilon_0 K_B T_e / e^2 N_{e0})^{1/2}$

and the reciprocal of the electron plasma frequency, $\omega_{pe}^{-1} = (\varepsilon_0 m_e / N_{e0} e^2)^{1/2}$, we obtain

$$n_i(\phi) = n_{i0} \left(1 - \frac{2\phi}{\sqrt{\mu} M^2} \right)^{-1/2}, \quad (6.6)$$

where $\mu = m_i/m_e$ is the ion to electron mass ratio, and M is now normalized with respect to v_{te} . Comparing equations (6.5) and (6.6), we see that normalizing with respect to the electron parameters (v_{te} , ω_{pi}^{-1} and λ_{De}), implies that allowed Mach numbers corresponding to solitary waves will be $(m_i/m_e)^{1/4}$ times the Mach numbers associated with the normalization in (6.5).

The species' densities in Eqs. (6.3), (6.4) and (6.5) are coupled with the help of Poisson's equation [Popel *et al.*, 1995]

$$\frac{d^2\phi}{d\xi^2} = n_e(\phi) - n_i(\phi) - n_p(\phi) = 0. \quad (6.7)$$

6.3 Linear Dispersion Relation

Ion-acoustic waves have characteristic velocities $(K_B T_i / m_i)^{1/2} \ll \omega/k \ll (K_B T_e / m_e)^{1/2}$. In a two-component (e-i) plasma the dispersion relation takes the form

$$\frac{\omega'^2}{k'^2} = \frac{C_s^2}{1 + k^2 \lambda_{De}^2}, \quad (6.8)$$

where $C_s = (K_B T_e / m_i)^{1/2}$ and $\lambda_{De} = (\varepsilon_0 K_B T_e / n_{e0} e^2)^{1/2}$. Note that in the above expression, k' and ω' are unnormalized wavenumber and frequency. It follows that one requires $T_i \ll T_e$, otherwise if $T_i \approx T_e$, then the ion thermal velocity will be comparable to the ion-acoustic wave phase velocity, which will lead to strong Landau damping.

In the presence of positrons (e-p-i plasma), the normalized and linearized species densities become

$$\begin{aligned} n_{e1} &\approx n_{e0}(1 - \beta)\phi_1; \\ n_{p1} &\approx -n_{p0}\sigma\phi_1 \quad \text{and} \\ n_{i1} &\approx n_{i0}(\omega^2/k^2)\phi_1, \end{aligned} \quad (6.9)$$

respectively, where n_{j1} ($j = e, p, i$) and ϕ_1 are the perturbed density and electrostatic potential, and now k and ω are normalized quantities. In addition, Poissons's equation becomes

$$k^2 \phi_1 = (n_{i1} - n_{e1} + n_{p1})/n_{i0}. \quad (6.10)$$

Substituting the densities from Eq. (6.9) into Eq. (6.10) we get

$$k^2/\omega^2 = [n_{i0}k^2 + (1 - \beta)n_{e0} + \sigma n_{p0}]/n_{i0}. \quad (6.11)$$

With $n_{e0} = 1$, $n_{p0} = p$ and $n_{i0} = 1 - p$, the dispersion relation in this case then becomes

$$\frac{\omega^2}{k^2} = \left\{ k^2 + \frac{\sigma p + (1 - \beta)}{1 - p} \right\}^{-1} \quad (6.12)$$

$$\equiv \frac{1}{(k^2 + 1/M_s^2)}, \quad (6.13)$$

where, as we will see in the subsequent section [see Eq. (6.16), for example], $M_s = \sqrt{(1 - p)/(1 - \beta + p\sigma)}$ is the critical (minimum) speed of the solitary structures in the moving frame. It follows from Eq. (6.13) that in the limit $k \rightarrow 0$, $\omega/k \rightarrow M_s$, that is, M_s is equivalent to the phase velocity of the propagating solitary structures in the long wavelength regime ($k \rightarrow 0$).

From the definition of M_s we see that when $p = 0$ (no positrons), and $\beta = 0$ (Maxwellian electrons), the dispersion relation (6.13) becomes $\omega^2 = k^2/(1 + k^2)$, which in unnormalized form is simply Eq. (6.8), for an electron-ion plasma.

6.4 Arbitrary Amplitude Solitary Waves

With the help of Eqs. (6.3), (6.4) and (6.5) we can integrate Eq. (6.7), leading to the energy integral relation

$$\frac{1}{2} \left(\frac{d\phi}{d\xi} \right)^2 + \Psi(\phi, M) = 0, \quad (6.14)$$

where the Sagdeev potential $\Psi(\phi, M)$ is defined by [Pakzad, 2009]

$$\begin{aligned} \Psi(\phi, M) = & (1 + 3\beta) - [1 + \beta(3 - 3\phi + \phi^2)] \exp(\phi) + \frac{p}{\sigma} [1 - \exp(-\phi \sigma)] \\ & + (1 - p)M^2[1 - (1 - 2\phi/M^2)^{1/2}], \end{aligned} \quad (6.15)$$

with the shorthand $p = n_{p0} = N_{p0}/N_{e0}$ being the normalized equilibrium positron density [Pakzad, 2009], and the charge neutrality condition (in the form) $n_{e0} = n_{p0} + n_{i0}$ (with $n_{e0} = 1$) has been used. For Maxwellian electrons ($\beta = 0$ or $\alpha = 0$), Eq. (6.15) reduces to Eq. (10) of Popel *et al.* [1995].

As a necessary (but not sufficient) condition for the existence of solitons (or double layers), we require that $\Psi''(0, M) < 0$ must hold. This condition leads to the soliton requirement [Pakzad, 2009]

$$M > M_s = \frac{\sqrt{(1-p)}}{\sqrt{1-\beta+p\sigma}}, \quad (6.16)$$

where M_s is the critical Mach number, equivalent to the acoustic phase velocity of the wave, obtained from $\Psi''(0, M_s) = 0$. Similarly, in the case of Maxwellian electrons (with $\beta = 0$), Eq. (6.16) is the same as Eq. (12) of Popel *et al.* [1995]. We can easily confirm that Popel's result (M_s decreases with increasing p) for $\beta = 0$ applies for all values of β . We note also that the value $p = 0$ implies an electron-ion plasma; $M_s \rightarrow (1-\beta)^{-1/2}$, increasing as β increases, with a minimum value $M_s = 1$, as expected for a Maxwellian distribution. On the other hand, for $p = 1$ we have a pure electron-positron plasma, ion-acoustic waves cannot be supported, and $M_s \rightarrow 0$.

If, instead of using Eq. (6.5) for the normalized ion density, we use the alternative normalization, (6.6), in Poisson's equation, the Sagdeev potential becomes

$$\begin{aligned} \Psi(\phi, M) = & \{ (1 + 3\beta) - [1 + \beta(3 - 3\phi + \phi^2)] \exp(\phi) \} + \frac{p}{\sigma} [1 - \exp(-\phi\sigma)] \\ & + \frac{(1-p)}{\sqrt{\mu}} M^2 [1 - (1 - 2\sqrt{\mu}\phi/M^2)^{1/2}]. \end{aligned} \quad (6.17)$$

Therefore in this case, the lower Mach number limit for the existence domain of solitons or double layers becomes [Pakzad, 2009]

$$M > M_s^* = \frac{\mu^{1/4} \sqrt{(1-p)}}{\sqrt{1-\beta+p\sigma}}, \quad (6.18)$$

where the factor $\sqrt{\mu}$ in (6.16) is a result of the different normalization used here. In particular, with the transformation $M^2 \rightarrow (\mu)^{1/2} M^2$, we get Eq. (6.16).

The lower bounding curves for solitons in Figs. 6.1 and 6.2 were obtained analytically using Eq. (6.16). However, the upper bounding curves were obtained numerically by sub-

stituting the upper soliton potential limit $\phi_{li} = M^2/2$ in Eq. (6.15), and solving for $M(p)$ for given values of β .

6.4.1 Numerical Results and Discussion

With the help of the Sagdeev potential in Eq. (6.15) we are in a position to delineate existence domains of solitons supported by the plasma model. First, the positron and electron densities are well behaved for all ϕ . However, it is easy to see from the ion density relation in Eq. (6.5) that the ions are infinitely compressed ($n_i \rightarrow \infty$) when $\phi \rightarrow \phi_{li} = M^2/2 > 0$. Since $\phi_{li} > 0$ for all $M > 0$, it implies that the existence of positive potential solitons require $S(\phi_{li}, M) > 0$ with the upper limit on M obtained at $\Psi(\phi_{li}, M) = 0$. Negative solitons, if they exist, could be limited by double layers, for which we require the relation $\Psi(\phi_{dl}, M_{dl}) = \Psi'(\phi_{dl}, M_{dl}) = 0$, where M_{dl} and ϕ_{dl} are the Mach number and potential amplitude corresponding to the negative double layer, respectively.

Assuming equal positron and electron temperatures ($\sigma = 1$), Pakzad [2009] showed typical Sagdeev potential plots in his Figs. 1 and 2 for $p = 0.01$ and different values of β but for the same Mach number. Thus, Pakzad [2009] showed that the soliton amplitude decreases with increasing β . However, his results for $\beta = 0.6$ (and $M = 1.45$) can not lead to a soliton solution, as that Mach number falls below $M_s \simeq 1.554$. Closer examination of the Sagdeev potential would have revealed that very close to the origin there is a hump, with $\Psi(\phi) > 0$, before it drops below zero, forming a well. As a result of the small positive hump, the pseudo particle would never be able to reach the well, and no soliton exists. In addition, as we have already pointed out, for $\beta > 4/7 \approx 0.571$, the Cairns distribution is no longer appropriate as a steady-state distribution [Verheest and Pillay, 2008a; Verheest, 2010a].

In Fig. 6.1 (left panel) we show a plot of the Mach number M versus p for a plasma with positrons having the same temperature as the electrons, and $\beta = 0.5$. The graph shows that positive potential solitons exist for the full range of p , bounded by the continuous and dotted green curves. These positive solitons are limited by infinite compression of the ion density ($n_i \rightarrow \infty$), that is, positive solitons have amplitudes less than $\phi_{li} = M^2/2$. In addition, we also observe negative solitons limited by double layers for a narrow range in p ($p \lesssim 0.05$), bounded by the dashed red curve. Thus these negative solitons and double

layers occur only in a plasma which is essentially an electron-ion plasma with positron impurity. In the allowable range of β ($\beta < 4/7$), as we shall see below, we have only found these negative solitary waves in a narrow range of β and p . These were not reported by Pakzad [2009].

In the right panel of Fig. 6.1 we show only positive potential solitons for different values of β : dotted ($\beta = 0.5$), dashed ($\beta = 0.3$) and continuous ($\beta = 0.1$), respectively. The graphs show that the variation of β has only a quantitative effect on the existence domain of positive solitons, with the domain becoming a little narrower as β increases. In addition, for fixed p in the range $0 < p < 1$, both the lower and upper Mach number limits for the existence domain increases as β increases; thus the normalized solitary wave speed values also increase. We see that for $p = 0$ (a pure electron-ion plasma) and $\beta = 0.1$, the range of M lies between 1.054 and 1.591, which is consistent with the standard range of $[1, 1.5852]$ that is well-known for the case of a plasma with Boltzmann electrons ($\beta = 0$) and fluid ions [Infeld and Rowlands, 2000].

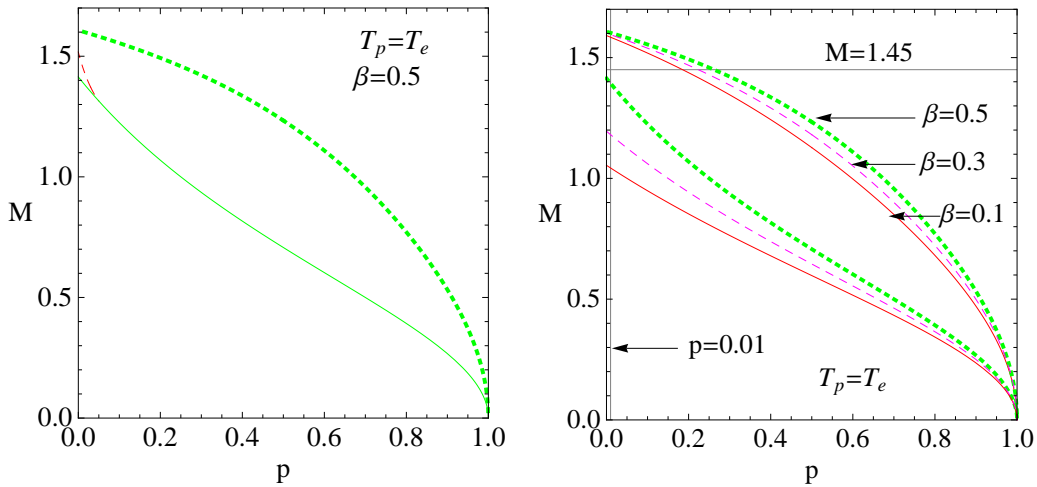


Figure 6.1: *Left panel:* Existence domain of solitons or double layers corresponding to a plasma with equal positron and electron temperatures ($\sigma = 1$) and $\beta = 0.5$. Positive solitons are bounded by the green (solid and dotted) curves; Negative solitons (limited by double layers) are bounded by the red dashed curve, occurring for low $p = N_{p0}/N_{e0}$ values. *Right panel:* Existence domain for positive potential solitons for different β values: dotted ($\beta = 0.5$), dashed ($\beta = 0.3$) and continuous ($\beta = 0.1$), respectively.

In Fig. 6.2 we show the existence domain of positive solitons, in the $[M - \beta]$ plane, for different values of p . For each value of p , the lower curves correspond to M_s (obtained using Eq. (6.16)) while the upper curves correspond to the upper M limit, obtained numerically

by solving the expression $S(\phi_{li}, M) = 0$. For the values of p used here ($p = 0.1, 0.01$, and 0.001) we confirm the results of Pakzad [2009] in his Fig. 4. In particular, our results show that positive potential solitons exist for, say, $\beta < 0.734$ ($p = 0.1$), $\beta < 0.626$ ($p = 0.01$) and $\beta < 0.616$ ($p = 0.001$), respectively, which agree with those of Pakzad [2009] in his Fig. 5. While these results show critical upper limits in β for the existence of positive potential solitons, they all correspond to $\beta > 4/7$, and hence, as we have seen earlier, are physically inappropriate. Thus the existence domains are more correctly cut off at $\beta = 0.57$ as shown in the figure.

We note that the calculations in Figs. 6.1 and 6.2 have been only for $T_e = T_p$. It is physically reasonable to assume this as a first approximation because of rapid thermalization of the leptons. We shall consider some aspects of $T_e \neq T_p$ below.

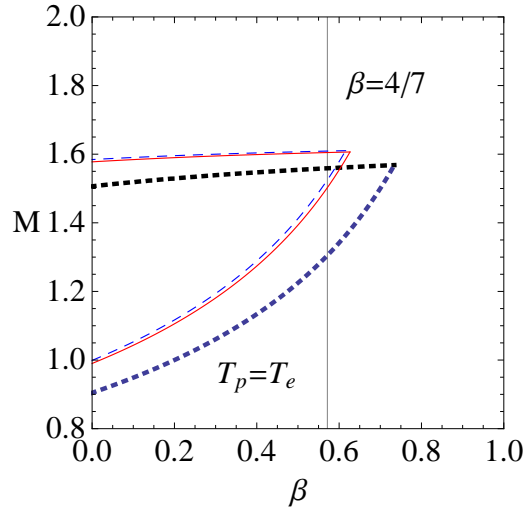


Figure 6.2: Existence domain of positive potential solitons, in the $(M - \beta)$ plane, for different values of p ; $p = 0.1$ (dotted), $p = 0.01$ (solid), and $p = 0.001$ (dashed). Solitons exist for $\beta < 0.734$ ($p = 0.1$), $\beta < 0.626$ ($p = 0.01$) and $\beta < 0.616$ ($p = 0.001$).

6.4.2 Critical Composition

In recent studies on solitary waves discussed in Chapters 4 and 5 [Baluku *et al.*, 2010a,b], and in [Verheest *et al.*, 2010], as well as in [Verheest and Hellberg, 2010], it has been found that the sign of $\Psi'''(\phi = 0, M_s)$ for a particular plasma configuration can aid in understanding the sign of the solitons, and whether “coexistence of solitons” is supported by the plasma model. In addition, if $\Psi(\phi, M_s)$ has a finite amplitude soliton, then for the same plasma parameters, Sagdeev potentials corresponding to $M > M_s$ will result in

solitons of both polarity.

From Eq. (6.15) the third derivative of the Sagdeev potential $\Psi(\phi, M)$ evaluated at $\phi = 0$ and $M = M_s$ is given by

$$\Psi'''(0, M_s) = p \sigma^2 - 1 + \frac{3(1 - \beta + p \sigma)^2}{1 - p}. \quad (6.19)$$

In the limit $p \rightarrow 0$, $\Psi'''(0, M_s) = 3\beta^2 - 6\beta + 2$, which gives the critical values of β as $\beta_{c1} = (3 - \sqrt{3})/3 \simeq 0.423$ and $\beta_{c2} = (3 + \sqrt{3})/3 \simeq 1.577$. However, from the definition of β , *i.e.*, $\beta = 4\alpha/(1 + 3\alpha)$, the maximum allowable value of β is $\beta = 4/3 \simeq 1.333$. The latter value (β_{c2}) is inappropriate as it exceeds this allowed upper limit. We note that $p \rightarrow 0$ yields an e-i plasma and thus β could then play the role of the critical parameter f which we encountered in previous chapters.

Figure 6.3 (upper panel) shows a plot of p versus β satisfying $\Psi'''(0, M_s) = 0$, for different values of $\sigma < 1$ ($T_e < T_p$). The lower panel shows a small range of the figure in the upper panel. For $0 < \sigma < 1$, $\Psi'''(0, M_s)$ is negative (positive) below (above) the curve corresponding to a particular value of σ . Note that for $\beta < \beta_{c1}$ we have $\Psi'''(0, M_s) > 0$ for all values of $p > 0$, implying that “KdV-like” solitons² (whose amplitudes vanish at M_s) supported for such values of β will have positive polarity; and if negative solitons exist for some values of p , they will be nonKdV-like with nonzero amplitudes at M_s [Baluku *et al.*, 2010a,b; Verheest, 2010a; Verheest *et al.*, 2010]. Figure 6.3 (upper panel) thus shows that for the physically appropriate β range ($\beta < 4/7$), negative potential “KdV-like” solitons (or double layers) exist only for very low values of p (less than about 0.2 for $\sigma \geq 0.5$). For fixed β , the range of p having negative solitary waves, decreases as σ increases and becomes negligible for T_e significantly greater than T_p .

On the other hand, for a particular value of p , negative solitary structures occur for the range $\beta_1 < \beta < 4/3$, where β_1 , which may be less than or greater than β_{c1} depending on the value of p , is the lower β cutoff at which the Mach number (M_{dl}) corresponding to a negative double layer equals M_s . In the case of $\beta_1 < \beta_{c1}$, the occurrence of these negative solitons or double layers would require a very small proportion of positrons (p values very close to 0), and are nonKdV-like.

²“KdV-like” solitons have amplitudes that go to zero as M goes to M_s while “nonKdV-like” solitons have finite nonzero amplitudes at M_s .

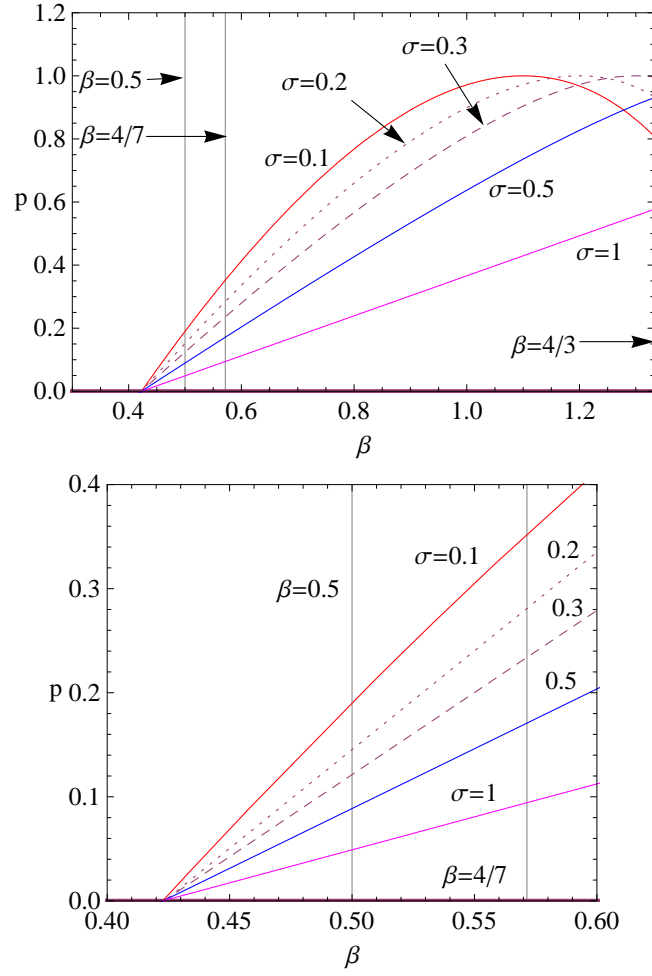


Figure 6.3: *Upper panel:* Curves for $\Psi'''(\phi = 0, M = M_s) = 0$ giving $p = p_c$ for different values of $\sigma = T_p/T_e$. Under the curves, $\Psi'''(\phi = 0, M = M_s) < 0$ and outside the curves $\Psi'''(\phi = 0, M = M_s) > 0$. The sign of $\Psi(\phi = 0, M = M_s)$ corresponds to the sign of the “KdV-like” solitons. *Lower panel:* Similar to the upper panel, here showing a small range of p and β .

Evaluating $\Psi'''(0, M_s) = 0$ from Eq. (6.19), for $\beta = 0.5$ and $\sigma = 1$, one finds a critical value of p , *i.e.*, $p_c \simeq 0.04904$. Typical examples of the Sagdeev potential curves are shown in Fig. 6.4 for $p = 0.03 < p_c$ (upper panel) and $p = 0.0494 > p_c$ (lower panel). For $p = 0.03$ we have $\Psi''(\phi = 0, M) = 0$, $\Psi'''(\phi = 0, M) < 0$, and obtain a positive soliton at M_s with finite amplitude $\phi \simeq 0.5$ (upper left panel). With a small increment in M of about 0.015 we also find a negative soliton of amplitude $|\phi| \approx 0.35$ (upper right panel), while the positive soliton has increased to $\phi \sim 0.6$. Thus this is a region where the two soliton polarities may coexist. In addition, if we increase M to $M = M_s + 0.019 = 1.372$, a negative potential double layer, of amplitude $|\phi| \sim 0.573$ can be obtained (not shown). Choosing a value

of $p > p_c$ (we consider $p = 0.0494$ in the lower panel), we show a finite negative soliton ($|\phi| \simeq 0.058$, lower left panel) obtained at M_s , with $\Psi''(\phi, M) = 0$, $\Psi'''(\phi = 0, M) > 0$, but there is no positive soliton. Finally, at $M \simeq M_s + 0.000018$ (lower right panel) we get a negative double layer ($|\phi| \sim 0.11$) and a positive soliton ($\phi \sim 0.016$), again demonstrating coexistence. The examples in Fig. 6.4 show that the existence of a finite positive (or negative) roots of $S(\phi, M)$ implies that neighbouring Sagdeev potentials have solitons of both polarities [Verheest *et al.*, 2010].

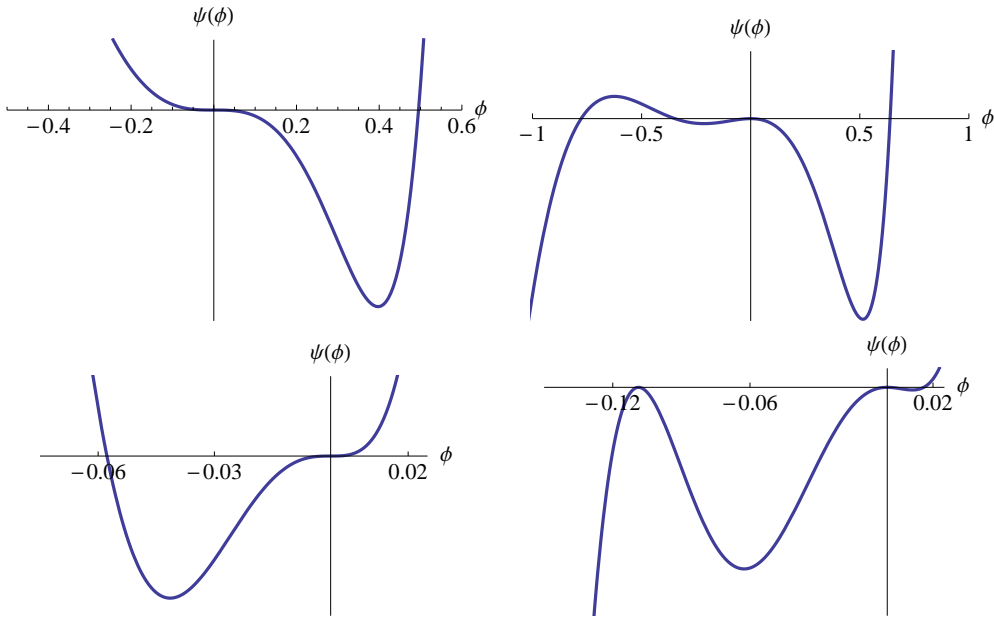


Figure 6.4: Typical Sagdeev potential curves for $\sigma = 1$, $\beta = 0.5$, and $p = 0.03 < p_c = 0.04904$ (*upper panel*) and $p = 0.0494 > p_c$ (*lower panel*). The left panel curves show Sagdeev potential curves at $M = M_s$ while the right panel curves are for $M_s + 0.015$ (upper right panel) with two solitons (one large and the other very small), and for $M = M_s + 0.000018$ (lower right panel) showing a negative double layer and a positive soliton.

6.5 Summary and Remarks

We have studied ion-acoustic solitary waves in an e-p-i plasma using the Sagdeev potential approach. This work is an extension of Pakzad [2009]. As shown in Fig. 1.2, the nonthermal particle distribution is multi-humped for values of $\beta > 4/7$, and therefore is then inappropriate to use as a stable non-Maxwellian distribution. Possibly another form of nonthermal distribution, such as a kappa distribution, may be used instead.

We have found (Fig. 6.2) that in addition to positive potential ion-acoustic solitons which are supported over the full range of fractional positron density, negative potential

solitons can be supported over a very limited range of low positron density ($p \lesssim 0.05$), and are limited by double layers. These negative solitary waves were not reported by Pakzad [2009].

In addition, our results show that in the region where both positive and negative potential solitons may be supported by the same plasma configuration, finite solitary structures can be obtained at the critical (minimum) Mach number, *i.e.*, at the true ion-acoustic speed of the plasma mix.

For some plasma configuration, with a specific value of β , there exists a critical value of the fractional positron density, p (denoted p_c) at which $\Psi'''(\phi, M) = 0$ for $\phi = 0$ and $M = M_s$. For example, with $\sigma = 1$, we find $p_c \simeq 0.01734$ ($\beta = 0.45$) and $p_c \simeq 0.04904$ ($\beta = 0.5$).

If p_c lies in the region where solitons of both polarity occur for the same plasma parameters, then for $p < p_c$ one gets negative “KdV-like” solitons and finite amplitude positive potential “nonKdV-like” solitons. Similarly, for $p > p_c$ one obtains positive “KdV-like” solitons that are of small amplitude and finite amplitude negative potential “nonKdV-like” solitons

Lastly, for a particular value of p , the lower value of β supporting negative potential solitons or double layers corresponds to the double layer Mach number M_{dl} being equal to M_s .

Ion-Acoustic Solitary Waves in a Plasma With Two-Temperature Electrons

In this chapter we use fluid equations to study ion-acoustic solitons in two temperature electron plasmas consisting of cold inertial ions, and cool and hot Boltzmann electrons. Though such a plasma model has been studied in the past by a number of authors, our further investigations have revealed new results that are presented in this work.

The results presented in this Chapter have been published as Baluku et al., Europhysics Letters 91, 15001 (2010)

7.1 Introduction

Using a plasma with a single electron component, Washimi and Taniuti [1966] discussed the one-dimensional long-time asymptotic behaviour of ion-acoustic waves of small but finite amplitudes using the Korteweg-de Vries (KdV) equation. They showed that the width of the solitary wave becomes larger for small amplitude, implying that steepening of the wave due to the weak nonlinearity is balanced by the dispersion in long wavelength for the weak solitary wave to be formed. Ion-acoustic solitary waves in a two-temperature plasma have been studied by a number of authors in the past [Buti, 1980; Nishihara and Tajiri, 1981; Baboolal *et al.*, 1990; Ghosh *et al.*, 1996]. Nishihara and Tajiri [1981] then considered a two-electron temperature plasma with both hot and cool electron components using fluid equations. Here, they showed that there are two regions of wave propagation

in the plasma model: the normal propagation and the anomalous propagation, where the anomalous propagation property is characterized by the steepening of the wave so as to decrease the density. Nishihara and Tajiri [1981] also showed that for a certain parameter region, finite amplitude rarefactive and compressive ion-acoustic solitons can both be supported (loosely, “coexist”) in the plasma, with the small amplitude rarefactive (or compressive) solitons existing only in the plasma configuration having anomalous (or normal) propagation properties. As will be seen in Sec. 7.3, in the terminology of the Sagdeev potential [Sagdeev, 1966], the two regions are separated by a curved surface obtained for parameters at which both the second and third derivatives of the Sagdeev potential vanish at the origin.

As the terminology “compressive” and “rarefactive” is not well-defined in a multi-fluid plasma, we point out that in this model, rarefactive solitons have negative potential while compressive solitons have positive potential. In this work we show that in the region of “coexistence”, if the negative solitons have amplitudes that vanish at the acoustic speed, as for Korteweg-de Vries (KdV) solitons [Swanson, 2003], then the positive solitons have finite amplitude at the acoustic speed, which cannot be obtained from the KdV description.

In plasma models where large amplitude solitons can exist, the reductive perturbation analysis, which leads to a KdV equation and weakly nonlinear solitons, is not appropriate. The Sagdeev approach [Sagdeev, 1966] is a useful tool in seeking solutions of arbitrary amplitude nonlinear solitary wave structures, far beyond the KdV results.

Using the Sagdeev approach, Baboolal *et al.* [1990] investigated the cutoff conditions for the existence of large amplitude ion-acoustic solitons and double layers in fluid plasmas consisting, *e.g.*, of two Boltzmann electron species (hot and cool) and a single cold ion species. They found that below a temperature threshold, both positive and negative potential solitons existed for an intermediate range of cool electron density ratio, with the negative solitons limited by double layers. Elsewhere, only positive potential solitons occurred. In addition, in the “coexistence” region, finite (nonzero) amplitude positive potential solitons were obtained at the critical Mach number M_s , equivalent to the acoustic speed, but they did not comment on them.

In this work we investigate these finite amplitude results at M_s in detail, and also report that positive double layers can also be supported by the plasma model for a restricted range

of cool electron densities. For a range of cool electron densities where these positive double layers can exist, we also obtain solitons having Mach numbers exceeding those supporting double layers, *i.e.*, the Mach numbers corresponding to double layers don't act as an upper Mach number limit, as expected.

7.2 Plasma Model and Basic Equations

We consider a plasma model consisting of two Boltzmann electron components, one hot (temperature T_h , density n_h) and the other cool (temperature T_c , density n_c), and cold inertial fluid ions that are singly charged. Such a model has been discussed by a number of authors [Buti, 1980; Nishihara and Tajiri, 1981; Baboolal *et al.*, 1990; Ghosh *et al.*, 1996], where Ghosh *et al.* [1996] used a plasma model with warm fluid ions instead.

The normalized densities of the cool and hot electrons are, respectively, given by

$$n_c(\phi) = f \exp(\alpha_c \phi) \quad \text{and} \quad (7.1)$$

$$n_h(\phi) = (1 - f) \exp(\alpha_h \phi), \quad (7.2)$$

where $f = N_{c0}/N_{i0}$ with $N_{i0} = N_{e0} = N_{c0} + N_{h0}$, N_{j0} ($j = c, h, i$) being the equilibrium densities; $1/\alpha_c = T_c/T_{\text{eff}}$ and $1/\alpha_h = T_h/T_{\text{eff}}$; and ϕ is the electrostatic potential, normalized to $K_B T_{\text{eff}}/e$. Here, K_B and e are the usual Boltzmann constant and electronic charge, respectively, while T_{eff} is an effective electron temperature defined by $T_{\text{eff}} = T_c/[f + (1-f)\tau]$, in terms of the temperature ratio $\tau = T_c/T_h$. Of course, n_h will play a role only when $\alpha_h \neq 0$, and hence $\tau \neq 0$.

The density of the cold ions is given by

$$n_i(\phi) = (1 - 2\phi/M^2)^{-1/2}, \quad (7.3)$$

where M is the Mach number, which gives the velocity of the solitary structures, normalized to the acoustic speed $C_s = (K_B T_{\text{eff}}/m_i)^{1/2}$, m_i being the mass of the ions.

In the Sagdeev approach [Sagdeev, 1966], the simple traveling waves satisfying Eq. (7.5) are solitary waves which are stationary in a frame moving with a velocity, M . Transforming to a moving frame with position $\xi = x - Mt$, the species' densities are coupled by Poisson's

equation to give

$$\frac{d^2\phi}{d\xi^2} + G(\phi) = 0, \quad (7.4)$$

where $G(\phi)$ is the sum of the species' densities.

After an integration, Eq. (7.4) can be expressed in the form of an energy integral [Sagdeev, 1966]

$$\frac{1}{2} \left(\frac{d\phi}{d\xi} \right)^2 + \Psi(\phi, M) = 0, \quad (7.5)$$

where $\Psi(\phi, M) = -\int_0^\phi G(\phi)d\phi$ is the pseudopotential or the Sagdeev potential of the plasma system.

In obtaining the expression for the Sagdeev potential $\Psi(\phi, M)$, following from Eq. (7.5), we ensure that $\Psi(\phi, M)$ and its derivative (with respect to the potential ϕ) vanish at the origin $\phi = 0$. The former, $\Psi(\phi, M) = 0$ for $\phi = 0$ ensures that the boundary conditions are satisfied in the integration while the latter (the vanishing of the derivative of the Sagdeev potential at the origin) ensures that the overall charge neutrality is zero in the absence of disturbances.

Thus the Sagdeev potential in Eq. (7.5) takes the form

$$\Psi(\phi, M) = \frac{f}{\alpha_c} [1 - \exp(\alpha_c \phi)] + \frac{(1-f)}{\alpha_h} [1 - \exp(\alpha_h \phi)] + M^2(1 - \sqrt{1 - 2\phi/M^2}). \quad (7.6)$$

As a prerequisite for the formation of solitary structures, the origin should be a local (unstable) maximum, which condition is usually interpreted as requiring that $\Psi''(0, M) < 0$ (where the prime denotes differentiation with ϕ). This condition leads to super-acoustic waves with $M > M_s = 1$, where M_s is the normalized acoustic linear phase velocity, obtained from $\Psi''(0, M_s) = 0$.

Though the general practice has been that the existence of solitons requires $M > M_s$, recent investigations [Baluku *et al.*, 2010a,b; Baluku and Hellberg, 2010; Verheest, 2010a; Verheest *et al.*, 2010] have shown that solitons can have finite amplitudes at M_s in the parameter regime where solitons of both polarity exist. In these cases $\Psi''(0, M) = 0$: the origin is a triple root such that the convexity condition is provided by the third derivative of $\Psi(\phi, M)$. With a triple root at the origin, in the presence of positive (negative) potential solitons, the origin is unstable (stable) for $\phi > 0$ ($\phi < 0$) but stable (unstable) for $\phi < 0$

($\phi > 0$).

In some instances the Mach number M may have an upper limit such that solitary structures will occur for a limited range in M , and in other instances, M is unbounded such that solitary structures can occur for all $M \geq M_s$; the equality sign only applies to particular plasma parameters in the region where both signs of potential can be supported. The constraints leading to the upper limit on M may be due to a number of factors such as, ensuring that the species densities remain real and nonzero, existence of sonic points, or by the occurrence of double layers if both solitary structures are supported by the plasma model in question.

For this model positive potential solitons are limited by infinite compression of the inertial ions, reached when $\phi \rightarrow \phi_{li} = M^2/2$, thus leading to a sufficient condition $\Psi(M^2/2, M) > 0$. However, depending on the value of the temperature ratio τ , positive potential double layers are also possible for a limited range in f . On the other hand, negative potential solitons are limited by double layers.

We shall now investigate the existence domain for the solitons and double layers that may be supported by this model.

From Eq. (7.6), the third derivative of $\Psi(\phi, M)$ at the origin ($\phi = 0$) for $M = M_s$, is given by

$$\Psi'''(0, M_s) = 3 - \frac{f}{(\tau(1-f) + f)^2} - \frac{(1-f)}{(1-f + f/\tau)^2}. \quad (7.7)$$

If $\Psi'''(0, M_s) = 0$, then for fixed τ , Eq. (7.7) gives the critical values of the cool electron density as

$$f_{c1,2} = \frac{(1-5\tau) \pm (1-10\tau + \tau^2)^{1/2}}{6(1-\tau)}, \quad (7.8)$$

provided $\tau \neq 1$. Here, f_{c1} and f_{c2} are the lower and upper values of the critical density given by the minus and plus signs in Eq. (7.8), respectively, and are real provided $\tau^2 - 10\tau + 1 \geq 0$, leading to a critical value of τ .

Thus, the existence of a finite, non complex critical density ratio $f = f_c$ requires $\tau \leq \tau_{c1}$, where $\tau_{c1} = (5 - 2\sqrt{6}) \simeq 0.10102$, that is, $T_h \geq (5 + 2\sqrt{6}) T_c \simeq 9.89898 T_c$, as was reported by Bezzerides *et al.* [1978] for rarefactive shocks in laser plasmas. At $\tau = \tau_{c1}$, the roots f_{c1} and f_{c2} in (7.8) coalesce into a single root $f_c \approx 0.092$. In addition, when $\tau \rightarrow 0$ we have $f_{c1} \rightarrow 0$ and $f_{c2} \rightarrow 1/3$. However, with the choice of normalization, when $\tau \rightarrow 0$,

$T_c/T_{\text{eff}} \rightarrow f$ and $T_h/T_{\text{eff}} \rightarrow \infty$. Such super hot conditions cannot be achieved in physical plasma situations, and, moreover, the model then breaks down.

The critical density f_c can also be obtained from the KdV description in the following way. Here we consider a normalized KdV equation of the form

$$\frac{d\phi}{d\zeta} + A\phi\frac{d\phi}{d\chi} + B\frac{d^3\phi}{d\chi^3} = 0, \quad (7.9)$$

where the second term describes the nonlinearity while the third term describes dispersion or dissipation. In obtaining Eq. (7.9) we have used the stretched coordinates $\chi = \epsilon^{1/2}(x - M_a t)$ and $\zeta = \epsilon^{3/2}t$, where M_a is the phase velocity normalized to C_s , and ϵ is a smallness parameter. The constants A and B in Eq. (7.9), involve the equilibrium density and temperature ratios, besides other parameters in the plasma model. In particular, it can easily be shown (see Chap. 5) that for this model

$$A = \frac{Q}{2}\alpha_{s1}^{1/2}(1 + 3\tau\alpha_{s1})^{-1/2}; \quad Q = 3 - \alpha_{s2}/\alpha_{s1}^2 \quad \text{and} \quad (7.10)$$

$$B = \alpha_{s1}^{-3/2}(1 + 3\tau\alpha_{s1})^{-1/2}, \quad (7.11)$$

where $\alpha_{s1} = \sum_s \tau_s N_{s0}/N_{e0}$; $\alpha_{s2} = \sum_s \tau_s^2 N_{s0}/N_{e0}$; $\tau_s = T_c/T_s$, with $s = c, h$ for the cool or hot electron constituent. Note that $\tau_c = 1$ and $\tau_h = T_c/T_h = \tau$.

Solutions to Eq. (7.9) are valid only for $A \neq 0$. However, when $A \rightarrow 0$, the balance between the nonlinearity and dispersion is not maintained for the solitary structures to propagate. The critical density f_c is then obtained by solving the equation $A = 0$ for f . For this particular model, it is clear from Eq. (7.10) that $A = 0$ when $Q = 0$. It also follows that $Q = \Psi'''(0, M_s)$ in Eq. (7.7), and hence the same critical f_c are found as those in Eq. (7.8) above. We point out that the expression Q reduces to Eq. (2.12) of Tajiri and Nishihara [1985]. Using an analogous three component plasm model with contaminating negative ions (instead of the cool electron component), Nakamura *et al.* [1985] experimentally observed a positive pulse, that propagated like a linear wave without change of its shape (except by damping), at the critical parameters for which the nonlinear coefficient A in the KdV equation vanished.

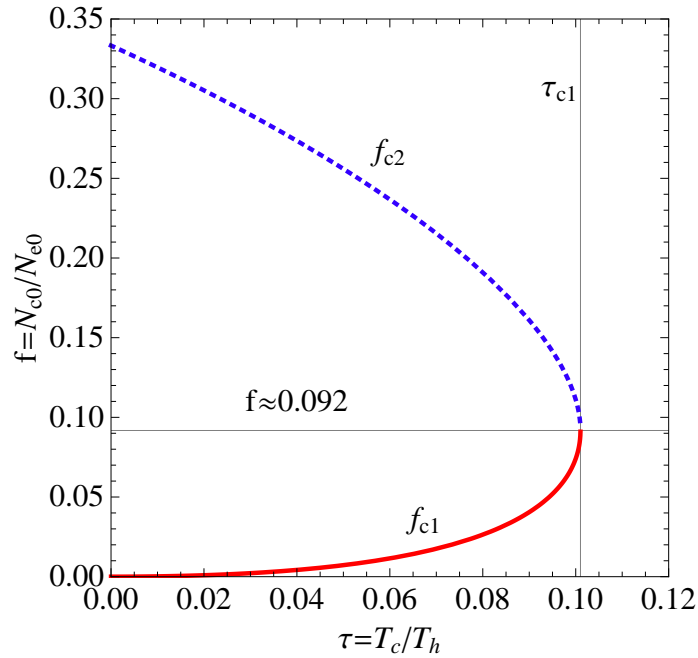


Figure 7.1: Variation of the critical density fraction, f_c , with τ . Along the curve, $\Psi'''(0, M_s) = 0$. Inside the curve, $\Psi'''(0, M_s) < 0$ while outside the curve, $\Psi'''(0, M_s) > 0$. Here, $f_{c1} = f_{c2}$ at the critical temperature ratio $\tau_{c1} = 5 - 2\sqrt{6}$.

7.3 Numerical Results and Discussion

In Fig. 7.1 we show the variation of f_c with temperature ratio τ , using Eq. (7.8). Along the curve we have $\Psi'''(0, M_s) = 0$; inside the curve $\Psi'''(0, M_s) < 0$, and outside the curve $\Psi'''(0, M_s) > 0$. Figure 7.1 is similar to Fig. 3, curve labeled B, of Nishihara and Tajiri [1981] (see also Tajiri and Nishihara [1985]) and Fig. 2 of Bezzerides *et al.* [1978], although in the latter, only one solution of f_c is shown. The region bounded by $\Psi'''(0, M_s) < 0$ is what is referred to as the region of anomalous propagation in Bezzerides *et al.* [1978] and Nishihara and Tajiri [1981], while the other region with $\Psi'''(0, M_s) > 0$ is the region of normal propagation.

7.3.1 $\tau > \tau_{c1} = 5 - 2\sqrt{6}$

To begin with, we consider a value of τ that is above $\tau_{c1} = 5 - 2\sqrt{6} \simeq 0.10102$, *i.e.*, where $\Psi(0, M_s) > 0$ for all f . Here an example is shown in Fig. 7.2, with $\tau = 1/5$. Only positive potential solitons limited by the ion density constraint ($\phi < \phi_{li} = M^2/2$) are supported by the model; The curve shows the Mach number ($M = M_{li}$) that gives the maximum amplitude limit due to the ion density constraint (ϕ_{li}) at which $\Psi(\phi_{li}, M) = 0$.

Positive potential double layers do not exist, and negative potential solitons or double layers are not supported. For these positive potential solitons, at $f = 0$ or $f = 1$, corresponding to a simple plasma with isothermal (Boltzmann) electrons and cold fluid ions, we recover the usual range [Infeld and Rowlands, 2000, p. 125] $1 < M < 1.5852$. The nature of these positive solitons, having the sign of $\Psi'''(0, M_s)$, is that their amplitudes tend to zero as M approaches M_s . Basically for $\tau \geq \tau_{c1}$ only positive potential solitons exist, as reported, for example, by Baboolal *et al.* [1990].

Figure 7.2 also shows that the maximum Mach number associated with positive solitons first decrease as f increases from $f = 0$, up to an intermediate value of f corresponding to the dip in the curve, beyond which the maximum Mach number increases with f up to $f = 1$. We have carried out some calculations and found that as τ decreases, the dip on the curve occurs for lower M values, and reaches $M_s = 1$ at critical τ value $\tau_{c2} \approx 0.075$, for $f \approx 0.0212$. Therefore, for $\tau < \tau_{c2}$, there is a range in f where any possible positive solitons that may exist, cannot be limited by the ion density constraint. If they are nevertheless to exist there, they must be limited by positive potential double layers. This point will be illustrated by some examples below.

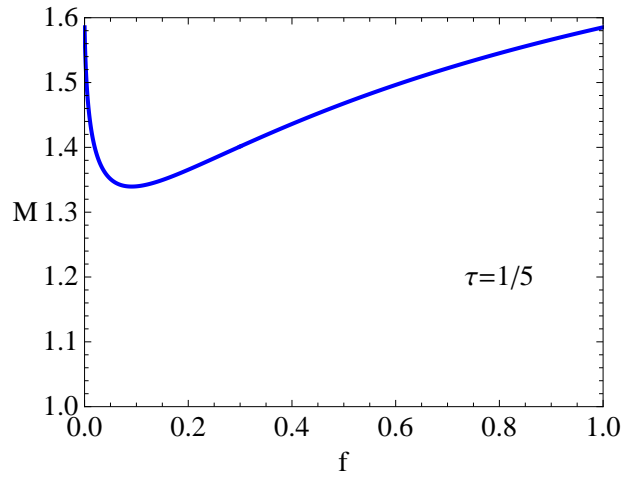


Figure 7.2: Existence domain of ion-acoustic solitons for $\tau = 1/5 > \tau_{c1}$. Positive potential solitons exist for the entire range of f from 0 to 1, and are bounded by the dashed blue curve.

7.3.2 $\tau_{c2} \simeq 0.075 < \tau < \tau_{c1}$

For the next example we consider a value of τ in the range $\tau_{c2} < \tau < \tau_{c1}$. In this range, $\Psi'''(0, M_s) < 0$ for some f , but ion density-limited positive solitons do still occur

for all $0 \leq f \leq 1$. For this purpose we first choose $\tau = 0.09$ for discussion. In Fig. 7.3 we present the existence domain (left panel) and soliton potentials at $M = M_s$ (right panel) for $\tau = 0.09$. The continuous (blue) curve is the upper limit for positive solitons. The dashed (blue) curve represents positive double layers for $f < f_{c1}$, while the dotted (red) curve shows negative double layers (for $f_{c1} < f < f_n$), that limit negative solitons. We note that f_{c1} is the boundary between the two double layer polarities, and here it is also the lower limit for the existence of negative solitons. For $f > f_n$, only positive solitons are supported. Thus, we see in Fig. 7.3 (left panel) that positive and negative solitons are both supported (“coexist”) over the range $f_{c1} < f < f_n$. This region, bounding negative potential double layers, is analogous to that corresponding to rarefactive shocks in Fig. 3 of Bezzerides *et al.* [1978]. We also observe from Fig. 7.3 (left panel) that the other value of f_c ($f_{c2} \simeq 0.161$) lies in the “coexistence” region. In addition, there is a surprising set of solitons (limited by the ions, bounded by the continuous blue curve in Fig. 7.3, left panel) that occur beyond the positive potential double layers [Baluku and Hellberg, 2010], *i.e.*, at values $M > M_{dl}$, where M_{dl} is the Mach number of the positive double layer. These

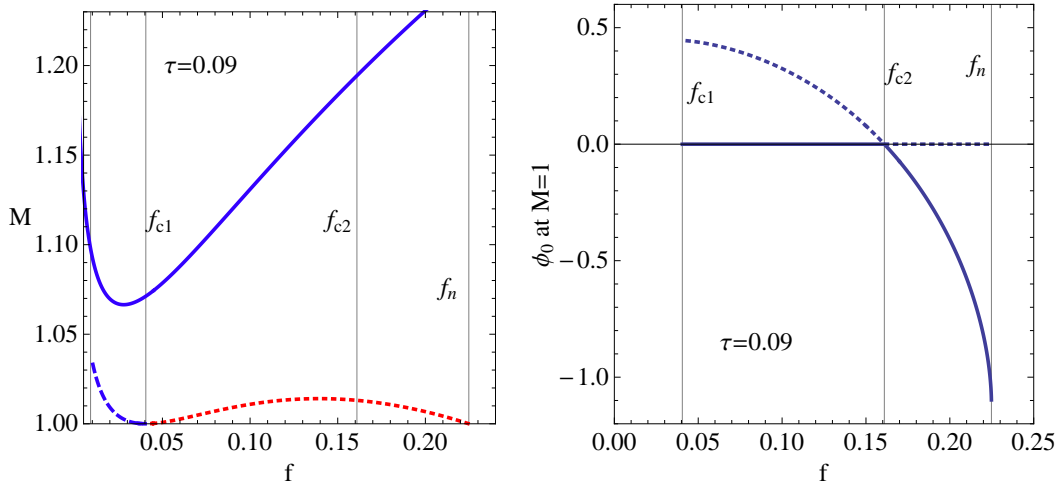


Figure 7.3: *Left panel:* Existence domain of ion-acoustic solitons for $\tau = 0.09$. *Right panel:* Typical soliton potential amplitude at the lowest Mach number $M = 1$ covering the range of f for “co-existence” of solitons of both polarities, shown in the left panel graph. Here $f_{c1} \simeq 0.041$, $f_{c2} \simeq 0.161$ and $f_n \simeq 0.225$.

positive double layers were not reported by the authors that have looked at this plasma model [Buti, 1980; Nishihara and Tajiri, 1981; Baboolal *et al.*, 1990]. However, using a fluid-dynamical approach, Verheest *et al.* [2006] showed that positive double layers that are

very weakly super-ion-acoustic, could be supported at small values of f in a two-electron temperature plasma with isothermal electron components. Note that at $f = 0$, other than at the origin ($\phi = 0$), the double layer requirements $\Psi(\phi, M) = 0$ and $\Psi'(\phi, M) = 0$ are not satisfied.

In the right panel of Fig. 7.3 we show the variation of soliton amplitude ϕ_0 (at $M = M_s$) with cool electron density f , over the interval $[f_{c1}, f_n]$. The continuous curve represents negative solitons, the dotted curve, positive solitons. The figure shows that between f_{c1} and f_{c2} , negative solitons have zero amplitude at M_s , (*i.e.*, they are KdV-like) while positive solitons have finite nonzero amplitudes at M_s (*i.e.*, they are nonKdV-like). These properties reverse for $f_{c2} < f < f_n$. Results similar to those in Fig. 7.3 (right panel) were also found for dust ion-acoustic solitons in a plasma with kappa-distributed electrons [Baluku *et al.*, 2010a].

We have already observed from Fig. 7.3 (left panel) that in the region where positive double layers can be obtained, for a given value of f , one can get solitons for Mach numbers that lie above those corresponding to the positive double layers.

Figure 7.4 shows the variation of soliton amplitude with M for fixed f (left panel), and the corresponding typical Sagdeev potential curves (right panel). In the left panel of Fig. 7.4, the end points of the lower curves for the different density ratios f give the amplitudes and Mach numbers of the positive double layers; after which there is a ‘jump’ in amplitude between the double layers and the next set of solitons (that are limited by the ions, that is, those solitons whose amplitude must not exceed $\phi_{li} = M^2/2$, to ensure that the ion density remains real). In the right panel of Fig. 7.4 all the Sagdeev potential curves ($A - F$) have a double root at the origin; the soliton curves A, B and $D - F$ have a single root outside the origin, and the double layer curve C has another double root outside the origin and an inaccessible single root beyond the double root. Such solitons forming beyond double layers for the same plasma composition (with $M > M_{dl}$) were also reported by Verheest [2009] in nonthermal plasmas consisting of cold fluid positive and negative dust particles and Cairns distributed electrons and ions (see his Fig. 4 and the discussion accompanying it).

In Fig. 7.5, we show typical soliton potential profiles (left panel) for the parameters in Fig. 7.4. Solitons below the double layer (with $M < M_{dl}$) are bell-shaped while those

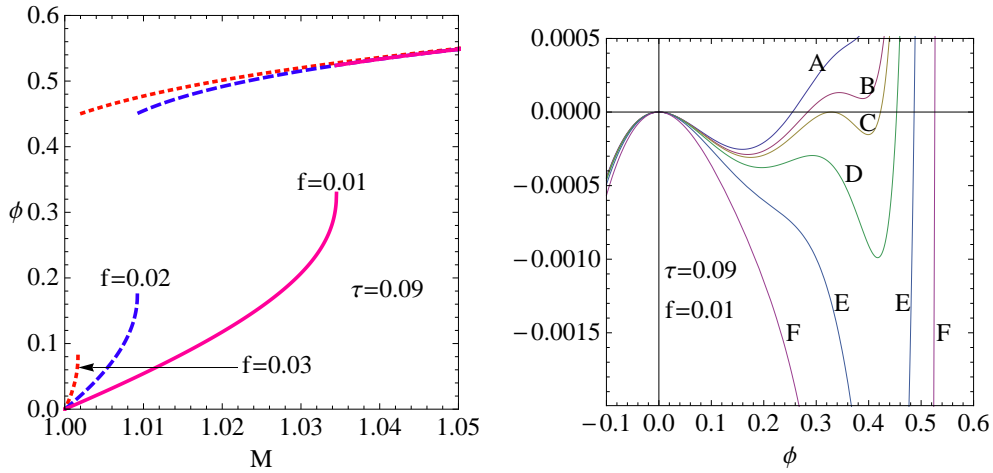


Figure 7.4: *Left panel:* Soliton amplitude variation with M for $\tau = 0.09$, and $f = 0.01$ (continuous curves), $f = 0.02$ (dashed curves) and $f = 0.03$ (dotted curves), respectively. *Right panel:* Typical Sagdeev curves corresponding to the results in the left panel with $f = 0.01$ and different Mach numbers, both below and above M_{dl} where $M_{dl} \simeq 1.0345$ is the Mach number that gives the positive double layer marked C. Other values of M are 1.033 (A), 1.034 (B), 1.036 (D), 1.04 (E) and 1.05 (F).

with $M > M_{dl}$ have a spiky shape. In Fig. 7.5 (right panel) we also show the phase space curves [Sagdeev, 1966; Infeld and Rowlands, 2000] for the Mach numbers used in Fig. 7.4. The figure shows that the amplitude size increases as M increases, and beyond the double layer, solitons have a flattened edge at the maximum potential while the double layer curve has an inaccessible extended closed lobe. The curves beyond the double layer correspond to the soliton curves $D - F$ in Fig. 7.4 (right panel).

Though we have given results for $\tau = 0.09$, we have also looked at other values of τ (especially close to $\tau_{c1} \simeq 0.10102$, such as $\tau = 0.10$ (Fig. 7.6, upper panel) and $\tau = 0.101$ (not shown)). In these cases we get the same trend of results as those discussed for $\tau = 0.09$: a “coexistence region” between f_{c1} and f_n , and below f_{c1} , positive potential double layers are also supported, *i.e.*, f_{c1} separates negative from positive double layers.

As τ approaches τ_{c1} , the region of coexistence becomes very narrow, and the associated M_{dl} are very close to M_s . For instance, the largest Mach number at which negative double layers occur are $M \simeq 1.014041$ (for $\tau = 0.099$, see Fig. 7.3), $M = M_a \simeq 1.000374$ (for $\tau = 0.1$, see Fig. 7.6) and $M \simeq 1.000001075$ (for $\tau = 0.101$, not shown), which is very close to $M_s = 1$. The region (of coexistence) eventually vanishes at $\tau = \tau_{c1}$, when f_{c1} and f_{c2} merge at $f \simeq 0.092$ (see Fig. 7.1). In other words, negative potential solitons or double

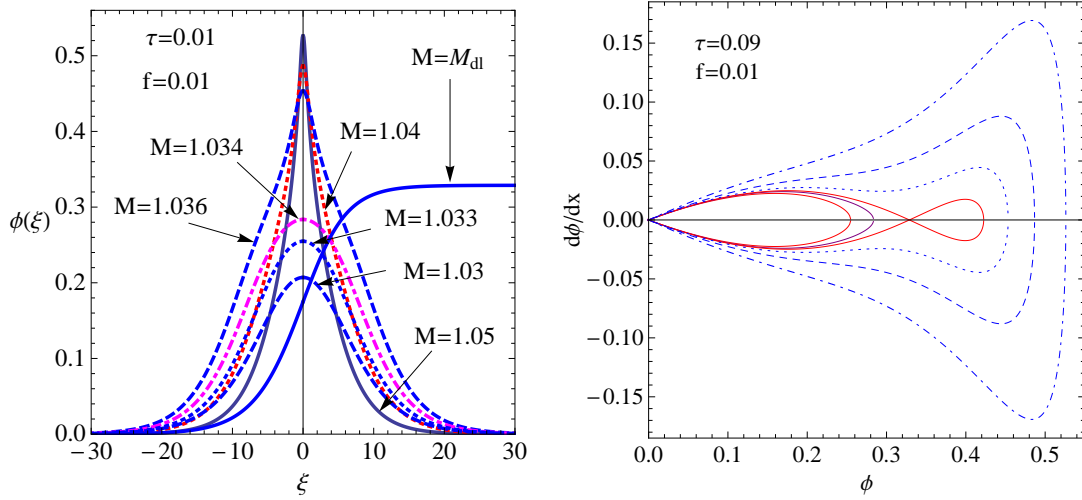


Figure 7.5: *Upper panel*: Typical soliton pulse curves corresponding to $\tau = 0.09$, $f = 0.01$ in Fig. 7.4 for different Mach numbers, both below and above the positive double layer: $M = 1.033$ (A), 1.034 (B), 1.036 (D), 1.04 (E) and 1.05 (F). *Lower panel*: Phase space curves for the parameters in (the *right panel*) Fig. 7.4. The innermost curve correspond to A and the outermost one to F (labels in Fig. 7.4).

layers exist only for $\tau < \tau_{c1}$.

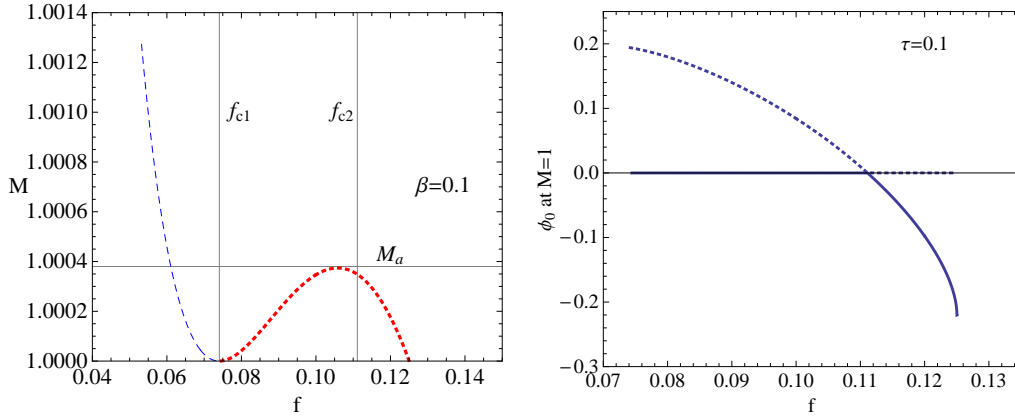


Figure 7.6: Existence domain (*left panel*) of ion-acoustic solitons, and soliton amplitudes at $M = M_s$ for the values of f encompassing the coexistence region (*right panel*), for $\tau = 0.1$. Here, $f_{c1} \approx 0.0741$ and $f_{c2} \approx 0.1111$.

7.3.3 $\tau < \tau_{c2} \simeq 0.075$

In the next examples we consider cases where τ is less than τ_{c2} . Here we look at three specific cases, that is, $\tau = 1/15 \approx 0.067$, $\tau = 1/30 \approx 0.033$ and $\tau = 1/100 = 0.01$. As the dip in the curve of Fig. 7.2 drops below M_s , it yields two apparent ion density cutoffs, *viz.*, f_{p1} , close to $f = 0$, and f_{p2} , the new lower limit of the coexistence region, satisfying $f_{p2} \geq f_{c1}$. However, as we shall see, f_{p1} plays no physical role.

Case I: $\tau = 1/15$

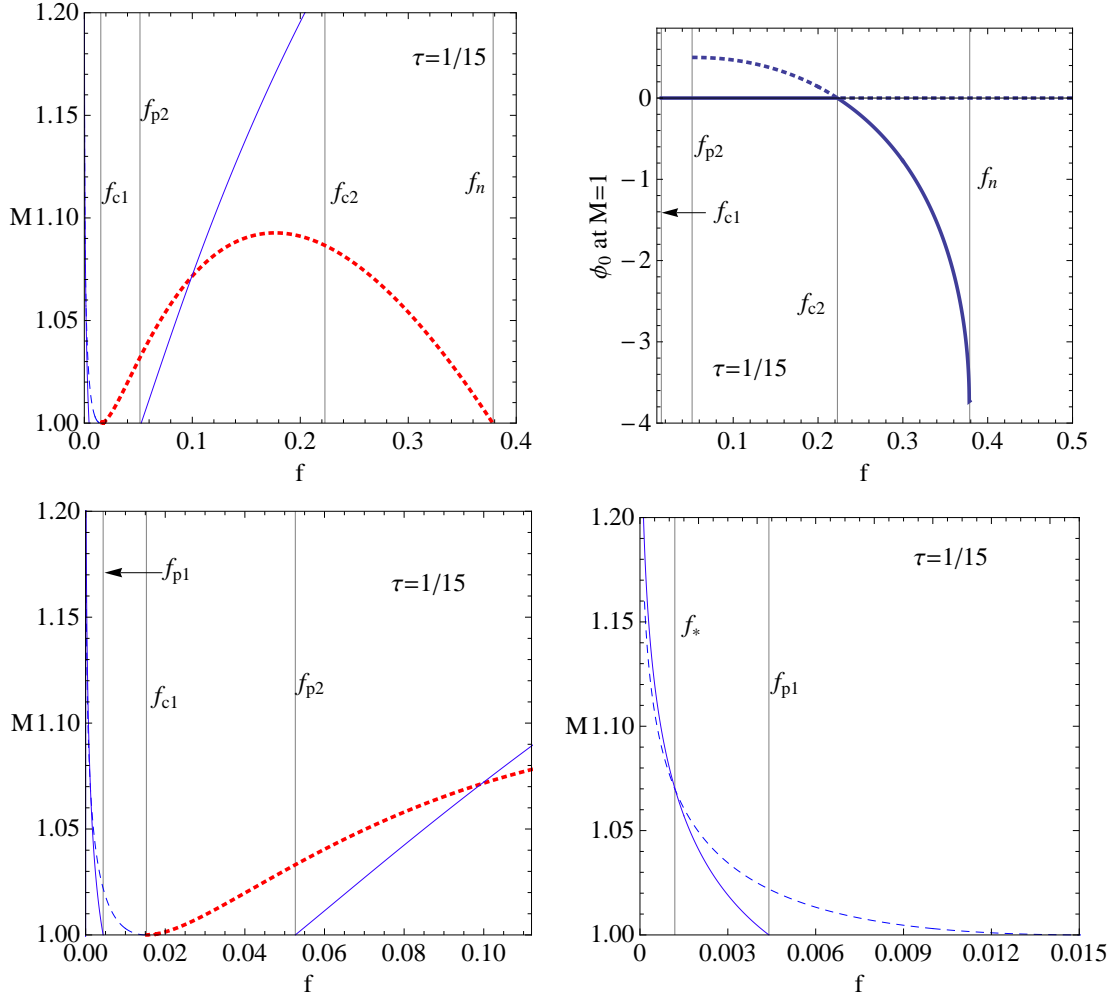


Figure 7.7: Existence domain of ion-acoustic solitons for $\tau = 1/15$ (upper left panel) and amplitude variation with f at $M = M_s$ (upper right panel), with $f_{c1} = 0.0153$, $f_{c2} = 0.2228$, $f_n = 0.3786$ and $f_{p2} = 0.0516$. Only positive solitons exist for $f > f_n$ and $f < f_{c1}$, both positive and negative potential solitons exist between f_{p2} and f_n , and only negative potential solitons exist between f_{c1} and f_{p2} . The lower panel shows the existence domain for values of f close to f_{c1} . In the lower panel, $f_* \approx 0.0012$ and $f_{p1} \approx 0.0044$. For $f_* < f < f_{p1}$, the occurrence of positive potential double layers dominate over the ion limit condition $\phi < \phi_{li} = M^2/2$ in providing a limitation on the existence of positive potential solitons, and the reverse is true for $f < f_*$.

Figure 7.7 (upper left panel) shows the existence domain for $\tau = 1/15 \approx 0.067$, with the range $f < f_{c1}$ clearly shown in more detail in the lower panels. Between 0 and f_{c1} only positive solitons and double layers are found; for $f_{c1} < f < f_{p2}$ only negative double layers and solitons occur; $f_{p2} < f < f_n$ is the coexistence region, and $f_n < f < 1$ supports positive solitons. The upper right panel, which is analogous to Fig. 7.3 (right panel), shows

a plot of the soliton amplitude at $M = M_s = 1$ versus density ratio f in the “coexistence” region. The figure also shows that in the region of “coexistence” the potentials of the two soliton types vanish at $M = M_s$ and $f = f_{c2}$: below (above) f_{c2} , positive (negative) solitons have finite amplitudes at M_s while above (below) f_{c2} , negative (positive) solitons have finite amplitudes at M_s , as was obtained with $\tau = 0.09$ and $\tau = 0.1$ [see Figs. 7.3 and 7.6 (right panels)]. Note that the finite positive potential solitons at $M_s = 1$ do not occur between f_{p2} and f_{c1} , since in this range only negative potential solitons (that are “KdV-like”) exist. As shown in the right lower panel of Fig. 7.7, we get positive double layers in the very narrow range, $0 < f < f_* \simeq 0.002$, with solitons beyond M_{dl} , but they are limited by the ion density (continuous curve), as in Fig. 7.4. At $f = f_*$, the double layer at $M_{dl} = M_{li}$ has $\phi_{dl} < \phi_{li}$. Despite the presence of the ion constraint curve in $f_* < f < f_{c1}$, it represents a spurious root, and positive solitons are limited by double layers (dashed curve). Thus f_{p1} also plays no physical role.

Other aspects of our results in Fig. 7.8 are consistent with those of Baboolal *et al.* [1990], where with $\tau = 1/15$ they showed that negative potential double layers exist for the cool electron density ratio (f) roughly between 0.02 and 0.35 (see their Fig. 2(b)). Compared to our case, this region lies between $f_{c1} \simeq 0.015$ and $f_n \simeq 0.38$. Similarly, in the case of positive potential solitons, Baboolal *et al.* [1990] obtained results with finite amplitudes at $M_s = 1$ for the range of f approximately between 0.1 and 0.25, although they never commented on them. In our case they are in the range $f_{p2} \simeq 0.05 < f < f_{c2} \simeq 0.22$. In the same way their results for $\tau = 1/30$ (see their Fig. 2(a)) are in agreement with ours, as can be seen in Fig. 7.11 (right upper panel) for $\tau = 1/30$.

The top panel of Fig. 7.8 shows the variation of solitary wave amplitude with density ratio f for $\tau = 1/15$. The continuous blue curve shows the maximum amplitude limit due to the ions ($\phi_{li} = M^2/2$ at which $\Psi(\phi_{li}, M) = 0$). Thus amplitudes of positive potential solitons limited by the ions need not exceed ϕ_{li} . Likewise, the dashed blue curve and the dotted red curve give the amplitudes of the positive and negative potential double layers, respectively. For graphical purposes we have scaled up the amplitudes of the positive double layers ($\times 10$) thus in interpreting these results, one has to bear that in mind. For instance, when $f < f_*$ (see lower right panel of Fig. 7.7 or upper right panel of Fig. 7.8), solitons are ultimately limited by the ion condition $\phi < \phi_{li} = M^2/2$ (and not by the

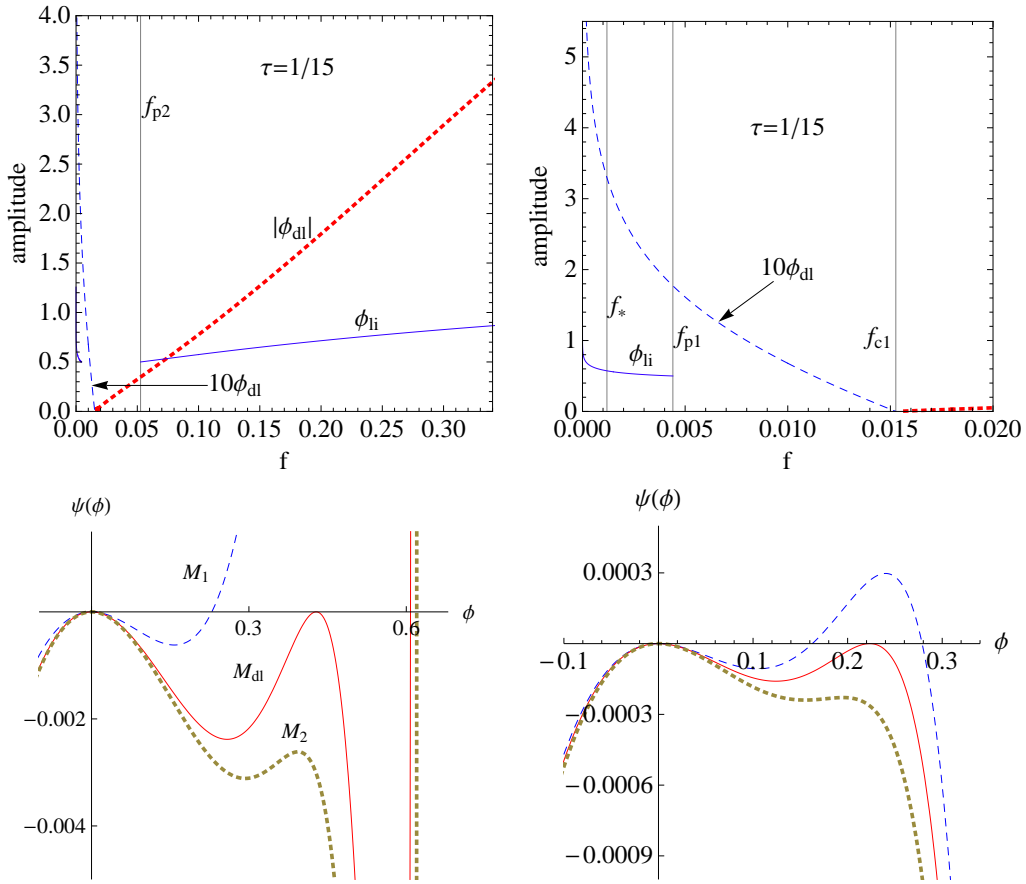


Figure 7.8: *Top panel (left)*: Variation of solitary structure amplitude with density ratio, f for $\tau = 1/15$. *Top panel (right)*: Similar to the figure on the left, now clearly showing amplitudes for positive potential double layers for $f < f_{c1}$. *Bottom panel*: Typical Sagdeev potential plots for $f = 0.0005$ (just 0.05% contribution to density from the cool electrons) on the left for three different Mach numbers, $M_{dl} \approx 1.1066$, $M_1 = M_{dl} - 0.0350$ and $M_2 = M_{dl} + 0.0075$, with a positive double layer occurring at $M = M_{dl}$, and for $f = 0.003$ on the right for $M_{dl} \approx 1.0346$ (continuous curve), $M_1 = M_{dl} - 0.0035$ (dashed curve) and $M_2 = M_{dl} + 0.0035$ (dotted curve). Note that the double layer in the lower right panel figure has amplitude less than $\phi_{li} = M^2/2$, the latter corresponding to a Mach number at which the ion density is infinitely compressed.

occurrence of double layers). The double layer amplitude in those cases is less than the potential limit ϕ_{li} , and solitons exist even beyond the double layer. A typical example is shown in the left lower panel of Fig. 7.8 with Sagdeev potential curves for $f = 0.0005 < f_*$ for three values of M , namely, $M_{dl} \approx 1.1066$, $M_1 = M_{dl} - 0.0350$ and $M_2 = M_{dl} + 0.0075$. At $M = M_{dl}$ we get a double layer with amplitude, $\phi_{dl} \approx 0.43$. For $M < M_{dl}$ (M_1) we get a soliton with amplitude $\phi_0 \sim 0.23$, and for $M > M_{dl}$ (M_2) we get a soliton with amplitude $\phi_0 \sim 0.62 > \phi_{dl}$. It is also observed that there is a large jump in amplitude between the double layer and the next set of solitons forming beyond the double layer, as was seen in

Fig. 7.3 (right panel). However, in the other example shown in the lower right panel of Fig. 7.8, for $f = 0.003 > f_*$ but less than f_{p1} , solitons are limited by the occurrence of double layers (not by the ion limit constraint), and no solitons exist beyond the double layer. For small τ , $f_* \rightarrow 0$, and positive solitons for $f < f_{c1}$ are limited by double layers only. Though the cool electron density is very small (very low f), in the case of positive double layers the resulting soliton/double layer amplitudes are significantly large.

Solitons for $M > M_{li}$?

At $f = f_*$, the Mach number $M = M_{dl}$, corresponding to a positive double layer of amplitude ϕ_{dl} , is equivalent to $M = M_{li}$, and satisfies $\Psi(\phi_{li}, M) = 0$, where $\phi_{li} = M^2/2$ is the potential at which the ions become infinitely compressed. Thus, at $f = f_*$ we get a double layer of amplitude $\phi_{dl} < \phi_{li}$ for $M = M_{li}$. On the one hand, when $0 < f < f_*$ we have $M_{dl} < M_{li}$: solitons are limited by the ion limit constraint, and not by the occurrence of double layers. Thus solitons exist even beyond the double layers, as was the case in Fig. 7.4. On the other hand, when $f_* < f < f_{p1}$ we have $M_{dl} > M_{li}$: solitons are limited by the occurrence of double layers, and not by the ion limit constraint. Thus in the range $f < f_{p1}$, positive potential solitons are limited by the maximum of M_{li} and M_{dl} .

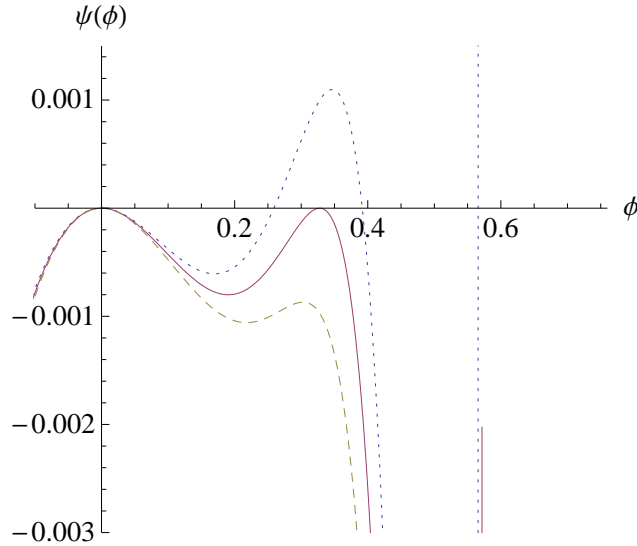


Figure 7.9: Sagdeev potential curves for $\tau = 1/15$, $f = f_* \approx 0.001212$, $M_{li} = M_{dl} \approx 1.06925$ (continuous curve), giving a double layer of amplitude $\phi_{dl} \approx 0.328 < \phi_{li} = 0.572$. The dotted and dashed curves are for $M = M_{dl} - 0.005$ and $M = M_{dl} + 0.005$, respectively.

In understanding the behaviour of solitons in the region $f_* < f < f_{p1}$, we look at Fig. 7.10 (left panel) showing Sagdeev potential curves for Mach numbers close to $M = M_{li}$

for $f = 0.003$, a value in the range $f_* < f < f_{p1}$ (similar to Fig. 7.8, lower right panel). The ion limitation $\Psi(\phi_{li} = M^2/2, M) = 0$ leads to $M = M_{li} \simeq 1.01911$, and therefore $\phi_{li} = M_{li}^2/2 \simeq 0.5193$. In other words, infinite compression of the ion density at $M = M_{li}$ occurs at $\phi = \phi_{li}$. The right panel of Fig. 7.10 is the same as the one on the left; here we show the behaviour of $\Psi(\phi, M)$ close to the value $\phi = \phi_{li}$ for which the ion density is infinitely compressed when $M = M_{li}$. Clearly, the right panel of Fig. 7.10 shows that for $M \geq M_{li}$, $\Psi(\phi, M)$ does not have a root in the vicinity of ϕ_{li} . However, as the left panel figure shows, for $M \geq M_{li}$ it is even possible that the density can remain finite such that a root(s) of $\Psi(\phi, M)$ is (are) encountered in the range $0 < \phi < \phi_{li}$. Actually, even at M_{li} , the ion density $n_i(\phi)$ remains finite provided $\phi < \phi_{li}$, and is complex for $\phi > \phi_{li}$. Thus, for the value of $f = 0.003$, a positive double layer occurs for $M = M_{dl} \simeq 1.3458 > M_{li}$, with amplitude $\phi_{dl} \simeq 0.2334$. As seen from Fig 7.10, when $M = M_{li}$ we get a soliton (first root of $\Psi(\phi, M)$ close to the origin) of amplitude $\phi_0 \approx 0.09 \ll \phi_{li}$. More roots of $\Psi(\phi, M)$ close to the origin in the interval $0 < \phi < \phi_{li}$ can also be obtained as M increases beyond M_{li} , leading to solitons, until a double layer, with amplitude $\phi_{dl} \simeq 0.2334 < \phi_{li}$, is encountered. These roots are shown in Table. 7.1. Beyond the double layer, $\Psi(\phi, M)$ has no roots, thus solitons in the range $f_* < f < f_{p1}$ are limited by double layers, and not by the ion limitation constraint; They are “KdV-like” (have amplitudes that go to zero as M approaches M_s), and lie outside the coexistence region ($f_{p2} < f < f_n$). Note that f_{p1} exists only for τ in the range given, approximately by $\tau_{c3} \simeq 0.0394 < \tau < \tau_{c2} \simeq 0.075$. In this range we get the same behaviour of positive solitons as described in Fig. 7.8 (lower panel) and Fig. 7.10. For $\tau < \tau_{c3}$, positive solitons that exist for $f < f_{c1}$ are limited by the occurrence of positive double layers; positive solitons limited by the ion limit constraint occur for $f_{p2} < f < 1$, and only negative solitons exist for $f_{c1} < f < f_{p2}$. The case for $\tau < \tau_{c3}$ is discussed below, where we consider $\tau = 1/30$ and $\tau = 1/100$.

Case II: $\tau = 1/30$ and $\tau = 1/100$

In the upper left panels of Figs. 7.11 and 7.12 we show plots of the variation of M and amplitude ϕ with f for both negative and positive solitons. Negative solitons are bounded by double layers (red dotted curve labeled M_{dl}) and the size of the amplitude of the negative double layers is indicated by the red dot-dashed curve (labeled $|\phi_{dl}|$) in

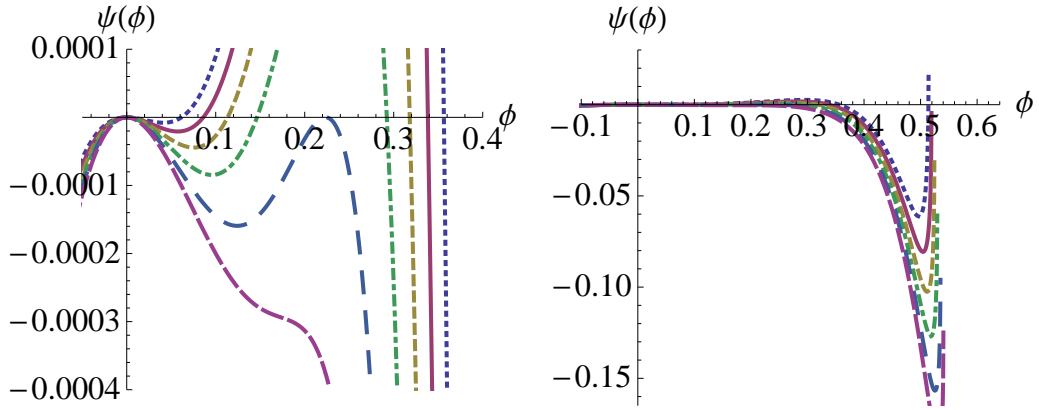


Figure 7.10: *Left panel:* Sagdeev potential curves for $\tau = 1/15$, $f = 0.003$, lying between f_* and f_{p1} , for Mach numbers very close to $M_{li} \approx 1.019$, the value of M at which $n_i(\phi)$ is infinitely compressed. Values of M used are: $M = M_{li} - 0.005$ (dotted curve), $M = M_{li}$ (continuous curve), $M = M_{li} + 0.005$ (dashed curve), $M = M_{li} + 0.01$ (dot-dashed curve), $M = M_{dl} \approx 1.03458$ (long dashed curve) and $M = M_{dl} + 0.005$ (short dashed curve). *Right panel:* Similar to left panel, now showing the behaviour of $\Psi(\phi, M)$ around $\phi = \phi_{li}$.

M	ϕ_{01}	ϕ_{02}^*	ϕ_{03}^*
$M_{li} - 0.010$	0.039	0.373	0.508
$M_{li} - 0.005$	0.062	0.356	0.514
$M_{li} \approx 1.019$	0.086	0.338	xx
$M_{li} + 0.005$	0.113	0.318	xx
$M_{li} + 0.010$	0.146	0.292	xx
$M_{dl} \approx 1.035$	0.233	0.233	xx
$M_{dl} + 0.005$	xx	xx	xx

Table 7.1: Table showing roots (ϕ_0) of $\Psi(\phi, M)$ (all below $\phi_{li} \approx 0.52$) for values of M close to M_{li} , the Mach number corresponding to the ion limit, obtained from $\Psi(M^2/2, M) = 0$. Roots with an asterisk are superfluous (inaccessible in the case of solitons as the soliton conditions are not satisfied beyond the first root, ϕ_{01}), and xx implies that the root does not exist. Other parameters are $\tau = 1/15$ and $f = 0.003$, lying in the range $f_* < f < f_{p1}$.

Fig. 7.11 and $0.1|\phi_{dl}|$ in Fig. 7.12, respectively). In other words, for a particular density ratio f , negative solitons will have amplitudes less than ϕ_{dl} . Similarly, positive potential solitons (limited by the ions) are bounded by the continuous blue curve (labeled M_{li}) and they have amplitudes less than ϕ_{li} (dot-dashed blue curve).

The upper right panel plots in Figs. 7.11 and 7.12 are analogous to Fig. 7.3 (right panel), showing the amplitudes at $M = M_s$. For clarity, the negative potential amplitude at M_s for $\tau = 1/100$ in Fig. 7.12 is suppressed (*i.e.*, the actual amplitude is 10 times what is shown on the graph).

We also point out that as we reduce τ to as low as $\tau = 1/30$ [Fig. 7.11 (upper)] or

further to $\tau = 1/100$ (as in Fig. 7.12), f_{c1} lies very close to $f = 0$, and therefore can not be differentiated from $f = 0$ as the range $[0, f_{c1}]$ becomes negligibly small, for example, see the top panels of Fig. 7.11 and 7.12. Below f_{c1} , only positive potential solitons (limited by double layers) are supported. Their existence domains for $\tau = 1/30$ and $\tau = 1/100$ are clearly shown in Figs. 7.11 and 7.12 [lower panels (left)], respectively, and the associated double layer amplitudes are shown in the graphs on the right of the lower panels. As was the case with $\tau = 1/15$, positive potential solitons do not occur for the full range of f (from 0 to 1).

Another observation from Figs. 7.11 and 7.12 is that as we reduce τ the Mach number at which negative double layers occur (along the dotted red curves) increases, implying that the amplitude of the double layer, for particular density ratio f , also increases. For instance, with $f = 0.3$ the amplitude increases from $|\phi_{dl}| = 2.9$ ($\tau = 1/15$) to $|\phi_{dl}| = 6.5$ ($\tau = 1/30$) and $|\phi_{dl}| = 25$ ($\tau = 1/100$). Thus we can say that a plasma with two temperature electron components, with a minimal contribution of cool electron density supports negative potential solitons with very large amplitudes, in addition to positive solitons limited by the ions. As can be seen in Fig. 7.11 and 7.12 (upper right panels), negative solitons at $M = M_s$ are several units large.

When $\tau = 0$, negative double layers discussed for the cases $0 < \tau < \tau_{c1}$ are no longer supported, and thus negative solitons exist for unbounded Mach numbers. In addition, positive potential solitons, bounded by the ion limit $\phi < \phi_{li} = M^2/2$, exist for $f_{p2} < f < 1$, and no positive potential double layers exist. This is due to the fact that for $\tau \rightarrow 0$, f_{c1} , the lower value of f_c goes to zero, as one may see from Eq. (7.8). However, as we mentioned earlier, this is an unlikely physical situation since the model breaks down as $\tau \rightarrow 0$.

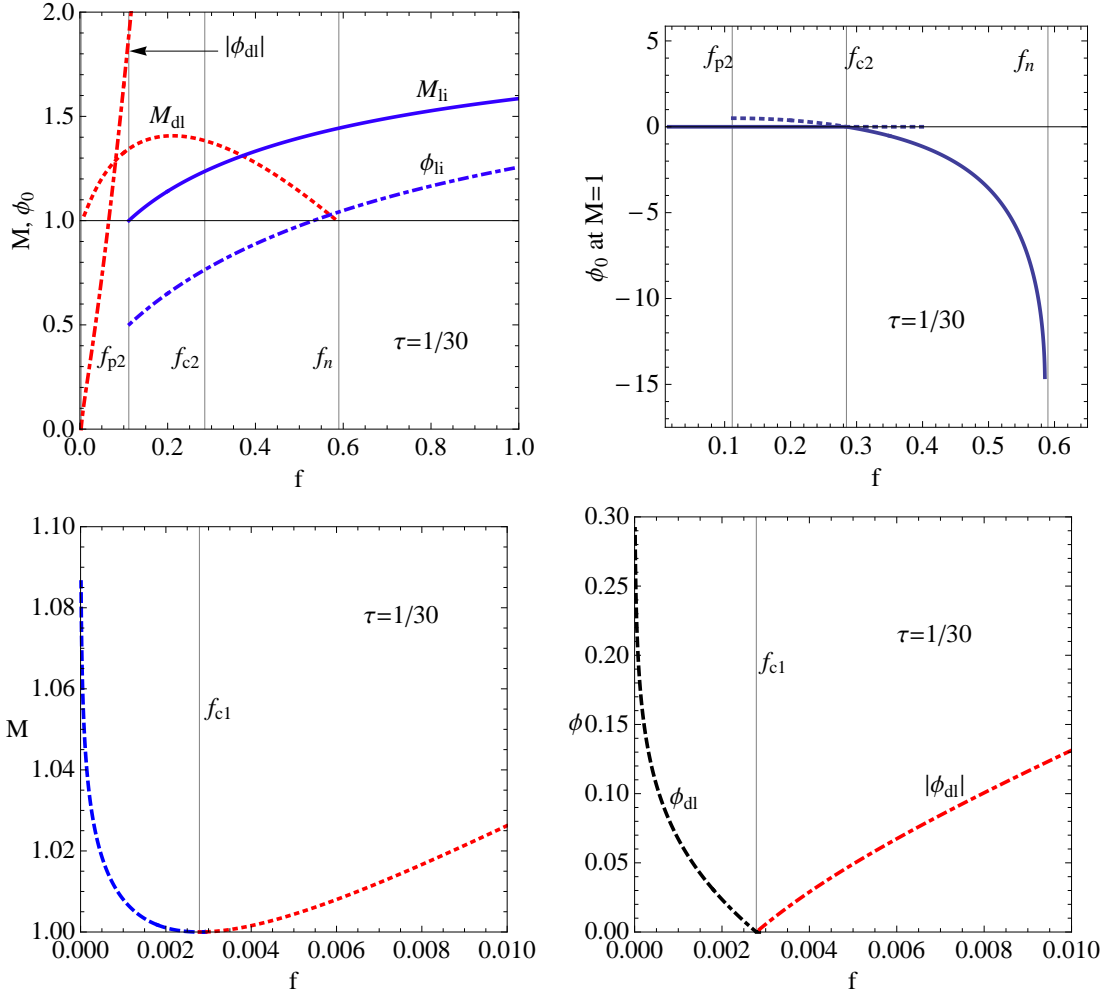


Figure 7.11: *Upper left panel:* Existence domain of ion-acoustic solitons for $\tau = 1/30$. Between $f_{p2} \approx 0.1115$ and $f_n \approx 0.59$, both positive and negative potential solitons are supported; between $f_{c1} \approx 0.0028$ and f_{p2} , only negative potential solitons are supported, and elsewhere ($f < f_{c1}$ and $f > f_n$), only positive potential solitons (limited by double layers) are supported. *Upper right panel:* Soliton amplitude variation at $M = M_s$ with f in the region of coexistence (between f_{p2} and f_n). *Lower panel:* Similar to upper panel, now showing the range of existence of positive double layers (*lower left panel*) and the associated amplitudes (*right left panel*) in the region close to f_{c1} . For $\beta = 1/30$, $f_{c2} \approx 0.2846$.

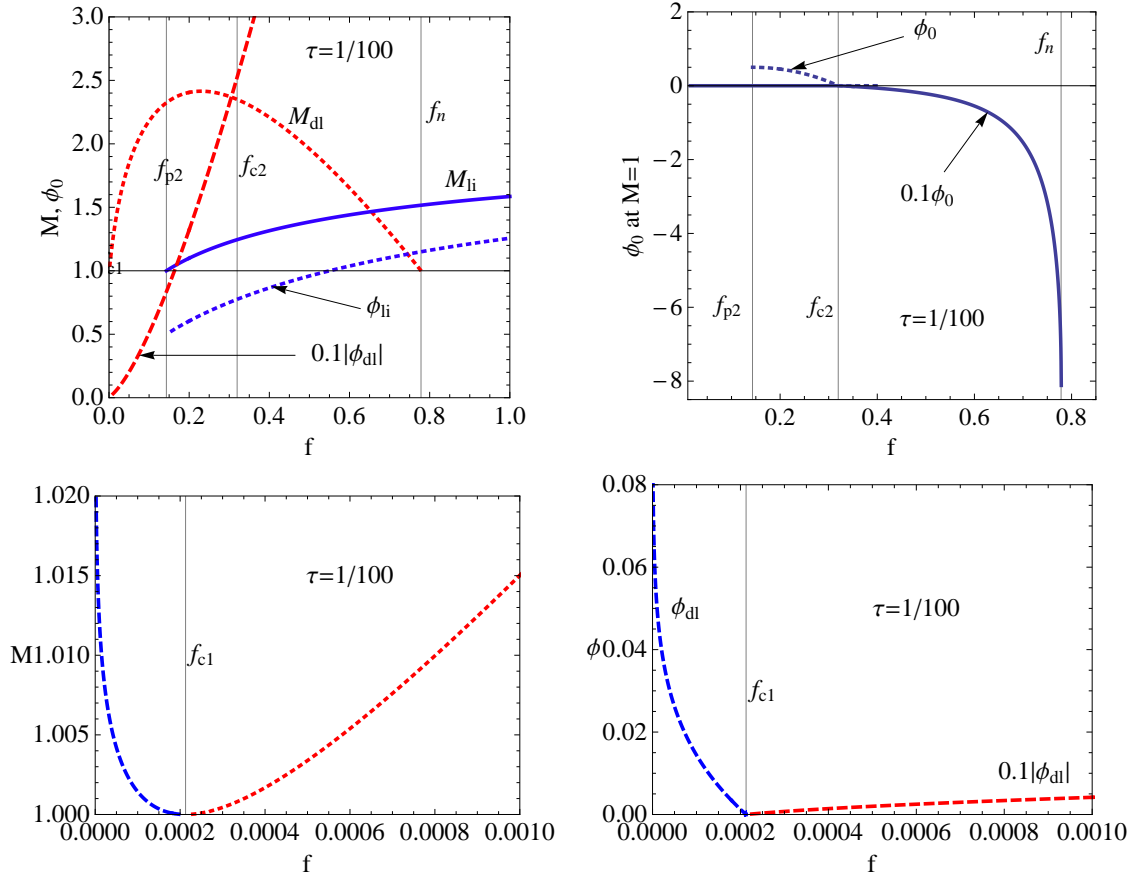


Figure 7.12: Existence domain of ion-acoustic solitons (upper left panel) and amplitude variation at $M = M_s$ with f in the coexistence region (upper right panel) for $\tau = 1/100$. *Lower panel:* Similar to upper panel, now showing the existence of positive double layers for $f < f_{c1}$. Here, $f_{c1} \approx 0.0002$, $f_{c2} \approx 0.3197$, $f_{p2} \approx 0.1433$ and $f_n \approx 0.7784$.

7.4 Conclusions and Chapter Summary

In this work we have revisited in detail the existence of ion-acoustic solitary waves in a plasma with two isothermal electron components. Our results have confirmed a number of earlier results [Buti, 1980; Nishihara and Tajiri, 1981; Baboolal *et al.*, 1990; Ghosh *et al.*, 1996; Verheest *et al.*, 2006] and have also gone far beyond them.

We have plotted the curve $\Psi'''(0, M_s) = 0$ in the space of cool density fraction and temperature ratio (*i.e.*, $f - \tau$), and shown that it agrees with an earlier representation [Nishihara and Tajiri, 1981], found by other means. At fixed $\tau < \tau_{c1} \simeq 0.10102$, it yields two critical values of f (f_{c1} and f_{c2}) which merge at $\tau = \tau_{c1}$.

Above τ_{c1} , only positive potential solitons (which are limited by the ion density constraint) are supported, as for a simple electron-ion plasma, and no positive double layers exist. These positive solitons are “KdV-like” in that their amplitudes tend to zero as M approaches M_s .

For $0 < \tau < \tau_{c1}$ both negative and positive potential double layers may occur over limited ranges of cool electron density fraction f . The former are well-known [Baboolal *et al.*, 1990; Ghosh *et al.*, 1996], and Verheest *et al.* [2006] previously identified a single case of the latter. Our calculations show that positive double layers exist over a narrow range $f < f_{c1}$, while negative double layers occur for $f_{c1} < f < f_n$, below a cut-off, f_n . Surprisingly, solitons may be obtained even beyond the positive double layer, *i.e.*, for $M > M_{dl}$, accompanied by a jump in amplitude. Thus, depending on the temperature ratio $\tau = T_c/T_h$, we may, for low f , get two sets of positive solitons, one bounded by the double layer limit, the other by the usual ion limit condition [Baboolal *et al.*, 1990]. As opposed to the usual bell-shape of the well-known positive solitons, the latter set have a sharply-pointed profile.

If $\tau_{c2} \simeq 0.075 < \tau < \tau_{c1}$ then f_{c1} also acts as the lower f limit of the “coexistence” region in which solitons of both polarities may exist. However, for $\tau < \tau_{c2}$, positive solitons are no longer supported for all f , and an interval $f_{c1} < f < f_{p2}$ is found where only negative potential solitons and double layers are obtained. As a result, the “coexistence” region becomes $f_{p2} < f < f_n$.

The existence of solitons even after a double layer has occurred depends on the position

of f_{p1} , where here we define f_{p1} as the value of f ($< f_{c1}$) at which $M = M_s$ satisfies $\Psi(M^2/2, M) = 0$. Also, f_{p1} exists only for τ in the range $\tau_{c3} \simeq 0.0394 < \tau < \tau_{c2}$. For $\tau < \tau_{c3}$, and $f < f_{c1}$, positive solitons are limited by the occurrence of positive double layers; when $f_{p2} < f < 1$, positive solitons are limited by the ion limit constraint, and only negative solitons exist for $f_{c1} < f < f_{p2}$.

Provided f_c (in this case, f_{c2}) lies in the region of existence of solitons of both polarities ($f_{p2} < f < f_n$), we observe the following:

(i) Contrary to the conventional wisdom that solitons are super-acoustic ($M > M_s$), we have found solitons at the critical Mach number M_s , thus showing that they can propagate at the ion-acoustic speed.

(ii) For $f < f_{c2}$ positive potential solitons have finite amplitude at M_s while negative potential solitons have zero amplitude at M_s , as is the case for “KdV-like” solitons. The negative sign associated with $\Psi'''(0, M_s)$ for $f < f_{c2}$ corresponds to the sign of the KdV-like solitons. Similarly, for $f > f_c$, the negative solitons have finite amplitudes at M_s (“nonKdV-like”) while the positive solitons are now KdV-like. The positive sign of $\Psi'''(0, M_s)$ for $f > f_{c2}$ thus corresponds to the sign of these positive potential (KdV-like) solitons near M_s . Hence, for $f_{p2} < f < f_{c2}$ one finds KdV-like negative soliton potentials accompanied by nonKdV-like positive solitons, and vice versa for $f_n > f > f_{c2}$.

(iii) The amplitudes of the nonKdV-like solitons [*i.e.*, those not corresponding to the sign of $\Psi'''(0, M_s)$] increase monotonically with $|f - f_c|$, but vanish at $f = f_{c2}$. For small values of τ , the negative nonKdV-like solitons develop large amplitudes at $M = M_s$ when $f \rightarrow f_n$. In addition, the largest value of M_{dl} increases rapidly with decreasing τ . Hence the normalized ϕ_{dl} increases rapidly and can reach several tens.

(iv) Positive solitons are limited from above by the requirement that $\phi < M^2/2$ so that the ion density remains real, and the negative solitons are limited by the occurrence of double layers.

If one defines the density ratio f in terms of the equilibrium density of the hot electron component N_{h0}/N_{e0} instead of the cool electron component N_{c0}/N_{e0} (as we have used here), then the transformation $f \rightarrow (1 - f)$ in Eq. (7.8) gives the appropriate range of f where the results discussed here apply (see Chapter 5).

We argue that the existence (and position) of a critical parameter, in this case, critical

density ratio, may give a hint on the polarity of solitons in a plasma model.

General Summary and Conclusions

In this thesis, we have investigated linear and nonlinear acoustic waves in various plasma models, which may occur in space. In the case of linear acoustic waves we have used a kinetic theoretical approach in the study of electron-acoustic waves in bi-kappa plasmas, with emphasis on Saturn's magnetosphere. The rest of the thesis deals with acoustic solitons and double layers in a variety of relevant three-component plasmas. In all cases we have used the Sagdeev pseudopotential (arbitrary amplitude) approach, while in some chapters we have also carried out expansions to find small amplitude solutions, along the lines of the KdV solutions.

In Chap. 1, we have given a detailed description of kappa distributions and their major features in Sec. 1.1. This section also highlights plasma environments where particles whose velocity distribution functions may be well described by kappa distributions have been reported to exist. We have also given a detailed discussion of dusty plasmas, solitary structures (solitons and double layers), and various methods that we have used to study these structures, in Sec. 1.2.

8.1 Linear Electron-Acoustic Waves

Using a kinetic theoretical approach, we have carried out a parameter survey of the dispersion and damping of electron-acoustic waves (EAW) and electron plasma waves (EPW)

relevant to the magnetosphere of Saturn, in which the electron distribution is well fitted by a superposition of two kappa distributions at different temperatures and kappa values. Our investigations for specific regions of the magnetosphere have shown that:

- Weakly damped electron-acoustic waves may occur in Saturn's outer magnetosphere around $13 - 18 R_S$ where (i) the densities of the hot and cool electron populations are of about the same order of magnitude; (ii) the temperatures differ by about two orders of magnitude, that is $T_h/T_c \sim 100$, and (iii) the kappa index values are more or less constant around $\kappa_c \simeq 2$ and $\kappa_h \simeq 4$.
- There is strong coupling between the EAW and the EPW in the intermediate magnetosphere ($9 R_S < R < 13 R_S$) with potentially observable waves that are EAW-like. This pattern is also obtained, for some cases, in the $R > 13 R_S$ region when the density ratio n_{h0}/n_{e0} is very small since the cool electron component density is very high compared to the hot electron component density.
- EAWs are strongly damped in the inner magnetosphere ($R < 9 R_S$); only the EPW is weakly damped. This may be attributed to the fact that the density ratio is very small. Thus, our results show that even in the presence of a second non-Maxwellian electron component, it is the dependence of the damping rate on parameters such as the hot-to-cool electron temperature ratio $\beta = T_h/T_c$ and the fractional hot electron density $f = n_{h0}/n_{e0}$ that determines the range in wavenumber (in terms of $k\lambda_{Dc}$) over which EAWs are weakly damped.

8.2 Nonlinear Acoustic Waves

In this thesis we have introduced a generalized density relation

$$N_s(\varphi) = N_{s0} \left[1 + \left(\frac{1}{\kappa_s - 3/2} \right) \frac{q_s \varphi}{K_B T_s} \right]^{-(\kappa_s - 1/2)}$$

for kappa distribution functions, which, in the limit $\kappa \rightarrow \infty$, reduces to the Maxwellian density function

$$N_s(\varphi) = N_{s0} \exp \left(\frac{-q_s \varphi}{K_B T_s} \right).$$

This density relation has been applied to various plasma models, including dust acoustic waves/solitons with κ -distributed ions and/or electrons (discussed in Chap. 3), dust ion-acoustic solitons (discussed in Chap. 4), and ion-acoustic solitons in bi-kappa plasmas – with both the cool and hot electrons being kappa distributed (discussed in Chap. 5).

DA Solitons: In Chapter 3 we investigated the existence of dust acoustic (DA) solitons in dusty plasmas with κ -distributed ions and/or electrons. We have used both the Sagdeev (pseudopotential) approach for the arbitrary amplitude solitary waves and the expanded Sagdeev potential approach, equivalent to the reductive perturbation technique, for the small amplitude solitary waves. A double layer relation was derived for the small amplitude solitary waves. However, in practice it was found that double layers are not supported by the plasma model.

We found that when the dust is negative, only negative potential solitons exist, and reducing the spectral indices (κ_e , κ_i) only affects the existence domains of the solitons quantitatively.

In the presence of positively charged dust, only positive potential solitons are found, but the ion to electron temperature ratio has significant quantitative effects: particularly for $T_e \gg T_i$ the results are very different from those for $T_e = T_i$. In both cases we find that the soliton polarity agrees with the sign of the charge of the cold, inertial species (dust), as observed in a number of other plasma models, albeit not universally so.

Our results are qualitatively similar to those obtained for dusty plasmas with Boltzmann or polytropic electrons and ions. However, there are quantitative differences, arising from the functional form of the number density for a κ -distribution as in Eq. (3.2).

Although the κ -distribution is nonthermal, the results reveal important differences from those found when one of the hot plasma species has a different nonthermal distribution, *viz.*, the Cairns distribution [Verheest and Pillay, 2008a,b]. In the latter, it was shown that for negative (positive) dust, positive (negative) solitons could also be found, limited by double layers, for sufficient nonthermality of the ions (electrons) and sufficiently low electron (ion) density. For nonthermal electrons (ions) only negative (positive) potential solitons were found, as in our case. This difference in results could be due to the fact that for the κ -distribution the main change from a Maxwellian lies in the ‘tail’ region, unlike

the case of the Cairns distribution.

DIA Solitons: In Chapter 4 we used the pseudopotential approach in studying arbitrary amplitude dust ion-acoustic solitons in a plasma of positive ions, κ -distributed electrons and charged dust grains. This was an extension of the work of Bharuthram and Shukla [1992], who studied a plasma model consisting of Boltzmann-distributed electrons, cold ions, and immobile negative dust in the bulk of the paper, and then presented a few results for mobile negative dust. In the case of small amplitude waves/solitons, we used the reductive perturbation technique, where we derived the associated KdV and mKdV equations. For these small amplitude solitons, the mKdV approach was only valid for plasma situations where the KdV solutions are unattainable.

For the case of *negative dust*, we have shown that for all $\kappa > 3/2$ the model supports both positive and negative potential solitons in a specific range of fractional electron density, where the Mach number for positive (negative) potential solitons is limited from above by the condition at which the ion density becomes complex (the dust is infinitely compressed). This agrees with the analysis of Verheest *et al.* [2005] for polytropic electrons, where it was found that both negative and positive potential dust ion-acoustic solitons may exist in a dusty plasma with negatively charged dust, positively charged ions and polytropic electrons.

Positive potential DIA solitons experience a low- f cutoff (f_p) which decreases with increasing κ (*i.e.*, with a decrease in excess superthermal particles), and hence this increases the range in (f, M) space over which positive solitons exist. Allowing for finite dust grain mobility has little or no effect on the existence domain for positive solitons; the smaller the value of z , that is the heavier the dust particles (assuming constant dust charge), the larger the domain in (f, M) space over which negative potential solitons can be obtained. Also, the variation of the ion temperature (through σ) has a weak effect of increasing the size of the existence domain as σ is increased. That is, the warmer the ions (the larger the value of σ) the larger the existence domain for solitons, with the region of existence decreasing as κ decreases.

Negative potential solitons do not exist above a κ -independent cutoff f_n lying approximately between $0.9 - 1$, the exact value of which depends significantly on the magnitude

of the dust mobility factor $z = Z_d m_i / m_d$. They are effectively not subject to an upper limit in M as $z \ll 1$ implies that $\phi_{\ell d} \gg 1$, and thus negative solitons may be very large.

A surprising result occurs over the range of fractional electron density f in which solitons of both polarities are supported. Here, finite amplitude solitary structures exist even at the DIA speed – behaviour which contradicts KdV theory. A similar result was found recently in another three-component plasma [Verheest and Hellberg, 2010], where, as here, the phenomenon is associated with a point of inflexion of the pseudopotential at $\phi = 0$ and $M = M_s$, rather than the usual maximum. The sign of $\Psi'''(\phi = 0; M = M_s; f)$ then designates the polarity of the KdV-like soliton that vanishes at $M = M_s$.

A critical role is played by f_c , the value of f at which the KdV coefficient $A = 0$, which also satisfies the constraint $\Psi'''(\phi = 0; M = M_s; f_c) = 0$. In particular, as f is varied, solitons of each polarity switch at $f = f_c$ from a KdV-like form to nonKdV-like behaviour. For $f_p < f < f_c$, positive solitons at $M = M_s$ have finite amplitude, increasing in size with $|f - f_c|$ as f approaches f_p , while negative solitons have zero magnitude at $M = M_s$, as expected from KdV theory. This situation reverses in polarity for solitons found for $f_c < f < f_n$.

In a plasma with *positive dust grains*, only positive potential (“KdV-like”) solitons are supported by the plasma model, with the upper limit on M provided by infinite compression of the ions, and the positively charged dust particles only contribute in neutralizing the electrons in the background. The Maxwellian case agrees with earlier results, using the fluid dynamic paradigm with polytropic electrons [Baluku *et al.*, 2008]. Decreasing κ leads to small reductions in both the accessible M and the existence range in M . The dusty plasma model with positive dust is similar to a two component ion-electron plasma, with modifications to the dynamics due to the presence of weakly mobile dust. The results are reminiscent of those found for ion-acoustic solitons in a two-ion plasma [McKenzie *et al.*, 2005], but for a much heavier second “positive ion”.

Double Kappa IAS: In Chapter 5 we considered a plasma model consisting of warm inertial fluid ions and two (cool and hot) electron components, that are both kappa distributed, as found in Saturn’s magnetosphere.

The main features of this work are:

(i) Both compressive ($\phi > 0$) and rarefactive ($\phi < 0$) solitons can be supported by the model. Here, compressive (rarefactive) solitons have a hump (dip) in the density as well as the electrostatic potential.

(ii) The effect of spectral index κ on the existence domain of solitons (or double layers) was that, compared to high values of kappa (which represent Maxwellian particles), low kappa values, which indicate increased superthermal particles in the high energy tail of the distribution, reduce the existence domain in the parameter space of (f, M) over which compressive solitons or both compressive and rarefactive solitons can exist.

(iii) For plasma configurations that support the existence of both hump ($\phi > 0$) and dip ($\phi < 0$) solitons, we found that there exists a critical density ratio, f_c at which both the second and third derivatives of the Sagdeev potential vanish, when evaluated at the origin for the critical Mach number M_s . In the vicinity of f_c , solitons of a polarity opposite to the sign of $\Psi'''(0, M_s)$ remained finite (nonzero) at M_s , a result that is contrary to the Korteweg-de Vries description. These solitons which exist at M_s can therefore propagate at a velocity equivalent to the phase velocity of the wave. This result means that the usually quoted Sagdeev requirement $\Psi''(0, M) < 0$ needs to be changed to $\Psi''(0, M) \leq 0$.

(iv) Comparison between the perturbation theory and the large amplitude techniques showed that whereas the former approach seems to be accurate for very small amplitudes, especially for Mach numbers close to M_s , that is, for structures that move with velocities close to the phase velocity of the wave, the method becomes less reliable for velocities far from the phase velocity. In addition, it cannot represent the second (nonKdV-like) soliton that has finite amplitude at $M = M_s$, when both polarities are supported. Thus the fully nonlinear (arbitrary amplitude) pseudopotential approach becomes indispensable.

(v) The large rarefactive potential solitons ($\phi < 0$) reported for this plasma model may be attributed to the fact that the small but finite electron mass, which is a measure of the electron inertia, is neglected in the electron density expression. If the electron inertia due to the finite electron mass were included, such a scheme would require obtaining the electron density expression from the fluid equations of motion, with the associated kappa distributed pressure term incorporated. The pressure expression associated with a kappa distribution function has been derived in Appendix A.1.2. However, this approach has not been applied in this work, but shall be considered as an extension to getting comprehensive

results for this model in the foreseeable future.

IAS in Electron-Positron-Ion Plasmas: In Chapter 6 we have considered a plasma consisting of electrons, positrons and positive ions. The electrons are nonthermally distributed, following a Cairns distribution function [Cairns *et al.*, 1995]; the positrons are Boltzmann distributed while the ions are modeled by hydrodynamic fluid equations. This is an extension of the plasma model discussed by Popel *et al.* [1995] for Boltzmann electrons, and is similar to the model discussed by Pakzad [2009]. In this work we confirm some results obtained by Pakzad [2009] and present more new results associated with ion-acoustic solitary waves in electron-positron-ion plasmas where the electrons are Cairns distributed.

We have pointed out that low values of β are appropriate for the use of the Cairns distribution for nonthermal particles. Values of $\beta > 4/7$ (see *e.g.*, Verheest and Pillay [2008a]) result in the nonthermal particle distribution being deformed (forming wings) so that it may not appropriately represent a stable nonthermal distribution. In such cases another form of nonthermal distribution, such as a kappa distribution, may be used instead.

Though Pakzad [2009] reported only the existence of positive potential solitons in the model under investigation, we have shown that in addition, negative potential solitons and double layers can also be supported, though for a limited range in the fractional positron density p .

In contrast to the usual assumption that solitons are explicitly super-acoustic, occurring for Mach numbers $M > M_s$, we have also obtained solitons at M_s . This implies that these solitons can propagate at the acoustic phase speed. This observation occurs only in the region of “coexistence”, where both positive and negative potential solitons may be supported by the same plasma parameter values.

In this work, we have obtained critical values of p (denoted p_c) at which $\Psi'''(\phi, M) = 0$ for $\phi = 0$ and $M = M_s$. If p_c lies in the region where solitons of both polarity occur for the same plasma parameters, then for $p < p_c$ one gets negative potential “KdV-like” solitons and positive potential “nonKdV like” solitons at M_s . The reverse polarities are found for $p > p_c$.

Double Boltzmann IAS: In Chapter 7 we consider ion-acoustic solitons in two temperature electron plasmas, where the electrons are Boltzmann-distributed. Such a plasma

model has been studied in the past, with negative potential solitons and double layers reported to be supported in addition to positive potential solitons. In this work we have carried out further investigations and showed that positive potential double layers can form below a critical density ratio, associated with the third derivative of the Sagdeev potential evaluated at the origin for the acoustic phase velocity of the wave. We also found out that for density ratios that support positive double layers, solitons were also reported beyond the double layers, depending on the cool-to-hot electron temperature ratio. This contradicts the usual belief, based on simpler forms of the Sagdeev potential, that double layers always represent a Mach number limit for solitons. As we have already indicated in chapters 4 and 5, when both polarities can be supported, solitary structures can propagate at the acoustic phase velocity of the wave, contrary to a KdV prescription

At fixed $\tau < \tau_{c1} \simeq 0.10102$, $\Psi'''(0, M_s) = 0$ yields two critical values of f (f_{c1} and f_{c2}) which merge at $\tau = \tau_{c1}$.

Above τ_{c1} , only positive potential solitons (which are limited by the ion density constraint) are supported, as for a simple electron-ion plasma, and no positive double layers exist. These positive solitons are “KdV-like” in that their amplitudes tend to zero as M approaches M_s .

For $0 < \tau < \tau_{c1}$ both negative and positive potential double layers may occur over limited ranges of cool electron density fraction f . The former are well-known [Baboolal *et al.*, 1990; Ghosh *et al.*, 1996], and Verheest *et al.* [2006] previously identified a single case of the latter. Our calculations show that positive double layers exist over a narrow range $f < f_{c1}$, while negative double layers occur for $f_{c1} < f < f_n$, below a cut-off, f_n . Surprisingly, solitons may be obtained even beyond the positive double layer, *i.e.*, for $M > M_{dl}$, accompanied by a jump in amplitude. Thus, depending on the temperature ratio $\tau = T_c/T_h$, we may, for low f , get two sets of positive solitons, one bounded by the double layer limit, the other by the usual ion limit condition [Baboolal *et al.*, 1990]. As opposed to the usual bell-shape of the well-known positive solitons, the latter set have a sharply-pointed profile.

For $\tau_{c2} \simeq 0.075 < \tau < \tau_{c1}$, f_{c1} also acts as the lower f limit of the “coexistence” region in which solitons of both polarities may exist. However, for $\tau < \tau_{c2}$, positive solitons are no longer supported for all f , and an interval $f_{c1} < f < f_{p2}$ is found where only negative

potential solitons and double layers are obtained. Here, f_{p2} is the value of f ($> f_{c1}$) at which $M = M_s$ satisfies $\Psi(M^2/2, M) = 0$.

The existence of solitons even after a double layer has occurred depends on the position of f_{p1} , where here we define f_{p1} as the value of f ($< f_{c1}$) at which $M = M_s$ satisfies $\Psi(M^2/2, M) = 0$. Also, f_{p1} exists only for τ in the range $\tau_{c3} \simeq 0.0394 < \tau < \tau_{c2}$. For $\tau < \tau_{c3}$, and $f < f_{c1}$, positive solitons are limited by the occurrence of positive double layers; when $f_{p2} < f < 1$, positive solitons are limited by the ion limit constraint, and only negative solitons exist for $f_{c1} < f < f_{p2}$. These results show that the existence (and position) of a critical parameter, in this case, critical density ratio, may give a hint on the polarity of solitons in a plasma model.

Finally, we reiterate that in our nonlinear studies of acoustic waves in three-component plasmas we have found two key results with wider repercussions. They are:

1. The existence of finite amplitude solitons (and double layers) at the acoustic speed, that are thus nonKdV-like, and also lead to a change to the usual Sagdeev condition $\Psi''(0, M) < 0$, which now becomes $\Psi''(0, M) \leq 0$.
2. The existence of solitons at Mach numbers exceeding that at which a double layer occurs, as opposed to the conventional wisdom that double layers always represent an upper Mach number limit to a sequence of solitons.

A.1 Derivation of Density and Pressure for Kappa Distributions

Before going into the details of deriving the density and pressure expressions following from kappa distribution functions, we first introduce some special integrals.

A.1.1 Special Integrals for Kappa Distributions

Consider the integral

$$I = \iint_{-\infty}^{\infty} \left(1 + \frac{v_x^2 + v_y^2 + v_z^2}{\kappa_\alpha \theta_\alpha^2} \right)^{-(\kappa_\alpha + 2)} dv_z dv_y. \quad (\text{A.1})$$

This can be written as

$$I = \int_{-\infty}^{\infty} \left(1 + \frac{v_x^2 + v_y^2}{\kappa_\alpha \theta_\alpha^2} \right)^{-(\kappa_\alpha + 2)} \int_{-\infty}^{\infty} \left(1 + \frac{v_z^2}{\kappa_\alpha \theta_\alpha^2 + v_x^2 + v_y^2} \right)^{-(\kappa_\alpha + 2)} dv_z dv_y.$$

Substituting $v_z^2 = (\kappa_\alpha \theta_\alpha^2 + v_x^2 + v_y^2)R$, where $R = R(v_z)$ is a function of v_z , we then have

$$dv_z = \frac{1}{2}(\kappa_\alpha \theta_\alpha^2)^{1/2} \left(1 + \frac{v_x^2 + v_y^2}{\kappa_\alpha \theta_\alpha^2} \right)^{1/2} R^{-1/2} dR.$$

Thus (A.1) becomes

$$\begin{aligned} I &= (\kappa_\alpha \theta_\alpha^2)^{1/2} B(1/2, \kappa_\alpha + 3/2) \int_{-\infty}^{\infty} \left(1 + \frac{v_x^2 + v_y^2}{\kappa_\alpha \theta_\alpha^2}\right)^{-(\kappa_\alpha + 3/2)} dv_y, \\ &= (\kappa_\alpha \theta_\alpha^2) B(1/2, \kappa_\alpha + 3/2) B(1/2, \kappa_\alpha + 1) \left(1 + \frac{v_x^2}{\kappa_\alpha \theta_\alpha^2}\right)^{-(\kappa_\alpha + 1)}, \end{aligned}$$

where the Beta function, $B(a, b)$ is defined by [Arfken and Weber, 1995, p. 614]; [Riley *et al.*, 1998, p. 981]

$$B(a, b) = \int_0^\infty x^{a-1} (1+x)^{-(a+b)} dx; \quad a, b > 0. \quad (\text{A.2})$$

Using the relations [Arfken and Weber, 1995; Riley *et al.*, 1998]

$$B(a, b) = \frac{\Gamma(a)\Gamma(b)}{\Gamma(a+b)}; \quad \Gamma(\alpha + 1) = \alpha\Gamma(\alpha) \quad \text{and} \quad \Gamma(1/2) = \pi^{1/2}, \quad (\text{A.3})$$

we obtain

$$I = \frac{\pi \kappa_\alpha \theta_\alpha^2}{(\kappa_\alpha + 1)} \left(1 + \frac{v_x^2}{\kappa_\alpha \theta_\alpha^2}\right)^{-(\kappa_\alpha + 1)}. \quad (\text{A.4})$$

Therefore

$$\iint_{-\infty}^{\infty} \left(1 + \frac{v_x^2 + v_y^2 + v_z^2}{\kappa_\alpha \theta_\alpha^2}\right)^{-(\kappa_\alpha + 2)} dv_z dv_y = \frac{\pi \kappa_\alpha \theta_\alpha^2}{(\kappa_\alpha + 1)} \left(1 + \frac{v_x^2}{\kappa_\alpha \theta_\alpha^2}\right)^{-(\kappa_\alpha + 1)}. \quad (\text{A.5})$$

Similarly,

$$\iint_{-\infty}^{\infty} \left(1 + \frac{v_x^2 + v_y^2 + v_z^2}{\kappa \theta^2}\right)^{-(\kappa + 1)} dv_z dv_y = \pi \theta^2 \left(1 + \frac{v_x^2}{\kappa \theta^2}\right)^{-\kappa}. \quad (\text{A.6})$$

A.1.2 Density and Pressure Expressions for Kappa Distributions

We consider the three dimensional isotropic kappa distribution function $F_\kappa(v)$, of particles of mass m and charge q in a plasma with electrostatic potential φ , given by

$$F_k(v) = A_\kappa \left(1 + \frac{v^2 + 2q\varphi/m}{\kappa \theta^2}\right)^{-(\kappa + 1)} = \left(1 + \frac{v_x^2 + v_y^2 + v_z^2 + 2q\varphi/m}{\kappa \theta^2}\right)^{-(\kappa + 1)}, \quad (\text{A.7})$$

where

$$A_\kappa = \frac{N_0}{(\pi \kappa \theta^2)^{3/2}} \frac{\Gamma(\kappa + 1)}{\Gamma(\kappa - 1/2)}.$$

The average number of particles per unit volume or simply the number density N_j for species of type j is given by [Gurnett and Bhattacharjee, 2005, p.138]; [Kivelson and Russell, 1995, p.34]

$$N_j = \iiint_{-\infty}^{\infty} F_\kappa(v) d^3v, \quad \text{where} \quad d^3v = dv_x dv_y dv_z. \quad (\text{A.8})$$

Using the procedure in appendix A.1.1 above, the density expression can easily be written in the form

$$N_j(\varphi) = A_\kappa (\kappa \theta^2)^{3/2} B(1/2, \kappa + 1/2) B(1/2, \kappa) B(1/2, \kappa - 1/2) \left(1 + \frac{2q\varphi}{m\kappa\theta^2} \right)^{-(\kappa-1/2)}. \quad (\text{A.9})$$

Upon using Eq. (A.3) and substituting for A_κ we obtain the density of species j with mass m_j , charge q_j , spectral index κ_j and initial density N_{j0} as

$$N_j = N_{j0} \left(1 + \frac{2q_j\varphi}{m_j\kappa_j\theta_j^2} \right)^{-(\kappa_j-1/2)}. \quad (\text{A.10})$$

The pressure associated with a kappa distribution is obtained from the pressure tensor $\overleftrightarrow{\mathbf{P}}_s = [\mathbf{P}_{ij}]$, given by [Gurnett and Bhattacharjee, 2005, p.138]

$$\overleftrightarrow{\mathbf{P}}_s = \int_V m_s (\mathbf{v} - \mathbf{U}_s) (\mathbf{v} - \mathbf{U}_s) f(\mathbf{v}, \mathbf{r}, t) d^3v, \quad (\text{A.11})$$

where \mathbf{U}_s is the average velocity of particles of type j , or simply the bulk velocity at which the distribution is peaked. Note that the pressure tensor $\overleftrightarrow{\mathbf{P}}_s$ gives the average rate at which momentum is transported in the i direction across surface j in a frame of reference moving at the average velocity, \mathbf{U}_s . In the pressure tensor expression, the term $(\mathbf{v} - \mathbf{U}_s)(\mathbf{v} - \mathbf{U}_s)$ is given by the matrix [Gurnett and Bhattacharjee, 2005, p.138]

$$(\mathbf{v} - \mathbf{U}_s)(\mathbf{v} - \mathbf{U}_s) = \begin{bmatrix} (v_x - U_{sx})(v_x - U_{sx}), (v_x - U_{sx})(v_y - U_{sy}), (v_x - U_{sx})(v_z - U_{sz}) \\ (v_y - U_{sy})(v_x - U_{sx}), (v_y - U_{sy})(v_y - U_{sy}), (v_y - U_{sy})(v_z - U_{sz}) \\ (v_z - U_{sz})(v_x - U_{sx}), (v_z - U_{sz})(v_y - U_{sy}), (v_z - U_{sz})(v_z - U_{sz}) \end{bmatrix}.$$

Thus if the bulk velocity is 0 (that is, the distribution function is peaked at $v = 0$) then the dialic term gives

$$(\mathbf{v} - \mathbf{U}_s)(\mathbf{v} - \mathbf{U}_s) = \begin{bmatrix} v_x^2 & v_x v_y & v_x v_z \\ v_y v_x & v_y^2 & v_y v_z \\ v_z v_x & v_z v_y & v_z^2 \end{bmatrix},$$

and therefore the pressure tensor becomes

$$P = \begin{bmatrix} P_{xx} & P_{xy} & P_{xz} \\ P_{yx} & P_{yy} & P_{yz} \\ P_{zx} & P_{zy} & P_{zz} \end{bmatrix},$$

where the components of \mathbf{P}_{ij} can be obtained as described below. For the distribution defined in Eq A.7 we have $P_{xx}/m = \iiint v_x^2 F_\kappa(v) dv_x dv_y dv_z$, giving

$$\frac{P_{xx}}{m} = A_\kappa \int_{-\infty}^{\infty} v_x^2 \left\{ \iint_{-\infty}^{\infty} \left[1 + \frac{v_x^2 + v_y^2 + v_z^2 + 2q\varphi/m}{\kappa\theta^2} \right]^{-(\kappa+1)} dv_z dv_y \right\} dv_x.$$

Using Eq. (A.6), the term in curly brackets is simply $\pi\theta^2 \left(1 + \frac{v_x^2 + 2q\varphi/m}{\kappa\theta^2} \right)^{-\kappa}$, and thus

$$\frac{P_{xx}}{m} = \pi\theta^2 A_\kappa \left(1 + \frac{2q\varphi/m}{\kappa\theta^2} \right)^{-\kappa} \int_{-\infty}^{\infty} v_x^2 \left(1 + \frac{v_x^2}{\kappa\theta^2 + 2q\varphi/m} \right)^{-\kappa} dv_x,$$

which simplifies to

$$\begin{aligned} \frac{P_{xx}}{m} &= \pi(\theta^2)^{3/2} A_\kappa B(3/2, \kappa - 3/2) \left(1 + \frac{2q\varphi/m}{\kappa\theta^2} \right)^{-(\kappa-3/2)} \\ &= \frac{N_0\theta^2}{2} \left(\frac{\kappa}{\kappa - 3/2} \right) \left(1 + \frac{2q\varphi/m}{\kappa\theta^2} \right)^{-(\kappa-3/2)}. \end{aligned}$$

Substituting $\theta^2 = \left(\frac{\kappa - 3/2}{\kappa} \right) \left(\frac{2K_B T}{m} \right)$ we then obtain

$$P_{xx} = N_0 K_B T \left(1 + \frac{1}{\kappa - 3/2} \frac{q\varphi}{K_B T} \right)^{-(\kappa-3/2)} \quad (\text{A.12})$$

as the pressure of particles propagating in one dimension. Similarly, $P_{yy} = P_{zz} = P_{xx}$. Note that in the limit $\kappa \rightarrow \infty$, $P_{xx} = N_0 K_B T \exp[-q\varphi/K_B T]$, thus if the particles have zero potential and pressure P_0 in the unperturbed equilibrium state, then $P_{xx}(\varphi \rightarrow 0) = P_0 = N_0 K_B T$, which is the ideal gas pressure equation for Maxwellian particles. However, P_{ij} , for $i \neq j$, may take a different form and will not be considered here.

B.1 Dispersion Relation of Electron-Acoustic Waves from Linear Kinetic Theory.

In deriving the appropriate dispersion relation for electron-acoustic waves discussed in Chap. 2 we use the assumption that on the electron-acoustic wave time scale, $V_{ti} \ll V_{tc} \ll \omega/k \ll V_{th}$, and with $\xi_\alpha \propto \omega/(kV_{t\alpha})$, it follows that $|\xi_i|, |\xi_c| \gg 1$, such that we can use the asymptotic expansion of $\mathcal{Z}(\kappa_\alpha, \xi_\alpha)$ for the ions and cool electrons. Similarly, $|\xi_h| \ll 1$, leading to the need to use the power series expansion of $\mathcal{Z}(\kappa_\alpha, \xi_\alpha)$ for hot electrons.

As the ions are Maxwellian, $\mathcal{Z}'(\kappa_i, \xi_i) \rightarrow Z'(\xi)$ in the limit $\kappa_i \rightarrow \infty$, where $Z'(\xi)$ is the derivative, with respect to the argument ξ , of the usual plasma dispersion function of Fried and Conte (see [Krall and Trivelpiece, 1989]).

The asymptotic expression for $Z'(\xi)$ (large ξ , $|\xi^{-1}| \ll 1$) becomes (see [Brambilla, 1989, pp.107–108]; [Swanson, 1989, pp.375–376])

$$Z'(\xi) \sim \frac{1}{\xi^2} + \frac{3}{2\xi^4} + \dots - \sigma(2i\sqrt{\pi})\xi e^{-\xi^2}, \quad (\text{B.1})$$

where

$$\sigma = \begin{cases} 0 & \text{for } \text{Im}(\xi) > 0, \\ 1 & \text{for } \text{Im}(\xi) = 0, \\ 2 & \text{for } \text{Im}(\xi) < 0. \end{cases} \quad (\text{B.2})$$

Thus for the ions with $|\xi_i| \gg 1$, we neglect terms of order higher than $0(\xi^{-2})$ in Eq. (B.1), giving

$$\mathcal{Z}'(\xi_i) \sim \left(\frac{2k^2 V_{ti}^2}{\omega^2} \right) - 2i\sigma \sqrt{\frac{\pi}{2}} \left(\frac{\omega}{kV_{ti}} \right) \exp\left(-\frac{\omega^2}{2k^2 V_{ti}^2} \right). \quad (\text{B.3})$$

For sufficiently small and large argument ξ [Hellberg and Mace, 2002], the power series and asymptotic expansion of $\mathcal{Z}(\kappa_\alpha, \xi_\alpha)$ are, respectively, given by

$$\mathcal{Z}(\kappa_\alpha, \xi_\alpha) = \frac{i\pi^{1/2}\Gamma(\kappa)}{\kappa^{1/2}\Gamma(\kappa - \frac{1}{2})} \frac{(\kappa)^\kappa}{(\kappa + \xi^2)^\kappa} - 2 \left(\frac{\kappa - \frac{1}{2}}{\kappa} \right) \xi + \frac{4}{3} \frac{(\kappa + \frac{1}{2})(\kappa - \frac{1}{2})}{\kappa^2} \xi^3 + \dots, \quad (\text{B.4})$$

and

$$\mathcal{Z}(\kappa_\alpha, \xi_\alpha) = \frac{\pi^{1/2}\kappa^{\kappa-1/2}\Gamma(\kappa)}{\Gamma(\kappa - \frac{1}{2})} \frac{[i - \tan(\kappa\pi)]}{(\kappa + \xi^2)^\kappa} - \left(\frac{1}{\xi} + \frac{\kappa}{2\kappa - 3} \frac{1}{\xi^3} + \dots \right). \quad (\text{B.5})$$

Note that Eq. (B.5) follows from Eq. (55) of Hellberg and Mace [2002], and corrects their Eq. (56).

In the case of hot electrons, neglecting terms of order higher than $0(\xi_h^2)$ for $\xi_h \ll 1$, Eq. (B.4) gives

$$\mathcal{Z}'(\kappa_h, \xi_h) = -2 \left(\frac{\kappa_h - 1/2}{\kappa_h} \right) - \frac{2i\sqrt{\pi}\Gamma(\kappa_h)}{\sqrt{\kappa_h}\Gamma(\kappa_h - 1/2)} \frac{\omega}{k\theta_h} \left(1 + \frac{\omega^2}{\kappa_h k^2 \theta_h^2} \right)^{-(\kappa_h+1)}. \quad (\text{B.6})$$

Similarly for the cool electrons, the asymptotic expansion in Eq. (B.5) gives

$$\mathcal{Z}'(\kappa_c, \xi_c) \sim \frac{-2\sqrt{\pi}\Gamma(\kappa_c)\xi_c}{\sqrt{\kappa_c}\Gamma(\kappa_c - 1/2)} (i - \tan \kappa_c \pi) (1 + \xi_c^2/\kappa_c)^{-(\kappa_c+1)} + \frac{1}{\xi_c^2} \left[1 + \frac{3\kappa_c}{2\kappa_c - 3} \frac{1}{\xi_c^2} \right].$$

With $|\xi_c| \gg 1$, we take the approximation $\xi_c(1 + \xi_c^2/\kappa_c)^{-(\kappa_c+1)} \approx \kappa_c^{\kappa_c+1}/\xi_c^{2\kappa_c+1}$, giving

$$\begin{aligned} \mathcal{Z}'(\kappa_c, \xi_c) \sim & \frac{k^2 \theta_c^2}{\omega^2} \left[1 + \frac{3\kappa_c}{2\kappa_c - 3} \frac{k^2 \theta_c^2}{\omega^2} \right] \\ & - \frac{2\sqrt{\pi} \kappa_c^{(\kappa_c+1/2)} \Gamma(\kappa_c)}{\Gamma(\kappa_c - 1/2)} (i - \tan \kappa_c \pi) \left(\frac{\omega}{k\theta_c} \right)^{-(2\kappa_c+1)}. \end{aligned} \quad (\text{B.7})$$

Substitution of equations (B.3), (B.6) and (B.7) into Eq. (2.2) gives

$$\begin{aligned} D(k, \omega) = & \left(1 + \frac{1}{k^2 \lambda_{\kappa_h}^2} \right) - \frac{\omega_{pc}^2}{\omega^2} \left(1 + \frac{\omega_{pi}^2}{\omega_{pc}^2} \right) - 3k^2 \lambda_{Dc}^2 \frac{\omega_{pc}^4}{\omega^4} \\ & - \frac{\sqrt{\pi} \kappa_c^{(\kappa_c+1/2)} \Gamma(\kappa_c + 1)}{\Gamma(\kappa_c + 1/2)} \left(\frac{\tan \kappa_c \pi}{k^2 \lambda_{\kappa_c}^2} \right) \left(\frac{\omega}{k\theta_c} \right)^{-(2\kappa_c+1)} \\ & + i \left\{ \frac{\sqrt{\pi} \kappa_c^{(\kappa_c+1/2)} \Gamma(\kappa_c + 1)}{\Gamma(\kappa_c + 1/2)} \frac{1}{k^2 \lambda_{\kappa_c}^2} \left(\frac{\omega}{k\theta_c} \right)^{-(2\kappa_c+1)} \right. \\ & + \frac{\sqrt{\pi} \sqrt{\kappa_h} \Gamma(\kappa_h)}{\Gamma(\kappa_h + 1/2)} \left(\frac{\omega}{k^3 \lambda_{\kappa_h}^2 \theta_h} \right) \left(1 + \frac{\omega^2}{\kappa_h k^2 \theta_h^2} \right)^{-(\kappa_h+1)} \\ & \left. + \sigma \sqrt{\frac{\pi}{2}} \frac{1}{k^2 \lambda_{Di}^2} \left(\frac{\omega}{kV_{th,i}} \right) \exp \left(-\frac{\omega^2}{2k^2 V_{ti}^2} \right) \right\} = 0, \end{aligned} \quad (\text{B.8})$$

where $\lambda_{\kappa_\alpha} = [(\kappa_\alpha - 3/2)/(\kappa_\alpha - 1/2)]^{1/2} \lambda_{D\alpha}$, with $\lambda_{D\alpha} = (\varepsilon_0 K_B T_\alpha / n_{0\alpha} e^2)^{1/2}$ being the Debye length of species α . The parameter λ_{κ_α} is the appropriate Debye length in a kappa plasma [Bryant, 1996; Mace *et al.*, 1998], which reduces to $\lambda_{D\alpha}$ in the limit $\kappa_\alpha \rightarrow \infty$.

In the case of weak damping we can expand $D(k, \omega)$ about ω_r , where $\omega = \omega_r + i\gamma$. Neglecting terms of order $(\omega - \omega_r)^2$ we obtain [Krall and Trivelpiece, 1989, p.389]

$$D(k, \omega) \simeq D(k, \omega_r) + i \gamma \frac{\partial D(k, \omega_r)}{\partial \omega_r}. \quad (\text{B.9})$$

However, $D(k, \omega_r)$ is itself a complex quantity (see Eq. (B.8)). Thus it can be written in the form

$$D(k, \omega_r) = D_r(k, \omega_r) + i D_i(k, \omega_r), \quad (\text{B.10})$$

where

$$D_r(k, \omega_r) = \left(1 + \frac{1}{k^2 \lambda_{\kappa h}^2}\right) - \frac{\omega_{pc}^2}{\omega_r^2} \left(1 + \frac{\omega_{pi}^2}{\omega_{pc}^2}\right) - 3k^2 \lambda_{Dc}^2 \frac{\omega_{pc}^4}{\omega_r^4} - \frac{\sqrt{\pi} \kappa_c^{(\kappa_c+1/2)} \Gamma(\kappa_c+1)}{\Gamma(\kappa_c+1/2)} \left(\frac{\tan \kappa_c \pi}{k^2 \lambda_{\kappa c}^2}\right) \left(\frac{\omega_r}{k \theta_c}\right)^{-(2\kappa_c+1)} \quad \text{and} \quad (\text{B.11})$$

$$D_i(k, \omega_r) = \frac{\sqrt{\pi} \kappa_c^{(\kappa_c+1/2)} \Gamma(\kappa_c+1)}{\Gamma(\kappa_c+1/2)} \frac{1}{k^2 \lambda_{\kappa c}^2} \left(\frac{\omega_r}{k \theta_c}\right)^{-(2\kappa_c+1)} + \frac{\sqrt{\pi} \sqrt{\kappa_h} \Gamma(\kappa_h)}{\Gamma(\kappa_h+1/2)} \left(\frac{\omega_r}{k^3 \lambda_{\kappa h}^2 \theta_h}\right) \left(1 + \frac{\omega_r^2}{\kappa_h k^2 \theta_h^2}\right)^{-(\kappa_h+1)} + \sigma \sqrt{\frac{\pi}{2}} \frac{1}{k^2 \lambda_{Di}^2} \left(\frac{\omega_r}{k V_{ti}}\right) \exp\left(-\frac{\omega_r^2}{2k^2 V_{ti}^2}\right). \quad (\text{B.12})$$

With the assumption that $|\gamma| \ll \omega_r$ and $|D_i(k, \omega_r)| \ll |D_r(k, \omega_r)|$, equations (B.9) and (B.10) give

$$D(k, \omega) \simeq D_r(k, \omega_r) + i \left\{ D_r(k, \omega_r) + \gamma \frac{\partial D_i(k, \omega_r)}{\partial \omega_r} \right\} = 0. \quad (\text{B.13})$$

Therefore equating the real and imaginary parts to zero, we obtain, respectively, the dispersion relation, $\omega_r \equiv \omega_r(k)$, and the damping rate, $\gamma \equiv \gamma(k) < 0$ or growth rate, $\gamma \equiv \gamma(k) > 0$ from [Krahl and Trivelpiece, 1989, p.389]:

$$D_r(k, \omega) = 0 \quad \text{and} \quad \gamma = \frac{-D_i(k, \omega_r)}{\partial D_r(k, \omega_r) / \partial \omega_r}. \quad (\text{B.14})$$

Since $m_e/m_i \simeq 1/1836 \ll 1$, it follows that provided $n_{h0}/n_{c0} \leq 1$ then $\omega_{pi}^2/\omega_{pc}^2 \ll 1$ is a valid approximation. Now assuming $\omega_{pi} \ll \omega_{pc}$ and neglecting the term proportional to $1/\xi_c^{2\kappa_c+1}$ for $\xi_c \gg 1$ in Eq. (B.11), we get

$$\left(1 + \frac{1}{k^2 \lambda_{\kappa h}^2}\right) \omega_r^4 - \omega_{pc}^2 \omega_r^2 - 3k^2 \lambda_{Dc}^2 \omega_{pc}^4 = 0,$$

with solution $\omega_r^2 > 0$ given by

$$\omega_r^2 = \omega_{pc}^2 \left\{ \frac{1 + [1 + 12k^2 \lambda_{Dc}^2 (1 + 1/k^2 \lambda_{\kappa h}^2)]^{1/2}}{2(1 + 1/k^2 \lambda_{\kappa h}^2)} \right\}. \quad (\text{B.15})$$

Similarly, as the frequencies have been normalized to ω_{pe} , Eq. (B.14) gives

$$\frac{\gamma}{\omega_{pe}} = -\frac{\omega_{pc}}{\omega_{pe}} \left(\frac{\omega_r}{\omega_{pe}} \right)^6 \frac{A_1(\kappa_c, \kappa_h)}{A_2(\kappa_c)} = - \left(1 - \frac{n_{h0}}{n_{e0}} \right)^{1/2} \left(\frac{\omega_r}{\omega_{pe}} \right)^6 \frac{A_1(\kappa_c, \kappa_h)}{A_2(\kappa_c)}, \quad (\text{B.16})$$

where

$$\begin{aligned} A_1(\kappa_c, \kappa_h) = & \frac{C_1(\kappa_c)}{k^2 \lambda_{Dc}^2} \left[\left(\frac{\kappa_c}{2\kappa_c - 3} \right)^{1/2} \frac{1}{(1 - n_{0h}/n_{0e})^{1/2}} \frac{\omega_r/\omega_{pe}}{k \lambda_{Dc}} \right]^{-(2\kappa_c+1)} \\ & + \frac{C_2(\kappa_h)}{k^3 \lambda_{Dc}^3} \left[1 + \frac{1/(1 - n_{0h}/n_{0e})}{(2\kappa_h - 3)(T_h/T_c)} \frac{\omega_r^2/\omega_{pe}^2}{k^2 \lambda_{Dc}^2} \right]^{-(\kappa_h+1)} \\ & + \frac{C_3(\sigma)}{k^3 \lambda_{Dc}^3} \exp \left[-\frac{1}{2} \frac{m_i/m_e}{(T_i/T_c)(1 - n_{0h}/n_{0e})} \frac{\omega_r^2/\omega_{pe}^2}{k^2 \lambda_{Dc}^2} \right]; \end{aligned} \quad (\text{B.17})$$

$$\begin{aligned} A_2(\kappa_c) = & 12k^2 \lambda_{Dc}^2 (1 - n_{h0}/n_{e0})^{5/2} + \frac{2(1 - n_{h0}/n_{e0})^{3/2}}{(\omega_r/\omega_{pe})^{-2}} \left[1 + \frac{m_e}{m_i} \left(1 - \frac{n_{h0}}{n_{e0}} \right)^{-1} \right] \\ & + \sqrt{2\pi} \frac{\tan(\kappa_c \pi)}{(\omega_r/\omega_{pe})^{-5}} \frac{\kappa_c^{\kappa_c+1}}{k^3 \lambda_{Dc}^3} \frac{(\kappa_c^2 - 1/4)}{(\kappa_c - 3/2)^{3/2}} \\ & \times \left[\frac{(2\kappa_c - 3)}{\kappa_c} \frac{1}{(1 - n_{h0}/n_{e0})^{1/2}} \frac{\omega_r/\omega_{pe}}{k \lambda_{Dc}} \right]^{-2(\kappa_c+1)}, \end{aligned} \quad (\text{B.18})$$

and

$$\begin{aligned} C_1(\kappa_c) = & \sqrt{\pi} \frac{(\kappa_c - 1/2)}{(\kappa_c - 3/2)} \frac{\Gamma(\kappa_c + 1)}{\Gamma(\kappa_c + 1/2)} \frac{\kappa_c^{(\kappa_c+1/2)}}{\omega_r/\omega_{pe}}; \\ C_2(\kappa_h) = & \frac{(\pi/2)^{1/2}}{(T_h/T_c)^{3/2}} \frac{(\kappa_h - 1/2)}{(\kappa_h - 3/2)^{3/2}} \frac{\Gamma(\kappa_h + 1)}{\Gamma(\kappa_h + 1/2)} \frac{(n_{0h}/n_{0e})}{(1 - n_{0h}/n_{0e})^{3/2}}; \\ C_3(\sigma) = & \sigma \frac{(\pi/2)^{1/2} (m_i/m_e)^{1/2}}{(T_i/T_c)^{3/2} (1 - n_{0h}/n_{0e})^{3/2}}. \end{aligned} \quad (\text{B.19})$$

The normalized frequency ω_r/ω_{pe} in Eqs. (B.16)–(B.18) satisfies $D_r(k, \omega_r) = 0$, and is obtained from (B.15).

Already we have seen that electron-acoustic waves require $\xi_h \ll 1$ and $\xi_c \gg 1$, that is, $\xi_h \ll \xi_c$. The latter implies that $\lambda_{Dc}/\lambda_{\kappa h} \ll (n_{0h}/n_{0e})^{1/2} [\kappa_c/(\kappa_c - 3/2)]^{1/2}$.

Now, if $(n_{0h}/n_{0e})^{1/2} [\kappa_c/(\kappa_c - 3/2)]^{1/2} \gtrsim 1$, that is, $f = n_{0h}/n_{0e} \gtrsim (2\kappa_c - 3)/(4\kappa_c - 3) \equiv f_c$, $\lambda_{Dc}/\lambda_{\kappa h} \ll 1$ is a valid approximation. Here, in the long wavelength regime, f_c is the threshold value of f below which EAWs may not be weakly damped. Also, $\lambda_{Dc}/\lambda_{\kappa h} \ll 1$

implies that $f \ll 1/\{1 + [(\kappa_h - 1/2)/(\kappa_h - 3/2)]/\beta\} \equiv f_h$, where $\beta = T_h/T_c$.

Also we assume that $12k^2\lambda_{Dc}^2(1 + 1/k^2\lambda_{\kappa_h}^2) \ll 1$ in (B.15), which holds only in the long wavelength regime ($k\lambda_{Dc} \ll 1$) and when $\lambda_{Dc} \ll \lambda_{\kappa_h}$ (provided $f \ll f_h$ and $f \gtrsim f_c$). Thus ignoring the negative solution, (B.15) leads to

$$\omega_r^2 = \omega_{pc}^2 \left\{ \frac{1 + 3k^2\lambda_{Dc}^2(1 + 1/k^2\lambda_{\kappa_h}^2)}{(1 + 1/k^2\lambda_{\kappa_h}^2)} \right\}. \quad (\text{B.20})$$

With $V_{tc} = \omega_{pc}\lambda_{Dc} = (K_B T_c/m_e)^{1/2}$ and $V_{s\kappa} = \omega_{pc}\lambda_{\kappa_h}$, (B.20) can be written as

$$\omega_r^2 = k^2 \left\{ 3V_{tc}^2 + \frac{V_{s\kappa}^2}{1 + k^2\lambda_{\kappa_h}^2} \right\}, \quad (\text{B.21})$$

which clearly shows that the phase velocity ω/k is modified by the hot electron parameters (through λ_{κ_h}).

However, if in addition we assume that $\lambda_{Dc} \ll \lambda_{\kappa_h}$, then Eq. (B.20) can be written in the form [Mace *et al.*, 1999]

$$\omega_r^2 = \omega_{pc}^2 \left(\frac{1 + 3k^2\lambda_{Dc}^2}{1 + 1/k^2\lambda_{\kappa_h}^2} \right). \quad (\text{B.22})$$

C.1 Derivation of the Modified Korteweg de-Vries (mKdV) Equation

We already saw from the KdV equation (1.27) in Sec. 1.2 that when the coefficient of the nonlinearity term $\partial\varphi^2/\partial\zeta$ vanishes, the soliton amplitude goes to infinity. In other words, the small amplitude method based on the KdV approach breaks down. In overcoming that scenario in the perturbation approach, we re-scale the stretched space-time variables ζ and \mathcal{T} . In this work, we have used the approach of Baboolal *et al.* [1989], by making use of the stretched variables $\zeta = \epsilon(X - Vt')$ and $\mathcal{T} = \epsilon^3 t'$. In addition, we expand the varying plasma parameters N_j , V_j and φ , that is, the density, velocity and electrostatic potential, respectively, in terms of the smallness parameter, ϵ , using the expansion [Nishihara and Tajiri, 1981; Mace *et al.*, 1991]:

$$\begin{aligned}
 N_j &= N_{j0} + \epsilon N_{j1} + \epsilon^2 N_{j2} + \dots \\
 V_j &= \epsilon V_{j1} + \epsilon^2 V_{j2} + \dots \\
 \varphi &= \epsilon \varphi_1 + \epsilon^2 \varphi_2 + \dots
 \end{aligned}
 \tag{C.1}$$

Here, parameters with subscript 0 correspond to the equilibrium state while those with subscripts 1, 2 \dots correspond to the first-, second-, \dots order perturbed states. The velocity of the individual particles in the equilibrium state is taken to be zero, and we have assumed

zero equilibrium potential since the electric field is assumed to be zero in the equilibrium state. We have not included the pressure expansion terms, since in the plasma models that will be discussed in this thesis, the pressure is expressed as a function of density using the adiabatic relation $P_j N_j^{-\gamma_j} = \text{constant} = P_{j0} N_{j0}^{-\gamma_j}$, where γ is the ratio of the heat capacities at constant volume, equal to unity for isothermal particles, and three for adiabatic particles.

Using the stretched variables $\zeta = \epsilon(X - Vt')$ and $\mathcal{T} = \epsilon^3 t'$, we have $\partial/\partial X = \epsilon \partial/\partial \zeta$ and $\partial/\partial t' = \epsilon^3 \partial/\partial \mathcal{T} - \epsilon V \partial/\partial \zeta$. Thus the continuity, momentum and Poisson's equations can be written, respectively, in the form:

$$\epsilon^3 \frac{\partial N_i}{\partial \mathcal{T}} - \epsilon V \frac{\partial N_i}{\partial \zeta} + \epsilon N_i \frac{\partial V_i}{\partial \zeta} + \epsilon V_i \frac{\partial N_i}{\partial \zeta} = 0, \quad (\text{C.2})$$

$$m_i N_i \left(\epsilon^3 \frac{\partial V_i}{\partial \mathcal{T}} - \epsilon V \frac{\partial V_i}{\partial \zeta} + \epsilon V_i \frac{\partial V_i}{\partial \zeta} \right) + \epsilon m_i C_{ti}^2 \left(\frac{N_i}{N_{i0}} \right)^{(\gamma_i-1)} \frac{\partial N_i}{\partial \zeta} + \epsilon N_i q_i \frac{\partial \varphi}{\partial \zeta} = 0, \quad (\text{C.3})$$

and

$$\epsilon^2 \epsilon_0 \frac{\partial^2 \varphi}{\partial \zeta^2} + N_i q_i + \sum_{s=c,h} N_{s0} \sum_{r=0}^{\infty} (-1)^r \nu_{sr} \varphi^r q_s = 0, \quad (\text{C.4})$$

where N_i , V_i and φ are defined in Eq. (C.1), and the thermal velocity of the ions, C_{ti} is defined by $C_{ti}^2 = \gamma_i P_{i0} / m_i N_{i0}$. Re-arranging order by order we have the following:

The continuity equation gives:

$$\bigcirc (\epsilon^2): N_{i0} \frac{\partial V_{i1}}{\partial \zeta} - V \frac{\partial N_{i1}}{\partial \zeta} = 0, \quad (\text{C.5})$$

$$\bigcirc (\epsilon^3): N_{i0} \frac{\partial V_{i2}}{\partial \zeta} - V \frac{\partial N_{i2}}{\partial \zeta} + N_{i1} \frac{\partial V_{i1}}{\partial \zeta} = 0, \quad (\text{C.6})$$

$$\bigcirc (\epsilon^4): \frac{\partial N_{i1}}{\partial \mathcal{T}} - V \frac{\partial N_{i3}}{\partial \zeta} + N_{i0} \frac{\partial V_{i3}}{\partial \zeta} + N_{i1} \frac{\partial V_{i2}}{\partial \zeta} + N_{i2} \frac{\partial V_{i1}}{\partial \zeta} = 0. \quad (\text{C.7})$$

The momentum equation gives:

$$\bigcirc(\epsilon^2) : m_i C_{ti}^2 \frac{\partial N_{i1}}{\partial \zeta} + N_{i0} q_i \frac{\partial \varphi_1}{\partial \zeta} - m_i N_{i0} V \frac{\partial V_{i1}}{\partial \zeta} = 0. \quad (\text{C.8})$$

$$\begin{aligned} \bigcirc(\epsilon^3) : m_i N_{i0} V_{i1} \frac{\partial V_{i1}}{\partial \zeta} - m_i N_{i0} V \frac{\partial V_{i2}}{\partial \zeta} - m_i N_{i1} V \frac{\partial V_{i1}}{\partial \zeta} + (\gamma_i - 1) m_i C_{ti}^2 \frac{N_{i1}}{N_{i0}} \frac{\partial N_{i1}}{\partial \zeta} \\ + m_i C_{ti}^2 \frac{\partial N_{i2}}{\partial \zeta} + N_{i0} q_i \frac{\partial \varphi_2}{\partial \zeta} + N_{i1} q_i \frac{\partial \varphi_1}{\partial \zeta} = 0. \end{aligned} \quad (\text{C.9})$$

$$\begin{aligned} \bigcirc(\epsilon^4) : m_i N_{i0} \frac{\partial V_{i1}}{\partial \mathcal{T}} - m_i N_{i0} V \frac{\partial V_{i3}}{\partial \zeta} - m_i N_{i1} V \frac{\partial V_{i2}}{\partial \zeta} - m_i V N_{i2} \frac{\partial V_{i1}}{\partial \zeta} + m_i N_{i0} V_{i1} \frac{\partial V_{i2}}{\partial \zeta} \\ + m_i N_{i0} V_{i2} \frac{\partial V_{i1}}{\partial \zeta} + m_i N_{i1} V_{i1} \frac{\partial V_{i1}}{\partial \zeta} + m_i C_{ti}^2 \frac{\partial N_{i3}}{\partial \zeta} + N_{i0} q_i \frac{\partial \varphi_3}{\partial \zeta} + N_{i1} q_i \frac{\partial \varphi_2}{\partial \zeta} \\ + (\gamma_i - 1) m_i C_{ti}^2 \frac{N_{i1}}{N_{i0}} \frac{\partial N_{i2}}{\partial \zeta} + (\gamma_i - 1) m_i C_{ti}^2 \frac{N_{i2}}{N_{i0}} \frac{\partial N_{i1}}{\partial \zeta} + N_{i2} q_i \frac{\partial \varphi_1}{\partial \zeta} = 0. \end{aligned} \quad (\text{C.10})$$

Similarly, Poisson's equation gives:

$$\bigcirc(\epsilon^0) : \sum_{s=c,h} N_{s0} q_s + N_{i0} q_i = 0, \quad (\text{C.11})$$

$$\bigcirc(\epsilon^1) : N_{i1} q_i - \sum_{s=c,h} q_s N_{s0} \nu_{s1} \varphi_1 = 0, \quad (\text{C.12})$$

$$\bigcirc(\epsilon^2) : N_{i2} q_i - \sum_{s=c,h} q_s N_{s0} \nu_{s1} \varphi_2 + \sum_{s=c,h} q_s N_{s0} \nu_{s2} \varphi_1^2 = 0, \quad (\text{C.13})$$

$$\begin{aligned} \bigcirc(\epsilon^3) : \varepsilon_0 \frac{\partial^2 \varphi_1}{\partial \zeta^2} + N_{i3} q_i - \sum_{s=c,h} q_s N_{s0} \nu_{s1} \varphi_3 \\ + 2 \sum_{s=c,h} q_s N_{s0} \nu_{s2} \varphi_1 \varphi_2 - \sum_{s=c,h} q_s N_{s0} \nu_{s3} \varphi_1^3 = 0, \end{aligned} \quad (\text{C.14})$$

where Eq. (C.11) is the charge neutrality condition of the un-perturbed plasma constituents at equilibrium.

The $\bigcirc(\epsilon^2)$ equations, (C.5) and (C.8), can easily be solved for the first-order perturbed velocity V_{i1} and density N_{i1} in terms of φ_1 giving

$$V_{i1} = \frac{V q_i / m_i}{V^2 - C_{ti}^2} \varphi_1 \quad \text{and} \quad N_{i1} = \frac{N_{i0} q_i / m_i}{V^2 - C_{ti}^2} \varphi_1. \quad (\text{C.15})$$

Again, the $\bigcirc(\epsilon^1)$ terms in Poisson's equation, (C.12), gives the linear dispersion relation

$$\frac{\omega_{pi}^2}{V^2 - C_{ti}^2} - \frac{1}{\lambda_{D\kappa}^2} = 0 \quad \text{or} \quad \frac{\omega_{pi}^2}{\omega^2 - k^2 C_{ti}^2} - \frac{1}{k^2 \lambda_{D\kappa}^2} = 0, \quad (\text{C.16})$$

from which the phase velocity, V is obtained as $V = (C_{i\kappa}^2 + C_{ti}^2)^{1/2}$, with $C_{i\kappa} = \omega_{pi} \lambda_{D\kappa}$

being the ion-acoustic sound speed of the plasma model.

Similarly, the $\mathcal{O}(\epsilon^2)$ terms in Poissons's equation (C.13) together with the $\mathcal{O}(\epsilon^3)$ terms in the continuity equation (C.6) give,

$$N_{i2} = \sum_{s=c,h} \frac{q_s N_{s0}}{q_i} \nu_{s1} \varphi_2 - \sum_{s=c,h} \frac{q_s N_{s0}}{q_i} \nu_{s2} \varphi_1^2 \quad \text{and}$$

$$V_{i2} = V \left\{ \sum_{s=c,h} \frac{q_s N_{s0}}{q_i N_{i0}} \nu_{s1} \varphi_2 - \sum_{s=c,h} \frac{q_s N_{s0}}{q_i N_{i0}} \nu_{s2} \varphi_1^2 - \frac{1}{2} \frac{q_i^2/m_i^2}{(V^2 - C_{ti}^2)^2} \varphi_1^2 \right\}.$$

In order to eliminate the third-order perturbation terms V_{i3} and N_{i3} , we use the $\mathcal{O}(\epsilon^4)$ continuity and momentum equations, and the $\mathcal{O}(\epsilon^3)$ Poisson's equation. That is, Eqs. (C.7), (C.10) and (C.14). After a single differentiation, Eq. (C.14) then becomes

$$\begin{aligned} \epsilon_0 \frac{\partial^3 \varphi_1}{\partial \zeta^3} + \frac{2N_{i0} V q_i^2/m_i}{(V^2 - C_{ti}^2)^2} \frac{\partial \varphi_1}{\partial \tau} + \left\{ \frac{N_{i0} q_i^2/m_i}{V^2 - C_{ti}^2} - \sum_{s=c,h} q_s N_{s0} \nu_{s1} \right\} \frac{\partial \varphi_3}{\partial \zeta} \\ + \varphi_2 \frac{\partial \varphi_1}{\partial \zeta} \left\{ \frac{N_{i0} q_i^2/m_i}{(V^2 - C_{ti}^2)^2} [2V^2 + (\gamma_i - 2)C_{ti}^2] \sum_{s=c,h} \frac{q_s N_{s0}}{q_i N_{i0}} \nu_{s1} + 2 \sum_{s=c,h} q_s N_{s0} \nu_{s2} \right\} \\ + \varphi_1 \frac{\partial \varphi_2}{\partial \zeta} \left\{ 2 \sum_{s=c,h} q_s N_{s0} \nu_{s2} + \frac{N_{i0} q_i^2/m_i}{(V^2 - C_{ti}^2)^2} \left[1 + \{V^2 + (\gamma_i - 1)C_{ti}^2\} \sum_{s=c,h} \frac{q_s N_{s0}}{q_i N_{i0}} \nu_{s1} \right] \right\} \\ - \varphi_1^2 \frac{\partial \varphi_1}{\partial \zeta} \left\{ 3 \sum_{s=c,h} q_s N_{s0} \nu_{s3} + \frac{3 N_{i0} V^2 q_i^4/m_i^3}{2 (V^2 - C_{ti}^2)^4} \right. \\ \left. + \frac{N_{i0} q_i^2/m_i}{(V^2 - C_{ti}^2)^2} [4V^2 + (3\gamma_i - 4)C_{ti}^2] \sum_{s=c,h} \frac{q_s N_{s0}}{q_i N_{i0}} \nu_{s2} \right\} = 0. \end{aligned} \quad (\text{C.17})$$

We observe from Eq. (C.12) that for $\varphi_1 \neq 0$, the coefficient of $\partial \varphi_3/\partial \zeta$ in Eq. (C.17) is zero, and therefore those terms drop out. Also, we assume that the terms $\varphi_2 \partial \varphi_1/\partial \zeta$ and $\varphi_1 \partial \varphi_2/\partial \zeta$ are proportional to the product of φ_1 and φ_2 , and therefore are of higher order and will be neglected. We then get

$$\begin{aligned} - \left\{ \frac{3 \omega_{pi}^2 V^2 q_i^2/m_i^2}{2 (V^2 - C_{ti}^2)^4} + 3 \sum_{s=c,h} \frac{q_s N_{s0}}{\epsilon_0} \nu_{s3} + \frac{\omega_{pi}^2 [4V^2 + (3\gamma_i - 4)C_{ti}^2]}{(V^2 - C_{ti}^2)^2} \sum_{s=c,h} \frac{q_s N_{s0}}{q_i N_{i0}} \nu_{s2} \right\} \varphi_1^2 \frac{\partial \varphi_1}{\partial \zeta} \\ + \frac{\partial^3 \varphi_1}{\partial \zeta^3} + \frac{2V \omega_{pi}^2}{(V^2 - C_{ti}^2)^2} \frac{\partial \varphi_1}{\partial \mathcal{T}} = 0. \end{aligned} \quad (\text{C.18})$$

Thus from Eq. (C.18), the modified KdV equation takes the form [Verheest, 2000]

$$\frac{\partial \varphi_1}{\partial \mathcal{T}} + C(V) \varphi_1^2 \frac{\partial \varphi_1}{\partial \zeta} + D(V) \frac{\partial^3 \varphi_1}{\partial \zeta^3} = 0, \quad (\text{C.19})$$

where again the phase velocity V is obtained from $V^2 = C_{ti}^2 + C_{i\kappa}^2$, and

$$C(V) = -A_3/A_1; \quad D(V) = B(V) = 1/A_1; \quad A_1 = \frac{2V \omega_{pi}^2}{(V^2 - C_{ti}^2)^2} \quad \text{and}$$

$$A_3 = \frac{3 \omega_{pi}^2 V^2 q_i^2 / m_i^2}{2 (V^2 - C_{ti}^2)^4} + 3 \sum_{s=c,h} \frac{q_s N_{s0}}{\varepsilon_0} \nu_{s3} + \frac{\omega_{pi}^2 [4V^2 + (3\gamma_i - 4)c_{ti}^2]}{(V^2 - C_{ti}^2)^2} \sum_{s=c,h} \frac{q_s N_{s0}}{q_i N_{i0}} \nu_{s2}.$$

C.2 Solution of the mKdV Equation

In getting the solution to the mKdV equation [(C.19)] we use the transformation $\chi = \xi - u_0 \mathcal{T}$. Thus Eq. (C.19) becomes

$$D \frac{\partial^2 \varphi_1}{\partial \chi^2} + \frac{C}{3} \varphi_1^3 \frac{\partial \varphi_1}{\partial \chi} - u_0 \varphi_1 \frac{\partial \varphi_1}{\partial \chi} = 0,$$

which can also be simplified, and written in the form:

$$\frac{\partial \varphi_1}{\partial \chi} = \left(\frac{u_0}{D} \right)^{1/2} \varphi_1 \left[1 - \left(\frac{C}{6u_0} \right) \varphi_1^2 \right]^{1/2}. \quad (\text{C.20})$$

Integrating Eq. (C.20), $\chi(\varphi_1)$ is obtained from the expression

$$\left(\frac{u_0}{D} \right)^{1/2} \chi = \int \frac{\partial \varphi_1}{\varphi_1 \left[1 - \left(\frac{C}{6u_0} \right) \varphi_1^2 \right]^{1/2}}. \quad (\text{C.21})$$

Introducing the substitution $Y(\varphi_1) = \left[1 - (C/6u_0) \varphi_1^2 \right]^{1/2}$ gives

$$\varphi_1 = \left(\frac{6u_0}{C} \right)^{1/2} [1 - Y(\varphi_1)^2]^{1/2}, \quad (\text{C.22})$$

and therefore the RHS of Eq. (C.21) is equivalent to $\ln[(1 - Y(\varphi_1))/(1 + Y(\varphi_1))]$, *i.e.*,

$$2 \left(\frac{u_0}{D} \right)^{1/2} \chi = \ln \left[\frac{1 - Y(\varphi_1)}{1 + Y(\varphi_1)} \right] \quad \text{or}$$

$$Y(\varphi_1) = \frac{1 - \exp[2(u_0/D)^{1/2}\chi]}{1 + \exp[2(u_0/D)^{1/2}\chi]}. \quad (\text{C.23})$$

Equations (C.22) and (C.23) give

$$\begin{aligned} \varphi_1 &= \left(\frac{6u_0}{C} \right)^{1/2} \frac{2}{\exp[(u_0/D)^{1/2}\chi] + \exp[-(u_0/D)^{1/2}\chi]} \\ &= \left(\frac{6u_0}{C} \right)^{1/2} \operatorname{sech} \left[\left(\frac{u_0}{D} \right)^{1/2} \chi \right]. \end{aligned} \quad (\text{C.24})$$

References

- H. Abbasi and H. H. Pajouh, Dust-ion-acoustic solitons in plasmas with non-Maxwellian electron distribution function, *Physics of Plasmas*, **14**, 012307(1–6), 2007.
- M. Abramowitz and I. A. Stegun, *Handbook of mathematical functions with formulas, graphs, and mathematical tables*, (National Bureau of Standards, Washington DC, USA, 1972)
- N. André, M. Blanc, S. Maurice, P. Schippers, E. Pallier, T. I. Gombosi, K. C. Hansen, D. T. Young, F. J. Crary, S. Bolton, E. C. Sittler, H. T. Smith, R. E. Johnson, R. A. Baragiola, A. J. Coates, A. M. Rymer, M. K. Dougherty, N. Achilleos, C. S. Arridge, S. M. Krimigis, D. G. Mitchell, N. Krupp, D. C. Hamilton, I. Dandouras, D. A. Gurnett, W. S. Kurth, P. Louarn, R. Srama, S. Kempf, H. J. Waite, L. W. Esposito and J. T. Clarke, Identification of Saturn’s magnetospheric regions and associated plasma processes: Synopsis of Cassini observations during orbit insertion, *Reviews of Geophysics*, **46**, RG4008(1–22), 2008.
- G. B. Arfken and H. J. Weber, *Mathematical Methods for Physicists, 4th edition*, (Academic Press, San Diego, USA, 1995)
- M. Ashour-Abdalla and H. Okuda, Electron acoustic instabilities in the geomagnetic tail, *Geophysical Research Letters*, **13**, 366–369, 1986.
- S. Baboolal, R. Bharuthram and M. A. Hellberg, Arbitrary-amplitude rarefactive ion-

-
- acoustic double layers in warm multi-fluid plasma, *Journal of Plasma Physics*, **40**(1), 163–178, 1988.
- S. Baboolal, R. Bharuthram and M. A. Hellberg, Arbitrary-amplitude theory of ion-acoustic solitons in warm multi-fluid plasmas, *Journal of Plasma Physics*, **41**(2), 341–353, 1989.
- S. Baboolal, R. Bharuthram and M. A. Hellberg, Cut-off conditions and existence domains for large-amplitude ion-acoustic solitons and double layers in fluid plasmas, *Journal of Plasma Physics*, **44**, 1–23, 1990.
- T. K. Baluku, Acoustic Solitons in a Plasma with Positive Dust, Master’s thesis, University of KwaZulu-Natal, Durban, South Africa, 2007.
- T. K. Baluku and M. A. Hellberg, Dust acoustic solitons in plasmas with kappa-distributed electrons and/or ions, *Physics of Plasmas*, **15**, 123705(1–11), 2008.
- T. K. Baluku and M. A. Hellberg, Ion acoustic solitary waves in a plasma with two-temperature kappa distributed electrons, in preparation, 2010.
- T. K. Baluku, M. A. Hellberg and R. L. Mace, Solitons in dusty plasmas with positive dust grains, *Physics of Plasmas*, **15**, 033701(1–11), 2008.
- T. K. Baluku, M. A. Hellberg, I. Kourakis and S. N. Saini, Dust ion acoustic solitons in a plasma with kappa distributed electrons, *Physics of Plasmas*, **17**, 053702(1–11), 2010a.
- T. K. Baluku, M. A. Hellberg, and F. Verheest, New light on ion acoustic solitary waves in a plasma with two temperature electrons, *Europhysics Letters*, **91**, 15001, 2010b.
- D. D. Barbosa and W. S. Kurth, On the generation of plasma waves in Saturn’s inner magnetosphere, *Journal of Geophysical Research*, **98**(A6), 9351–9356, 1993.
- A. Barkan, R. L. Merlino and N. D’Angelo, Laboratory observation of the dust-acoustic wave mode, *Physics of Plasmas*, **2**, 3563–3565, 1995.
- A. Barkan, N. D’Angelo and R. N. Merlino, Experiments on ion-acoustic waves in dusty plasmas, *Planetary and Space Science*, **44**(8), 239–242, 1996.

REFERENCES

- R. Bharuthram and P. K. Shukla, Large amplitude ion-acoustic solitons in dusty plasma, *Planetary and Space Science*, **4**(7), 973–977, 1992.
- V. I. Berezhiani, M. Y. El-Ashry, and U. A. Mofiz, Theory of strong-electromagnetic-wave propagation in an electron-positron-ion plasma, *Physical Review E*, **50**, 448–452, 1994.
- B. Bezzerides, D. W. Forslund and E. L. Lindman, Existence of rarefaction shocks in a laser-plasma corona, *Physics of Fluids*, **21**, 2179–2185, 1978.
- L. P. Block, A double layer review, *Astrophysics and Space Science*, **15**, 59–83, 1978.
- T. J. M. Boyd and J. J. Sanderson, *The Physics of Plasmas*, (Cambridge University Press, Cambridge, UK, 2003), p. 8
- M. Brambilla, *Kinetic Theory of Plasma Waves (Homogeneous Plasmas)*, (Oxford University Press, New York, USA, 1989), pp. 107–109
- D. A. Bryant, Debye length in a kappa-distribution plasma, *Journal of Plasma Physics*, **56**, 87–93, 1996.
- B. Buti, Ion-acoustic holes in a two-electron-temperature plasma, *Physics Letters A*, **76**, 251–254, 1980.
- R. A. Cairns, A. A. Mamun, R. Bingham, R. Boström, R. O. Dendy, C. M. C. Nairn and P. K. Shukla, Electrostatic solitary structures in non-thermal plasmas, *Geophysical Research Letters*, **22**(20), 2709–2712, 1995.
- T. Cattaert, F. Verheest and M. A. Hellberg, Potential hill electron-acoustic solitons and double layers in plasmas with two electron species, *Physics of Plasmas*, **12**(4), 042901(1–10), 2005.
- Y. F. Chateau and N. Meyer-Vernet, Electrostatic noise in non-Maxwellian plasmas: Generic properties and “Kappa” distributions, *Journal of Geophysical Research*, **96**(44), 5825–5836, 1991.
- F. F. Chen, *Introduction to Plasma Physics*, (Plenum Press, New York, USA, 1984)

- S. P. Christon, D. G. Mitchell, D. J. Williams, L. A. Frank, C. Y. Huang and T. E. Eastman, Energy spectra of plasma sheet ions and electrons from about 50 eV/e to about 1 MeV during plasma temperature transitions, *Journal of Geophysical Research*, **93**, 2562–2572, 1988.
- J. H. Chu and L. I, Direct observation of Coulomb crystals and liquids in strongly coupled rf dusty plasmas, *Physical Review Letters*, **72**, 4009–4012, 1994.
- S. H. Chuang and L. N. Hau, The characteristics of ion acoustic solitons in non-Maxwellian plasmas, *Journal of Plasma Physics*, **16**, 0022901(1–6), 2009.
- N. D’Angelo, Coulomb solids and low-frequency fluctuations in RF dusty plasmas, *Journal of Physics D: Applied Physics*, **28**, 1009–1010, 1995.
- N. D’Angelo, Low-frequency waves in collisional positive dust plasmas, *Journal of Physics D: Applied Physics*, **37**, 860–862, 2004.
- K. Dialynas, S. M. Krimigis, D. G. Mitchell, D. C. Hamilton, N. Krupp and P. C. Brandt, Energetic ion spectral characteristics in the Saturnian magnetosphere using Cassini/MIMI measurements, *Journal of Geophysical Research*, **114**, A01212(1-7), 2009.
- M. K. Dougherty, N. Achilleos, N. André, C. S. Arridge, A. Balogh, I. C. Bertucci, M. E. Burton, S. W. H. Cowley, G. Erdos, G. Giampieri, K.-H. Glassmeier, K. K. Khurana, J. Leisner, F. M. Neubauer, C. T. Russell, E. J. Smith, D. J. Southwood and B. T. Tsurutani, Cassini Magnetometer observations during Saturn Orbit Insertion, *Science*, **307**, 1266–1270, 2005.
- P. O. Dovner, A. I. Eriksson, R. Boström, and B. Holback, Freja multiprobe observations of electrostatic solitary structures, *Geophysical Research Letters*, **21**(17), 1827–1830, 1994.
- D. H. E. Dubin and T. M. O’Neil, Computer simulation of ion clouds in a Penning trap, *Physical Review Letters*, **60**(6), 511–514, 1988.
- V. Formisano, G. Moreno, F. Palmiotto and P. C. Hedgecock, Solar wind interaction with the Earth’s magnetic field: 1. Magnetosheath, *Journal of Geophysical Research*, **78**, 3714–3730, 1973.

REFERENCES

- V. E. Fortov, A. P. Nefedov, V. M. Torchinsky, V. I. Molotkov, O. F. Petrov, A. A. Samarian, A. M. Lipaev and A. G. Khrapak, Crystalline structures of strongly coupled dusty plasmas in dc glow discharge strata, *Physics Letters A*, **229**, 317–322, 1997.
- B. D. Fried and S. D. Conte, *The Plasma Dispersion Function*, (Academic Press, New York, USA, 1961)
- W. Fu and L. Hau, Vlasov-Maxwell equilibrium solutions for Harris sheet magnetic field with Kappa velocity distribution, *Physics of Plasmas*, **12**(7), 070701(1–4), 2005.
- S. P. Gary, Electron/electron acoustic instability, *Physics of Fluids*, **30**(9), 2745–2749, 1987.
- S. P. Gary and R. L. Tokar, Electron-acoustic mode, *Physics of Fluids*, **28**(8), 2439–2441, 1985.
- L. J. Gelinas, K. A. Lynch, M. C. Kelley, S. Collins, S. Baker, Q. Zhou and J. S. Friedman, First observation of meteoritic charged dust in the tropical mesosphere, *Geophysical Research Letters*, **25**, 4047–4050, 1998.
- S. S. Ghosh and A. N. Sekar Iyengar, Anomalous width variations for ion acoustic rarefactive solitary waves in a warm ion plasma with two electron temperatures, *Physics of Plasmas*, **4**(9), 3204–3210, 1997.
- S. S. Ghosh, K. K. Ghosh, and A. N. Sekar Iyengar, Large Mach number ion acoustic rarefactive solitary waves for a two electron temperature warm ion plasma, *Physics of Plasmas*, **3**(11), 3939–3946, 1996.
- S. Ghosh, S. Sarkar, M. Khan and M. R. Gupta, Nonlinear properties of small amplitude dust ion acoustic solitary waves, *Physics of Plasmas*, **7**(9), 3594–3599, 2000a.
- S. Ghosh, S. Sarkar, M. Khan and M. R. Gupta, Dust ion acoustic shock waves in a collisionless dusty plasma, *Physics Letters A*, **7**(275), 109–117, 2000b.
- S. L. Gilbert, J. J. Bollinger and D. J. Wineland, Shell-structure phase of magnetically confined strongly coupled plasmas, *Physical Review Letters*, **60**(20), 2022–2025, 1988.

-
- C. K. Goertz, Dusty plasmas in the solar system, *Reviews of Geophysics*, **27**, 271–292, 1989.
- R. J. Goldston and P. H. Rutherford, *Introduction to Space Physics*, (IOP, Bristol, U.K., 1995), p. 12;
- D. A. Gurnett and A. Bhattacharjee, *Introduction to Plasma Physics with Space and Laboratory Applications*, (Cambridge University Press, Cambridge, UK, 2005), pp. 5–12; 77
- D. A. Gurnett, W. S. Kurth and F. L. Scarf, Plasma waves near Saturn: Initial results from Voyager 1, *Science*, **212**, 235–239, 1981.
- D. A. Gurnett, W. S. Kurth, G. B. Hospodarsky, A. M. Persoon, T. F. Averkamp, B. Cecconi, A. Lecacheux, P. Zarka, P. Canu, N. Cornilleau-Wehrin, P. Galopeau, A. Roux, C. Harvey, P. Louarn, R. Bostrom, G. Gustafsson, J.-E. Wahlund, M. D. Desch, W. M. Farrell, M. L. Kaiser, K. Goetz, P. J. Kellogg, H. P. L. G. Fischer, H. Rucker, H. Alleyne and A. Pedersen, Radio and plasma wave observations at Saturn from Cassini's approach and first orbit, *Science*, **307**, 1255–1259, 2005.
- Q. Haque and H. Saleem, Ion acoustic and drift wave vortices in electron-positron-ion plasmas, *Physics of Plasmas*, **10**, 3793–3795, 2003.
- A. Hasegawa, K. Mima and M. Duong-van, Plasma distribution function in a superthermal radiation field. *Physical Review Letters*, **54**(24), 2608–2610, 1985.
- L. Hau and W. Fu, Mathematical and physical aspects of kappa velocity distribution, *Physics of Plasmas*, **14**(11), 110702(1–4), 2007.
- O. Havnes, Dusty plasmas in the ionosphere and its environment, In *Dusty Plasmas in the New Millennium: Proceedings of the Third International Conference on the Physics of Dusty Plasmas*, held, 20–24 May 2002, Durban, South Africa, edited by R. Bharuthram, M. A. Hellberg, P. K. Shukla and F. Verheest (American Institute of Physics, New York, USA, 2002), pp. 13–21.
- Y. Hayashi and K. Tachibana, Observation of Coulomb-crystal formation from Carbon

- particles grown in a Methane plasma, *Japanese Journal of Applied Physics*, **33**, L804–L806, 1994.
- M. A. Hellberg and R. L. Mace, Generalized plasma function for a plasma with a kappa-Maxwellian velocity distribution, *Physics of Plasmas*, **9**(5), 1495–1504, 2002.
- M. A. Hellberg and F. Verheest, Ion-acoustic solitons in plasmas with two-temperature ions, *Physics of Plasmas*, **15**(6), 062307(1–8), 2008.
- M. A. Hellberg, M. A. Raadu, and R. L. Mace, On fluid models of stationary, acoustic double layers, In *Double Layers–Potential Formation and Related Nonlinear Phenomena in Plasmas*, edited by “S. P. Forum” (World Scientific, Singapore, 1997), pp. 1–13
- M. A. Hellberg, R. L. Mace, R. J. Armstrong and G. Karlstad, Electron-acoustic waves in the laboratory: an experiment revisited, *Journal of Plasma Physics*, **64**(04), 433–443, 2000.
- M. A. Hellberg, R. L. Mace and T. Cattaert, Effects of superthermal particles on waves in magnetized space plasmas, *Space Science Reviews*, **121**(1), 127–139, 2006.
- M. A. Hellberg, F. Verheest and T. Cattaert, Existence domains for nonlinear structures in complex two-ion-temperature plasmas, *Journal of Physics A: Mathematical and General*, **39**(12), 3137–3146, 2006.
- M. A. Hellberg, R. L. Mace, T. K. Baluku, I. Kourakis and N. S. Saini, Comment on “Mathematical and physical aspects of Kappa velocity distribution” [Phys. Plasmas **14**, 110702 (2007)], *Physics of Plasmas*, **16**(5), 094701(1–5), 2009.
- M. Horányi, Dusty plasmas in the solar system, In *Dusty Plasmas in the New Millennium: Proceedings of the Third International Conference on the Physics of Dusty Plasmas*, held, 20–24 May 2002, Durban, South Africa, edited by R. Bharuthram, M. A. Hellberg, P. K. Shukla and F. Verheest (American Institute of Physics, New York, USA, 2002), pp. 22–31.
- E. Infeld and G. Rowlands, *Nonlinear Waves, Solitons, and Chaos*, (Cambridge University Press, Cambridge, UK, 2000)

-
- G. H. Jones, E. Roussos, N. Krupp, U. Beckmann, A. J. Coates, F. Crary, I. Dandouras, V. Dikarev, M. K. Dougherty, P. Garnier, C. J. Hansen, A. R. Hendrix, G. B. Hospodarsky, R. E. Johnson, S. Kempf, K. K. Khurana, S. M. Krimigis, H. Krüger, W. S. Kurth, A. Lagg, H. J. McAndrews, D. G. Mitchell, C. Paranicas, F. Postberg, C. T. Russell, J. Saur, M. Seif, F. Spahn, R. Srama, D. F. Strobel, R. Tokar, J. E. Wahlund, R. J. Wilson, J. Woch and D. Young, Multi-instrument analysis of electron populations in Saturn's magnetosphere, *Science*, **319**(1380), 1567–1572, 2008.
- H. Kakati and K. S. Goswami, On the existence of small amplitude double layers in an electron-positron-ion plasma, *Physics of Plasmas*, **7**, 808–813, 2000.
- G. Karlstad, J. Trulsen and R. J. Armstrong, Electron plasma waves in a d. p. machine, In *Proceedings of the International Conference on Plasma Physics: Contributed Papers*, edited by M. Q. Tran and M. L. Swaley (Lausanne, Switzerland, 1984), **1**, 12.
- Y. Kawai, Y. Nakamura, T. Itoh, T. Hara and T. Kawabe, Propagation of electron waves in a non-Maxwellian plasma, *Journal of the Physical Society of Japan*, **38**(3), 876–881, 1975.
- S.-H. Kim and R. L. Merlino. Charging of dust grains in a plasma with negative ions. *Physics of Plasmas*, 13(5):052118(1–7), 2006.
- M. G. Kivelson and C. T. Russell, *Introduction to Space Physics*, (Cambridge University Press, Cambridge, UK, 1995)
- N. A. Krall and A. W. Trivelpiece, *Principles of Plasma Physics*, (McGraw-Hill, New York, USA, 1989)
- S. M. Krimigis, J. F. Carbary, E. P. Keath, T. P. Armstrong, L. J. Lanzerotti and G. Gloeckler, General characteristics of hot plasma and energetic particles in the Saturnian magnetosphere - Results from the Voyager spacecraft, *Journal of Geophysical Research*, **88**, 8871–8892, 1983.
- S. M. Krimigis, D. G. Mitchell, D. C. Hamilton, N. Krupp, S. Livi, E. C. Roelof, J. Dandouras, T. P. Armstrong, B. H. Mauk, C. Paranicas, P. C. Brandt, S. Bolton, A. F. Cheng, T. Choo, G. Gloeckler, J. Hayes, K. C. Hsieh, W. H. Ip, S. Jaskulek, E. P.

REFERENCES

- Keath, E. Kirsch, M. Kusterer, A. Lagg, L. J. Lanzerotti, D. LaVallee, J. Manweiler, R. W. McEntire, W. Rasmuss, J. Saur, F. S. Turner, D. J. Williams and J. Woch, Dynamics of Saturn's Magnetosphere from MIMI during Cassini's Orbital Insertion, *Science*, **307**, 1270–, 2005.
- N. Krupp, A. Lagg, J. Woch, S. M. Krimigis, S. Livi, D. G. Mitchell, E. C. Roelof, C. Paranicas, B. H. Mauk, D. C. Hamilton, T. P. Armstrong and M. K. Dougherty, The Saturnian plasma sheet as revealed by energetic particle measurements, *Geophysical Research Letters*, **32**, L20S03(1–5), 2005.
- W. S. Kurth, F. L. Scarf, D. A. Gurnett and D. D. Barbosa, A survey of electrostatic waves in Saturn's inner magnetosphere, *Journal of Geophysical Research*, **88**(11), 8959–8970, 1983.
- M. P. Leubner, A nonextensive entropy approach to kappa-distributions, *Astrophysics and Space Science*, **282**, 573–579, 2002.
- M. P. Leubner, Fundamental issues on kappa-distributions in space plasmas and interplanetary proton distributions, *Physics of Plasmas*, **11**, 1308–1316, 2004.
- E. P. Liang, S. C. Wilks and M. Tabak, Pair production by ultraintense lasers, *Physical Review Letters*, **81**, 4887–4890, 1998.
- G. Livadiotis and D. J. McComas, Beyond kappa distributions: Exploiting Tsallis statistical mechanics in space plasmas, *Journal of Geophysical Research*, **114**(1), A11105, 2009.
- R. L. Mace, Linear and Nonlinear electron-acoustic waves in plasmas with two electron components, Master's thesis, University of Natal, Durban, South Africa, 1991.
- R. L. Mace and M. A. Hellberg, Higher-order electron modes in a two-electron temperature plasma, *Journal of Plasma Physics*, **43**, 239–255, 1990.
- R. L. Mace and M. A. Hellberg, Electron-acoustic and cyclotron-sound instabilities driven by field-aligned hot-electron streaming, *Journal of Geophysical Research*, **98**(4), 5881–5891, 1993.

-
- R. L. Mace and M. A. Hellberg, A dispersion function for plasmas containing suprathermal particles, *Physics of Plasmas*, **2**, 2098–2109, 1995.
- R. L. Mace and M. A. Hellberg, The Korteweg-de Vries-Zakharov-Kuznetsov equation for electron-acoustic waves, *Physics of Plasmas*, **8**, 2649–2656, 2001.
- R. L. Mace and M. A. Hellberg, A new formulation and simplified derivation of the dispersion function for a plasma with kappa velocity distribution, *Physics of Plasmas*, **16**, 072113(1–9), 2009.
- R. L. Mace and R. D. Sydora, Parallel whistler instability in a plasma with an anisotropic bi-kappa distribution, *Journal of Geophysical Research*, **115**, A07206(1–14),
- R. L. Mace, S. Baboolal, R. Bharuthram and M. A. Hellberg, Arbitrary-amplitude electron-acoustic solitons in a two electron-component plasma, *Journal of Plasma Physics*, **45**, 323–338, 1991.
- R. L. Mace, M. A. Hellberg, and R. Truemann, Electrostatic fluctuations in plasmas containing suprathermal particles, *Journal of Plasma Physics*, **59**, 393–416, 1998.
- R. L. Mace, G. Amery and M. A. Hellberg, The electron-acoustic mode in a plasma with hot suprathermal and cool Maxwellian electrons, *Physics of Plasmas*, **6**(1), 44–49, 1999.
- M. Maksimovic, V. Pierrard and J. F. Lemaire, A kinetic model of the solar wind with Kappa distribution functions in the corona, *Astronomy & Astrophysics*, **324**, 725–734, 1997.
- A. A. Mamun, Solitary potentials in dusty plasmas, *Physics of Plasmas*, **3**(2), 702, 1996.
- A. A. Mamun, Effects of ion temperature on electrostatic solitary structures in nonthermal plasmas, *Physical Review E*, **55**(2), 1852–1857, 1997.
- A. A. Mamun and N. Jahan, Roles of adiabaticity and dynamics of electrons and ions on dust-ion acoustic KdV solitons, *Europhysics Letters*, **T98**, 35001, 2008.
- A. A. Mamun and P. K. Shukla, Electrostatic solitary and shock structures in dusty plasmas, *Physica Scripta*, **T98**, 107–114, 2002.

REFERENCES

- A. A. Mamun and P. K. Shukla, Nonlinear waves and structures in dusty plasmas, *Plasma Physics and Controlled Fusion*, **47**(5A), A1–A9, 2005.
- A. A. Mamun and P. K. Shukla, Electron-acoustic solitary waves in dusty plasmas, In *New Aspects of Plasma Physics: Proceedings of the 2007 ICTP Summer College on Plasma Physics, Trieste, Italy*, edited by P. K Shukla, L. Stenflo and B. Eliasson (World Scientific, Danvers, USA, 2008), p. 374.
- E. Marsch and S. Livi, Coulomb collision rates for self-similar kappa distributions, *Physics of Fluids*, **28**(5), 1379–13868, 1985.
- J. A. M. McDonnell, J. C. Zarnecki, R. E. Olearczyk, S. C. Chakaveh, G. S. A. Pankiewicz and S. T. Evans, Giotto observations of Comet Halley dust, *Royal Society of London Philosophical Transactions Series A*, **323**, 381–395, 1987.
- J. F. McKenzie, The ion-acoustic soliton: A gas-dynamic viewpoint, *Physics of Plasmas*, **9**, 800–805, 2002a.
- J. F. McKenzie, The fluid-dynamic paradigm of the dust-acoustic soliton, *Journal of Plasma Physics*, **67**, 353–362, 2002b.
- J. F. McKenzie, Electron acoustic Langmuir solitons in a two-component electron plasma, *Journal of Plasma Physics*, **69**, 199–210, 2003.
- J. F. McKenzie and T. B. Doyle, A unified view of acoustic-electrostatic solitons in complex plasmas, *New Journal of Physics*, **5**, 26(1–10), 2003.
- J. F. McKenzie, T. B. Doyle, F. Verheest, and M. A. Hellberg, Compressive and rarefactive ion-acoustic solitons in a two component electron plasma, *Journal of Plasma Physics*, **71**, 2163–176, 2004a.
- J. F. McKenzie, F. Verheest, T. B. Doyle, and M. A. Hellberg, Compressive and rarefactive ion-acoustic solitons in bi-ion plasmas, *Physics of Plasmas*, **11**(5), 1–8, 2004b.
- J. F. McKenzie, F. Verheest, T. B. Doyle, and M. A. Hellberg, Note on rarefactive and compressive ion-acoustic solitons in a plasma containing two ion species, *Physics of Plasmas*, **12**(12), 102305(1–6), 2005.

-
- A. Melzer, T. Trottenberg and A. Piel, Experimental determination of the charge on dust particles forming Coulomb lattices, *Physics Letters A*, **191**, 301–308, 1994.
- D. A. Mendis and M. Rosenberg, Cosmic dusty plasma, *Annual Review of Astronomy and Astrophysics*, **32**(1), 419–463, 1994.
- C. A. Mendoza-Briceño, S. M. Russel and A. A. Mamun, Large amplitude electrostatic solitary structures in a hot non-thermal dusty plasma, *Planetary and Space Science*, **48**, 599–608, 2000.
- R. L. Merlino, A. Barkan, C. Thompson and N. D’Angelo, Experiments on waves and instabilities in dusty plasmas, *Plasma Physics and Controlled Fusion*, **39**(5A), A421–A429, 1997.
- R. L. Merlino, A. Barkan, C. Thompson and N. D’Angelo, Laboratory studies of waves and instabilities in dusty plasmas, *Physics of Plasmas*, **5**, 1607–1614, 1998.
- K. Miyamoto, *Fundamentals of Plasma Physics and Controlled Fusion*, (Iwanami Book Service Center, Tokyo, Japan, 1997)
- W. M. Moslem, I. Kourakis, P. K. Shukla and R. Schlickeiser, Nonlinear excitations in electron-positron-ion plasmas in accretion disks of active galactic nuclei, *Physics of Plasmas*, **14**(10), 102901, 2007.
- Y. Nakamura and H. Sugai, Experiments on ion acoustic solitons in a plasma, *Chaos, Solitons & Fractals*, **7**(7), 102–1031, 1996.
- Y. Nakamura, J. L. Ferreira, and G. O. Ludwig, Experiments on ion-acoustic rarefactive solitons in a multi-component plasma with negative ions, *Journal of Plasma Physics*, **33**, 237–248, 1985.
- Y. N. Nejoh, Effects of positron density and temperature on large amplitude ion-acoustic waves in an electron-positron-ion plasma, *Australian Journal of Physics*, **50**, 309–317, 1997.
- K. Nishihara and M. Tajiri, Rarefaction ion acoustic solitons in two electron temperature plasma, *Journal of the Physical Society of Japan*, **50**(12), 4047–353, 1981.

- S. Olbert, Summary of experimental results from M.I.T. detector on IMP-1, In *Physics of the Magnetosphere: Proceedings of the Conference held, 19–28 June 1967, at Boston College*, edited by R. L. Carovillano, J. F. McClay and H. R. Radoski (Riedel Publishing Company, Dordrecht, Netherlands, 1968), pp. 641–659.
- A. Olsson and P. Janhunen, A case study of electron precipitation in the late substorm growth phase on and nearby a preonset arc, *Annales de Geophysicae*, **16**(12), 1567–1572, 1998.
- H. H. Pajouh and H. Abbasi, Dust-ion-acoustic solitons in plasmas with non-Maxwellian electron distribution function, *Physics of Plasmas*, **15**, 103705, 2008.
- H. R. Pakzad, Ion acoustic solitary waves in plasma with nonthermal electron and positron, *Physics Letters A*, **373**, 847–850, 2009.
- G. K. Parks, *Physics of Space Plasmas : An Introduction*, (Westview Press, Boulder, 2004)
- V. Pierrard and J. Lemaire, Lorentzian ion exosphere model, *Journal of Geophysical Research*, **101**(A4), 7923–7934, 1996.
- V. Pierrard, H. Lamy and J. Lemaire, Exospheric distributions of minor ions in the solar wind, *Journal of Geophysical Research*, **109**, A02118, 2004.
- J. J. Podesta, Spatial Landau damping in plasmas with three-dimensional κ distributions, *Physics of Plasmas*, **12**, 052101, 2005.
- S. I. Popel, S. V. Vladimirov and P. K. Shukla, Ion-acoustic solitons in electron-positron-ion plasmas, *Physics of Plasmas*, **2**, 716–719, 1995.
- F. Postberg, S. Kempf, R. Srama, S. F. Green, J. K. Hillier, N. McBride and E. Grün, Composition of jovian dust stream particles, *Icarus*, **183**, 122–134, 2006.
- R. Pottelette, R. E. Ergun, R. A. Treumann, M. Berthomier, C. W. Carlson, J. P. McFadden and I. Roth, Modulated electron-acoustic waves in auroral density cavities: FAST observations, *Geophysical Research Letters*, **26**, 2629–2632, 1999.
- M. A. Raadu and P. Carlqvist, Electrostatic double layers and a plasma evacuation process, *Astrophysics and Space Science*, **74**, 189–206, 1981.

-
- M. A. Raadu and J. J. Rasmussen, Dynamical aspects of electrostatic double layers, *Astrophysics and Space Science*, **144**, 43–71, 1981.
- A. Rahman, F. Sayed and A. A. Mamun, Dust ion-acoustic shock waves in an adiabatic dusty plasma, *Physics of Plasmas*, **14**, 034503(1–3), 2007.
- N. N. Rao, P. K. Shukla, and M. Y. Yu. . *Planetary and Space Science*, 38:543–546, 1990.
- W. K. M. Rice, M. A. Hellberg, R. L. Mace and R. Bharuthram, Finite electron mass effects on ion-acoustic solitons in a two electron temperature plasma, *Physics Letters A*, **174**, 416–420, 1993.
- K. F. Riley, M. P. Hobson, and S. J. Bence, *Mathematical Methods for Physics and Engineering* , (Cambridge University Press, Cambridge, UK, 1998)
- K. Roy Chowdhury, S. N. Paul and A. Roy Chowdhury, Effect of electron inertia on double layers in a relativistic hot plasma, *Australian Journal of Physics*, **47**, 785–793, 1994.
- R. Z. Sagdeev, Cooperative phenomena and shock waves in collisionless plasmas, In M. A. Leontovich, editor, *Reviews of Plasma Physics*, **4**, 23–91, Consultants Bureau, New York, 1966.
- N. S. Saini, I. Kourakis and M. A. Hellberg, Arbitrary amplitude ion-acoustic solitary excitations in the presence of excess superthermal electrons, *Physics of Plasmas*, **16** (12), 062903(1–9), 2009.
- H. Saleem, Q. Haque, and J. Vranjes, Nonlinear drift waves in electron-positron-ion plasmas, *Physical Review E*, **67**(5), 057402, 2003.
- A. A. Samarian, O. S. Vaulina, A. P. Nefedov, V. E. Fortov, B. W. James and O. F. Petrov, Positively charged particles in dusty plasmas, *Physical Review E*, **64**(5), 056407(1–8), 2001.
- F. Sayed, M. M. Haider, A. A. Mamun, P. K. Shukla, B. Eliasson and N. Adhikary, Dust ion-acoustic solitary waves in a dusty plasma with positive and negative ions, *Physics of Plasmas*, **15**, 63701(1–7), 2008.

- P. Schippers, M. Blanc, N. André, I. D. G. R. Lewis, L. K. Gilbert, A. M. Persoon, N. Krupp, D. A. Gurnett, A. J. Coates, S. M. Krimigis, D. T. Young and M. K. Dougherty, Multi-instrument analysis of electron populations in Saturn's magnetosphere, *Journal of Geophysical Research*, **113**, A07208(1–10), 2008.
- J. D. Scudder, On the causes of temperature change in inhomogeneous low-density astrophysical plasmas (299–319); Why all stars should possess circumstellar temperature inversions (319–349), *Astrophysical Journal*, **398**, 1992.
- B. Shizgal, Suprathermal particle distributions in space physics: Kappa distributions and entropy, *Astrophysics and Space Science*, **312**, 227–237, 2007.
- P. K. Shukla, Waves in dusty plasmas, In *The Physics of Dusty Plasmas: Proceedings of the Sixth Workshop on the Physics of Dusty plasmas*, edited by D. A. Mendis, V. W. Chow and P. K. Shukla (World Scientific, Singapore, 1996), pp. 107–121.
- P. K. Shukla, Dust acoustic wave in a thermal dusty plasma, *Physical Review E*, **61**, 7249–7251, 2000a.
- P. K. Shukla, New collective processes in dusty plasmas: applications to space and laboratories, *Plasma Physics and Controlled Fusion*, **42**(12), B213–B221, 2000b.
- P. K. Shukla and A. A. Mamun, *Introduction to Dusty Plasma Physics*, (IOP, Bristol, UK, 2002)
- P. K. Shukla and A. A. Mamun, *New Journal of Physics*, **5**, 17(1–37), 2003,
- P. K. Shukla and V. P. Silin, Dust Ion-Acoustic Wave, *Physica Scripta*, **45**, 508, 1992.
- S. V. Singh and G. S. Lakhina, Generation of electron acoustic waves in the magnetosphere, *Planetary and Space Science*, **49**, 107–114, 2001.
- E. C. J. Sittler, K. W. Ogilvie and J. D. Scudder, Survey of low energy plasma electrons in Saturn's magnetosphere: Voyagers 1 and 2, *Journal of Geophysical Research*, **88**, 8847–8870, 1983.

-
- R. A. Smith, On the role of double layers in astrophysical plasmas, In *IAU SYMPOSIUM: Unstable Current Systems and Plasma Instabilities in Astrophysics*, edited by M. R. Kundu and G. D. Holman, **107**, 113–122, 1985.
- D. Summers and R. M. Thorne, The modified plasma dispersion function, *Physics of Fluids B: Plasma Physics*, **3**, 1835–1847, 1991.
- D. G. Swanson, *Plasma Waves, 1st edition*, (Academic Press, Boston, USA, 1989)
- D. G. Swanson, *Plasma Waves, 2nd edition*, (IOP, Bristol, U.K., 2003)
- M. Tajiri and K. Nishihara, Solitons and shock waves in two-electron-temperature plasmas, *Journal of the Physical Society of Japan*, **54**, 572–578, 1985.
- H. Thomas, G. E. Morfill, V. Demmel, J. Goree, B. Feuerbacher and D. Möhlmann, Plasma crystal: Coulomb crystallization in a dusty plasma, *Physical Review Letters*, **73**, 652–655, 1994.
- N. Thomas and H. U. Keller, Comet P/Halley’s dust production rate at Giotto encounter derived from Halley Multicolour Camera observations, *Astronomy & Astrophysics*, **249**, 258–268, 1991.
- R. L. Tokar and S. P. Gary, Electrostatic hiss and the beam driven electron acoustic instability in the dayside polar cusp, *Geophysical Research Letters*, **11**(12), 1180–1183, 1984.
- R. A. Treumann, Generalized-Lorentzian Thermodynamics, *Physica Scripta*, **59**(3), 204–214, 1999.
- C. Tsallis, Possible generalization of Boltzmann-Gibbs statistics, *Journal of Statistical Physics*, **52**, 479–487, 1988.
- C. Tsallis, Non-extensive thermostatics: brief review and comments, *Physica A: Statistical Mechanics and its Applications*, **221**, 277–290, 1995.
- C. Tsallis, Nonextensive statistics: Theoretical, experimental and computational evidences and connections, *Brazilian Journal of Physics*, **29**, 1–35, 1999.

- V. M. Vasyliunas, A Survey of low-energy electrons in the evening sector of the magnetosphere with OGO 1 and OGO 3, *Journal of Geophysical Research*, **73**(9), 2839–2884, 1968.
- F. Verheest, Dusty plasmas in application to astrophysics, *Plasma Physics and Controlled Fusion*, **41**(3A), A445–A451, 1999.
- F. Verheest, *Waves in Dusty Space Plasmas*, (Kluwer, Dordrecht, Netherlands, 2000)
- F. Verheest, Nonlinear acoustic waves in nonthermal plasmas with negative and positive dust, *Physics of Plasmas*, **16**(1), 013704(1–9), 2009.
- F. Verheest, Nonlinear acoustic waves in nonthermal dusty or pair plasmas, *Physics of Plasmas*, **17**, 062302(1–10), 2010a.
- F. Verheest and T. Cattaert, Nonlinear electromagnetic modes in astrophysical plasmas with dust distributions, *Astronomy & Astrophysics*, **421**, 17–21, 2004.
- F. Verheest and M. A. Hellberg, Bohm sheath criteria and double layers in multispecies plasmas, *Journal of Plasma Physics*, **57**(2), 465–477, 1997.
- F. Verheest and M. A. Hellberg, Nonthermal effects on existence domains for dust-acoustic solitary structures in plasmas with two-temperature ions, *Physics of Plasmas*, **17**, 023701(1–10), 2010.
- F. Verheest and S. R. Pillay, Large amplitude dust-acoustic solitary waves and double layers in nonthermal plasmas, *Physics of Plasmas*, **15**, 013703(1–11), 2008a.
- F. Verheest and S. R. Pillay, Dust-acoustic solitary structures in plasmas with nonthermal electrons and positive dust, *Nonlinear Processes in Geophysics*, **15**, 551–555, 2008b.
- F. Verheest, T. Cattaert, and M. A. Hellberg, Ion-and dust-acoustic solitons in dusty plasmas: Existence conditions for positive and negative potential solutions, *Physics of Plasmas*, **12**, 082308, 2005.
- F. Verheest, T. Cattaert, M. A. Hellberg and R. L. Mace, On the existence of ion-acoustic double layers in two-electron-temperature plasmas, *Physics of Plasmas*, **13**, 042301(1–9), 2006.

-
- F. Verheest, M. A. Hellberg and T. K. Baluku, Finite amplitude electrostatic solitons at the acoustic speed, submitted to *Journal of Plasma Physics* (under review), 2010.
- F. Verheest, M. A. Hellberg and I. Kourakis, Acoustic solitary waves in dusty and/or multi-ion plasmas with cold, adiabatic, and hot constituents, *Physics of Plasmas*, **15** (11), 112309(1–11), 2008.
- J.-E. Wahlund, R. Boström, G. Gustafsson, D. A. Gurnett, W. S. Kurth, T. Averkamp, G. B. Hospodarsky, A. M. Persoon, P. Canu, A. Pedersen, M. D. Desch, A. I. Eriksson, R. Gill, M. W. Morooka and M. André, The inner magnetosphere of Saturn: Cassini RPWS cold plasma results from the first encounter, *Geophysical Research Letters*, **32**, L20S09(1–4), 2005.
- H. Washimi and T. Taniuti, Propagation of ion-acoustic solitary waves of small amplitude, *Physical Review Letters*, **17**(19), 996–998, 1966.
- T. Watanabe and T. Taniuti, Electron-Acoustic mode in a plasma of two-temperature electrons, *Journal of the Physical Society of Japan*, **43**(5), 1819–1890, 1977.
- D. T. Young, J.-J. Berthelier, M. Blanc, J. L. Burch, S. Bolton, A. J. Coates, F. J. Crary, R. Goldstein, M. Grande, T. W. Hill, R. E. Johnson, R. A. Baragiola, V. Kelha, D. J. McComas, K. Mursula, E. C. Sittler, K. R. Svenes, K. Szegö, P. Tanskanen, M. F. Thomsen, S. Bakshi, B. L. Barraclough, Z. Bebesi, D. Delapp, M. W. Dunlop, J. T. Gosling, J. D. Furman, L. K. Gilbert, D. Glenn, C. Holmlund, J.-M. Illiano, G. R. Lewis, D. R. Linder, S. Maurice, H. J. McAndrews, B. T. Narheim, E. Pallier, D. Reisenfeld, A. M. Rymer, H. T. Smith, R. L. Tokar, J. Vilppola and C. Zinsmeyer, Composition and Dynamics of Plasma in Saturn’s Magnetosphere, *Science*, **307**, 1262–1266, 2005.